Raman spectroscopic studies of friction modifier Molybdenum DialkyldiThioCarbamate (MoDTC)

Doris Nekesa Khaemba

Submitted in accordance with the requirements for the degree of
Doctor of philosophy

The University of Leeds
School of Mechanical Engineering
Leeds, UK

February, 2016

The candidate confirms that the work submitted is her own, except where work which has formed part of jointly authored publications has been included. The contribution of the candidate and other co-authors in published work from this thesis has been clearly indicated. The candidate confirms that appropriate credit has been given within the thesis where reference has been made to the work of others.

In the papers contributing to this thesis, the candidate (first author) carried out all the experiments, analysis and preparation of the manuscripts. All other authors contributed by proof reading and providing insight on the discussions. Simulation results presented in Figure 10-5 were done by Ali Ghanbarzadeh.

This copy has been supplied on the understanding that it is copyright material and that no quotation from this thesis may be published without proper acknowledgement.

Papers contributing to this thesis

- Khaemba, D.N., Neville A., Morina, A. A methodology for Raman characterisation of MoDTC tribofilms and its application in investigating the influence of surface chemistry on friction performance of MoDTC lubricants. Tribology Letters, Volume 59, Issue 3, pp.1-17, 2015

- Khaemba, D.N., Neville A., Morina, A. New insights on the decomposition mechanism for molybdenum DialkyldiThioCarbamate (MoDTC): A Raman spectroscopic study. RSC advances, 2016, **DOI:** 10.1039/C6RA00652C

Acknowledgements

First, I would like to appreciate my supervisors, Professors Ardian Morina and Anne Neville who have been very instrumental in ensuring the successful completion of this work. I thank Prof. Ardian for his guidance regarding my experimental plan and discussions on my results. His probing questions have made me a better researcher. I would like to thank Prof. Anne for her ever useful discussions into the direction of my work and understanding novelty in my work. I could not have asked for better supervisors, it has truly been a pleasure working with you both.

I am very thankful to all members of the ENTICE project. I really enjoyed working with other research fellows and developing friendships. I always looked forward to project meetings and enjoyed getting feedback on my work. It was a privilege to be part of ENTICE.

I am thankful to Adrian Eagles for training me on using NPLEX machine, Chun Wang for providing advice of Raman analysis whenever I needed it, technicians in iFS for providing technical assistance with tribometers and other equipment. I also want to thank Benardette for training me on using MTM and conducting a few tests on my behalf. I am very grateful to Benoit, Frederic and members the tribology group at TOTAL for hosting me during my one month secondment at TOTAL Research Centre, Solaize. I also want to thank Morris Owen from Everlube for providing me with MoS_2 coatings. I also want to thank Fiona for her administrative support in the institute.

I would also like to thank my office mates Zahra, Frederick, Lukman, MacDonald, Ali, Evan, Earle, James, Bethan, Lubna and Mohsen for creating a wonderful working environment for me. I want to thank Farnaz, Kirjen, Nic, Shola, Rafaella, Thawhid, Yugal, Jide, Shahriar and John for being very good friends to me. Finally, I would like to thank my family for their support.

Abstract

Presently, there is a strong push towards improving fuel economy in passenger cars. Poor fuel economy is attributed to high friction in various components within car engines. About 5% of the friction losses in internal combustion engines occur in the boundary lubrication regime where metal-metal contact is present. Lubrication in boundary lubrication regime is achieved by using lubricants containing chemically active additives which react with the surfaces to form thin films known as tribofilms. The formed tribofilms provide friction reduction and wear protection due to their physicochemical properties. Molybdenum DialkyldiThioCarbamate (MoDTC) is an additive added in engine oil mainly as a friction modifier. MoDTC reduces friction by degradation of the additive to form discrete MoS_2 at the tribocontact. There is however little knowledge on the degradation process of MoDTC at the tribocontact.

In this thesis, tribochemical reactions that occur in steel/steel tribocontacts in the presence of MoDTC additive have been investigated. Tribological tests were conducted using model oils comprising of MoDTC additive in mineral base oil. Tests were conducted under unidirectional linear sliding and sliding/rolling conditions. Raman spectroscopy was used to conduct chemical characterisation of the rubbed surfaces.

Results show that mechanical activation accelerates the rate of MoDTC degradation. Under tribological conditions, MoDTC decomposes to form three main compounds; MoS_2, MoS_x and $FeMoO_4$. MoDTC decomposition products formed at the tribocontact are dependent on test conditions. The mechanism for the degradation process has been proposed. MoDTC tribofilms were observed to grow rapidly within generated wear scars until a limiting thickness was achieved. The limiting thickness was dependent on contact parameters.

The chemical composition of MoDTC tribofilms determined the friction observed in tribotests. In sliding/rolling conditions, low friction values (μ=0.04-0.05) were obtained when the tribofilms are composed of MoS_2 while higher friction (μ=0.06-0.08) was observed when the tribofilms were composed of Fe_2O_3, Fe_3O_4, MoS_x and $FeMoO_4$.

MoDTC provided wear protection to the steel substrates only at test conditions which allowed MoDTC tribofilms to be present at the contact. In conditions where MoDTC tribofilms were missing from the contact, severe wear of the substrate was observed.

The durability of MoDTC tribofilms when rubbed in MoDTC-free lubricant was observed to be dependent on the sliding configuration. MoDTC tribofilms were less durable in sliding/rolling contacts than in unidirectional sliding contacts. In unidirectional sliding conditions, it was also observed that MoDTC tribofilms formed on fresh steel samples were more durable than those formed on oxidised steel samples. This is because the adhesion of MoS_2 on iron oxide is less than on steel.

Table of Contents

List of Figures

List of Tables

Nomenclature

Terms	Definition	Units
$\Delta H^{\ddagger}$	Activation enthalpy	kJ/(K mol)
$\Delta S^{\ddagger}$	Activation entropy	J/(K mol)
μ_i	Induced dipole moment	C m
A_o	Pre-exponential factor	Dependent on reaction order
E_{elec}	Electric field	N/C
E_0	Amplitude of electric field	N/C
E^*	Reduced Young's modulus	Pa
E_a	Activation energy	kJ/mol
E_1, E_2	Young's Modulus of body 1 and 2	Pa
R^*	Radius of curvature	m
T_{max}	Maximum temperature rise	K
U_s	Relative sliding velocity $|U_2-U_1|$	m/s
h_{max}	Maximum tribofilm thickness	nm
h_{mean}	Mean tribofilm thickness	nm
k_B	Boltzmann constant	J/K
k_c	Tribofilm formation reaction constant	
k_{thermo}	Reaction constant for a thermally-activated reaction	Dependent on reaction order
k_{tribo}	Reaction constant for a mechanically-activated reaction	Dependent on reaction order
t_i	Induction time	min
v_1, v_2	Poisson ratio of body 1 and 2	-
α_p	Polarisability tensor	C m²/V
η_0	Dynamic viscosity	Pa s
τ_{growth}	Rate of tribofilm growth	nm³/s
τ_0	Pre-exponential factor for tribofilm growth	Dependent on reaction order

Terms	Definition	Units
ΔV	Activation volume	Å^3
µ	Friction coefficient	-
A	Absorption coefficient	cm^{-1}
C	Additive concentration	wt%
F	Friction force	N
h	Planck constant	J s
h_{min}	Minimum film thickness	nm
K	Thermal conductivity	W/(m K)
N	Number of atoms in a molecule	-
P	Pressure	Pa
Pe	Peclet number	-
P_{max}	Maximum Hertzian contact pressure	Pa
P_{mean}	Mean Hertzian contact pressure	Pa
q	Rate of heat generated per unit area of contact	W/m^2
Q	Molecular vibrational co-ordinates	-
R_s	Radius of laser spot	nm
R	Gas constant	J/(K mol)
r	Rate of reaction	s^{-1}
R_1, R_2	Radius of body 1 and 2	m
R_a	Centre line average roughness	nm
R_q	Root mean square roughness	nm
S	Speed	m/s
T	Temperature	K or $^{\circ}$C
t	Time	min
V	Material constant	m^3
W	Load	N
λ	Ratio of minimum film thickness to surface roughness	-
λ	Light wavelength	nm

Terms	Definition	Units
C_p	Specific heat capacity	J/(Kg K)
U	Entrainment speed $U = (U_1 + U_2)/2$	m/s
a	Radius of contact area	m
k	Thermal diffusivity	m/s^2
δ	Laser penetration depth	nm
ζ	Transmission coefficient	-
κ	Extinction index	-
ω	Angular frequency	rad/s
α	Pressure viscosity coefficient	Pa^{-1}
ρ	Density	kg/m^3
σ	Shear stress	Pa

Abbreviations

Abbreviation	Definition
AES	Auger Electron Spectroscopy
AFM	Atomic Force Microscope
ATR-FTIR	Attenuated Total Reflection Fourier Transform Infrared
BO	Base Oil
CCD	Charge-Coupled Device
DLC	Diamond-Like Coatings
DMF	Dimethylformamide
DoE	Design of Experiment
EDX	Energy Dispersive X-ray analysis
GMO	Glycerol Mono-Oleate
HRC	Rockwell Hardness
HSPOD	High Speed Pin-on-Disc
MoDTC	Molybdenum DialkyldiThioCarbamate
MTM	MiniTraction Machine
N.A	Numerical Aperture
PAO	Poly Alpha Olefin
SEM	Scanning Electron Microscopy
SLIM	Spacer Layer Image Mapping
SRR	Slide-Roll Ratio
VI	Viscosity Index
VPN	Vickers Pyramid Number
XAS	X-ray Absorption Spectroscopy
XPS	X-ray Photoelectron Spectroscopy
ZDDP	Zinc Dialkyl DithioPhosphate

Chapter 1   Introduction

Presently, fuel efficiency in passenger cars is gaining a lot of attention in the automotive industry. Studies by Holmberg et al. [1] showed that about 11.5% of fuel energy in passenger vehicles is lost due to friction losses in the internal combustion engine (Figure 1-1). Friction losses in engines occur in the piston assembly, bearings, valve train, pumping and hydraulic systems. Friction loss is highest in the piston assembly in comparison to the other components. About 10% of friction losses in the piston assembly occur in the boundary lubrication regime [2]. In boundary lubrication regime, there is metal-metal contact which is responsible for high friction observed within this regime. Since friction is highest in the boundary lubrication regime even a slight friction reduction in this regime can lead to huge energy savings. For this reason, a great deal of research is presently geared towards reducing friction in the boundary lubrication regime.
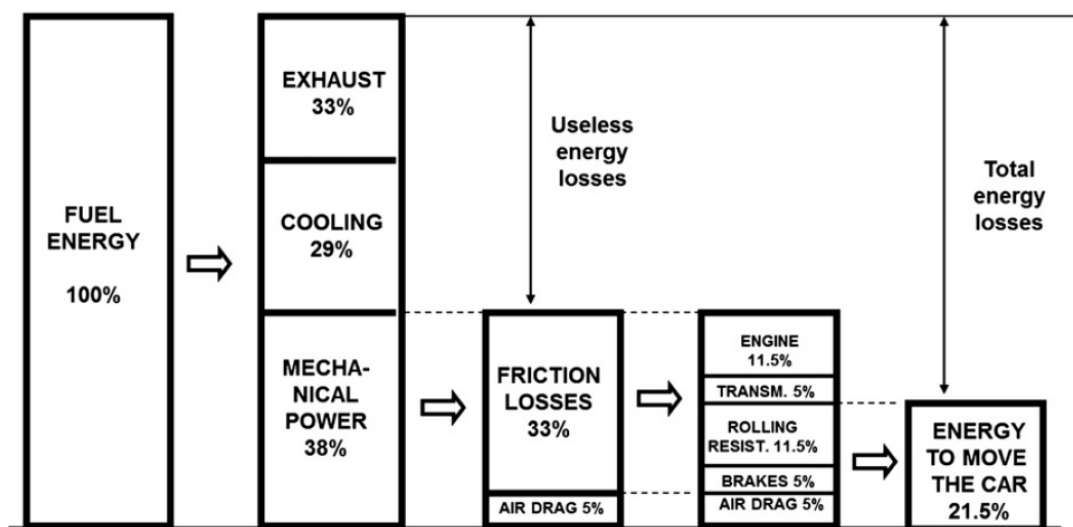
Figure 1-1. Energy losses in passenger cars [1]

Friction in boundary lubrication regime is normally reduced using lubricants containing additives known as friction modifiers. Examples of commonly used friction modifiers are Molybdenum DialkyldiThioCarbamate (MoDTC),

polyamidoalcohol, alkenoic ester and glycerol mono Oleate (GMO) [3, 4]. These oil-soluble friction modifiers form boundary films capable of reducing friction at the asperity-asperity contact (Figure 1-2). There is also a growing interest toward the possible use of a different class of friction modifiers which are not oil-soluble in nature such as MoS_2, WS_2 and H_3BO_3 nanoparticles [5-8]. Besides friction modifiers, low friction coatings such as Diamond-Like Coatings (DLC) are commonly used to achieve low friction [9, 10].
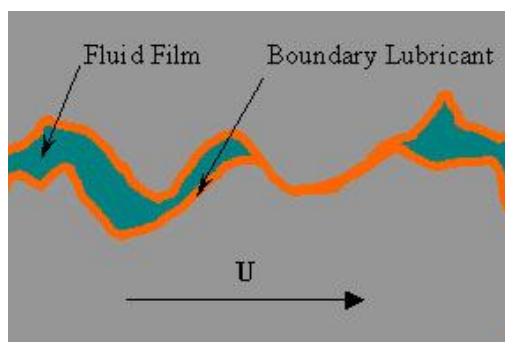
Figure 1-2. Lubrication films formed in boundary lubrication regime [11]

MoDTC is by far the most used friction modifier and has been found to be very effective in steel/steel contacts. Within tribocontacts, MoDTC decomposes to form MoS_2 which is responsible for low friction due to its low shear strength and lattice layer structure. Although MoDTC is expected to provide low friction, studies have shown that parameters such temperature, MoDTC concentration and surface roughness can affect the friction performance [12]. Under some test conditions, such as low MoDTC concentration, low temperatures and smooth surfaces, high friction is observed instead of low friction. The reason why these test conditions result in high friction is currently unknown. Since MoDTC decomposition is key to friction reduction it is important to have a good understanding of the decomposition process. It is also important to study the influence of test conditions on MoDTC decomposition in order to optimise the friction performance of this additive.

In order to study the decomposition of additives within tribocontacts it is necessary to employ techniques which can probe the rubbing interface to

provide chemical and physical information. In most studies, the rubbed surfaces are analysed *ex-situ* after tests. Examples of chemical characterisation techniques that are mostly used in *ex-situ* analysis are Raman spectroscopy, X-ray Photoelectron Spectroscopy (XPS), Energy Dispersive X-ray analysis (EDX). Techniques such as Scanning Electron Microscopy (SEM), Atomic Force Microscopy (AFM) and profilometry are used to study morphology and topography of the rubbed surfaces. *In-situ* analysis can provide more information on the reaction kinetics. Examples of *in-situ* chemical characterisation techniques that have been proposed in recent years include Attenuated Total Reflection Fourier Transform Infrared (ATR-FTIR) [13, 14] and Ultra-High Vacuum X-ray Photoelectron Spectroscopy/Auger Electron Spectroscopy (UHV-XPS/AES) [15, 16]. *In-situ* physical characterisation has been achieved with optical interferometry using Spacer Layer Image Mapping in a Mini-Traction Machine (SLIM-MTM) [4, 17] and *in-situ* AFM studies [18].

1.1   Objectives of this study

The aim of this study is to develop a better understanding of the interfacial processes (additive decomposition, tribofilm formation and removal) that occur within steel/steel contacts during tests with MoDTC containing lubricant. Raman spectroscopy will be employed in *ex-situ* chemical characterisation of the MoDTC decomposition products formed at the tribocontact. The objectives of the study are as follows:

(1) Understanding interfacial processes during tests with MoDTC containing lubricants

- To investigate the influence of contact parameters on MoDTC decomposition and how this impacts tribofilm formation, friction and wear performance of MoDTC lubricants.

- To investigate the durability of MoDTC tribofilms

(2) Determining the suitability of Raman spectroscopy in characterising MoDTC-derived tribofilms

- To investigate suitable parameters (i.e. laser wavelength, laser power, exposure time) for Raman analysis of MoDTC tribofilms. This will ensure that information provided from the analysis is accurate and not an artefact of the analysis process.

- To investigate the effect of lubricant film during Raman analysis of uncleaned samples. Knowledge gained from this investigation will be useful for *in-situ* Raman studies of lubricated surfaces.

1.2   Thesis outline

- Chapter Two: Fundamental theory relevant to this study is presented

- Chapter Three: Literature review on MoDTC additive and Raman studies on MoS_2 is presented.

- Chapter Four: Materials, equipment and experimental procedures used in this study are presented.

- Chapter Five: Results obtained from thermal decomposition of MoDTC in non-tribological conditions are presented.

- Chapter Six: The influence of acquisition parameters during Raman analysis of MoDTC tribofilms is investigated and suitable parameters are recommended.

- Chapter Seven: Surface chemistry changes that occur at the tribocontact during the evolution of MoDTC tribofilms is investigated. In addition, results on the influence of lubricant layer during analysis of rubbed surfaces are presented.

- Chapter Eight: The influence of temperature, MoDTC concentration and contact pressure on the chemical composition of MoDTC decomposition products formed in unidirectional linear sliding conditions are investigated.

- Chapter Nine: The influence of contact parameters on friction and wear performance of MoDTC lubricants in sliding/rolling conditions is investigated.

- Chapter Ten: The influence of surface roughness and slide-roll ratio on friction, morphology and chemical composition of MoDTC tribofilms is investigated.

- Chapter Eleven: The durability of MoDTC tribofilms under unidirectional linear sliding and sliding/rolling conditions is investigated.

- Chapter Twelve: Discussion on results obtained from Chapter Five to Chapter Eleven is presented.

- Chapter Thirteen: Main conclusions from this study are detailed and recommendations for future studies are outlined.

Chapter 2   Fundamental theory

2.1   Tribology

Tribology refers to the study of surfaces in relative motion [19]. Tribology entails the study of three main aspects; friction, wear and lubrication [20]. Friction refers to the resistance to motion which is encountered by one body when it is moved tangentially against another body. Wear refers to material loss from one body due to movement of another body against it. Lubrication refers to the use of compounds in gas, liquid or solid form between two bodies in relative motion so as to reduce friction and wear [21].

2.2   Contact between surfaces

2.2.1   Herztian contact pressure

When a load is applied to two bodies which are in contact the bodies can deform either plastically or elastically [22]. Plastic deformation occurs when extremely high stresses, above the elastic limit of the materials, are applied leading to permanent damage of the bodies. Stresses below the elastic limit of the materials in contact will lead to elastic deformation. In cases where elastic deformation occurs, equations developed by Hertz have been used to define the contact. There are different types of contacts depending on the shape of the rubbing surfaces. The contact can be defined as ball-on-ball, ball-on-flat, cylinder-on-cylinder, cylinder-on-flat or flat-on-flat contact. In ball-on-ball and ball-on-flat contacts, the contact is generally considered to be a point contact. In cylinder-on-cylinder and cylinder-on-flat contacts, the contact is considered to be a line contact.

Figure 2-1 shows a schematic diagram for a point contact. For point contacts, equations shown in Table 2-1 are normally used to calculate the contact areas

and contact pressures. A separate set of equations are available for calculating contact areas and pressures in line contacts.
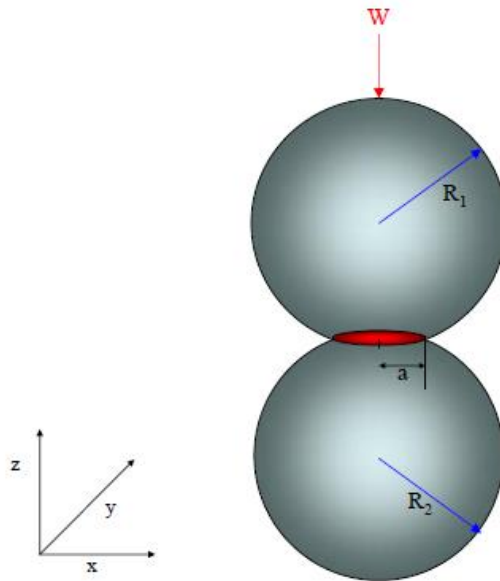
Figure 2-1. Schematic diagram showing two bodies in a point contact [23]

Table 2-1. Equations for calculating Hertzian contact pressure for point contacts

Radius of contact area, a	$a = \left(\dfrac{3WR^*}{4E^*}\right)^{\frac{1}{3}}$	2-1
Relative radius of curvature, R^*	$R^* = \left(\dfrac{1}{R_1} + \dfrac{1}{R_2}\right)^{-1}$	2-2
Reduced Young's modulus, E^*	$E^* = \dfrac{2E_1 E_2}{(1 - v_1{}^2)E_2 + (1 - v_2{}^2)E_1}$	2-3
Maximum contact pressure, P_{max}	$P_{max} = \dfrac{1}{2\pi}\left(\dfrac{3WE^{*2}}{R^{*2}}\right)^{\frac{1}{3}}$	2-4
Mean contact pressure, P_{mean}	$P_{mean} = \dfrac{2}{3}P_{max}$	2-5

Where W [N] is the applied load. E_1, E_2 and v_1, v_2 are elastic moduli and Poisson's ratios, respectively, of body 1 and body 2.

2.2.2   Real surfaces

The Hertzian contact pressure calculated by Equation 2-4 assumes that the surfaces of the bodies in contact are smooth. However, real surfaces are generally not smooth in nature instead they have a surface which is depicted by peaks (asperities) and valleys as can be seen in Figure 2-2. Roughness of surfaces is mostly defined by parameters such as the centre line average roughness (R_a) and root mean square roughness (R_q).

In real surfaces with peaks and valleys, the real contact area is much lower than the nominal contact area calculated using the contact radius derived by Equation 2-1. In some cases, the real contact area can be as low as 1% of the nominal contact area. The load is thus supported by few asperities which can result in extremely high local pressures.

(a)

(b)
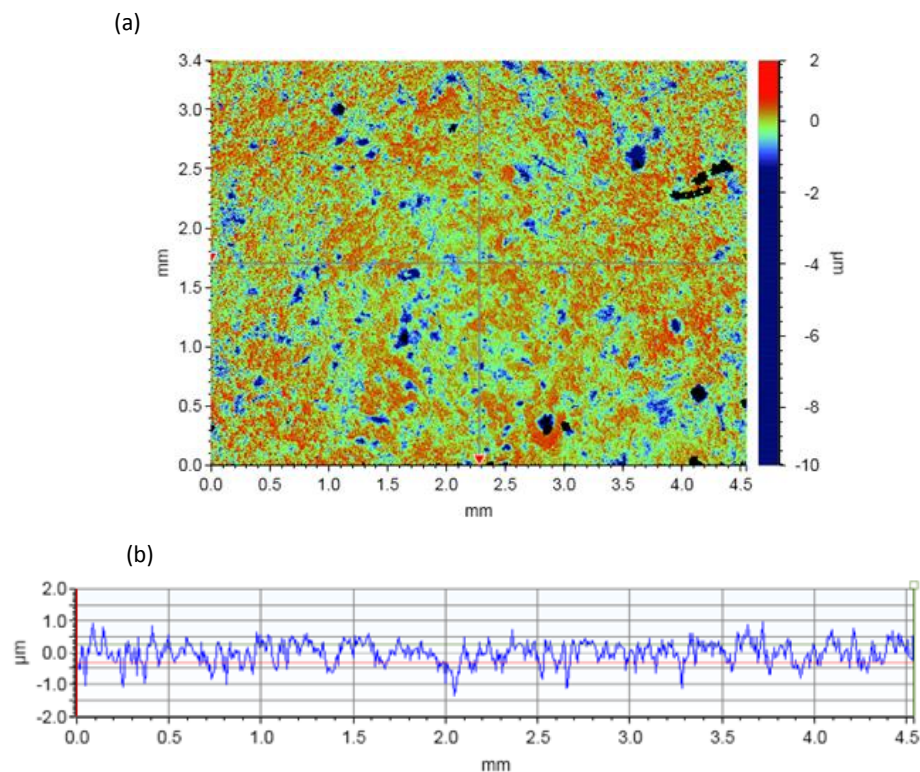
Figure 2-2. (a) 2D image of a steel surface showing variation in height (b) depth profile across the steel surface

2.2.3   Flash temperatures

When two bodies slide against each other, frictional heating occurs at the contact causing a rise in temperature. The high temperature is commonly referred to as flash temperature. Since it is difficult to directly measure temperature rise in a contact, numerical models have been developed to provide an estimate of the temperature rise [24-27].

For a circular Hertzian contact the maximum temperature rise (T_{max}) during sliding at high speeds is estimated using Equation 2-6. At slow sliding speeds, the two bodies are considered to be stationary and the temperature rise is not dependent on the sliding speed. At slow speeds, the temperature is estimated using Equation 2-7. The maximum temperature rise at all sliding velocities is estimated using Equation 2-8.

$$T_{max} = \frac{qa}{K\sqrt{\pi Pe}} \quad (Pe > 10) \qquad\qquad \text{2-6}$$

$$T_{max} = \frac{qa}{K} \quad (Pe < 0.2) \qquad\qquad \text{2-7}$$

$$T_{max} = \frac{qa}{K\sqrt{\pi(1.2373 + Pe}} \qquad\qquad \text{2-8}$$

Pe is the Peclet number and is given by $Pe = U_s a/2k$. U_s is the relative sliding velocity |U_2-U_1|, a the radius of contact area and k the thermal diffusivity ($k = K/\rho C_p$). K is the thermal conductivity, ρ the density and C_p the specific heat capacity of the material. q is the heat supply rate given by $q = \mu P U_s$ where μ is the friction coefficient and *P* the contact pressure.

2.3   Lubrication regimes

When a lubricant is added to a tribological contact the minimum film thickness (h_{min}) of the lubricant between the tribopair is dependent on applied load,

entrainment speed and viscosity of the lubricant. The minimum film thickness is determined using Equation 2-9 [28].

$$\frac{h_{min}}{R_x} = 3.63 \left(\frac{U\eta_0}{E^*R_x}\right)^{0.68} (\alpha E^*)^{0.49} \left(\frac{W}{E^*R_x{}^2}\right)^{-0.073} (1 - e^{-0.68k}) \qquad \text{2-9}$$

Where R_x is the radius of curvature in the x-direction [m], U is the entrainment speed [m/s], E^* the reduced Young's Modulus [Pa], η_0 the dynamic viscosity of the lubricant [Pa s], α the pressure-viscosity coefficient [Pa^{-1}], W the applied load [N], k=1. The entrainment speed is the average speed of the two bodies in contact, $U = (U_1 + U_2)/2$. The reduced Young's Modulus (E^*) is determined using Equation 2-3.

The viscosity of the lubricant is influenced by temperature and pressure [29]. Lubricant viscosity and pressure-viscosity coefficient generally decreases with increase in temperature [30]. Therefore, by employing Equation 2-9, it can be seen that thinner lubricant films are formed at high temperatures and low speeds.

The separation between two surfaces in a lubricated contact is further defined by the specific film thickness or lambda ratio (λ). The lambda ratio is determined by Equation 2-10. Where $R_{q(1)}$ and $R_{q(2)}$ represent the surface roughness of the two surfaces.

$$\lambda = \frac{h_{min}}{\sqrt{R_{q(1)}{}^2 + R_{q(2)}{}^2}} \qquad \text{2-10}$$

Figure 2-3 shows friction coefficient (μ) plotted against λ. Friction coefficient is the ratio between the applied load (W) and the friction force (F), $\mu = F/W$. This plot is known as the Stribeck diagram and is used to determine lubrication regimes in tribological contacts. The schematic diagram in Figure 2-4 illustrates the different lubrication regimes.
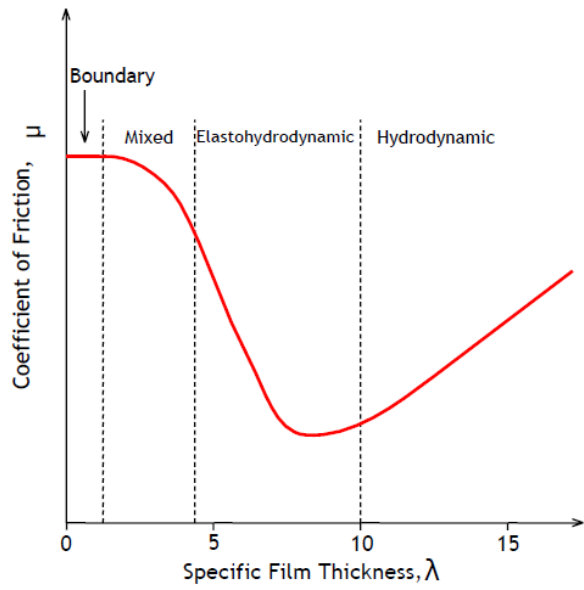
Figure 2-3. Stribeck diagram showing different lubrication regimes [31].
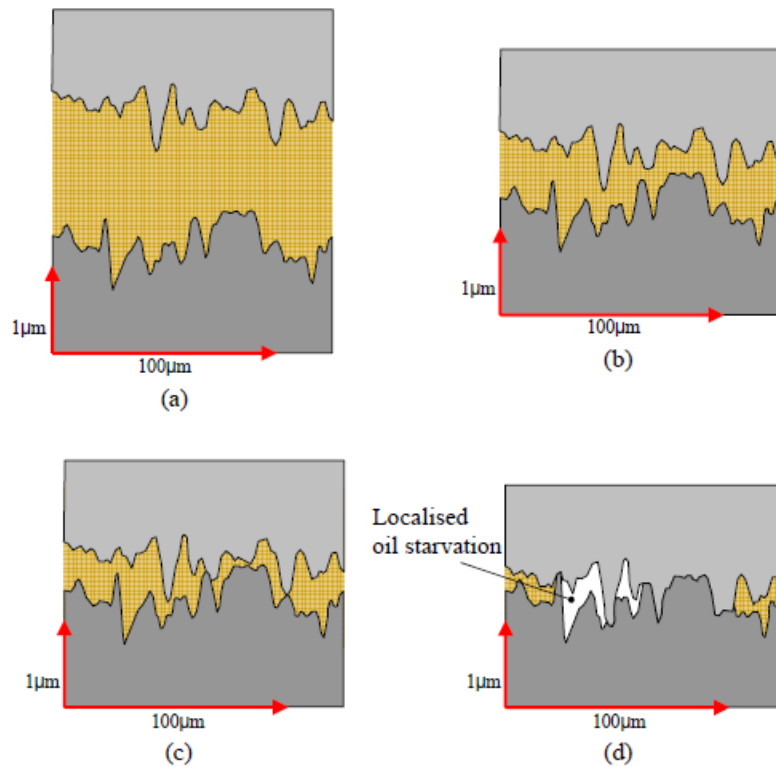
Figure 2-4. Schematic diagram illustrating different lubrication regimes (a) hyrodynamic (b) elastohydrodynamic (c) mixed (d) boundary [23]

11

2.3.1   Hydrodynamic lubrication regime

This lubrication regime occurs at $\lambda > 10$. The two surfaces in contact are completely separated by a lubricant film such that there is no asperity-asperity contact. The load is thus supported by the fluid film.

2.3.2   Elastohydrodynamic lubrication (EHD)

This lubrication regime occurs at $4 < \lambda < 10$. The two surfaces are completely separated with a lubricant film although the film is thinner than that in the hydrodynamic lubrication regime. The contact experiences high pressures which can result in elastic deformation of the tribopair.

2.3.3   Mixed lubrication

This lubrication regime occurs at $1 < \lambda < 4$. Asperities from both surfaces are separated by a fluid film in some regions and in other regions there is asperity-asperity contact. The load is thus supported by both the fluid film and the asperities. This lubrication regime is considered to be a mixture of elastohydrodynamic lubrication and boundary lubrication.

2.3.4   Boundary lubrication

This lubrication regime occurs at $\lambda < 1$. In this regime the thickness of the lubricant separating the two surfaces is less than the roughness of the two surfaces in contact. As a result, asperities from the two rubbing surfaces are in contact. The load in the rubbing contact is thus shared partially between the asperities peaks and the lubricant film. Of all the lubrication regimes, boundary lubrication exhibits the highest friction coefficient. Boundary lubrication regime normally occurs under low speed and high load conditions. In internal combustion engines, this lubrication regime is observed in components such as piston ring/liner interface, cam/tappet interface, gears, bearings, pumps and transmissions [32].

2.4   Lubricants

Engine lubricants are used to reduce friction and wear in internal combustion engines. A lubricant is composed of many additives that have been blended together into a base oil. Additives are chemical compounds that are added to base oils in order to improve the performance of the base oil. The base oil is usually obtained through refining petroleum products or synthetic synthesis [33]. A lubricant ideally consists of more than 20 additives with a total weight concentration of about 20% in the base oil [33].

2.4.1   Base oils

Base oils are grouped into five main categories namely; Group I, Group II, Group III, Group IV and Group V base oils. Table 2-2 shows the criteria used for the grouping.

Table 2-2 Base oil categories

Base oil	Viscosity Index (VI)	Aromatic content (%)	Sulphur content (%)	Source
Group I	80-120	15-35	>0.03	Crude oil
Group II	80-120	<7	<0.03	Crude oil
Group III	>120	<7	<0.03	Crude oil
Group IV	>120	0	0	Chemical synthesis
Group V	All other oils such as phosphate esters, polyalkene glycol and polyolesters.			

Ideally, a good base oil should be moderately viscous, inert towards surfaces, thermally stable, less volatile, provide wear and friction reduction and have good additive solubility [34]. However, in reality, base oils are neither thermally stable nor inert to metal surfaces; they undergo oxidation reactions at high temperatures via free radical mechanism resulting in polymerisation and thermal decomposition [35-37].

13

2.4.2   Additives

Table 2-3 lists additives present in engine lubricants and their functions. These additives can be grouped in two major groups; those that are chemically inert and those that are chemically active. Additives that are chemically inert are usually used to improve the physical characteristics of base oils and include pour point depressants, viscosity modifiers and foam inhibitors [38]. Additives that are chemically active normally interact chemically or physically with the surface or with other chemically active additives. Chemically active additives include corrosion inhibitors, detergents, friction modifiers, rust inhibitors, dispersants, antiwear agents and extreme pressure agents [39].

Table 2-3. Lubricant additives and their functions [39].

	Lubricant additive	Function
Chemically inactive additives	Pour point depressant	Prevents formation of large wax crystals
	Viscosity index improver	Increases VI of lubricant
	Foam inhibitor	Destabilizes foam in oil
Chemically active additives	Oxidation inhibitor	Prevents or slow oxidation of base oil at high temperatures
	Storage stabilizer	Prevents or slow oxidation at low temperatures over long periods
	Corrosion inhibitor	Limits corrosion of non-ferrous metals
	Rust inhibitor	Limits rusting of ferrous metals
	Detergent	Prevents build-up of varnishes on surfaces. If basic also neutralizes acids.
	Dispersant	Prevents formation of solid deposits in cold engine
	Friction modifier	Lowers friction and wear of rubbing surfaces
	Antiwear	Reduces wear of rubbing surfaces
	Extreme pressure (EP)	Prevents seizure of rubbing surfaces

Interactions of different additives can result in either synergy or antagonism which respectively leads to enhanced performance or reduced performance of the additive [39]. Synergy occurs when the combined effects of two or more

14

additives is more than the sum of the effects of individual additives. Antagonism occurs when the presence of one additive supresses the function of the other additives. Figure 2-5 shows the synergetic and antagonistic interactions of additives.
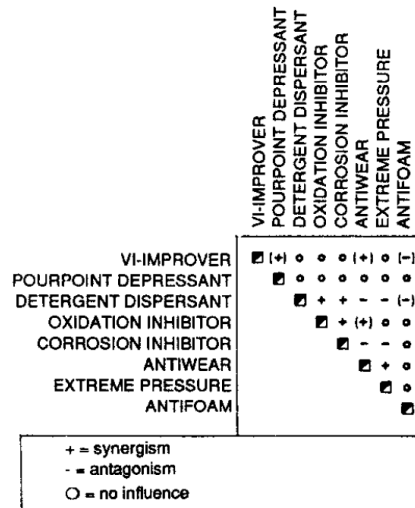
Figure 2-5. Interaction between various surface active additives [39].

2.4.3   Lubrication in different regimes

Lubrication in different lubrication regimes is achieved using different strategies as discussed below.

2.4.3.1   Hydrodynamic lubrication

Components in hydrodynamic lubrication do not experience wear since the surfaces are separated from each other. Thus, friction is the main concern in this regime. Bulk oil properties of the oil, particularly the viscosity, play an important role in friction performance. To reduce friction, oils with low viscosities are normally preferred.

15

2.4.3.2   Elastohydrodynamic lubrication regime

Similar to the hydrodynamic lubrication regime, friction rather than wear is mostly considered in this regime. Similarly, the bulk oil properties play an important role in friction performance. An oil with a high pressure-viscosity index is preferable since it can withstand the high pressures at the tribocontact.

2.4.3.3   Mixed lubrication

The presence of asperity-asperity contact in this lubrication regime results in wear of the substrate and high friction. The bulk properties of the base oil are not enough to provide wear protection and friction reduction. Thus, additives present in the base oil play a big role in providing lubrication. The mechanisms by which these additives provide lubrication are discussed in Section 2.4.3.4.

2.4.3.4   Boundary lubrication regime

Lubrication in boundary lubrication regime is achieved by formation of thin boundary films (also known as tribofilms). These boundary films are formed either through physical/chemical adsorption of the additive or by a chemical reaction between the additive and the rubbing surface [40]. Lubricant additives are therefore of particular importance in this lubrication regime.

Friction and wear reduction in boundary lubrication regime occurs via different mechanisms depending on the physicochemical properties of the boundary films formed. Spikes [4] proposed the following three main mechanisms by which friction is reduced in the boundary lubrication regime.

- Mechanism 1: Formation of lubrication films with low-shear strength or films that have lattice layer structure. These films are formed by friction modifiers such as carboxylic salts and soluble molybdenum additives such as MoDTC.

- Mechanism 2: Formation of a high-viscosity film on the rubbing surfaces which promote fluid film entrainment at low speeds. Oil soluble polymers and high-viscosity polar oils such as esters in less polar oils such as poly alpha olefins (PAO) reduce friction via this mechanism.

- Mechanism 3: Smoothening of the rubbing surfaces. Colloidal oil solutions containing nanoparticles such as gold reduce friction through this mechanism.

Wear protection, on the other hand, is achieved through formation of boundary films with low-shear strength which act as sacrificial layers during rubbing [32]. Zinc Dialkyl DithioPhosphate (ZDDP) is an example of additives that forms such antiwear films.

Boundary films may function as both antiwear and friction modifiers although this is not possible in all cases. For example, ZDDP, a commonly used antiwear additive, forms films which protect the rubbing surfaces from wear but do not provide friction reduction. It is therefore difficult to have an ideal boundary film that can provide both wear protection and friction reduction. Hsu and Gates [32] suggested that if an ideal boundary lubricating film existed, its structure would resemble that depicted in Figure 2-6. The boundary film would comprise of three separate layers; a solid layer, a liquid layer and a mobile phase. The solid layer would provide load carrying capacity under high stress conditions and the liquid layer would provide an easily deformable layer which would distribute loads at the asperities. The mobile phase at the top would provide a layer that can be sheared off easily. This layer would also store additive molecules which would react with the surface to form new films during severe wear.
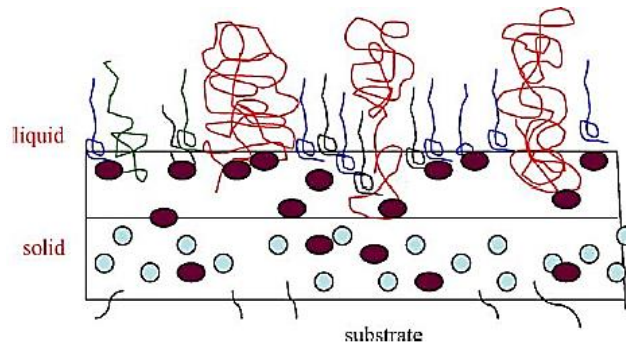
Figure 2-6. An ideal structure for an effective boundary lubricating film [32].

2.5   Tribochemistry

Tribochemistry belongs to a branch of chemistry known as mechanochemistry. Mechanochemistry refers to the chemistry studies which involve chemical and physical changes in matter due to mechanical force [41]. Tribochemistry is a special form of mechanochemistry which occurs specifically in tribological contact where chemical reactions at the tribocontact are activated by shear stress, friction and wear process [42].

Tribochemistry is very important in the boundary lubrication regime because there is asperity-asperity contact. In the absence of lubricants, sliding in boundary regime causes oxidation of the rubbing surfaces. When lubricants (gases or liquid) are used, mechanical rubbing has been shown to initiate and accelerate the rate of decomposition of additives resulting in the formation of tribofilms [43]. Tribofilms formed at the tribocontact provide wear protection and friction reduction. Tribochemical reactions can also cause wear of the tribopair [44].

Two mechanisms have been proposed as the driving force for tribochemical reactions resulting in the formation of boundary films [45]

- **Mechanisms 1**: High flash temperatures at the asperities which causes thermally-induced reactions.

18

- **Mechanism 2**: Shear stress at the tribocontact which causes mechanically-induced reactions.

2.5.1 Thermally-induced reactions

Reaction kinetics of thermally-induced chemical reactions is described by the transition state complex theory also known as the activated complex theory. According to this theory, formation of a reaction product *C* occurs via a reaction route where an activated complex $[AB]^{\ddagger}$ of the reactants *A* and *B* is formed (reaction 2-11)

$$A + B \leftrightarrows [AB]^{\ddagger} \rightarrow C \qquad\qquad 2\text{-}11$$

The rate of formation of product *C* is given by Equation 2-12.

$$\frac{d[C]}{dt} = r = k_{thermo}[A][B] \qquad\qquad 2\text{-}12$$

Where $[A]$ and $[B]$ are the concentrations of the reactants A and B, respectively. k_{thermo} is the reaction constant and is obtained from Eyring Equation 2-13.

$$k_{thermo} = \zeta \frac{k_B T}{h} e^{\frac{\Delta S^{\ddagger}}{R}} e^{\frac{-\Delta H^{\ddagger}}{RT}} \qquad\qquad 2\text{-}13$$

Where ζ is the transmission coefficient ($\zeta=1$), $\Delta S^{\ddagger}$ is the activation entropy, $\Delta H^{\ddagger}$ the activation enthalpy, k_B the Boltzmann constant, h the Planck constant, R the gas constant and T the absolute temperature. In order to calculate the activation energy E_a, Equation 2-13 is sometimes simplified in the form of Arrhenius Equation 2-14. A_0 is the pre-exponential factor ($A_0 = \zeta \frac{k_B T}{h}$).

$$k_{thermo} = A_0 e^{\frac{-E_a}{RT}} \qquad\qquad \text{2-14}$$

Thermally-activated reactions are normally dependent on temperature and the concentration of the reactants. Generally, faster reactions occur at high temperatures and high concentrations.

It is proposed that flash temperature at asperity-asperity contacts in boundary lubrication regime increases the rate of reaction at the tribocontact. However, in most tribological tests where lubricants are used, calculated flash temperatures are very low to initiate or accelerate reactions at the tribocontact [43].

2.5.2 Mechanically-induced reactions

Mechanically-induced reactions have been found to be different from thermally-activated reactions [42]. Several models have been proposed for calculating the rates of reactions in tribological contacts [46-48]. In some reports, it has been suggested that the rate of degradation of the additives in a tribocontact can be described by the modified Arrhenius equation shown in Equation 2-15 [49, 50].

$$k_{tribo} = A_o \, exp^{\frac{\sigma V - E_a}{k_B T}} \qquad\qquad \text{2-15}$$

Where A_o is the pre-exponential factor, σ the shear stress, V the material constant, E_a the activation energy, k_B the Boltzmann constant and T the temperature. Mechanically-induced reactions can occur at lower temperatures than thermally activated reactions since the activation energy is reduced by the shear stress component (σV).There are reports on additives which have been mechanically degraded in tribological contacts [50, 51].

Chapter 3 Literature review

The main aim of this study is to investigate tribochemical reactions that occur within tribocontacts in tests with MoDTC containing lubricants using Raman spectroscopy. Therefore, in this chapter a comprehensive literature review will be conducted on MoDTC additive and Raman spectroscopy.

3.1   Molybdenum DialkyldiThioCarbamate (MoDTC)

In engine oil lubricants, MoDTC is mostly used as a friction modifier although it also functions as an extreme pressure additive and an antioxidant [52]. The term MoDTC can represent compounds with varying molecular structures as shown in Table 3-1. The molecular structure of MoDTC is dependent on the synthesis process.

Table 3-1. Molecular structures of MoDTC

(I) di-μ-thio-dioxo-bis(dialkyldithiocarbamate) dimolybdenum

(II) di-μ-thio-dithio-bis(dialkyldithiocarbamate) dimolybdenum

(III) di-μ-oxo-dithio-bis(dialkyldithiocarbamate) dimolybdenum

(IV) di-μ-oxo-oxo-thio-bis(dialkyldithiocarbamate) dimolybdenum

Farmer and Rowan [53] first reported the synthesis of MoDTC with molecular structure (**III**) and (**IV**) in 1967. The synthesis reaction occurred according to Equation 3-1. Sakurai et al. [54] proposed an additional step to the reaction shown in 3-1 which led to the formation of MoDTC with structures (**I**) and (**II**). This additional step is shown in Equation 3-2.

$$MoO_3 + HNR_2 + nCS_2 \xrightarrow{105°C/\ DMF} Mo_2O_2S_2\ [R_2NCS_2]_2 \text{ or }$$
$$Mo_2O_3S[R_2NCS_2]_2 \tag{3-1}$$

$$MoO_3 + HNR_2 + nCS_2 \xrightarrow{105°C/\ DMF} Mo_2O_2S_2\ [R_2NCS_2]_2 \text{ or }$$
$$Mo_2O_3S[R_2NCS_2]_2 \xrightarrow{P_2S_{10}/xylene} Mo_2S_2O_2\ [R_2NCS_2]_2 \text{ or }$$
$$Mo_2S_4[R_2NCS_2]_2 \tag{3-2}$$
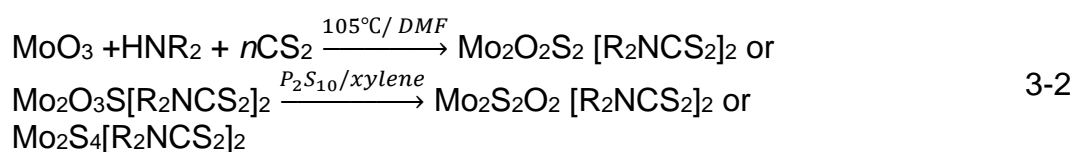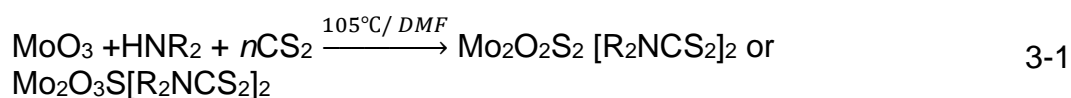
3.2   Thermal degradation of MoDTC

The thermal decomposition of MoDTC with structures **II**, **III** and **IV** has been reported in literature [54, 55]. Sakurai et al. [54] observed that thermal degradation of $Mo_2S_4[R_2NCS_2]_2$ (structure **II**) occurred in three main stages.

- Stage 1: CH_3CH_2SH and CH_3CH_2NS were formed at 200°C.

- Stage 2: CS_2, H_2S, C_4H_4S and MoS_2 were formed at 295°C.

- Stage 3: MoO_3 was formed at 435°C.

Thermal decomposition of $Mo_2S_4[R_2NCS_2]_2$ in nitrogen was observed to occur in only two stages; the first and second stage. Decomposition temperatures in the various stages were dependent on the alkyl groups. $Mo_2S_4[R_2NCS_2]_2$ with branched-chain alkyl groups decomposed at higher temperatures than those with straight chain alkyl groups. For $Mo_2S_4[R_2NCS_2]_2$ with straight-chain alkyl groups, the decomposition temperatures increased as the chain became shorter. MoDTC with molecular structures (**III**) and (**IV**) decomposed in a similar manner to structure (**II**) discussed above. The only notable difference was that MoDTC with oxygen atoms decomposed at slightly lower

22

temperatures than MoDTC without oxygen atoms [55]. Figure 3-1 shows the mechanism proposed for thermal decomposition of $Mo_2S_4[R_2NCS_2]_2$ [54].
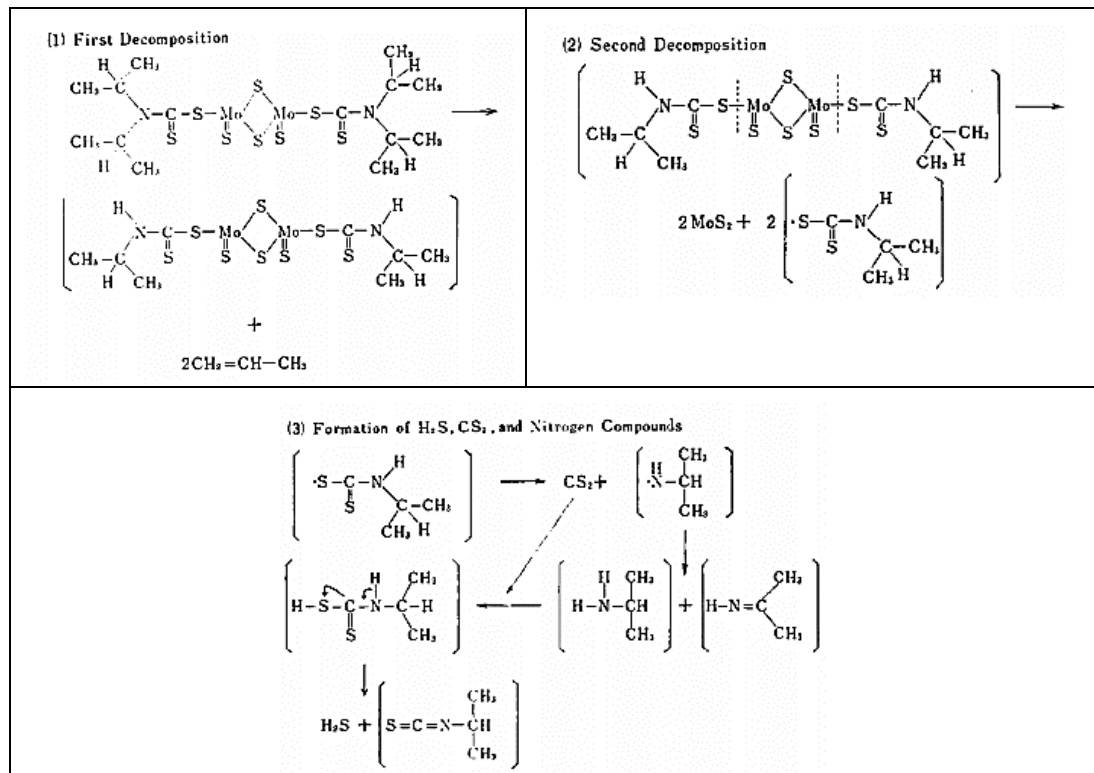
Figure 3-1. Proposed mechanism for thermal decomposition of $Mo_2S_4[R_2NCS_2]_2$, R is isopropyl [54]

3.3 Tribological tests with MoDTC

The literature review presented in the following sections refers to tests with MoDTC which has molecular structure (**I**) in Table 3-1. This review only focuses on tribological tests conducted in steel/steel contacts using lubricants which contain MoDTC in base oil unless otherwise mentioned.

Tribological tests conducted with MoDTC result in friction curves such as the one shown in Figure 3-2. Generally, there is high friction at the start of the test followed by a friction drop to low steady values after rubbing for a short period. The time taken for friction to drop from the start of the test to the time low steady values are observed is known as the induction time. The friction

23

coefficient can be as low as 0.04 in air and as low as 0.02 in vacuum environment [56]. The low friction values obtained in tests with MoDTC lubricant has been shown to be due to the presence of MoS_2 at the tribocontact. MoS_2 is formed as a result of MoDTC degradation. Decomposition of MoDTC leads to formation of thin films at the tribocontact. These films are commonly known as MoDTC tribofilms.
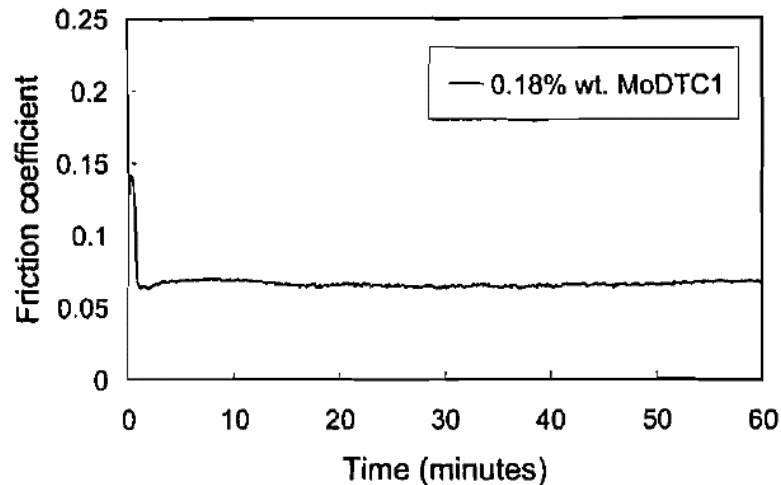
Figure 3-2. Typical friction curve obtained during tests with MoDTC lubricant [12]

It has been observed that friction and wear performance of MoDTC lubricants is influenced by test conditions. The influence of various test parameters on friction and wear performance of MoDTC lubricants is reviewed in the following sub-sections.

3.3.1 Influence of MoDTC concentration

In the study by Miklozic et al. [57], high friction (μ=0.15) was observed when lubricants containing 0.05 wt% MoDTC were used while low friction (μ=0.075) was observed when 0.125 wt% MoDTC was used (see Figure 3-3). MoS_2 was found to be present at the tribocontact at higher MoDTC concentrations observed while no MoS_2 was observed at low MoDTC concentrations. Using X-ray photoelectron spectroscopy (XPS) analysis, Yamamoto and Gondo [58]

reported that the intensity of MoS_2 peaks increased with MoDTC concentration suggesting that the quantity of MoS_2 increased with MoDTC concentration. Additionally, it was observed that friction coefficient decreased with increase in MoS_2 peak intensity.
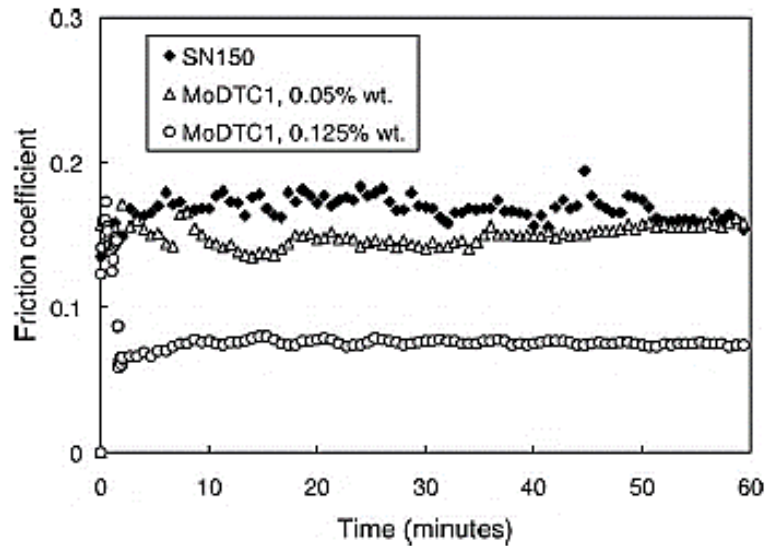
Figure 3-3. Influence of MoDTC concentration on friction [57]

It has also been observed that induction time and wear decreases with increase in MoDTC concentration [12, 58]. MoS_2 was detected using XPS after sliding for 5s at high MoDTC concentrations while at lower MoDTC concentrations, MoS_2 was only detected after sliding for 2-3 minutes [58]. The reduction in induction time with increase in MoDTC concentration can thus be attributed to the faster rate of MoS_2 formation at higher concentrations.

MoS_2 has a lower shear strength compared to steel substrates therefore if it is present at the tribocontact it would protect the substrate from wear by acting as a sacrificial layer. Therefore, the higher the amount of MoS_2 at the tribocontact the lower the wear of the substrate. The decrease in wear with increase in MoDTC concentration can thus be attributed to a higher MoS_2 concentration at the tribocontact.

3.3.2 Influence of temperature

In tests with MoDTC lubricants, friction generally decreases with increase in temperature [12, 57, 59]. Using Energy Dispersive X-ray analysis (EDX) Morina et al. [60] found that the concentration of Mo and S species increased with increase in temperature. Also, the top surface of the MoDTC tribofilms formed at low temperatures (30ºC) had a higher concentration of molybdenum oxides than MoS_2. The lower MoS_2 concentration on the surface of MoDTC tribofilms can explain the high friction values observed at low temperature tests. While the increase in Mo and S content (MoS_2) with increase in temperature explains the low friction observed at high temperatures.

Alkyl groups on MoDTC determine the temperature at which low friction is observed. Graham et al. [12] found that low friction was observed at 70ºC and 100ºC for MoDTC with 2-ethylhexyl and 2-methylbutyl groups, respectively. The observed difference can be attributed to differences in the decomposition temperature of the two additives. MoDTC with short-chain alkyl groups (2-methylbutyl) have higher decomposition temperatures than those with long chain alkyl groups (2-ethylhexyl).

Morina et al. [60] found that wear increased slightly with increase in temperature from 30ºC to 100ºC and then levelled off at higher temperatures. The increase in wear was attributed to increased metal-metal contact due to decreased lubricant thickness at high temperatures.

Previous studies have shown that the friction performance of MoDTC has a strong temperature-MoDTC concentration dependence as can be seen in Figure 3-4. This friction behaviour varies depending on the type of MoDTC (type of alkyl chains, presence of impurities) [12]. It has been suggested that the varying friction behaviour can be attributed to different MoDTCs having different reaction mechanisms (for example, simple thermal-activation, adsorption-controlled).
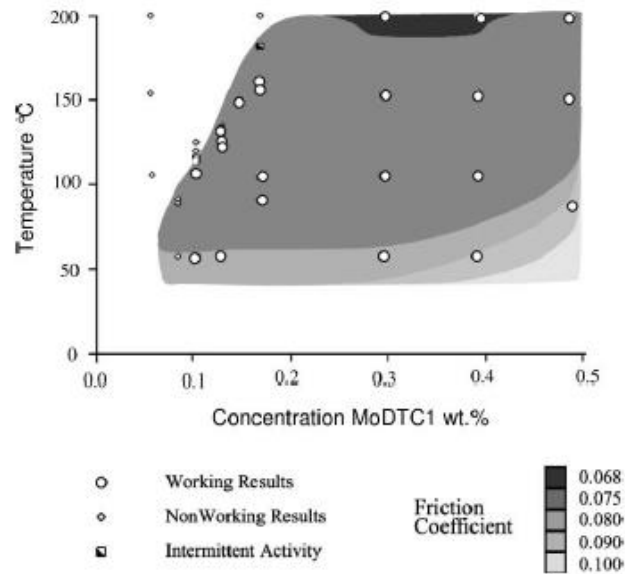
Figure 3-4. The effect of temperature and MoDTC concentration on friction. MoDTC has 2-ethylhexyl alkyl groups and contains impurities [57].

3.3.3 Influence of surface roughness

The effect of surface roughness on friction performance was studied by Graham et al. [12]. In the mentioned study, tests were carried out using smooth (R_a=10 nm) and rough (R_a=150-200 nm) discs rubbing against smooth balls (R_a=10 nm). It was observed that smooth discs showed high friction (μ=0.12) which did not reduce even after long test durations while rough discs showed low friction values (μ=0.04) after a short induction time. Using Raman spectroscopy analysis, MoS_2 was observed in tests with rough discs while no MoS_2 was observed in tests with smooth discs. It was suggested that micro-elastohydrodynamic (EHD) lubricating films were formed during tests with smooth discs preventing metal-metal contact [12]. Metal-metal contact is necessary for the formation of MoS_2 at the tribocontact. Therefore, the lack of metal-metal contact in smooth surfaces hindered the formation of MoS_2 hence the high friction.

27

3.3.4 Influence of sliding conditions

In a reciprocating sliding contact, it was observed that friction decreased with increase in stroke length [57]. Raman analysis across the stroke length revealed that the concentration of MoS_2 was high at the middle of the stroke and low at the reversal points of the stroke. The proportion of the stroke occupied by MoS_2 increased as the stroke length was increased. Therefore, decrease in friction with increase in stroke length was believed to be due to the overall increase in MoS_2 concentration.

It has been reported that higher loads were needed to achieve low friction in sliding/rolling contacts than in pure sliding contact [12]. In a pure sliding contact, a load of 30 N was sufficient to provide friction reduction while in a sliding/rolling contact (10% slide-roll ratio), a load of 70 N was necessary to achieve friction reduction. It was suggested that micro-EHD films were formed in sliding/rolling contacts than in sliding contacts preventing metal-metal contact. Due to the presence of micro-EHD films in sliding/rolling contacts, higher loads were required to ensure metal-metal contact which would promote MoDTC decomposition.

3.3.5 Influence of the environment

Yamamoto and Gondo [61] studied the friction performance of MoDTC under different environments. It was observed that friction reduction was achieved in environments with high oxygen concentrations whereas friction reduction was not observed in argon and nitrogen environments. The reason for the varying friction performance was attributed to differences in the chemical composition of tribofilms formed in the different environments. XPS analysis of MoDTC tribofilms formed in argon showed that the Mo 3d peaks were at a slightly lower binding energy compared to peaks from MoDTC tribofilms generated in air. Lower binding energies in tribofilms formed in argon/nitrogen indicated the formation of molybdenum compounds with molybdenum at a

lower oxidation state than +4 (typical for MoS_2). In air, MoDTC tribofilms were composed of MoS_2. Molybdenum compounds formed in argon and nitrogen had poor friction and wear performance in comparison to MoS_2 formed in air. It was observed that an oxygen concentration above 6.5 vol% was necessary to ensure the formation of friction reducing-MoDTC tribofilms.

3.3.6 Influence of other additives

Graham et al. [62] found that the presence of antioxidants in MoDTC lubricants increased the durability of MoDTC tribofilms. This is because in the presence of other antioxidants, oxidation inhibition by MoDTC is reduced therefore there is less degradation of the additive and more MoDTC is available to provide friction reduction for longer periods.

There are several studies on the influence of ZDDP, an antiwear additive, on friction and wear behaviour of MoDTC [30, 63-65]. The presence of ZDDP in MoDTC lubricants results in lower wear. The improved wear performance in the presence of ZDDP is due to formation of antiwear ZDDP tribofilms [65]. Morina and Neville [66] observed that addition of ZDDP to MoDTC lubricant led to a reduction in the induction time. This was believed to be either due to (1) formation of ZDDP tribofilms which prevented wear and in turn enhanced adsorption of MoS_2 at the tribocontact (2) ZDDP supplied sulphur to promote the formation of MoS_2 or (3) formation of a rougher surface which promoted MoS_2 formation [67]. Graham et al. [62] observed that addition of ZDDP to MoDTC lubricant resulted in gradual friction reduction instead of the rapid friction reduction observed in MoDTC lubricants. MoDTC has also been reported to reduce friction in fully formulated oils when rough surfaces are used [68]

3.3.7 Durability of MoDTC tribofilms

In a study by Graham et al. [62] it was observed that in a unidirectional sliding contact, the friction reducing capability of MoDTC was lost after rubbing for

about 1h at 120ºC. In the mentioned study, two mechanisms were proposed to explain this behaviour. One mechanism involves the depletion of MoDTC at the rubbing contact and the other mechanism involves the conditioning (polishing) of the surface which reduces its reactivity with MoDTC.

Morina and Neville [66] studied the durability of MoDTC tribofilms by rubbing pre-formed MoDTC tribofilms in base oil. It was observed that there was an instant rapid friction increase after replacing MoDTC lubricant with base oil. It was concluded that MoDTC tribofilms were not durable when rubbed in a MoDTC-free lubricant.

3.4 Properties of MoDTC tribofilms

3.4.1 Mechanical properties of MoDTC tribofilms

In the study conducted by Bec et al. [69] it was observed that MoDTC tribofilms have a hardness of 0.4-0.5 GPa and a Young's modulus of 7-8 GPa, respectively. The study also showed that the structure of MoDTC tribofilms is composed of a single layer, thus its mechanical properties are homogenous and do not vary across the depth of the tribofilm. Atomic Force Microscopy (AFM) analysis showed that MoDTC tribofilms appear as elliptical or circular pads on asperities of the tribopair [57]. The MoDTC pads are 10-25 nm in diameter. The thickness of the tribofilms can vary depending on the test conditions and values ranging from 2 to 75 nm have been reported [69].

3.4.2 Chemical composition of MoDTC tribofilms and thermal films

Chemical characterisation of MoDTC tribofilms with Raman spectroscopy and XPS reveal that MoDTC tribofilms are composed of MoS_2 and amorphous carbon. XPS analysis has shown that MoDTC tribofilms are also composed of molybdenum oxides such as MoO_2 and MoO_3 [60, 65]. MoDTC films formed from tribological tests (tribofilms) have different chemical composition from films formed through thermal decomposition of the additive (thermal films).

MoDTC thermal films formed on steel substrates for 6h at 150ºC have been found to be composed of a mixture of unreacted MoDTC and alkyl/aryl sulphide [70].

3.4.3 Raman spectroscopy and X-ray Photoelecton Spectroscopy (XPS) analysis of MoDTC tribofilms

Chemical characterisation of MoDTC tribofilms with Raman spectroscopy and XPS reveal conflicting results. XPS analysis suggests the presence of MoO_2 and MoO_3 while Raman spectroscopy has not shown the presence of these species. During tribotests with MoDTC in steel/steel contacts, the tribocontact has varying concentrations of Mo, S, Fe and O. The presence of these elements can lead to formation of various compounds as depicted in Figure 3-5. Using a characterisation technique that can clearly distinguish these chemical species is desired in tribological studies with MoDTC. Raman analysis of MoDTC tribofilms is conducted by obtaining spectra from the tribofilms and determining the chemical species based on Raman peaks observed. Each chemical specie in Figure 3-5 has it own unique Raman fingerprint as can be seen in Figure 3-6.
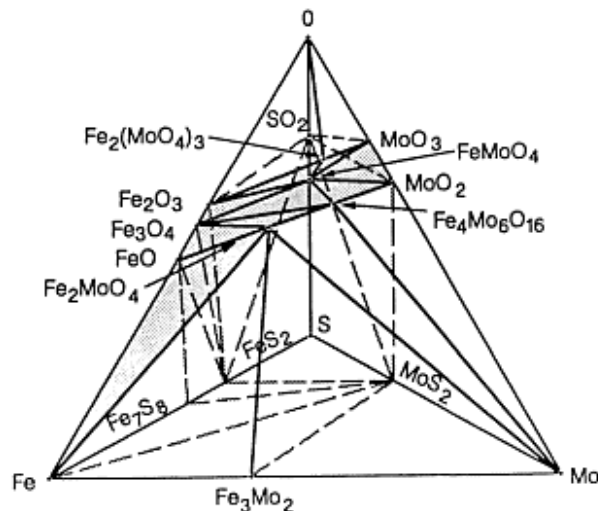
Figure 3-5. Quaternary phase diagram for a Mo-O-S-Fe system [71]
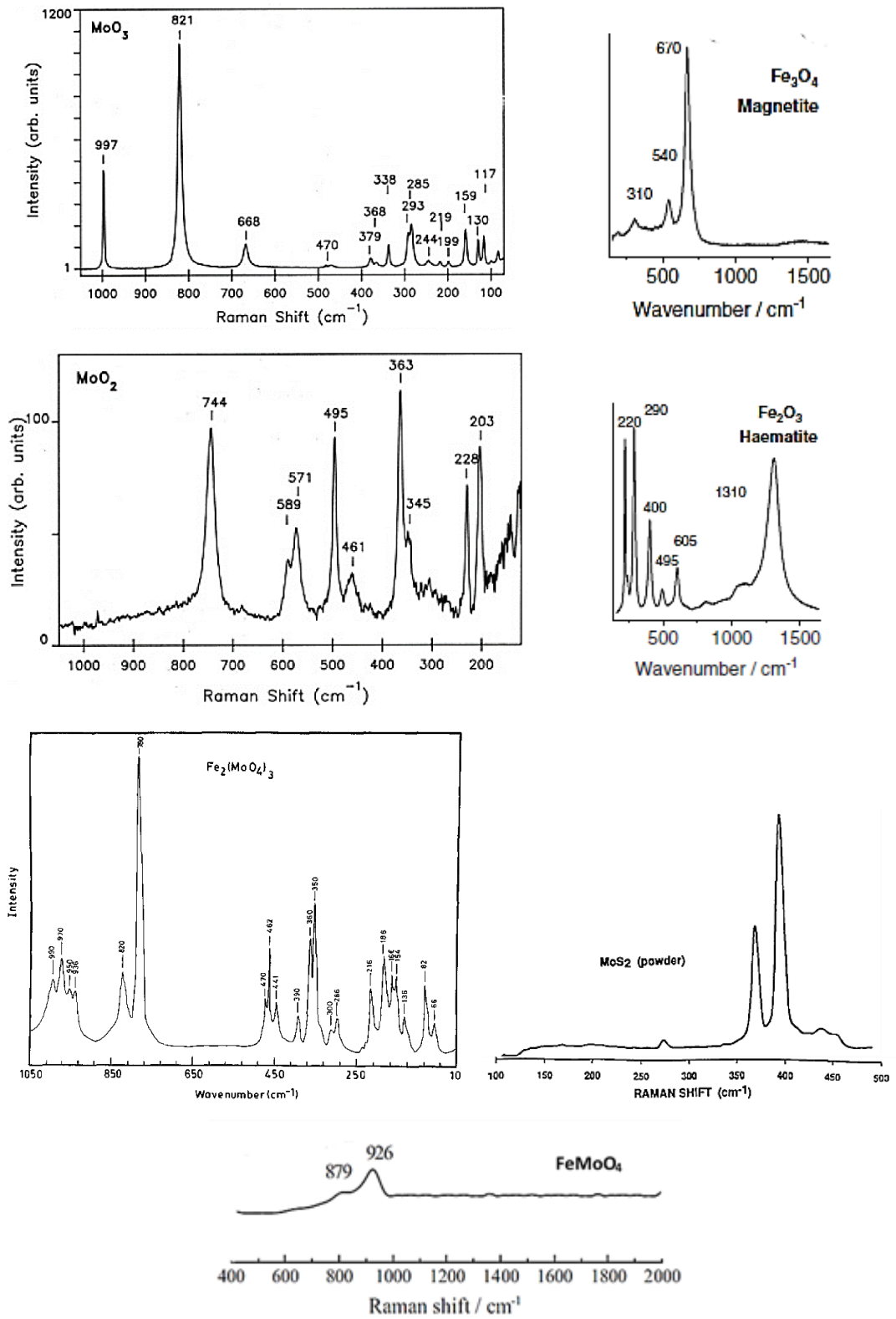
Figure 3-6. Raman spectra of MoS₂, MoO₃, MoO₂, Fe₃O₄, Fe₂O₃, Fe₂(MoO₄)₃ and FeMoO₄ [72-76]

In literature, spectra from MoDTC tribofilms have been reported to have two distinct Raman peaks around 382 and 412 cm^{-1} which are attributed to MoS_2 (Figure 3-7) [57]. The presence of Fe_3O_4 peaks and amorphous carbon peaks has also been reported [12]. However, peaks belonging to molybdenum oxides (MoO_2, MoO_3) have not been reported [57].
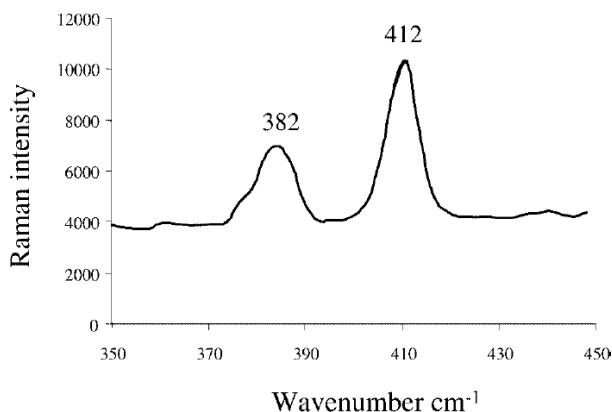
Figure 3-7. Raman spectra obtained from MoDTC tribofilm [57]

XPS analysis of MoDTC tribofilms is conducted by obtaining spectra at different binding energies. XPS spectra from MoDTC tribofilms are normally compared to spectra from reference model compounds in order to determine chemical species in the tribofilm. In analysis of MoDTC tribofilms, XPS spectra of model compounds Mo, MoS_2, MoO_2 and MoO_3 are commonly used. Figure 3-8 shows XPS spectra of model molybdenum compounds. The binding energies of the different molybdenum compounds are presented in Table 3-2.

Figure 3-9 shows a typical XPS spectrum obtained from MoDTC tribofilms. A broad peak with three local peaks is observed in the region 225-240 eV showing the presence of molybdenum compounds. In literature, the broad peak is normally deconvoluted with spectra from model compounds such as MoS_2, MoO_2 and MoO_3 and the contribution of the each compound is determined. In Figure 3-9 for example, MoDTC tribofilm was considered to be a mixture of MoS_2, MoO_3 and MoO_2.
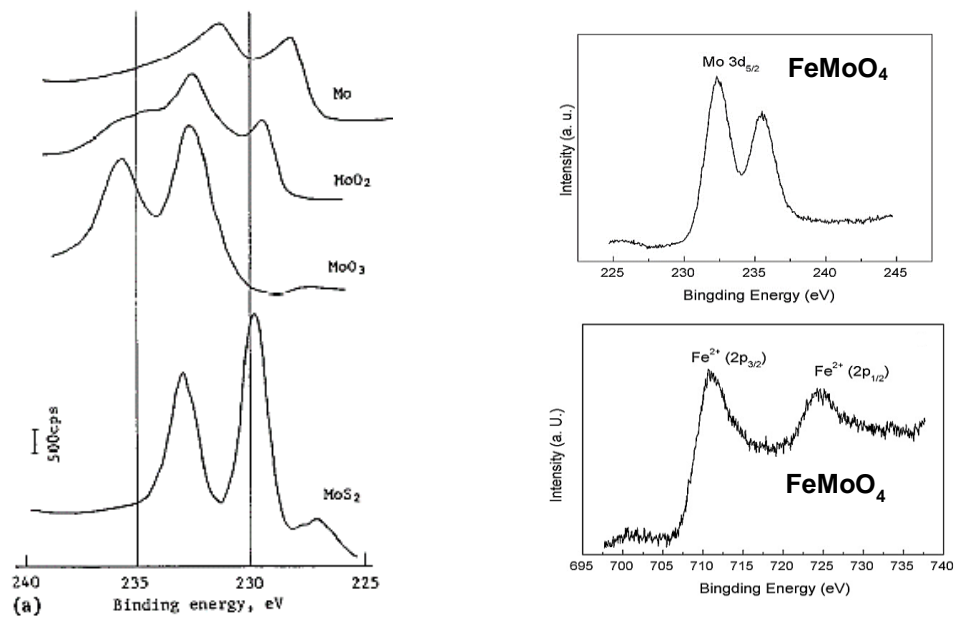
Figure 3-8. XPS spectra of Mo, MoO$_2$, MoO$_3$, MoS$_2$, FeMoO$_4$ [77, 78]

Table 3-2. Binding energies of various molybdenum compounds

Compound	Binding energy (eV)				Ref
	Mo 3d$_{5/2}$	O (1s)	S (2p$_{3/2}$)	Fe 2p$_{3/2}$	
Mo (0)	227.8				[79]
MoO$_2$ (+4)	229.2	529.9			[72]
MoS$_2$ (+4)	229.0		161.9		[77]
MoS$_3$ (+4)	229.1		161.6		[80]
MoS$_4$ (+4)	229		163.1		[81]
MoDTC (+5)			163.5		
MoS$_x$O$_y$ (+5)	231.1		161.7		[82]
MoO$_3$ (+6)	232.3	530.6			[72, 77]
FeMoO$_4$ (+6)	232.3	531.9		710.5	[78, 83]

The oxidation state of molybdenum in the compounds is indicated in brackets
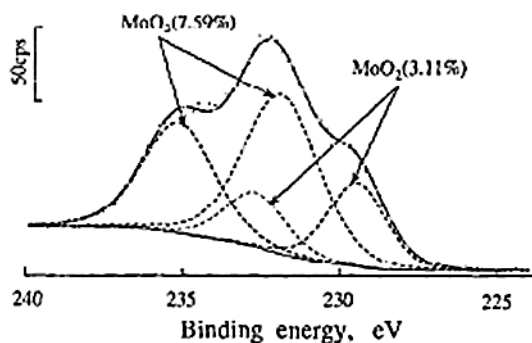
Figure 3-9. Typical spectrum obtained from MoDTC tribofilm [64]

XPS analysis of MoDTC tribofilms provides information on the oxidation states of different elements. However, XPS is incapable of clearly distinguishing different compounds in the tribofilms. For example, MoO_3 and $FeMoO_4$ have molybdenum in the same oxidation state (+6) which means that they have similar Mo 3d peaks (Table 3-2). Thus, peaks designated as MoO_3 can also be assigned as $FeMoO_4$. To distinguish MoO_3 from $FeMoO_4$, the Fe 2p peak has to be analysed. However, in the case of MoDTC tribofilms, such analysis would not yield much results. MoDTC tribofilms have been shown to be composed of Fe_2O_3 with Fe at an oxidation state of +2 which is similar to that of Fe in $FeMoO_4$. It is therefore difficult to definitely assign the Mo (+6) peaks to MoO_3 or $FeMoO_4$. Using XPS it may also be difficult to differentiate MoO_2 and MoS_2 peaks using Mo 3d peaks since they have similar Mo (+4) binding energies. In this case, the S 2p binding energy would be used to differentiate MoO_2 from MoS_2. However, other sulphur compounds with S at an oxidation state of -2, for example as FeS, can be formed in MoDTC tribofilms making it impossible to assign Mo (+4) peaks to MoS_2.

From the discussion above, it can be seen that Raman spectroscopy can distinguish molybdenum compounds better than XPS. Thus, the conflicting information regarding the chemical composition of MoDTC tribofilms can be attributed to the different distinguishing capabilities of Raman spectroscopy and XPS. MoO_2 and MoO_3 observed in MoDTC tribofilms using XPS could be

due to the presence of other Mo compounds with oxidation states +4 and +6, respectively.

Raman spectroscopy is also superior to XPS in determining the crystallinity of compounds. With XPS analysis, MoS_3 which is amorphous in nature cannot be differentiated from crystalline MoS_2 since they have similar Mo 3d peaks (Table 3-2). With Raman spectroscopy, MoS_3 and MoS_2 can be clearly differentiated since they have different Raman peaks [80]. Raman spectroscopy can also differentiate amorphous MoO_2 and MoO_3 from their crystalline forms [84, 85].

XPS analysis is a surface sensitive technique (<10 nm). However, XPS can be used to analyse the bulk of the tribofilm by employing the argon ion etching technique. One problem with etching MoDTC tribofilms is that it causes the binding energy to shift to lower energies as can be seen in Figure 3-10 [61]. Since identification of species is dependent on the position of the binding energy, shifting of the peaks with etching can affects the interpretation of the XPS spectra.
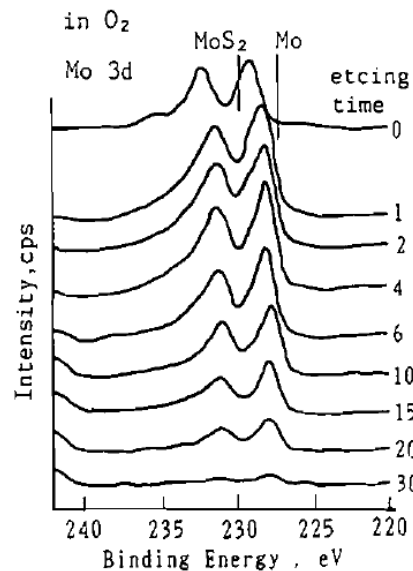
Figure 3-10. Shift in binding energy during argon ion etching of MoDTC tribbofilms. The numbers represent the etching time in seconds [61]

36

Although Raman spectroscopy is a bulk sensitive technique, it is has been shown to the capable of analysing films as thin as 1 nm [86]. Spectra obtained from MoDTC tribofilm with Raman spectroscopy can therefore be considered to contain chemical information from the top surface as well as the bulk of the tribofilm.

From the above discussion, it can be seen that Raman spectroscopy is better suited for chemical characterisation of MoDTC tribofilms than XPS and can provide a better understanding of tribochemical reactions involving MoDTC in ferrous contacts.

3.5   Mechanisms

3.5.1   Mechanism for MoDTC decomposition within a tribocontact

In literature, two mechanisms have been proposed for the decomposition of MoDTC in tribocontacts. One is based on chemical characterisation of the MoDTC tribofilms while the other one is based on molecular dynamics simulation.

Grossiord et al. [56] proposed that MoDTC decomposed at the tribocontact following the mechanism illustrated in Figure 3-11. The mechanism was derived following analysis of MoDTC tribofilms using XPS. XPS spectra obtained from MoDTC tribofilm was compared with spectra obtained from model compounds MoS_2 and MoO_3 as seen in Figure 3-12. The MoDTC spectra was found to be a mixture of Mo (IV), Mo (V) and Mo (VI). MoS_2 and MoO_3 were suggested as compounds with Mo (IV) and (V) oxidation states, respectively. The Mo (V) compound was suggested to be residual MoDTC or molybdenum oxysulphide species (MoS_xO_{2-x}). According to this mechanism, MoDTC first decomposes into three radicals due to electron transfer that occurs at the Mo-S bond on both sides of the molecule. Two of these radicals combine to form thiuram disulphide and the other radical cleaves to form MoS_2

and MoO_2. MoO_2 is later oxidised to MoO_3. The presence of thiuram disulphide was not confirmed in the mentioned study probably because it was dissolved in the lubricant.
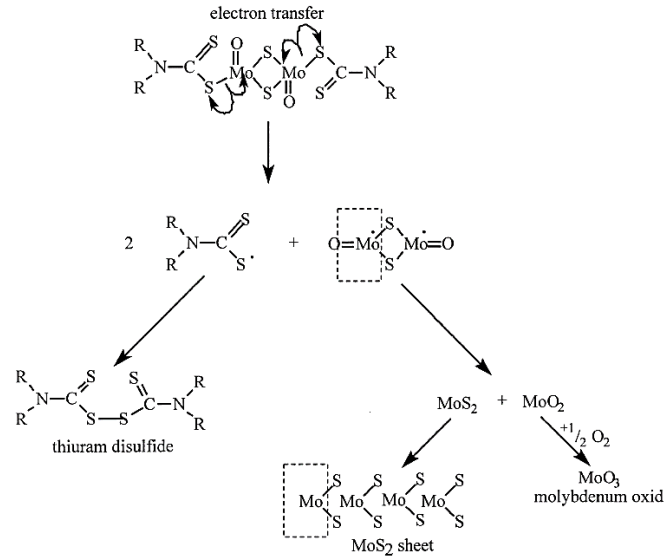
Figure 3-11. Decomposition mechanism for MoDTC leading to the formation of MoS₂ and MoO₃ [56].
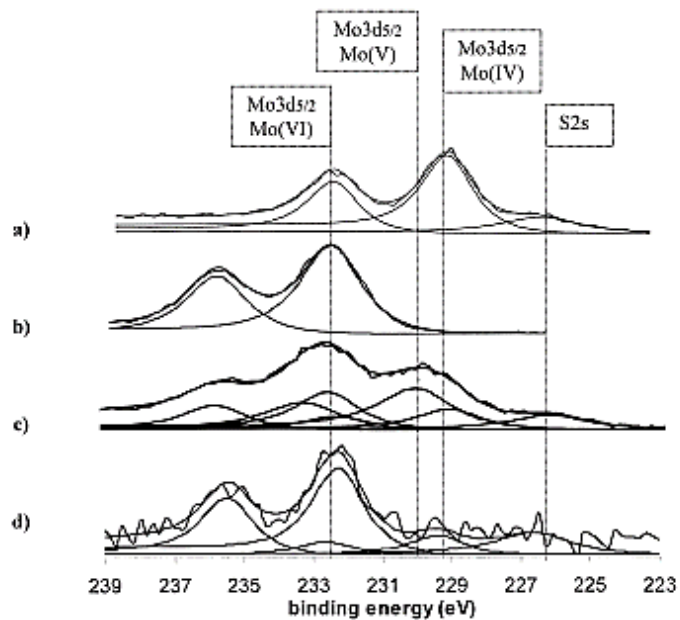
Figure 3-12. XPS spectra of (a) pure MoS₂ (b) pure MoO₃ (c) MoDTC tribofilm (d) outside regions of MoDTC tribofilm [56]

Molecular dynamics simulation studies by Onodera et al. [87] showed that MoDTC in the bulk lubricant changed to form a linkage isomer LI-MoDTC at high temperatures (425 K) (Figure 3-13).
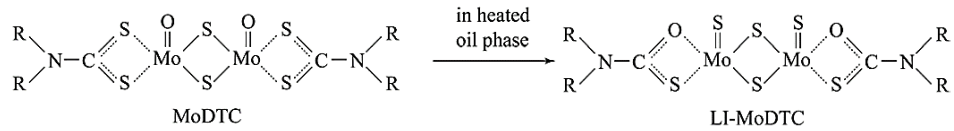
Figure 3-13. Structure of linkage MoDTC isomer (LI-MoDTC) formed at high temperatures [87]

It was demonstrated that LI-MoDTC adsorbed on the nascent Fe surface via the S atoms as shown in Figure 3-14. When sliding (100 m/s) and pressure (1 GPa) were applied to the adsorbed LI-MoDTC, O-Mo bonds were ruptured resulting in the formation of a Mo_2S_4 and two thiocarbamic acid molecules. The friction simulation was conducted for a short duration (320 fs) therefore the formation of MoS_2, typically observed in MoDTC tribofilms, was not observed. It was however concluded that MoS_2 was formed from the formed Mo_2S_4 core.
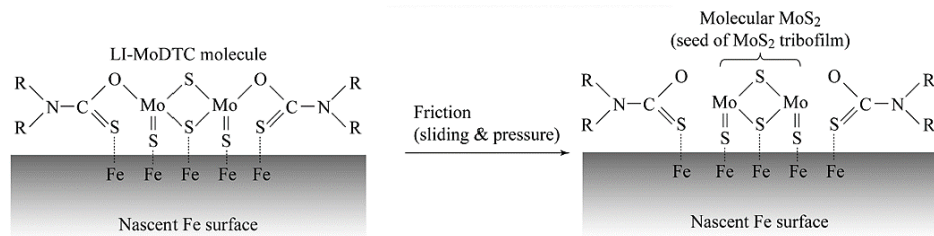
Figure 3-14. Structural changes occuring to LI-MoDTC in the presence of friction [87]

3.5.2 Mechanism for low friction in MoS₂

Tribotests carried out in an ultra-high vacuum (UHV) tribometer using an uncoated pin on already formed MoDTC tribofilm revealed that friction reduction occurred only after transfer of the MoS_2 sheets to the uncoated pin [56]. The authors noted that friction reduction was not due to intra-sliding of

39

MoS$_2$ sheets in the lattice structure but rather it was due to sliding between two separate MoS$_2$ sheets at the rubbing contact. Also, it was observed that only a few MoS$_2$ sheets were sufficient for friction reduction to be achieved.

The actual mechanism responsible for low friction in MoS$_2$ was investigated using molecular dynamics. Onodera et al. [88] reported that coulombic repulsion between sulphur atoms on adjacent MoS$_2$ sheets was responsible for low friction. Lower friction was achieved when MoS$_2$ sheets were adsorbed on nascent Fe surfaces. This is because adsorbed MoS$_2$ sheets receive electrons from the Fe surface becoming more negatively charged. Consequently, the repulsive forces between sulphur atoms increase resulting in lower friction. It was also reported that the presence of O atoms in the MoS$_2$ sheets generated atomic-scale roughness and decreased friction. Figure 3-15 shows a schematic diagram describing the mechanism of friction reduction in MoS$_2$.
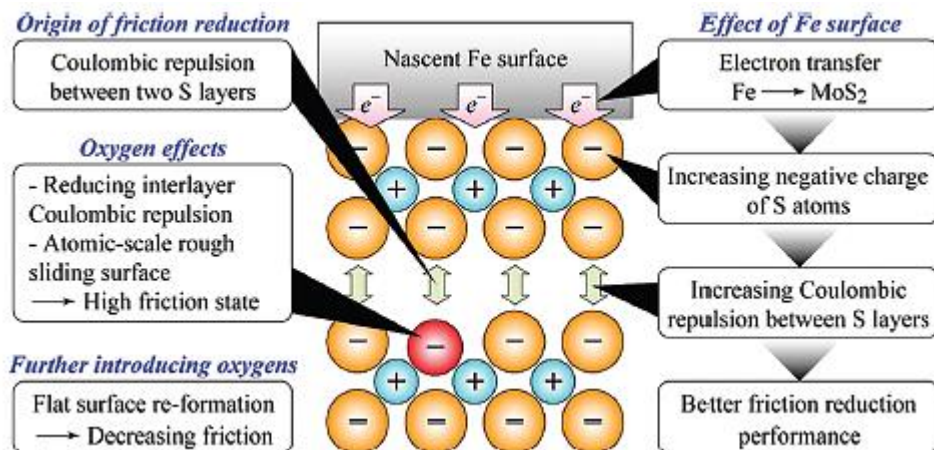
Figure 3-15. Low friction in MoS$_2$ sheets [88]

3.5.3   Reaction kinetics for growth of tribofilms

In literature, MoDTC tribofilms of varying thicknesses have been reported. However, there are still no studies on the growth of the tribofilms or the influence of contact conditions on the growth rate. Studying the growth of tribofilms requires measurement of the tribofilm thickness in real time. This

requires the use of *in-situ* analysis techniques. Recently, spacer layer image mapping (SLIM) and Atomic Force Microscopy (AFM) have become popular techniques for measuring tribofilm thickness *in-situ*. Although these two techniques are yet to be used to study the growth of MoDTC tribofilms, the techniques have been employed to study the growth of ZDDP tribofilms.

Fujita and Spikes [17] studied the growth of ZDDP tribofilm using SLIM. Using this technique, interference images of tribofilms formed on the ball are obtained at different time intervals during tribotests. The thickness of the tribofilms is then calculated from the obtained images. Figure 3-16 shows an example of interference images obtained during the formation of ZDDP tribofilms. It was observed that the surface coverage by ZDDP tribofilms increased with rubbing time.
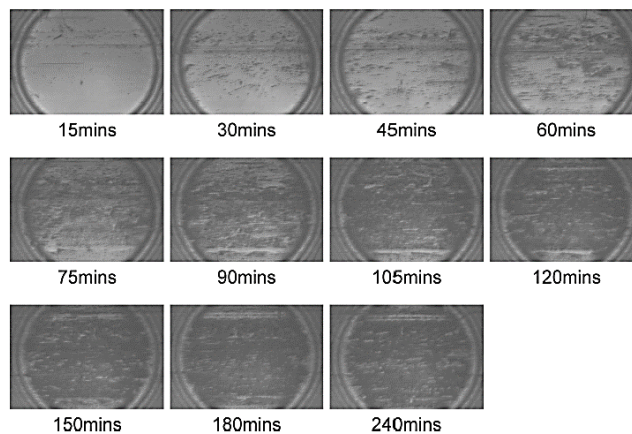
Figure 3-16. Optical images showing the growth of ZDDP tribofilms with rubbing time [89].

A kinetic model for the growth of ZDDP tribofilms was developed by assuming a simple coverage model (Equation 3-3). In this model, the rate of film growth is assumed to be proportional to the area not yet covered by the tribofilm.

$$h_{mean} = h_{\max}(1 - e^{-k_c(t-t_i)}) \qquad\qquad 3\text{-}3$$

Where h_{mean} is the mean film thickness, h_{max} the maximum film thickness, t_i the induction time and k_c the rate constant. k_c and h_{max} values for each experiment were determined by curve fitting experimental data. The model was found to fit experimental values well when an induction time of 30 minutes was assumed. By assuming a thermally-activated reaction (Equation 2-14), the activation energy (E_a) for the formation of ZDDP tribofilms was found to be 4 kJ/mol.

Gosvami et al. [18] monitored the growth of ZDDP tribofilms using *in-situ* AFM. With this technique, AFM images of the rubbed surfaces are obtained during the test and the volume of the formed tribofilms is determined from the images. It was observed that the thickness of ZDDP tribofilm increased with sliding time (cycles) as shown in Figure 3-17
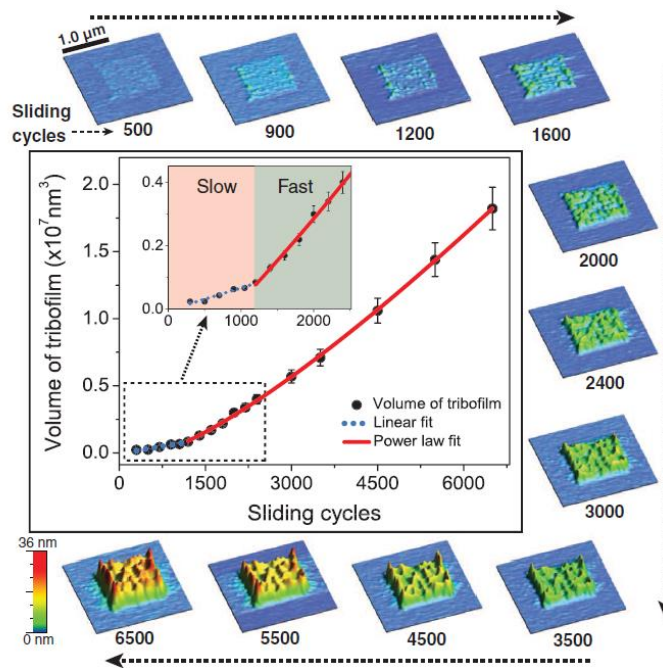
Figure 3-17. Growth of ZDDP tribofilms with rubbing cycles [18]

The maximum thickness of ZDDP tribofilm was found to be dependent on the applied pressure and temperature. The rate of growth of ZDDP tribofilm was described by Equation 3-4.

$$\tau_{growth} = \tau_0 \, exp^{\frac{\sigma \Delta V - E_a}{k_B T}} \qquad \text{3-4}$$

Where τ_0 is the pre-exponential factor and is dependent on the volume of the growth species and attempt frequency, σ is the applied shear stress taken as the contact pressure, ΔV is the activation volume, E_a the activation energy, k_B the Boltzmann constant and T the absolute temperature. The activation energy for the growth of ZDDP tribofilms was found to be 0.8 eV (77.2 kJ/mol).

From above, it can be seen that values for the activation energy vary by an order of 1 depending on the growth model used. By incorporating both shear stress and temperature in the growth model of ZDDP tribofilms, the activation energy was found to be much higher (77.2 kJ/mol) than when only temperature was considered, (4 kJ/mol). This shows that assuming a thermally-activated reaction for the growth of tribofilms greatly underestimates the activation energy.

ZDDP and MoDTC tribofilms are formed from different decomposition mechanisms [90, 91]. Thus, the growth of the tribofilms may not be exactly similar. However, from studies conducted ZDDP tribofilms it can be envisioned that the growth rate of MoDTC tribofilms will be affected by contact parameters.

3.6   Raman studies on MoS$_2$

Raman studies have revealed that MoDTC tribofilms are composed of MoS$_2$. MoS$_2$ is a naturally-occurring crystal with a hexagonal lattice structure [92]. It is composed of separate layers; each layer consists of molybdenum atoms sandwiched between sulphur atoms (Figure 3-18). Adjacent MoS$_2$ layers are weakly bonded via Coulombic forces [88]. In sub-sections below, literature review on Raman analysis of MoS$_2$ is presented.
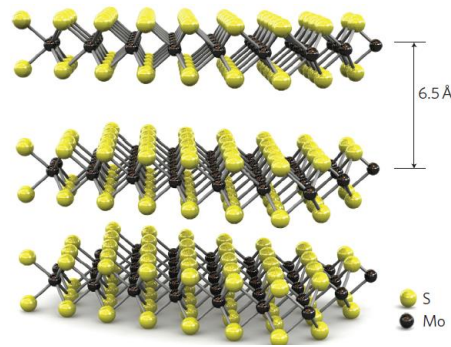
Figure 3-18. Structure of MoS$_2$ showing three individual layers [93].

3.6.1 MoS$_2$ first-order Raman peaks

When excited with electromagnetic waves at ambient conditions, Mo and S atoms within MoS$_2$ lattice structure vibrate both in-plane and out-of-plane Figure 3-19 shows the various vibration modes in MoS$_2$. These vibration modes can be Raman active, infrared active, inactive or both Raman and infrared active. Table 3-3 shows the classification of the various vibration modes.
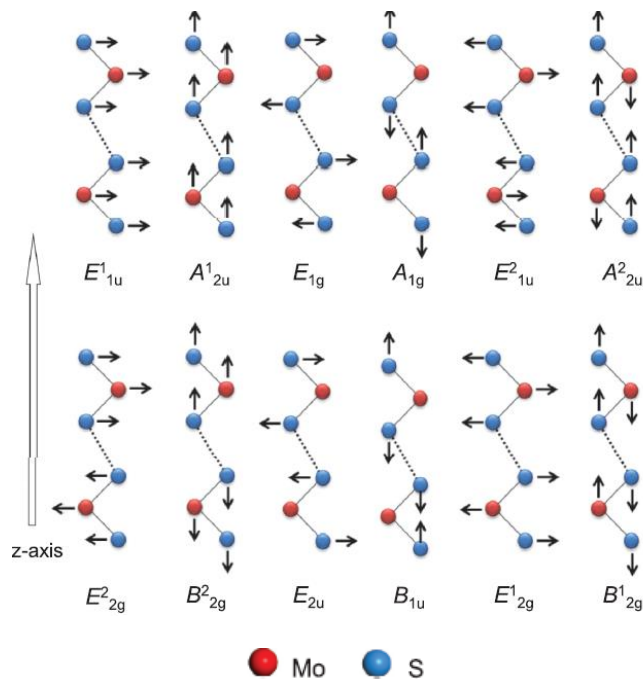
Figure 3-19. Vibration modes in MoS$_2$ [94]

Table 3-3. Classification of MoS$_2$ vibration modes [94, 95]

	Infrared active	Raman active	Inactive
In-plane	E^1_{1u} E^2_{1u}	E^2_{2g} E_{1g} E^1_{2g}	E_{2u}
Out of plane	A^1_{2u} A^2_{2u}	A_{1g}	B^2_{2g} B_{1u} B^1_{2g}

First-order Raman modes are the E^2_{2g}, E_{1g}, E^1_{2g} and A_{1g} and are observed at 34 cm⁻¹, 287 cm⁻¹, 383 cm⁻¹ and 409 cm⁻¹, respectively [96]. The E^2_{2g} and E^1_{2g} modes involve the vibration of both Mo and S atoms while the E_{1g} mode involves the vibration of only S atoms. The A_{1g} mode involves the vibration of S atoms away from the Mo atom in both directions of the MoS$_2$ layer.

The E^2_{2g} mode involves vibration of adjacent MoS$_2$ layers and is a relatively weak vibration compared to the other three modes [97]. The E_{1g} mode is also a weak mode and is sensitive to the polarisation of the laser on the incident plane. This mode is intense when *p*-polarised light is used (i.e. the electric field of the incident laser light is parallel to the basal plane of MoS$_2$) [97]. The orientation of the MoS$_2$ crystal also determines whether the E_{1g} mode is observed or not. Wieting and Verble [98] showed that E_{1g} mode was only observed when the observation plane was along the *z*-axis.

Of the four first-order Raman modes, the E^1_{2g} and A_{1g} modes have peaks with the highest intensities as can be seen in Figure 3-20 (a). For a given laser polarisation, the peak intensity ratio of E^1_{2g} to A_{1g} mode is dependent on the collection angle of the scattered light. Raman studies by Wang et al. [99] on a single MoS$_2$ monolayer found that the intensity of the A_{1g} mode was highest when the angle between the incident and scattered light was at 0° (i.e. backscattering configuration) or 180° and lowest at 90° and 270° while the

intensity of the E^1_{2g} mode was not affected by the collection angle (Figure 3-20b).
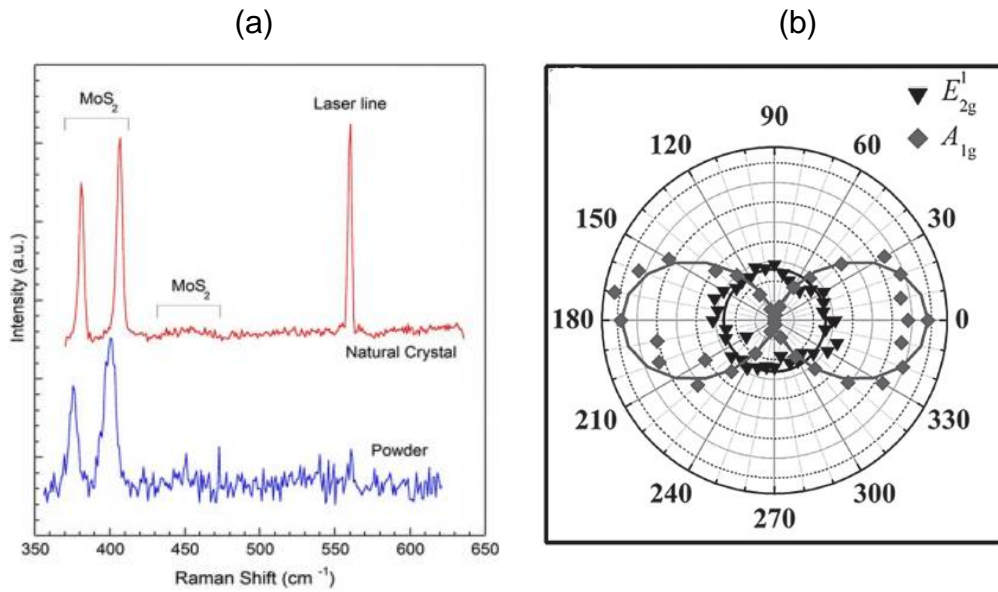
Figure 3-20. (a) Raman spectra of MoS$_2$ powder and natural crystal obtained with 488 nm wavelength laser [100] (b) MoS$_2$ E$^1_{2g}$ and A$_{1g}$ Raman peak intensities as a function of the angle between the incident and scattered light [99]

Polarisation of laser light has also been shown to affect peak intensities of MoS$_2$ first-order modes. Chen and Wang [97] found that the intensity of the A$_{1g}$ mode was twice that of the E$^1_{2g}$ mode using *s*-polarised laser (when the electric field is perpendicular to the basal plane). The intensity of both modes was comparable when *p*-polarised laser (electric field parallel to the plane of incidence) was used.

3.6.2   MoS$_2$ second-order Raman peaks

In addition to first-order peaks, second-order peaks are observed when laser wavelengths close to the absorption band of MoS$_2$ are used due to resonance effect. Absorption in MoS$_2$ occurs at 1.9 eV and 2.1 eV which corresponds to 652.6 nm and 590.5 nm laser wavelengths, respectively [101]. Table 3-4 summarizes Raman peaks observed under resonance conditions and their

assignments obtained from literature. Second-order peaks observed at 150 cm⁻¹ and 188 cm⁻¹ are due to a difference process and are therefore not observed at very low temperatures [97, 102]. MoS_2 nanoparticles have been found to have additional second-order peaks which are observed at 226 cm⁻¹, 247 cm⁻¹, 495 cm⁻¹ and 545 cm⁻¹ [102].

Table 3-4. Assignment of Raman bands due to resonance Raman scattering

Peak frequency (cm⁻¹)	First-order modes	Second-order modes	References
34	E^2_{2g}		[97, 103]
150		E^1_{2g} - LA(M)	[97, 100]
188		A_{1g} - LA(M)	[100, 102]
226, 247	LA(M)		[102]
287	E_{1g}		[96]
383	E^1_{2g}		[96, 100]
408	A_{1g}		[96, 100]
422		E^2_{1u}	[100]
455, 495		2LA(M)	[97, 102]
466		A_{1u}	[102]
526, 545		E_{1g} + LA(M)	[100, 102]
567		$2E_{1g}$	[97, 104]
596		E^1_{2g} + LA(M)	[97, 104]
641		A_{1g} + LA(M)	[104]
750		$2E^1_{2g}$	[97, 100]
778		A_{1g} + E^1_{2g}	[97, 104]
820		$2A_{1g}$	[97, 100, 104]

3.6.3   Application of MoS_2 Raman peaks

First-order and second-order MoS_2 peaks have been used to study disorder in MoS_2 films [75] and size in nanoparticles [102]. It has been reported that disorder in MoS_2 films and size reduction in nanoparticles results in broadening of peaks. First-order peaks have also been particularly useful in determining the thickness of a few MoS_2 layers (up to 4 layers) [86, 94, 103, 105]. The E^1_{2g} peak has been observed to red shift (move to lower

wavenumbers) while the A_{1g} peak blue shifts (shifts to higher wavenumbers) from a monolayer to four layer. Therefore, the difference in peak frequency can be used as a measure for layer thickness. Furthermore, the peak width (full width at half maxima, FWHM) of the A_{1g} mode has been found to decrease with increase in the number of layers from two layers to about six layers. Second-order peaks have also been shown to be layer dependent [106].

3.6.4 Influence of stress, temperature and laser power on MoS₂ Raman peaks

MoS₂ peak frequencies are greatly affected by stress-induced disorder. Studies have shown that under strain, the A_{1g} and E^1_{2g} peaks shift to higher wavenumbers and have pressure coefficients of 3.7 cm⁻¹/GPa and 1.8 cm⁻¹/GPa, respectively [107-109]. Figure 3-21 shows the shift in MoS₂ peaks at different pressures.
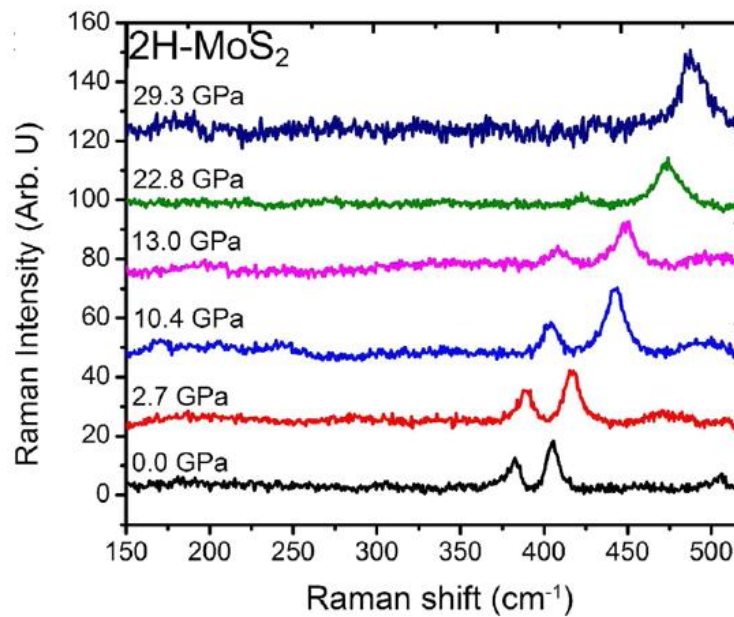
Figure 3-21. Pressure dependence of MoS₂ Raman peaks [110]

Peak frequencies and widths are also affected by temperature (Figure 3-22). At temperatures below 500 K, the A_{1g} and E^1_{2g} peaks red shift linearly with increase in temperature with first-order temperature coefficients of $-1.23 \times$

10^{-2} cm⁻¹/K and -1.32×10^{-2} cm⁻¹/K, respectively [108, 111-114]. The peak widths also increase linearly with increase in temperature. At higher temperatures, a non-linear relationship is observed in the peak frequency shift [115].
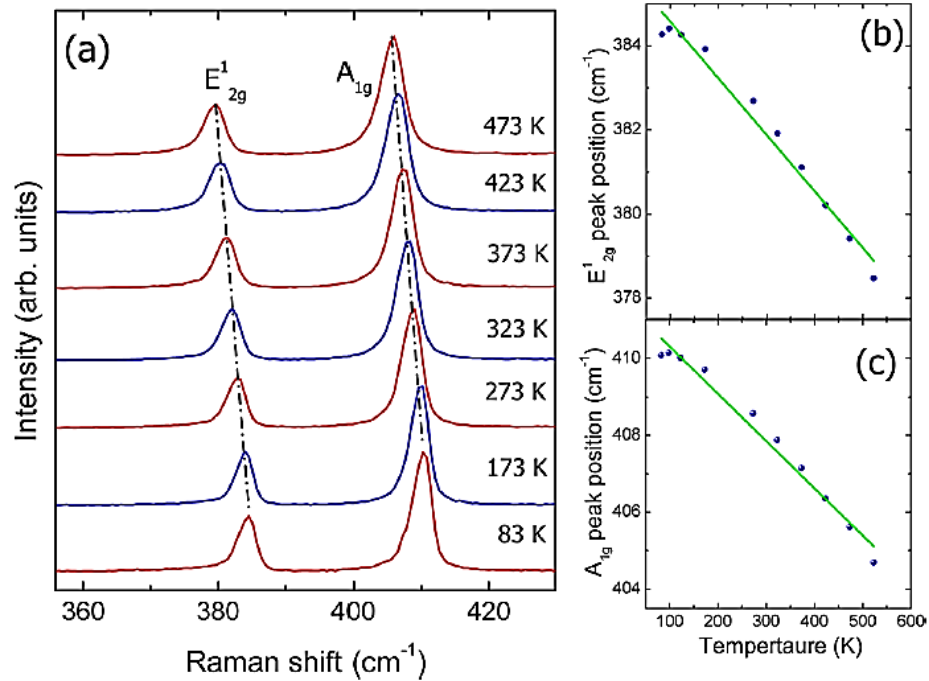
Figure 3-22. (a) MoS₂ peak frequency changes with increase in temperature (b) the E¹₂g peak position as a function of tempereture (c) A₁g peak position as a function of temperature [111]

During Raman spectra acquisition, laser heating may cause the local temperature of MoS₂ to rise resulting in a shift in the peak frequency [116]. The A₁g peak has been observed to shift to lower wavenumbers with increase in laser power at a rate of 5.4 ± 0.3 cm⁻¹/mW [111]. At very high laser powers, MoS₂ is partially oxidised to MoO₃ and peaks due to the formation of the oxide are observed at 279 cm⁻¹, 820 cm⁻¹ and 994 cm⁻¹ [100].

3.7   Summary

3.7.1   Current understanding on tribological processes of MoDTC

From currently available literature, the following information on MoDTC and its tribological performance is known. Friction reduction in tests with MoDTC lubricant is dependent on MoDTC concentration, temperature, surface roughness and sliding speed. Low friction is obtained when MoS_2 is observed within the rubbed surfaces while high friction is obtained the rubbed surfaces are composed of iron oxides (Fe_3O_4). The mechanism for MoDTC decomposition within tribocontacts has been proposed where thiuram disulphide, MoS_2 and MoO_3 are the decomposition products.

3.7.2   Knowledge gaps

There are still knowledge gaps in the current understanding of MoDTC tribochemical reactions and tribological performance. These knowledge gaps are discussed below and form the basis of this study. Figure 3-23 summarises what is currently known, unclear and unknown with regards to MoDTC.

It is known that contact parameters affect the friction performance. The effect of contact parameters on MoDTC decomposition products at the tribocontact is however still unknown. In this study, the influence of contact parameters on MoDTC decomposition will be investigated by analysing the chemical composition of wear scars after tribological tests. The mechanism for MoDTC decomposition is still unclear. According to the mechanism proposed in literature, MoS_2 and MoO_3 are the main MoDTC decomposition products. However, MoO_3 has not been detected in MoDTC tribofilms using Raman spectroscopy. Also, at certain test conditions, iron oxides are formed at the tribocontact instead of MoS_2 despite tests being conducted using MoDTC lubricant. The mechanism currently available does not explain why iron oxide is formed and not MoS_2. This study will therefore seek to have a better insight on the mechanism of MoDTC decomposition.
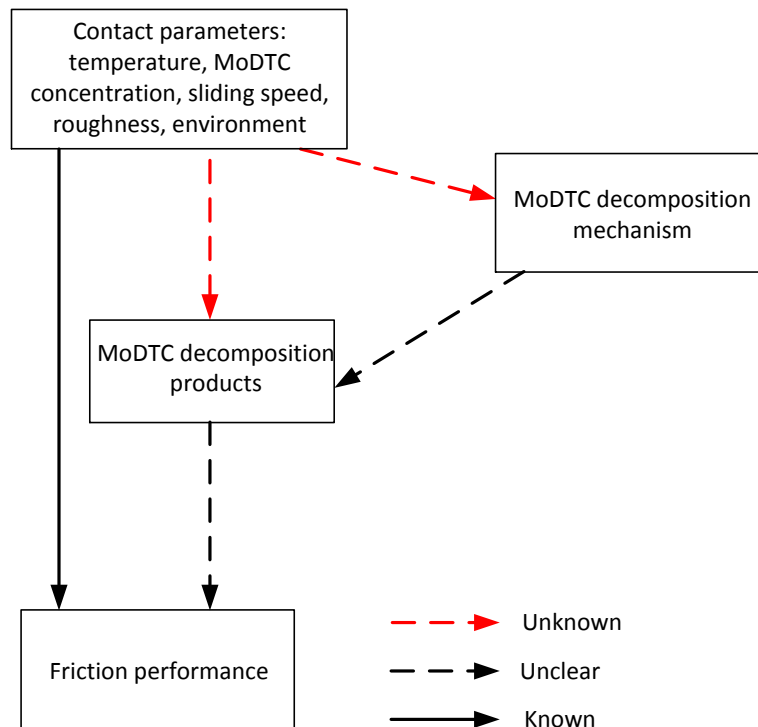
Figure 3-23. Schematic diagram summarising the current knowledge and knowledge gaps in the friction performance of MoDTC

The influence of MoDTC decomposition products on friction performance is also still unclear. From literature, it has been shown that friction coefficient can vary from 0.04 to 0.1 depending on test conditions. Low friction has been attributed to the presence of MoS_2 while high friction has been attributed to the presence of iron oxides at the tribocontact. There is however no information on chemical composition during intermediate friction values. The presence of intermediate friction values suggests that chemical species other than MoS_2 and iron oxides are being formed. In this study, chemical characterisation will be conducted on samples generated when intermediate friction values are observed so as to investigate the chemical composition of the MoDTC decomposition products.

Raman and XPS analysis provide conflicting information on chemical composition of MoDTC tribofilms. XPS shows the presence of MoO_2 and MoO_3 in the tribofilms while Raman analysis does not show the presence of

these molybdenum oxides. XPS can clearly distinguish different elements in a given compound however it is very difficult to differentiate compounds which have elements in the same oxidation state. For example, it is difficult to differentiate MoO_2 from MoS_2 since the oxidation state of molybdenum in both compounds is the same (+4). MoO_2 and MoS_2 have completely different Raman spectra which make it possible to clearly differentiate the two compounds. The presence of Mo (6+) peaks in XPS spectra has led to the conclusion that MoO_3 is present in MoDTC tribofilms. MoO_3 has a very distinct Raman spectrum which is different from MoO_2 and MoS_2 spectra. MoO_3 has not been detected in MoDTC tribofilms using Raman spectroscopy which suggests that the Mo (6+) peak observed in XPS analysis could be due to the presence of other molybdenum compounds besides MoO_3 which have Mo at an oxidation state of (6+). Raman spectroscopy is thus better suited for characterising MoDTC tribofilms than XPS. For this reason, chemical characterisation of MoDTC tribofilms in this study was conducted using Raman spectroscopy.

In the absence of MoDTC additive at the tribocontact high friction is observed and it has been concluded that the high friction is due to the removal of MoDTC tribofilms at the tribocontact. There has been no study on the growth and removal of MoDTC tribofilms. In this study, physical and chemical changes occurring during MoDTC tribofilm formation and removal are investigated.

Chapter 4 Experimental methodology

In this Chapter, information on materials, experimental procedures and analysis techniques used in this study are presented.

4.1 Materials

4.1.1 Additives and base oil

Additives (ZDDP and MoDTC) were supplied as concentrates (55-65 wt% in mineral oil). The ZDDP additive was a secondary ZDDP. MoDTC used in this study had the molecular structure shown in Figure 4-1. R groups in MoDTC were a mixture of C8 and C13 alkyl chains. The base oil used was a Group III mineral oil. Model oils were prepared by blending the additives in the base oil at various concentrations. Table 4-1 shows the model oils used in this study and their designation. The additive concentrates and the mineral base oil were supplied by Total Raffinage, Solaize, France.
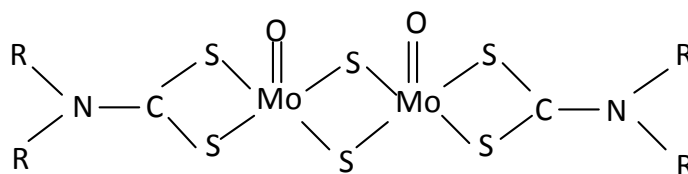
Figure 4-1. Molecular structure of MoDTC used in this study

Table 4-1. Model oils used in the study

Designation	Lubricant
BO	Group III mineral oil
MoDTC	0.1 - 0.9 wt% MoDTC + Group III mineral oil
ZDDP	1 wt% ZDDP + Group III mineral oil

4.1.2 Powders

Pure powders of MoS_2, MoO_2, MoO_3, Fe_3O_4, Fe_2O_3 and $Fe_2(MoO_4)_3$ were obtained from Sigma Aldrich (UK). Raman spectra of the different compounds are shown in Appendix C. The spectra were used as references in this study.

4.1.3 MoS_2 coatings

Steel discs (AISI 52100) such as the one shown in Figure 4-2 (a) were coated with MoS_2 according to the following procedure. The discs were first coated with a thin layer of phenolic resin to improve the adherence properties of the coating to the steel surface. The discs where then sprayed with a solution containing MoS_2 in a solvent solution. The solvent in the sprayed discs was then "flash off" by heating the coatings at 120ºC for 10 minutes before curing the discs at 200ºC for 1h. The thickness of the MoS_2 coatings ranged from 20 to 30 μm. Figure 4-2 (b) shows a steel disc coated with MoS_2. The steel discs were coated at Everlube Products (UK). The MoS_2 coated discs were used in tribological tests using the high speed pin-on-disc tribometer.
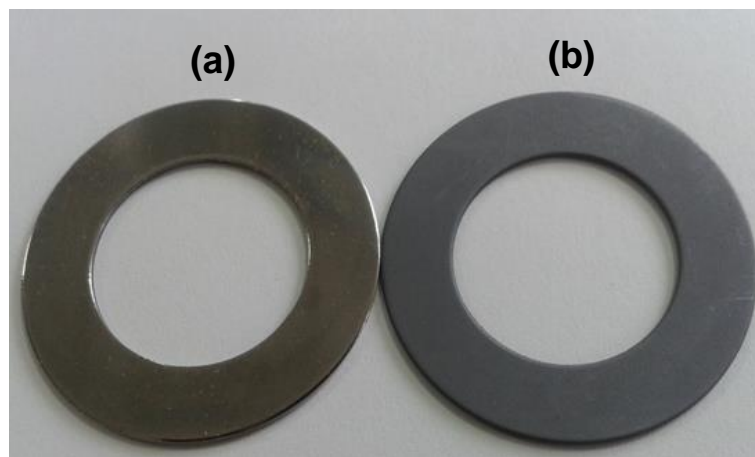
Figure 4-2. (a) Steel disc before coating with MoS_2 (b) steel disc after coating with MoS_2

4.2   Thermal degradation of MoDTC

4.2.1   Thermal decomposition of MoDTC additive and lubricants

Thermal degradation of MoDTC additive concentrate was carried out by heating a small quantity of the concentrate in a glass beaker at 100°C for 1h in air. Thermal degradation of 1 wt% MoDTC lubricant was carried out by heating 100 ml of the lubricant in a glass beaker at 150°C while stirring for 5h. A small amount of the lubricant was sampled every hour for Raman analysis. In a separate test, 5 wt% Fe_3O_4 was added to 0.5 wt% MoDTC lubricant and the mixture was heated at 100°C for 1h. The resulting Fe_3O_4 deposits after thermal decomposition of the lubricant were analysed. All samples were allowed to cool down before Raman analysis was conducted.

4.2.2   Generating MoDTC thermal films on discs

MoDTC thermal films were generated by placing clean steel discs in a glass beaker containing MoDTC lubricant heated at 100°C. The lubricant was heated for 1h. After the test, excess lubricant on the disc was removed by holding the discs vertically with tweezers and allowing the oil to drip off. The discs were then analysed using Raman spectroscopy without rinsing with an organic solvent.

4.3   High Speed Pin-on-Disc (HSPOD) tribotests

4.3.1   HSPOD tribometer

Figure 4-3 shows images of the HSPOD tribometer used in this study. The disc is mounted on top of the motor while the ball is fixed on the loading arm. The loading arm rests on top of the disc so that the ball and the disc are in contact as shown in Figure 4-3 (b). The load is applied to the ball by hanging appropriate weights to the loading arm. In this tribometer, the ball is fixed while the disc rotates simulating unidirectional linear sliding conditions.
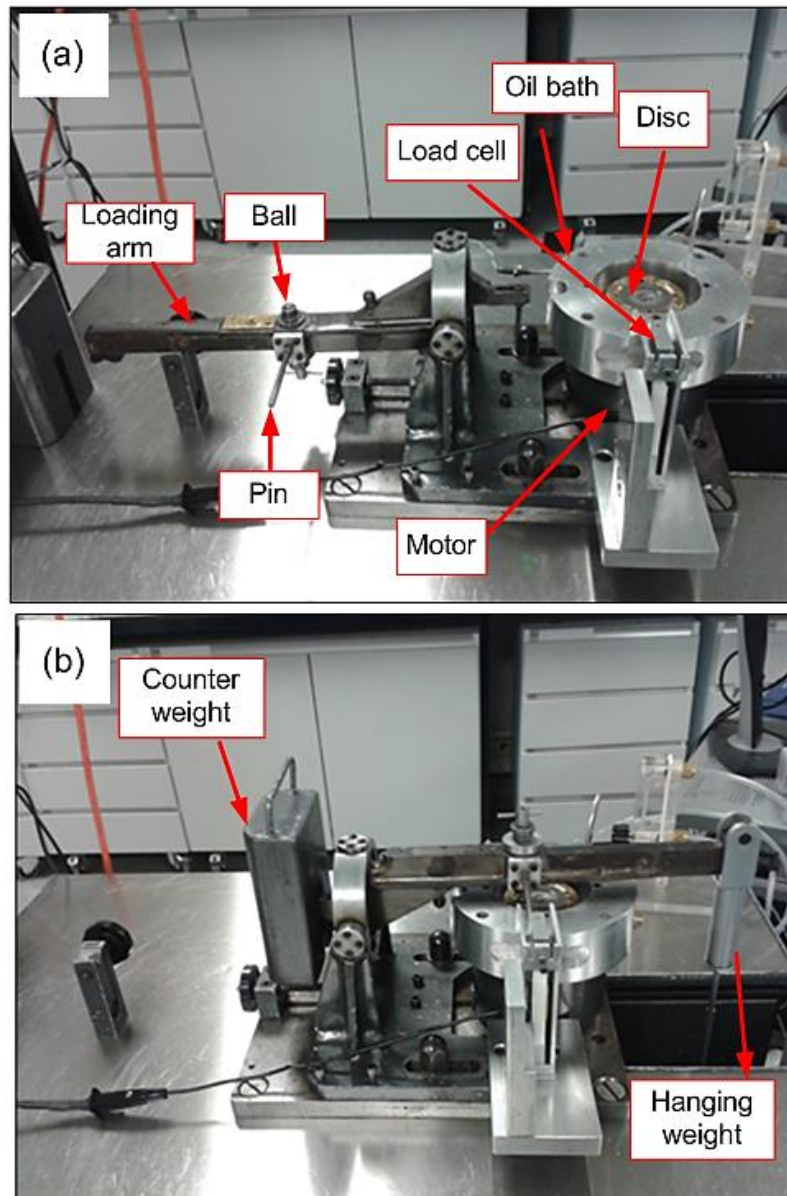
Figure 4-3. Images of the High Speed Pin-on-Disc (HSPOD) tribometer

In tests with lubricants, the lubricant is poured into the oil bath until the disc is fully submerged. The lubricant is heated by heating the steel oil bath to a set temperature. The oil bath is covered with a lid when lubricants are used so as to avoid oil spillage during tests. Frictional torque on the ball during tests is recorded by the load cell as friction voltage. The load cell is calibrated prior to the test so that the voltage obtained during tests can be converted to friction force. Friction voltage from the load cell is recorded every second using a LabVIEW program.

4.3.2   Test conditions for HSPOD tribotests

Material properties of balls and discs used to carry out tribotests using the HSPOD tribometer are summarised in Table 4-2. Tribotests were carried out at test conditions shown in Table 4-3. Contact pressures given in Table 4-3 are the initial maximum Hertzian contact pressures calculated using Equation 2-4. For calculations, the elastic modulus and Poisson's ratio of the tribopair (ball and disc) were taken as 210 GPa and 0.28, respectively.

Table 4-2. Material properties of tribopair samples used in HSPOD tribotests

	Ball	Disc
Material	AISI 52100	AISI 1050
Dimensions	Diameter: 6.5 mm	Inner diameter 25 mm Outer diameter: 42 mm Thickness: 1 mm
Roughness, R_a	13 nm	112 nm
Hardness	60-67 HRC	60-64 HRC
Young's Modulus	190-210 GPa	190-210 GPa

Table 4-3 Test conditions during HSPOD tribotests

Test condition	Parameters
Lubricants	BO, 0.1 - 0.9 wt% MoDTC
Temperature	20-100ºC
Contact pressure	0.98 - 2.12 GPa
Sliding speed	200 rpm (0.3m/s), 400 rpm (0.6 m/s)
Test duration	1 min - 6h
Lambda ratio, λ	0.02 - 0.14

Figure 4-4 shows images of the tribopair after HSPOD tribotests. A circular wear track was generated on the disc and a wear scar several hundred

micrometres in diameter was generated on the ball. The wear scars generated after HSPOD tests were further analysed to determine chemical composition and morphology.
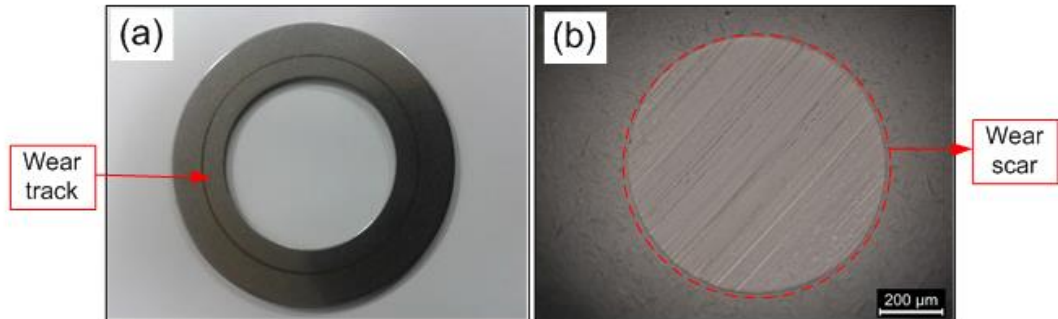
Figure 4-4. Examples of wear scars generated on the (a) disc and (b) ball after tests on the HSPOD tribometer

4.4 MiniTraction Machine (MTM) tribotests

4.4.1 MTM equipment

Figure 4-5 shows images of the MTM from PCS Instruments (Acton, UK) that was used in the study. The ball is fitted on the shaft while the disc is fixed at the bottom of the oil bath and sits on top of a motor as shown in Figure 4-6. Lubricant in the oil bath is heated using heaters and the temperature is controlled by the thermocouple inside the oil bath. As shown in Figure 4-6, both the ball and discs are rotated during tests. As such, MTM tests simulate sliding/rolling conditions. Tests are run using pre-programmed test profiles which have information on the temperature, speeds, load, test sequence and the rate of data acquisition.

An optical system was attached to the MTM and was used to obtain interference images of the ball at various time intervals during tests. Figure 4-5 (c) shows the optical system attached to the MTM. To obtain interference images during tests, the test is stopped momentarily and the ball is loaded against the glass window [89].
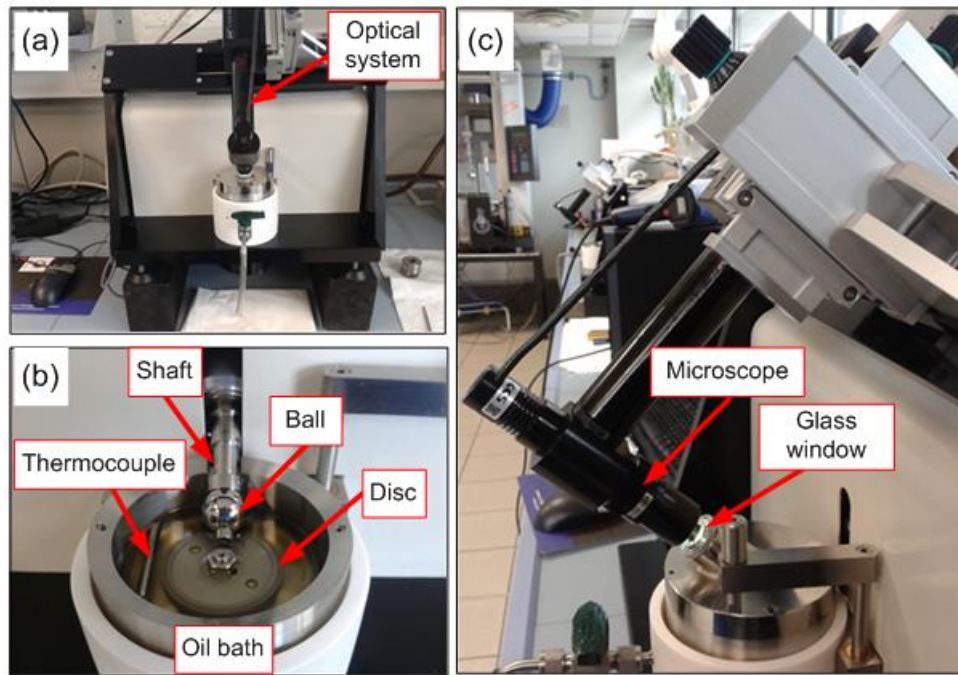
Figure 4-5. Images of the MiniTraction Machine
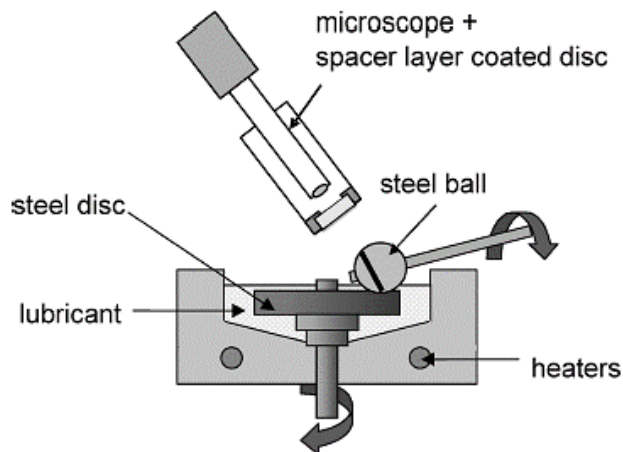
Figure 4-6. Schematic diagram showing the MTM [89].

Images of the ball were obtained using the spacer layer interferometry technique (Figure 4-7). In this technique, a glass disc coated with a semi-reflective chromium layer is attached to the glass window. When light passes through this disc, part of the light is reflected at the chromium layer while the remaining light passes through and is reflected by the steel ball. When the two beams recombine, an interference image is formed since the beams travel

different distances. With proper calibration, the thickness of the lubricant film or tribofilm between the glass disc and steel ball can be obtained.
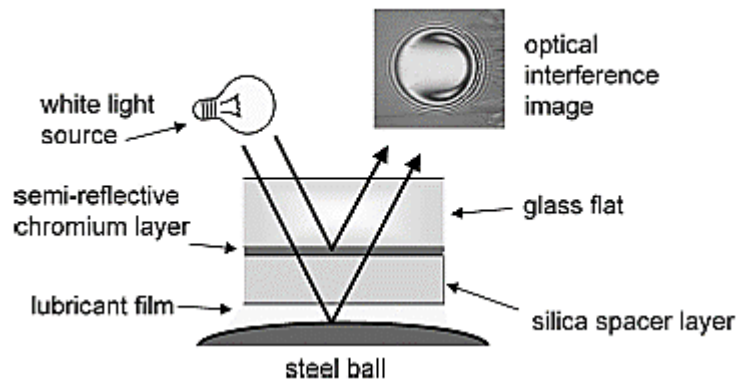
Figure 4-7. Schematic diagram showing how interference images are obtained using SLIM [89]

In order to obtain accurate film thickness from interference images, it is necessary to know the exact refractive index of the film. Interference images of ZDDP tribofilms have been widely studied and are estimated to have a refractive index of 1.5 - 1.6 with the assumption that they are composed of zinc phosphates. Using this refraction index, a calibration scale based on the colour of the ZDDP films has been established for mapping analysis with MTM. Commercial MTMs use this calibration by default. This calibration can provide inaccurate values when films being analysed have refractive indexes which are different from that of ZDDP films. This was the case with films formed using MoDTC lubricant. Figure 4-8 shows interference images during tests with ZDDP and MoDTC lubricants. As it can be seen from the images, ZDDP tribofilms have a brown colour while those from MoDTC tribofilm have a blue colour. Using the default calibration in the MTM, negative film thickness values were obtained for MoDTC tribofilms while positive values were obtained for ZDDP tribofilms. Contrary to the results from interference images, optical and 3D images clearly showed that thick MoDTC tribofilms had been formed on the ball. Thus, using the current in-built calibration in MTM, thickness information during tests with MoDTC lubricant could not be obtained from interference images. Tests in this study were conducted using MoDTC

60

lubricants, therefore interference images obtained during tests were only used to monitor changes on the ball wear track with rubbing time.
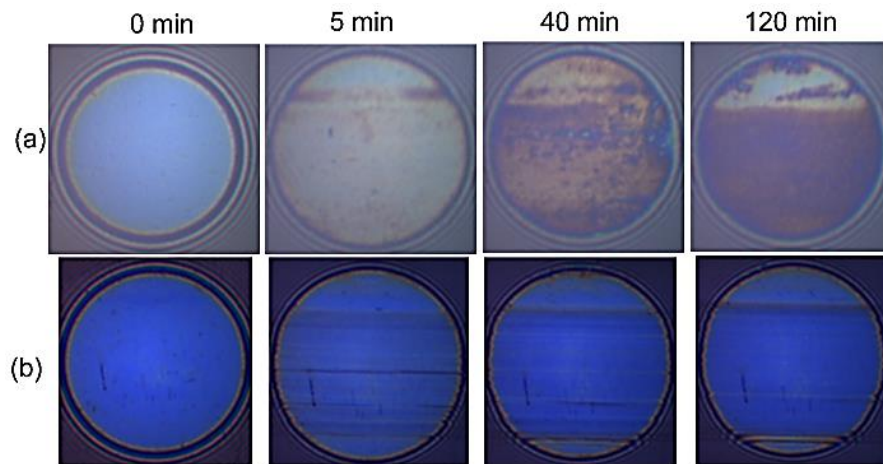
Figure 4-8. Interference images obtained during MTM tests with (a) ZDDP and (b) MoDTC lubricants

4.4.2 Test conditions for MTM tribotests

Tests in MTM were conducted using steel balls and discs (AISI 52100) with 750-770 VPN hardness. Two discs with different roughness were used; R_a=10 nm (smooth discs) and R_a=150 (rough discs). The steel balls had a diameter of 19 mm and roughness of R_a=10 nm. Tests were conducted at test conditions shown in Table 4-4.

Slide-roll ratio (SRR) is the ratio (as a percentage) of the sliding speed (U_s) to entrainment speed (U), $U_s/U \times 100$. Given that U_B and U_D are the speeds of the ball and disc, respectively. The sliding speed (U) is given by U_s=|U_B-U_D| while the entrainment speed (U) is given by U=(U_B+U_D)/2 [89]. It should be highlighted that since the shaft of the ball was not fixed, the ball was rolling even when the speed of the ball was 0 m/s (at SRR=200%) due to the motion of the disc.

Table 4-4. Test conditions during MTM tribotests

Test condition	Parameters
Temperature	100ºC
Contact pressure	1 GPa (40 N)
Lubricant	BO, 0.5 wt% MoDTC
Speed (SRR=100%)	0.45 m/s (disc), 0.15 m/s (ball)
Speed (SRR=200%)	0.6 m/s (disc), 0 m/s (ball)
Test duration	5 min - 4h
Ball material	AISI 52100 steel (R_a=10 nm)
Disc material	AISI 52100 steel (R_a=10 nm, 150 nm)

Figure 4-9 shows an example of the tribopair immediately after an MTM test. It can be observed that circular wear tracks developed on both the disc and ball. These wear tracks were further analysed for chemical composition and morphology.

Figure 4-9. Wear tracks generated on the tribopair after MTM tribotests

4.5   Design of Experiments (DoE)

The central composite design was used in the Design of Experiment for results presented in Chapter 9. This experimental design allows for estimation of linear, quadratic and two-way interactive effects of the variables on a response (friction, in this case) [117]. Tribotests were conducted in the MTM using rough discs (R_a=150 nm) at SRR=100%. All tests were conducted for 2h. Table 4-5 shows important factors and levels that were considered in this study.

Table 4-5. Important factors and levels

Parameters	Notation	Unit	Levels				
			-2	-1	0	1	+2
Pressure	*P*	GPa	-	0.7	1	1.3	-
Speed	*S*	m/s	0.2	0.4	0.6	0.8	1
Temperature	*T*	ºC	20	50	80	110	140
MoDTC concentration	*C*	wt%	0.1	0.3	0.5	0.7	0.9

Table 4-6 shows the total number of experiments conducted and the test conditions used. The first 16 tests were based on a full factorial design (2^4=16) of the levels -1 and +1. Exp. No.17 to No. 22 were carried out using the intermediate levels (0), the lowest (-2) and the highest levels (+2). The remaining three tests were carried out at the intermediate level (0). Applied loads of 15 N, 40 N and 75 N were used to give initial maximum Hertzian pressures of 0.7 GPa, 1 GPa and 1.3 GPa, respectively. All the tests were repeated twice to check for repeatability.

Table 4-6. Experimental test matrix

Exp. No	Parameters				Initial film thickness (h_{min})	Initial lambda ratios (λ)
	P	S	T	C		
1	0.7	0.4	50	0.3	28	0.19
2	1.3	0.4	50	0.3	25	0.17
3	0.7	0.8	50	0.3	45	0.30
4	1.3	0.8	50	0.3	40	0.27
5	0.7	0.4	110	0.3	8	0.05
6	1.3	0.4	110	0.3	7	0.05
7	0.7	0.8	110	0.3	12	0.08
8	1.3	0.8	110	0.3	11	0.07
9	0.7	0.4	50	0.7	28	0.19
10	1.3	0.4	50	0.7	25	0.17
11	0.7	0.8	50	0.7	45	0.30
12	1.3	0.8	50	0.7	40	0.27
13	0.7	0.4	110	0.7	8	0.05
14	1.3	0.4	110	0.7	7	0.05
15	0.7	0.8	110	0.7	12	0.08
16	1.3	0.8	110	0.7	11	0.07
17	1	0.2	80	0.5	9	0.06
18	1	1.0	80	0.5	26	0.17
19	1	0.6	20	0.5	60	0.40
20	1	0.6	140	0.5	5	0.03
21	1	0.6	80	0.1	19	0.12
22	1	0.6	80	0.9	19	0.12
23	1	0.6	80	0.5	19	0.12
24	1	0.6	80	0.5	19	0.12
25	1	0.6	80	0.5	19	0.12

4.6   Lubricant changing procedure

To study the durability of MoDTC tribofilms, tests were conducted using the lubricant changing procedure detailed in reference [66]. In summary, tests were run in one lubricant for a certain duration after which the test was stopped and the lubricant was removed using a syringe and replaced with another lubricant without removing the tribopair. Figure 4-10 shows the three procedures that were used. Separate tests were also conducted where the tests were stopped at different stages before changing the lubricants.
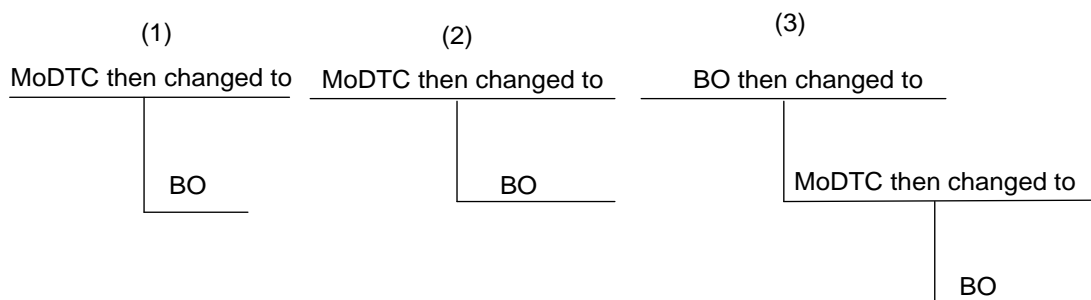
Figure 4-10. Schematic diagram showing the three procedures used to study MoDTC tribofilm removal. Procedure (1) was conducted using the MTM while procedures (2) and (3) were conducted in the HSPOD tribometer

4.7   Pre-test and Post-test sample treatment

Before any tribological tests, the tribopair was cleaned with acetone in an ultrasonic bath for a few minutes. The samples were then dried with tissue paper before being fixed in the tribometers.

After tribological tests, the tribopair samples were cleaned with heptane in an ultrasonic bath for 1 minute before Raman analysis. Figure 4-11 (a) shows an image of the disc immediately after tribological test with MoDTC and after cleaning with heptane. In the uncleaned sample, wear debris was observed on the outside regions of the rubbing track. The presence of the wear debris

made it impossible to distinguish the wear track. Rinsing the disc in heptane removed the loose wear debris from the disc surface and the wear track became distinct as can be seen in Figure 4-11 (b)

Figure 4-11. Images of the disc after tests on the HSPOD tribometer (a) before rinsing (b) after rinsing in heptane for 1 minute

Although Raman analysis can be carried out on uncleaned samples, most samples in this study were cleaned so as to obtain good Raman signals from the wear scars. Uncleaned samples have a layer of lubricant on the surface and when analysed with Raman spectroscopy they show very strong peaks from the mineral base oil. The strong Raman peaks from the mineral base oil make it impossible for weak peaks from MoDTC decomposition products to be observed. Removing the lubricant from the sample by rinsing in heptane allows Raman peaks of MoDTC decomposition products to be distinctly observed in the spectrum.

In some samples, Raman analysis was conducted on uncleaned samples so as to investigate the effect of lubricant layer in Raman analysis. These samples were generated using the HSPOD tribometer and after tribotests the lubricant was removed from the steel bath using a syringe and the excess oil on the disc surface was drained off by spinning the disc at high speeds for a

few minutes. The disc was then analysed with Raman spectroscopy without any further cleaning.

4.8   White light interferometry

3D images of wear tracks generated after tribotests were obtained by white light interferometry using NPFLEX from Bruker, UK. Basic theory of how images are obtained using the equipment is as follows. White light is radiated towards a beam splitter which splits the light into two beams. The first beam is directed towards an internal reference mirror while the second beam is directed towards the sample being analysed. Reflected light from the sample is later recombined with the first beam and the two beams are directed to a detector. Since the two beams travel different distances, they form interference images when they recombine. With suitable analysis software, the interference images are used to provide information on the topography of the samples being analysed. In this study, interference images obtained from NPLEX were analysed using Vision64 software from Bruker.

4.9   Raman spectroscopy

4.9.1   Theory: Classical interpretation of the Raman Effect

Raman scattering occurs due to interaction between induced dipoles and the incident radiation [118]. When an electromagnetic radiation is radiated on a molecule the electromagnetic field exerts a force on charged particles of the molecules causing an induced dipole. The induced dipole moment (μ_i) is given by Equation 4-1.

$$\mu_i = \alpha_p E_{elec} \qquad\qquad 4\text{-}1$$

Where α_p is the polarisability tensor and E_{elec} is the electric field.

Polarisability is a molecular quantity which describes the ease with which electrons can be moved by the electromagnetic radiation relative to the nuclear framework. Polarisability of a molecule with N atoms is given by Equation 4-2. n is the refractive index of the molecule.

$$\alpha_p = \frac{3}{4\pi N} \frac{n^2 - 1}{n^2 + 2}$$
4-2

Oscillation of the electric field of the electromagnetic radiation is given by Equation 4-3.

$$E_{elec} = E_0 \cos \omega t$$
4-3

Where E_0 is the amplitude of the electric field and ω the angular frequency of the incident light. The induced dipole moment in the molecule μ_i can therefore be written as:

$$\mu_i = \alpha_p E_0 \cos \omega t$$
4-4

The molecule undergoes constant vibrational motion along its 3N-6 molecular vibrational coordinates Q. Vibration of the molecule along its vibrational coordinates is given by Equation 4-5. ω_m is the frequency of the mth normal coordinate.

$$Q = Q_0^m \cos \omega_m t$$
4-5

Where m can have all values between 1 and 3N-6. The polarisability α_p of the molecule is also modulated at the vibrational frequencies of the molecule. For the mth coordinate, Q_m, polarisability can be expanded in a Taylor series as shown in Equation 4-6.

$$\alpha_p = \alpha_0 + \frac{d\alpha_p}{dQ_m} Q_m + \cdots$$
4-6

Normally, only the first and second terms of the Taylor series are considered. Therefore, polarisability of a molecule is described by Equation 4-7.

$$\alpha_p = \alpha_0 + \frac{d\alpha_p}{dQ_m} Q_0^m \cos \omega_m t \qquad\qquad 4\text{-}7$$

Taking into account Equation 4-7, the induced dipole moment can be rewritten as

$$\mu_i = \alpha_0 E_0 \cos \omega t + \frac{d\alpha_p}{dQ_m} Q_0^m E_0 \cos \omega_m t \cos \omega t \qquad\qquad 4\text{-}8$$

Using the trigonometric identity $(\cos A + \cos B) = \frac{1}{2}[\cos(A+B) + \cos(A-B)]$ Equation 4-8 is also written as:

$$\mu_i = \alpha_0 E_0 \cos \omega t + \frac{1}{2}\frac{d\alpha_p}{dQ_m} Q_0^m E_0[\cos(\omega - \omega_m)t + \cos(\omega + \omega_m)t] \qquad 4\text{-}9$$

The induced dipole moment therefore oscillates at the following frequencies: ω, $\omega - \omega_m$ and $\omega + \omega_m$. When the induced dipole oscillates at ω this is known as Rayleigh scattering. When the induced dipole oscillates at $\omega - \omega_m$ and $\omega + \omega_m$ this is referred to as stokes and anti-stokes Raman scattering, respectively.

Figure 4-12 shows a schematic diagram illustrating Rayleigh and Raman scattering. In Rayleigh scattering, the energy of light radiated on the molecule remains unchanged. In stokes Raman scattering, the scattered light is at a lower energy while in anti-stokes scattering the scattered light is at a higher energy than the incident light. Anti-stokes Raman scattering occurs when the molecule was initially at a higher energy level (excited state) for example when it is heated. In most cases however, molecules are in unexcited states and as such most Raman equipment record stokes Raman scattering. On the x-axis of Raman spectra, normally labelled as Raman shift (cm⁻¹), is the difference

in wavenumber ($1/\lambda$) between the incident light and Raman scattered light. On the *y*-axis of Raman spectra is the intensity of the scattered light.

When light is radiated on a sample, most of the light is scattered at the same energy (Rayleigh scattering) while only 0.0001% of the light undergoes Raman scattering.
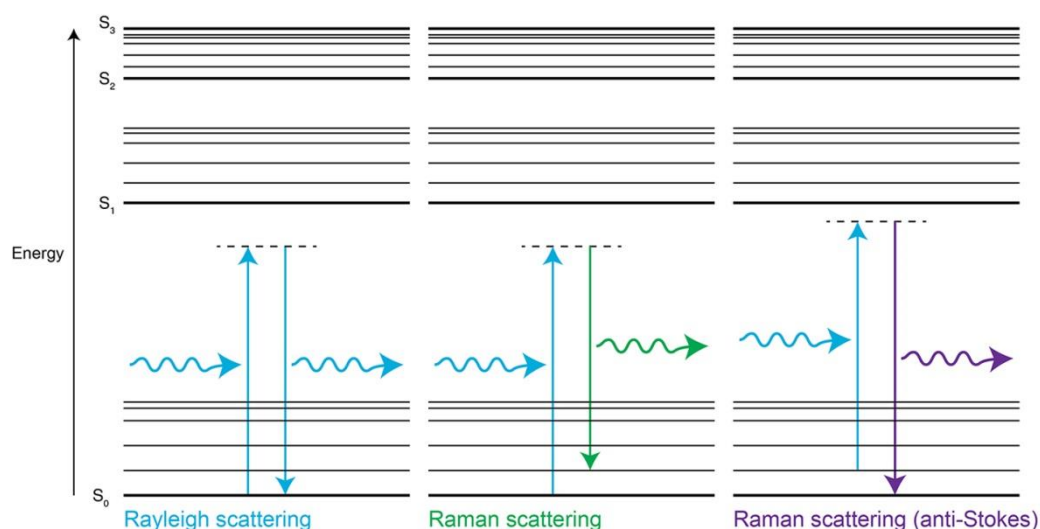
Figure 4-12. Schematic diagram illustrating Raman scattering phenomenon [119].

4.9.2   Raman equipment

The Renishaw InVia spectrometer (UK) shown in Figure 4-13 was used in this study. This Raman equipment is equipped with two lasers; 488 nm and 785 nm wavelength lasers operating at a maximum laser power of 10 mW and 220 mW at the source, respectively. This Raman equipment has 5x, 20x and 50x short distance objectives and 50x long distance objective. Samples are placed on the motorized stage and analysed with lasers focused through the objective lenses. The Raman equipment is connected to a PC which is used to collect spectral data during analysis. Samples on the stage can be viewed through the eye piece or on the PC. The analysis area is in a chamber with an

enclosure door. During analysis, the enclosure door is shut so as to prevent exposure to lasers which can be harmful.
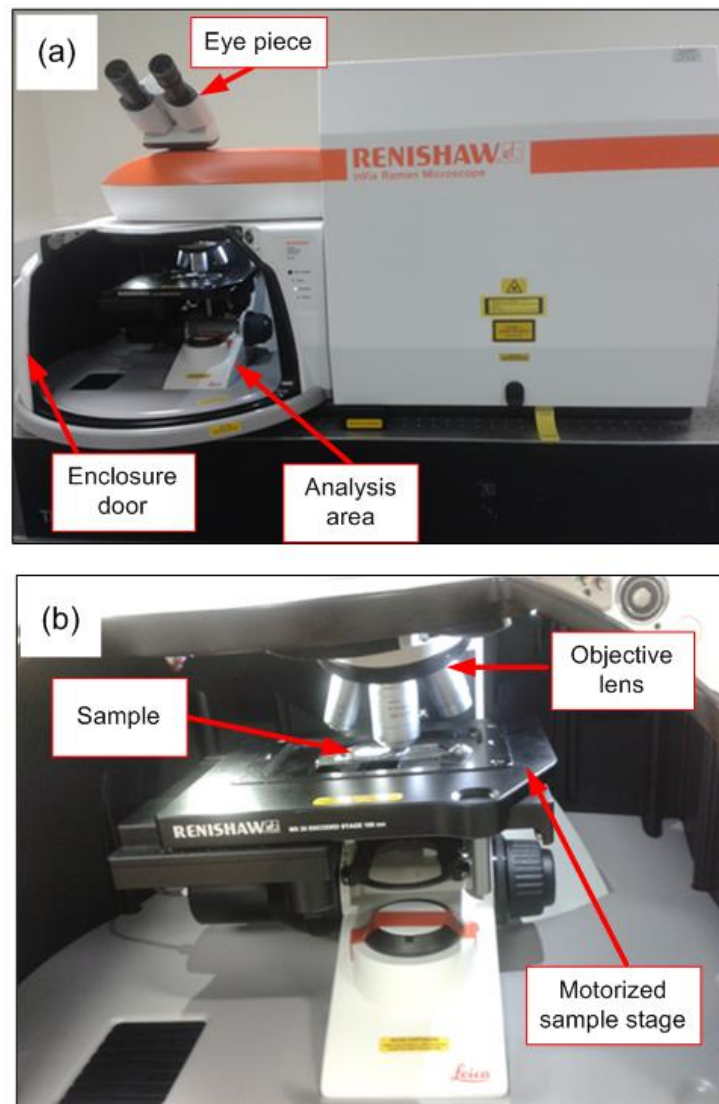
Figure 4-13. (a) Image of the Raman equipment used for analysis (b) inside the analysis chamber of the Raman equipment

4.9.3 Instrumentation

Figure 4-14 shows a schematic diagram of the Raman equipment used. Basically, the Raman equipment consists of the following: Laser sources, lenses, filters, microscope, diffraction grating and a detector (CCD camera). The lenses are used to focus the light beam from the laser source to the

sample. Scattered light is collected from the sample at 180º by the same lenses used to radiate the samples. This collection configuration is known as backscattering. The holographic filters are used to separate reflected light from the laser source from scattered light from the sample. The filters block light reflected from the laser source and allows scattered light from the sample to pass through to the diffraction grating. At the diffraction grating, the scattered light is split into different colours before being focused on the CCD camera which is used to detect the various colours. The 2400 l/mm and 1200 l/mm diffraction gratings were used for the 488 and 785 nm lasers, respectively.
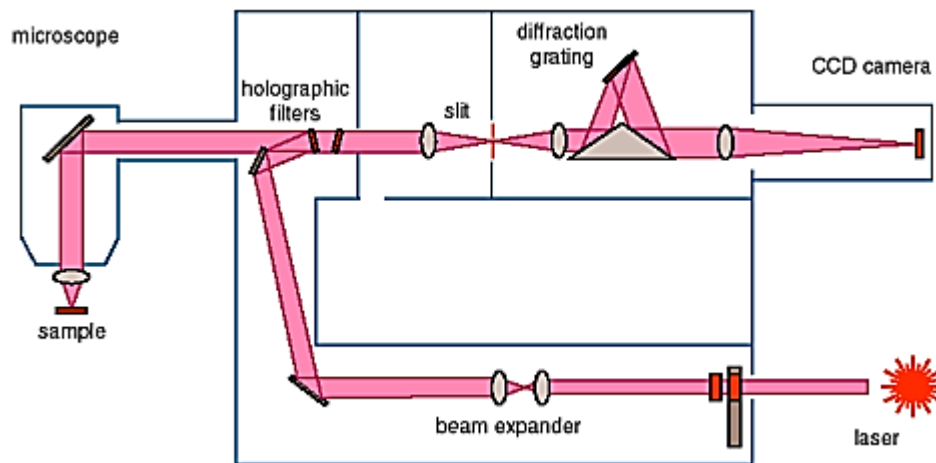
Figure 4-14. Schematic diagram of the Raman spectrometer [120].

The objective lenses used in the microscope determine the relative energy density of light that is delivered to the sample and the numerical aperture ($N.A$) of the microscope. The energy density increases with increase in magnification. It is therefore best to use objective lenses with high magnification. The numerical aperture ($N.A$) is a parameter used as a measure of light collected from the sample and is given by Equation 4-10.

$$N.A = n \, sin \, (\theta_{back})$$

4-10

Where n is the refractive index of the medium through which the laser light is passing through, n=1 if the medium is air. θ_{back} is half the angle of the maximum cone ($2\theta_{back}$) of light collected by the lens from the sample. θ_{back} is dependent on magnification of the objective lenses. For 50x magnification, $2\theta_{back}$ is 97.2 and *N.A*=0.75.

For opaque samples the radius of the laser spot (R_s) that is observed on the sample is determined by the laser wavelength (λ) and *N.A* and is calculated using Equation 4-11.

$$R_s = 0.61\lambda/N.A \qquad\qquad\qquad 4\text{-}11$$

At 50x magnification, the theoretical radius of laser spots for the 488 nm and 785 nm lasers is 400 nm and 640 nm, respectively. The size of the laser spot defines the spatial resolution of the Raman equipment. The penetration depth of lasers (δ) into samples is given by Equation 4-12.

$$\delta = \frac{1}{A} = \frac{\lambda}{4\pi n \kappa} \qquad\qquad\qquad 4\text{-}12$$

Where A is the absorption coefficient of the sample, n and κ are refraction and extinction indexes, respectively [121]. For backscattering configuration, the laser penetration depth is roughly $\delta = {}^{1}/_{2A}$ [122]. Laser penetration depth is thus dependent on the laser wavelength and optical properties of the material being analysed. Unfortunately, absorption coefficient values for most materials are not available therefore it is impossible to calculate penetration depths. Calculating the penetration depth becomes even more difficult when the analysed sample is a composite material such as tribofilms. To accurately determine the laser penetration depth in tribofilms the absorption coefficient of the tribofilm has to be measured.

4.9.4 Raman spectra acquisition from samples

Cleaned samples after tribotests were analysed with the short distance 50x objective. Uncleaned tribopair samples after tribotests, lubricants and powders were analysed using the long distance 50x objective. Raman analysis was conducted using both 488 nm and 785 nm lasers. With the Raman equipment, spectra can be obtained from samples in two ways:

1. Single spot analysis: With this analysis option, a single spectrum is obtained from a single spot on the sample

2. Spot-to-spot mapping: With this option, several spectra are obtained from different spots on the samples in a single analysis. This option is possible since the motorised stage can be programmed to move the sample to different positions during analysis. This mapping option makes it possible for larger areas of the sample to be analysed. Raman mapping is however very time-consuming.

In this study, spectra were obtained using the single spot analysis option. To check for uniformity in chemical composition, different regions of the sample were analysed. All spectra reported in this thesis were obtained at room temperature. Peak analysis was conducted using the Renishaw WiRE program where Raman peaks were fitted with mixed Gaussian/Lorentzian curves to determine the peak frequency, full width at half maxima (FWHM) and peak intensity.

Chapter 5

Chemical characterisation of MoDTC decomposition products formed under non-tribological conditions

5.1   Introduction

Tribochemical reactions are a combination of thermal and mechanically activated reactions. Therefore understanding how additives decompose independently under thermal and mechanical conditions can provide insight on the reactions that take place within a tribocontact. In this Chapter, thermal decomposition of MoDTC under non-tribological conditions was investigated. MoDTC additive concentrate and MoDTC containing lubricants were heated in air and the resulting samples were analysed using Raman spectroscopy. Raman analysis was also conducted on MoDTC thermal films formed on steel discs.

5.2   Raman spectra of oils and MoDTC additive

5.2.1   Group III mineral oil (base oil)

Figure 5-1 shows the Raman spectrum of Group III mineral oil used as the base oil in this study. Table 5-1 shows the assignment of the Raman peaks.

Table 5-1. Assignment of Raman peaks from base oil

Raman peak (cm^{-1})	Assignment	Reference
849, 1071, 1148,	C-C stretching	[123]
1301, 1444	Deformation of methyl groups and scissoring of the CH_2 groups	[123-125]
2727, 2849	Symmetrical and asymmetrical stretching of C-H bonds	[124]
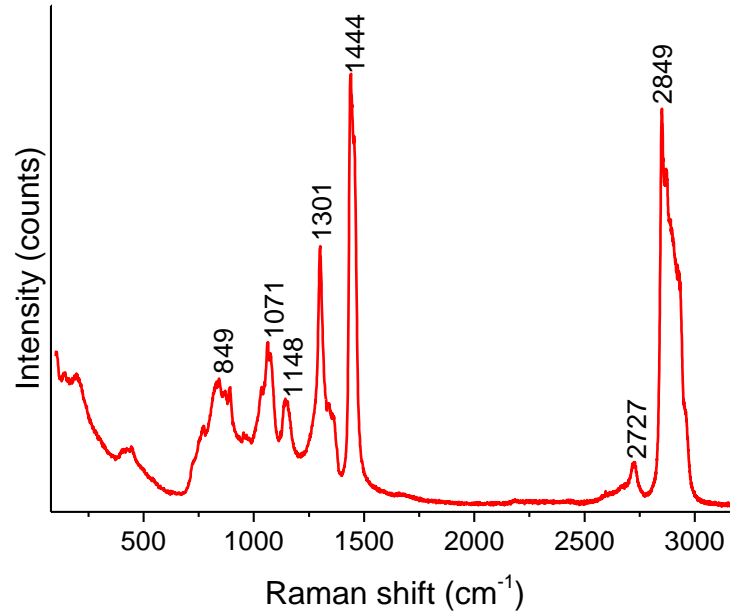
Figure 5-1. Raman spectrum of the Group III mineral oil used as base oil in this study

5.2.2 MoDTC additive concentrate

Figure 5-2 shows the Raman spectrum obtained from MoDTC additive concentrate. Assignment of the Raman peaks is shown in Table 5-2
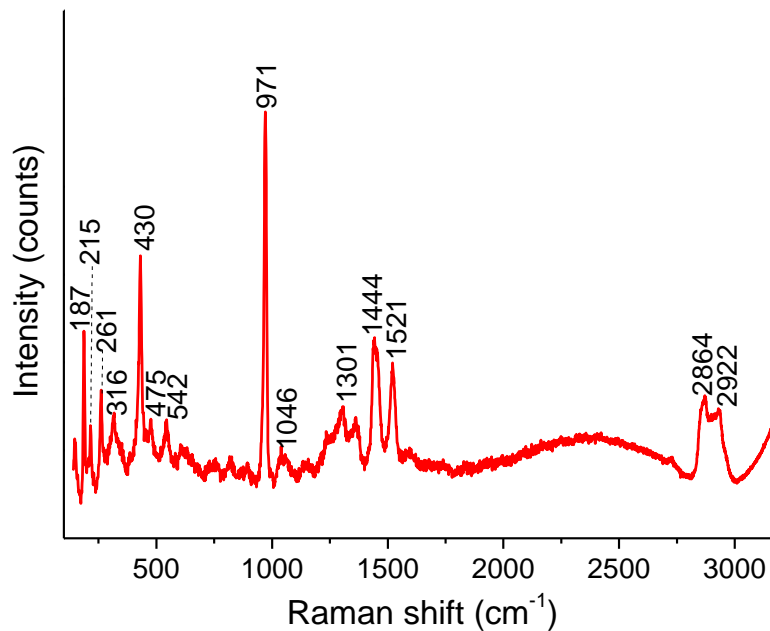
Figure 5-2. Raman spectrum of MoDTC additive concentrate

Table 5-2. Assignment of Raman peaks from MoDTC additive concentrate

Raman peak (cm⁻¹)	Assignment	Reference
187, 215, 261	v(Mo-Mo) vibration	[126, 127]
316	v(Mo-S) vibration outside the Mo-S$_2$-Mo ring	[128, 129]
430	v(Mo-S) vibration within the Mo-S$_2$-Mo ring	[130-133]
971	v(Mo=O) vibration	[130-133]
1521	v(C-N) vibration	[54]
1301, 1444, 2864, 2922	Stretching and bending of alkyl groups in MoDTC or in the mineral oil used to prepare the MoDTC concentrate	

5.2.3   MoDTC lubricant

Figure 5-3 shows Raman spectra obtained from MoDTC lubricant with varying MoDTC concentrations.
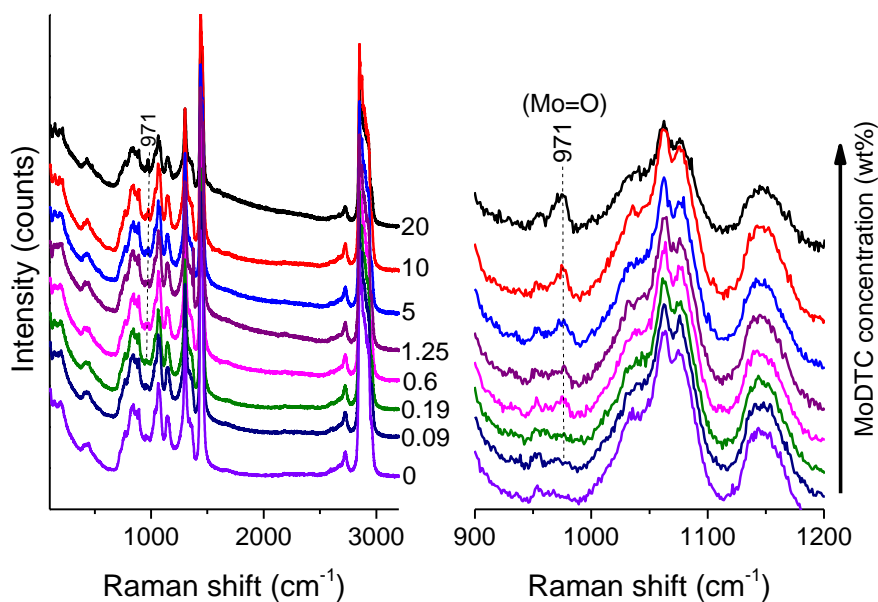
Figure 5-3. Raman spectra at various MoDTC concentrations. The intensity of the 971 cm⁻¹ peak increases with MoDTC concentration

The spectra obtained from the different blends were similar and showed strong Raman peaks from the base oil. The only notable peak from MoDTC was observed at 971 cm⁻¹ due to v(Mo=O) vibration. The MoDTC peak at 971 cm⁻¹ was very weak in comparison to peaks from the base oil and was barely noticeable at lower MoDTC concentrations. The lower intensity of MoDTC peaks in comparison to base oil peaks indicate that the base oil is more Raman active than MoDTC.

5.3   Thermal degradation of MoDTC additive concentrate

Figure 5-4 shows Raman spectra of MoDTC concentrate after 1h heating at 100⁰C.
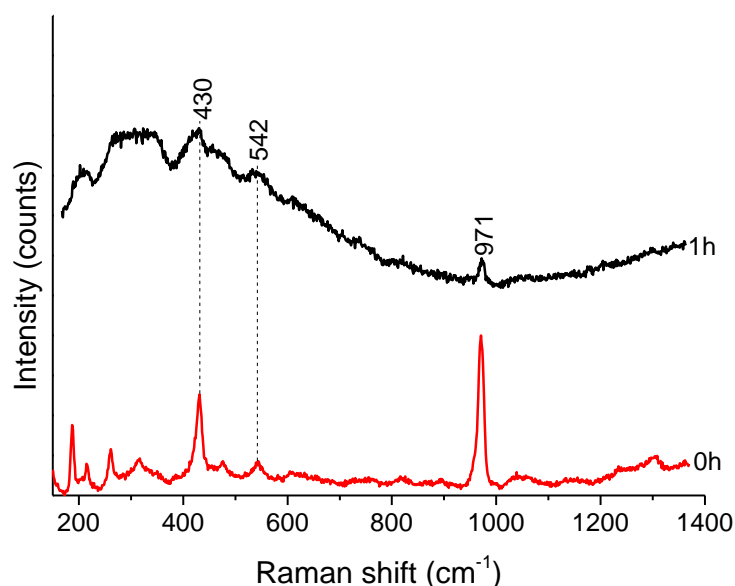
Figure 5-4. Raman spectra obtained from heating MoDTC additive concentrate in air at 100⁰C for 1h

Significant differences in the spectra patterns were observed at lower wavenumbers after heating the MoDTC concentrate. Two broad peaks were observed in the regions 250-400 cm⁻¹ and 400-500 cm⁻¹ region instead of the sharp peaks observed in the fresh concentrate. The peak at 971 cm⁻¹ observed in the fresh concentrate was also observed after heating the

concentrate for 1h indicating that (Mo=O) bonds were still present after heating the MoDTC concentrate. The broad peaks at 250-400 cm⁻¹ and 400-500 cm⁻¹ indicate formation of an amorphous molybdenum sulphur compound with varying Mo-Mo and Mo-S bond lengths (MoS$_x$) [134, 135].

5.4 Thermal degradation of MoDTC lubricant in air

5.4.1 Fresh lubricant without Fe₃O₄

Figure 5-5 shows Raman spectra of fresh MoDTC lubricant (1 wt%) and after heating the lubricant at 150ºC for 3h. The spectrum obtained after 3h of heating was similar to that of the fresh lubricant.
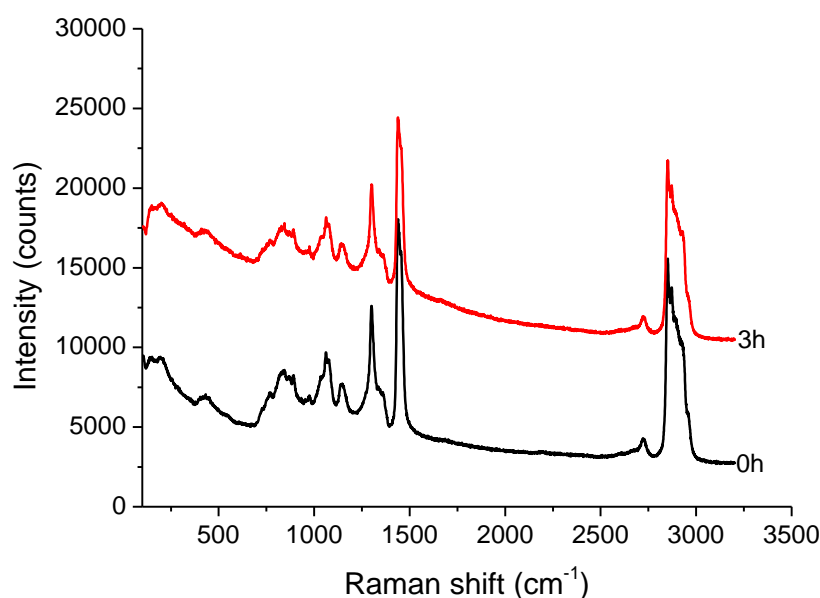
Figure 5-5. Raman spectra of 1 wt% MoDTC lubricant before heating (0h) and after heating at 150ºC for 3h.

After 3h thermal degradation, it was observed that the colour of the lubricant was similar to that of the fresh lubricant. However, after heating for 5h, brown deposits were observed in the lubricant. Figure 5-6 (a) shows a typical Raman spectrum obtained from deposits formed after 5h of heating MoDTC lubricant. Broad peaks were observed at 250-400 cm⁻¹, 400-500 cm⁻¹, 540 cm⁻¹

indicating the presence of amorphous molybdenum sulphur compounds (MoS_x) [135, 136]. At low wavenumbers (< 700 cm^{-1}), the spectral pattern from the deposits was similar to that obtained after heating MoDTC concentrate at 100°C for 1h (Figure 5-6b) suggesting that similar compounds (MoS_x) were formed in both instances.
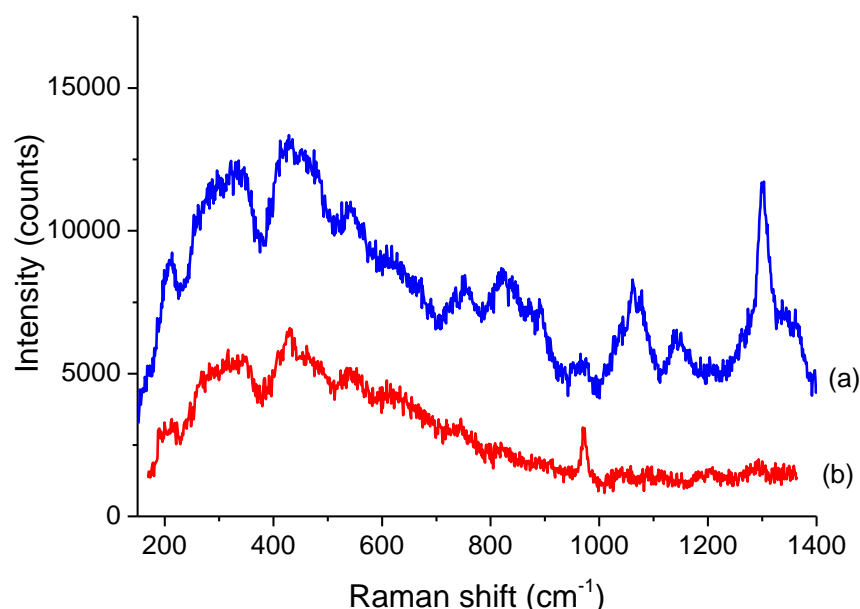
Figure 5-6. (a) Spectrum obtained from deposits after heating 1 wt% MoDTC in air for 5h at 150°C (b) Spectrum obtained from MoDTC additive concentrate after heating for 1h at 100°C

5.4.2   Fresh lubricant with Fe_3O_4 powder

MoDTC-containing lubricants have been shown to have good tribological performance when used on ferrous contacts. Surfaces of these ferrous substrates are composed of iron/iron oxides. It is therefore important to investigate the role of iron/iron oxides in thermal decomposition of MoDTC. MoDTC lubricant (0.5 wt%) containing 5 wt% Fe_3O_4 was heated at 100°C for 1h and the resulting Fe_3O_4 deposits were analysed. Figure 5-7 (a) shows an optical image of the Fe_3O_4 deposits in MoDTC lubricant after heating, these deposits will be referred to as MoDTC/Fe_3O_4 deposits hereafter.
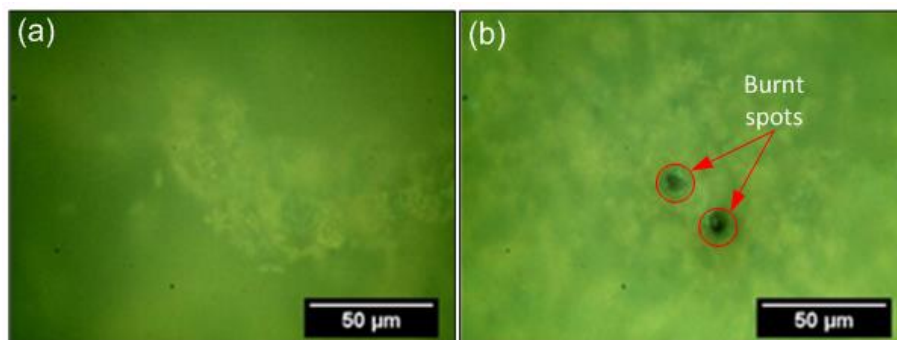
Figure 5-7. Optical images of the analysed MoDTC/Fe$_3$O$_4$ deposits after analysis at (a) 1 mW (b) 10 mW laser power. Raman spectra were obtained using the 488 nm wavelength laser

During Raman analysis of MoDTC/Fe$_3$O$_4$ deposits, it was observed that the spectra obtained were affected by the laser power. Therefore, to study the influence of laser power, the same spot on the deposits was probed at 1 and 10 mW laser power. The spot was first analysed at 1 mW followed by the 10 mW laser power. Figure 5-8 shows Raman spectra obtained from MoDTC/Fe$_3$O$_4$ deposits at different laser powers. Table 5-3 shows assignment of the Raman peaks. Reference spectra of the pure powders are shown in Appendix C.

The addition of Fe$_3$O$_4$ to MoDTC lubricant resulted in the formation of MoS$_2$ and FeMoO$_4$ after only 1h of heating. In the absence of Fe$_3$O$_4$, MoDTC required at least 5h before it was decomposed to MoS$_x$. These results indicate that Fe$_3$O$_4$ enhanced the decomposition rate of MoDTC in the lubricant.

Probing the MoDTC/Fe$_3$O$_4$ deposits at 10 mW laser power resulted in intense MoO$_2$ peaks appearing in the spectrum as well as burn spots being observed on the deposits (Figure 5-7 (b)). These results show that MoS$_2$ was oxidised to MoO$_2$ at high laser powers.
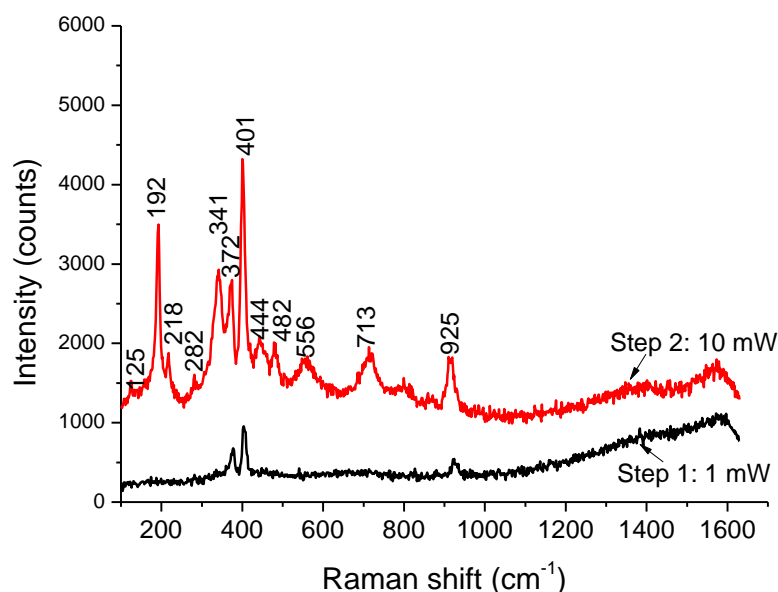
Figure 5-8. Spectra obtained from MoDTC/Fe₃O₄ deposits after heating at 100⁰C for 1h. In Step 1 the spectrum was obtained with 1 mW laser power. In Step 2 the same spot was analysed using 10 mW laser power. In both steps the spectra were obtained with 488 nm laser at 1s exposure time and 20 accumulations

Table 5-3. Assignment of Raman peaks obtained from MoDTC/Fe₃O₄ deposits

Laser power	Raman peak (cm⁻¹)	Assignment	Reference
1 mW	372, 402	MoS_2	Pure powders
	925	$FeMoO_4$	[83, 137]
10 mW	372, 401	MoS_2	Pure powders
	192,218, 282, 341, 444, 482, 556, 713	MoO_2	Pure powders
	925	$FeMoO_4$	[83, 137]

5.5   MoDTC thermal films

MoDTC thermal films were generated on steel discs at 100⁰C for 1h. These steel discs were analysed without cleaning. Figure 5-9 shows a typical Raman spectrum obtained from the thermal films at 1 mW laser power. This spectrum

82

shows Raman peaks belonging to the base oil which is expected for MoDTC lubricants. This results are in agreement with those in reported literature [70].
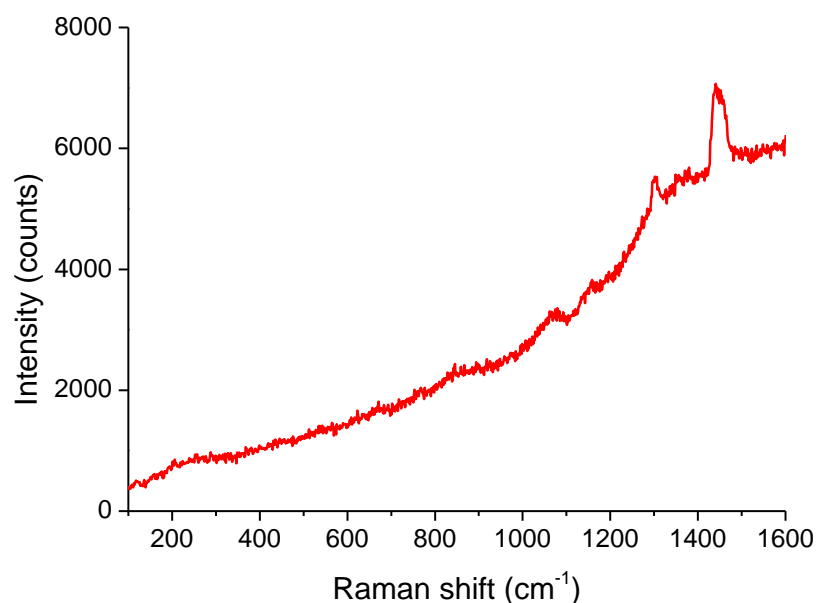
Figure 5-9. Raman spectum obtained from MoDTC thermal film formed at 100ºC for 1h. The spectrum was obtained with 488 nm laser at 1 mW laser power, 1s exposure time

To study the influence of laser power on spectra obtained from the MoDTC thermal film, spectra were obtained at varying laser powers. Figure 5-10 shows spectra obtained from the same spot on MoDTC thermal films at varying laser powers. MoDTC thermal film formed was first analysed using 1 mW laser power. The same spot was then analysed at 10 mW and then finally analysed at 1 mW laser power. The spectrum obtained in Step 1 at 1 mW laser power did not show any peaks in the lower wavenumbers. Peaks were only visible at high wavenumbers and were assigned to the mineral base oil. When the same spot was probed at 10 mW laser power in Step 2, distinct MoS_2 peaks were observed at 370 cm^{-1} and 399 cm^{-1}, these peaks were not observed in Step 1. To determine whether the appearance of the MoS_2 peaks was a result of the increased laser power, which increased the signal-to-noise ratio, the same spot was then probed at 1 mW laser power in Step 3. It was observed that the MoS_2 peaks remained distinct even at the lower laser

power. The fact that MoS$_2$ peaks were not initially observed at low laser power but were visible at low laser power after radiation with high laser power suggests laser-induced transformation of the adsorbed MoDTC to MoS$_2$ upon radiation at high laser power.
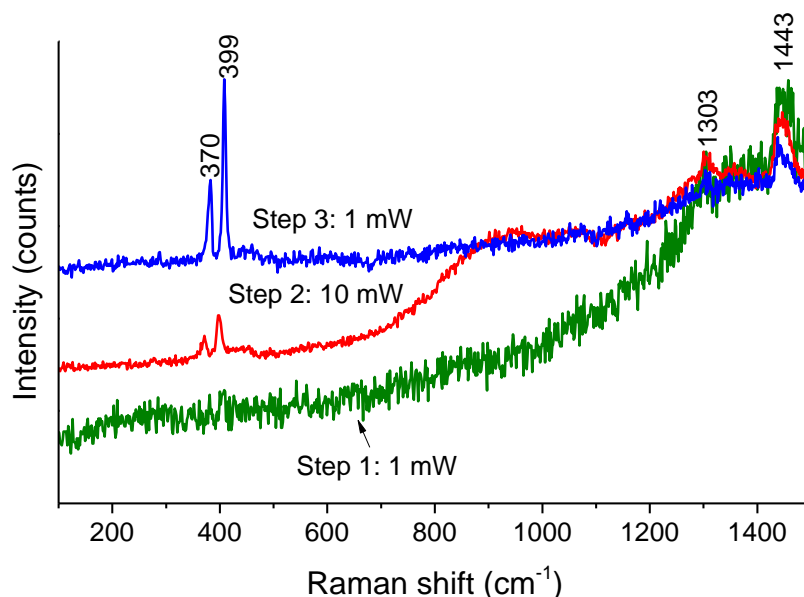
Figure 5-10. Spectra obtained from the same spot in three consecutively steps from Step 1 to Step 3 at laser power indicated in the Figure. All spectra were obtained at 1s exposure time

To further study the possibility of laser-induced transformation of MoDTC thermal films, spectra were obtained at 10 mW laser power and at longer laser exposure time (20s). Figure 5-11 shows two spectra obtained from the same spot using the 10 mW laser power at 1s and 20s exposure times. The first spectrum was obtained using 10 mW laser power at 1s exposure time. The second spectrum was then obtained at 20s exposure time. When the spot was initially analysed at 1s exposure time, MoS$_2$ peaks were observed but when the exposure time was increased to 20s, several additional peaks were observed. The additional peaks were due to formation of MoO$_2$ [138]. Figure 5-12 shows other spectra obtained at 10 mW, 20s exposure time from different positions on MoDTC thermal film. Additional peaks were observed at 661, 818 and 991 cm^{-1} and were assigned to MoO$_3$ [100].
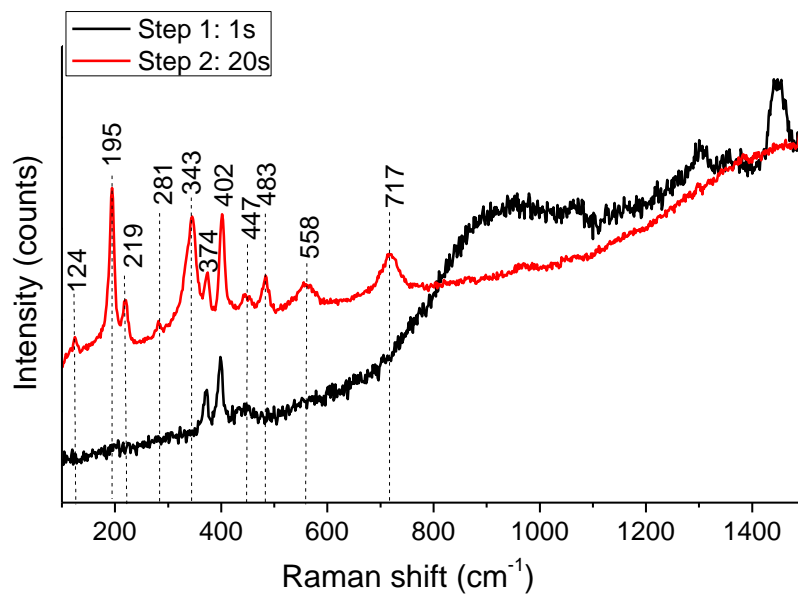
Figure 5-11. Raman spectra of MoDTC thermal films obtained from the same spot with 10 mW laser power in two consecutive steps. In Step 1 the spectrum was obtained at 1s exposure time. In Step 2, the spectrum was obtained at 20s exposure time
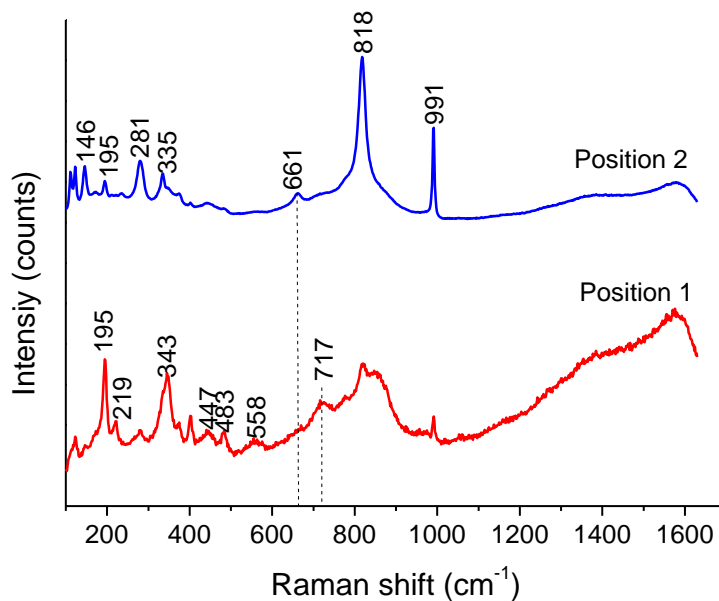
Figure 5-12. Raman spectra obtained from different positions on MoDTC thermal film. The spectra were obtained at 10 mW laser power, 20s exposure time

Table 5-4 summarises the chemical composition of MoDTC thermal films at different Raman acquisition parameters. By increasing the laser power from 1 mW to 10 mW, MoS_2 peaks appear in spectra obtained from MoDTC thermal films while increasing the exposure time at 10 mW laser power results in peaks assigned to MoO_2 and MoO_3 being observed in the obtained spectra. From these results it can be seen that spectra obtained from MoDTC thermal films are significantly affected by the laser power and exposure time.

Table 5-4. Chemical composition of MoDTC thermal films at different Raman acquisition parameters

Laser power	Exposure time	Chemical composition
1 mW	1s	MoDTC lubricant
10 mW	1s	MoS_2
	20s	MoS_2, MoO_2, MoO_3

5.6   Summary

- Mineral base oil has strong Raman signals which make it difficult to detect peaks from MoDTC additive in MoDTC lubricants.

- Heating MoDTC additive concentrate at 100ºC in air for 1h results in decomposition of MoDTC to an amorphous molybdenum sulphur compound (MoS_x).

- Heating 1 wt% MoDTC lubricant in air at 150ºC did not result in decomposition of MoDTC after 3h. However, after heating the lubricant for 5h, MoDTC decomposed and brown deposits appeared in the lubricant. Raman analysis of the brown deposits showed that they were composed of MoS_x.

- Addition of Fe_3O_4 to MoDTC lubricant resulted in decomposition of MoDTC to MoS_2 and $FeMoO_4$ at 100ºC.

- Raman analysis of MoDTC thermal films formed after 1h at low laser powers showed that the thermal films were composed of the MoDTC.

- Analysis of MoDTC lubricant films at high laser powers and longer exposure times led to laser-induced reactions which resulted in formation of MoS_2, MoO_2 and MoO_3.

Chapter 6

Selection of parameters for Raman spectra acquisition of MoDTC tribofilms

6.1   Introduction

Chemical characterisation of MoDTC tribofilms with Raman spectroscopy is key for achieving the objectives of this thesis. With this technique, spectra are obtained from MoDTC tribofilms and based on the peaks in the spectra the chemical composition of the films is determined. Previous Raman studies have shown MoDTC tribofilms to be composed of MoS_2 [57]. As discussed in Section 3.6, the Raman spectrum of MoS_2 is affected by laser acquisition parameters such as laser wavelength, power, exposure time and polarisation. Depending on the laser acquisition parameters the chemical composition obtained from Raman analysis can be an artefact of the analysis and not the actual chemical composition of the sample. Fluorescence is also an important aspect to consider when obtaining Raman spectra from MoDTC samples as it can greatly affect analysis. Fluorescence is dependent on the laser wavelength. If fluorescence occurs during Raman spectra acquisition, it causes the spectrum to have broad peaks which obscure peaks due to Raman scattering. The resulting Raman spectrum will therefore be less informative [139]. It is therefore important to have good understanding of the influence of these laser parameters so as to ensure that accurate characterisation of MoDTC tribofilms is conducted.

In this Chapter, the influences of laser parameters during Raman analysis of MoDTC tribofilms are investigated. The MoDTC tribofilms analysed in this Chapter were generated using the high speed pin-on-disc tribometer. Tribological tests were conducted using 0.5 wt% MoDTC lubricant at 100ºC, 200 rpm (0.3 m/s), 2.12 GPa for 1h.

6.2   Influence of laser wavelength

The laser wavelength can significantly alter the Raman spectra of MoS_2 especially when the wavelength is close to the absorption band of MoS_2 which occurs at 590 nm and 650 nm [101]. The Raman equipment used in the analysis has 488 nm and 785 nm wavelength lasers. The influence of these two laser wavelengths on spectra obtained from MoDTC tribofilms was investigated.

Figure 6-1 (a) shows a typical Raman spectrum obtained from MoDTC tribofilms using the 488 nm wavelength laser. A Raman spectrum of MoS_2 microcrystalline powder has been included as a reference for MoS_2 peaks. Assignment of Raman peaks is shown in Table 6-1. In the spectrum obtained from MoDTC tribofilm, MoS_2 first-order modes were observed. This is in agreement with previous reports [12, 57]. A broad peak was also observed around 200 cm^{-1}. Assignment of the broad peak at 200 cm^{-1} is discussed in detail in Chapter 7. In the spectrum obtained from MoS_2 microcrystalline powder, MoS_2 first-order and second-order peaks were observed. It was interesting to observe second-order peaks when the 488 nm laser was used as its energy is far from the MoS_2 absorption bands.

Figure 6-1 (b) shows spectra obtained with the 785 nm wavelength laser. The spectrum from MoDTC tribofilm did not show any significant peaks except for the peak at 410 cm^{-1} and the broad peak round 1300 cm^{-1}. A high background was observed in the region where MoS_2 first-order modes were expected to be observed. It was puzzling that when the same spot showed MoS_2 peaks when probed with the 488 nm laser, no MoS_2 peaks were observed when the laser was switched to 785 nm laser. When MoS_2 powder were analysed with 785 nm laser, first-order and second-order MoS_2 peaks were observed.
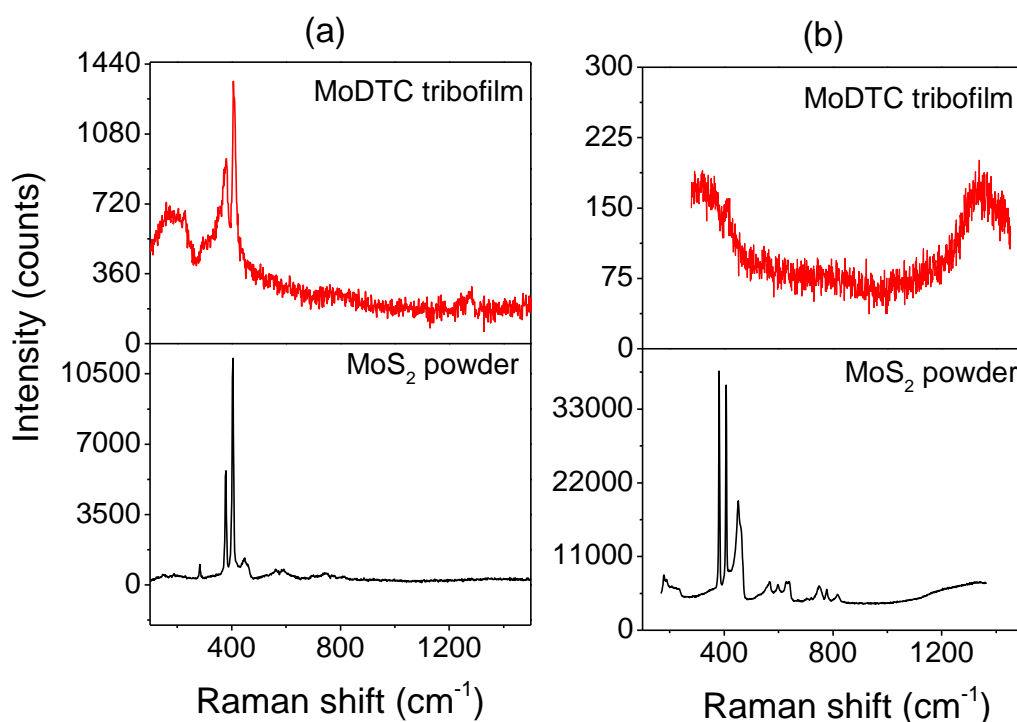
Figure 6-1. (a) Raman spectra of MoDTC tribofilm and MoS$_2$ microcrystalline powder obtained using the 488 nm wavelength laser at 1 mW laser power, 1s exposure time, 20 accumulations. (b) Raman spectra of MoDTC tribofilm and MoS$_2$ microcrystalline powder obtained using the 785 nm wavelength laser at 22 mW laser power, 1s exposure time, 1 accumulation. The spectra are plotted on different scales as indicated.

The peak frequency of MoS$_2$ first-order peaks obtained by different lasers are expected to be similar except when lasers close to the absorption band of MoS$_2$ are used. When the laser wavelength is close to the absorption band of MoS$_2$, additional peaks are observed and both the peak frequency and intensity of the first-order peaks can be altered. Since MoS$_2$ first-order and second-order peaks were observed in MoS$_2$ powder with both 785 nm and 488 nm lasers it was expected that first-order peaks would be observed in spectra from MoDTC tribofilm when probed with the 785 nm laser. However, this was not the case even when the laser power and exposure times were increased.

Table 6-1. Assignment of Raman peaks from spectra obtained from MoDTC tribofilms and MoS$_2$ powder

Laser wavelength	Sample	Raman peak (cm^{-1})	Assignment	
488 nm	MoDTC tribofilm	380	E^1_{2g}	MoS$_2$ first-order peaks
		409	A_{1g}	
	MoS$_2$ powder	281	E_{1g}	MoS$_2$ first-order peaks
		374	E^1_{2g}	
		400	A_{1g}	
		444	2LA(M)	MoS$_2$ second-order peaks
		458	A_{1u}	
		555	$2E_{1g}$	
		584	E^1_{2g} + LA(M)	
		738	$2E^1_{2g}$	
		812	$2A_{1g}$	
785 nm	MoDTC tribofilm	410		
		1300		
	MoS$_2$ powder	382	E^1_{2g}	MoS$_2$ first-order peaks
		407	A_{1g}	
		452	2LA(M)	MoS$_2$ second-order peaks
		464	A_{1u}	
		562	$2E_{1g}$	
		598	E^1_{2g} + LA(M)	
		640	A_{1g} + LA(M)	
		749	$2E^1_{2g}$	
		778	A_{1g} + E^1_{2g}	
		817	$2A_{1g}$	

In a study by Miklozic et al. [57], MoDTC tribofilms were analysed using the 532 nm wavelength laser and MoS$_2$ peaks were observed at 382 cm^{-1} and 412 cm^{-1}. MoS$_2$ peaks have also been observed using the 632 nm wavelength laser in wear scars generated using fully formulated lubricants [140]. The reason why MoDTC tribofilms could not be characterised with the 785 nm laser is not clear yet. Since no significant peaks were observed when the

785 nm laser was used, only the 488 nm laser was used in subsequent Raman analysis in this Chapter.

6.3   Influence of laser power

Thin films are easily damaged or transformed by lasers especially when high laser powers and long exposure times are used [141, 142]. It is therefore important to study the effect of laser power on MoDTC tribofilms for accurate chemical characterisation. The Raman equipment that was used was equipped with a microscope. It was therefore possible to obtain optical images of the wear scar before and after Raman analysis in order to physically determine whether laser damage had occurred or not. Figure 6-2 shows optical images of the tribopair wear scars. As can be seen the ball wear scar had a smoother morphology compared to the disc wear scar. Due to the rough nature of the disc wear scar it was difficult to observe any physical changes that occurred as a result of laser damage. On the other hand, the smooth topography of the ball wear scar allowed changes on the tribofilm due to laser damage to be observed. The effect of laser power on MoDTC tribofilms was observed to be similar on both the ball and the disc wear scars. Here, only the results from the ball wear scar are presented since it was also possible to observe changes on the tribofilm as a result of laser damage.
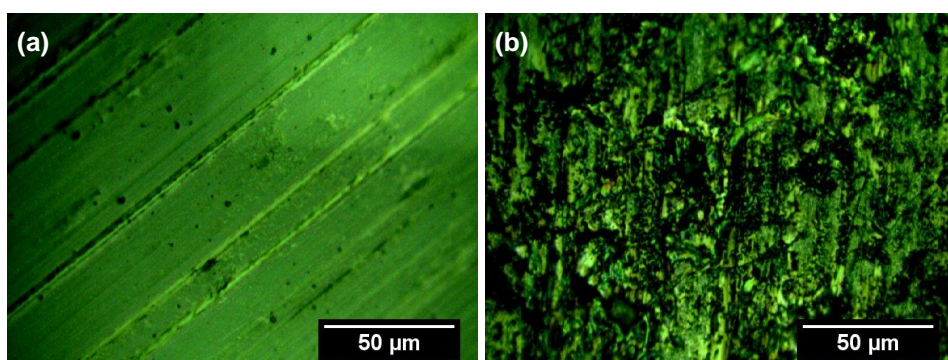
Figure 6-2. Optical images of wear scars on the (a) ball and (b) disc after tests.

Figure 6-3 shows Raman spectra obtained from the ball wear scar at various laser powers ranging from 0.5 mW to 10 mW. It should be noted that all spectra were obtained from the same spot starting with the lowest laser power to the highest. At laser powers lower than 0.5 mW there was very low signal-to-noise ratio (SNR) such that MoS_2 peaks were not clearly distinguished. The SNR increased with increase in laser power and at 5 mW laser power, the SNR was high and MoS_2 peaks were very distinct. At 10 mW laser power, additional peaks were observed at 212 cm⁻¹, 274 cm⁻¹ and 567 cm⁻¹. Also, an additional peak seemed to have formed around 390 cm⁻¹ and overlaps with the E^1_{2g} and A_{1g} peaks. These additional peaks were assigned to the formation of Fe_2O_3 [74]. The analysed region was observed to have developed dark spots after analysis with 10 mW laser power as seen in Figure 6-4. Similar spots were observed at 1 mW and 5 mW when the exposure time was increased.
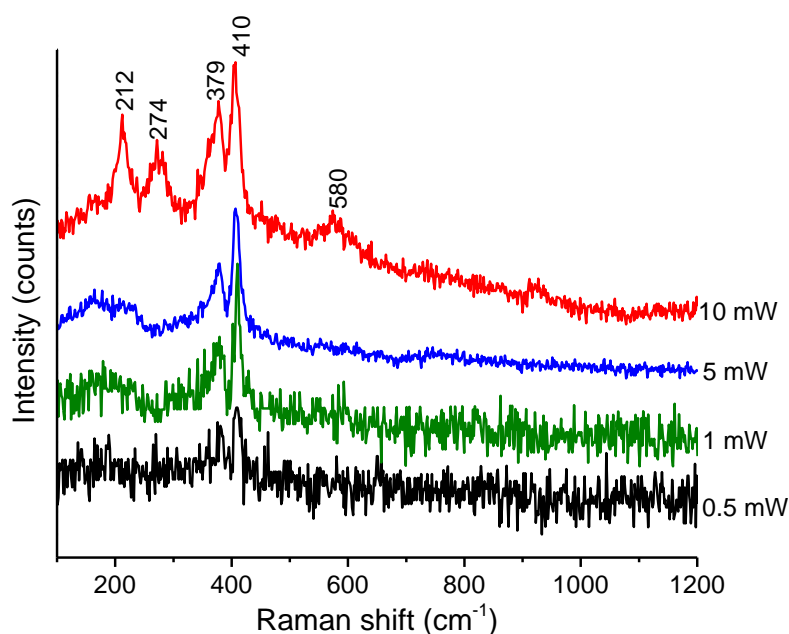
Figure 6-3. Raman spectra of MoDTC tribofilm generated on the ball wear scar after 60 minutes sliding. The spectra were acquired with 488 nm wavelength laser at various laser powers. The spectra were obtained at 1s exposure time and 1 accumulation. The spectra are plotted on different scales and have been vertically shifted for clarity.
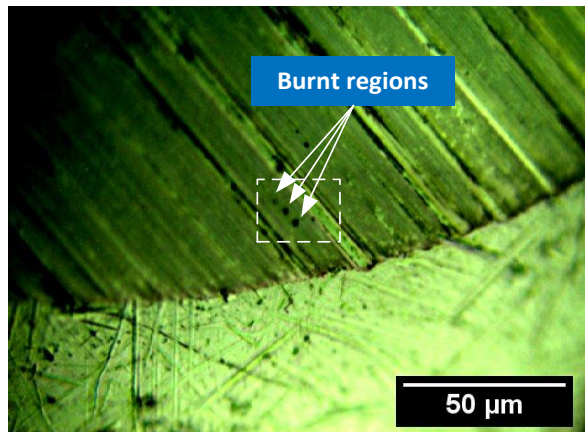
Figure 6-4. Optical image showing dark burn spots on the ball wear scar after analysis at 10 mW laser power

Figure 6-5 shows changes in MoS_2 peak frequencies in MoDTC tribofilms with increase in laser power. There were only slight changes when the laser power was increased from 0.5 mW to 10 mW. The E^1_{2g} peak shifted from 380 cm⁻¹ to 379 cm⁻¹ while the A_{1g} peak shifted from 410 cm⁻¹ to 406 cm⁻¹ (-4 cm⁻¹).
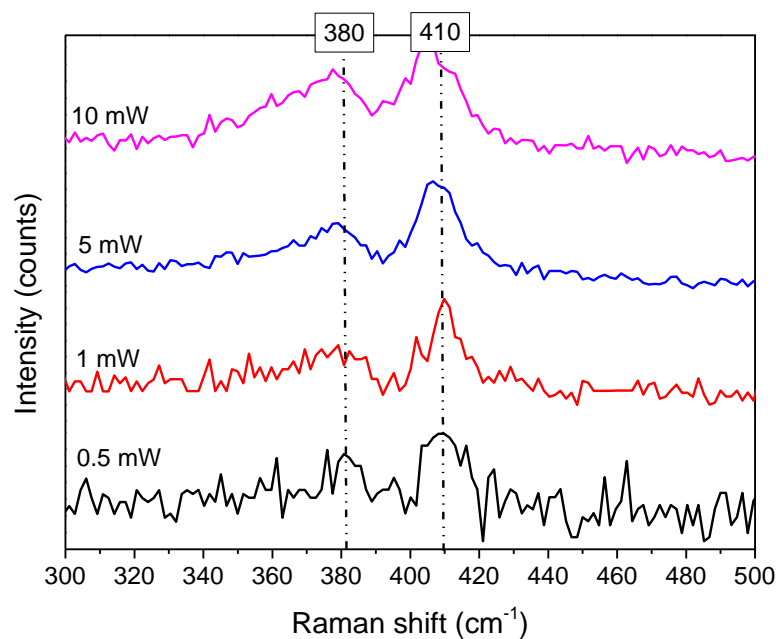
Figure 6-5. Influence of laser power on MoS_2 peak frequencies in MoDTC tribofilms. The spectra were obtained with 488 nm laser at 1s exposure time, 1 accumulation.

The effect of laser power on MoDTC tribofilms was compared to that of MoS$_2$ microcrystalline powder. Figure 6-6 shows spectra obtained from MoS$_2$ powder at various laser powers. Above 0.5 mW laser power, the intensity of MoS$_2$ peaks decreased with increase in laser power. At laser powers above 1 mW, MoS$_2$ powders were partially oxidised to MoO$_3$ as evidenced by dark spots on the powder sample after analysis and the emergence of strong peaks at 817 cm^{-1} and 989 cm^{-1} and less intense peaks at 227 cm^{-1}, 279 cm^{-1} and 334 cm^{-1} [72]. It has been proposed that the reaction shown in Equation 6-1 occurs in MoS$_2$ at high laser powers [100].
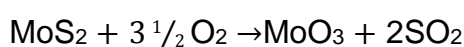
$$MoS_2 + 3\,^1/_2\,O_2 \rightarrow MoO_3 + 2SO_2 \hspace{3cm} 6\text{-}1$$
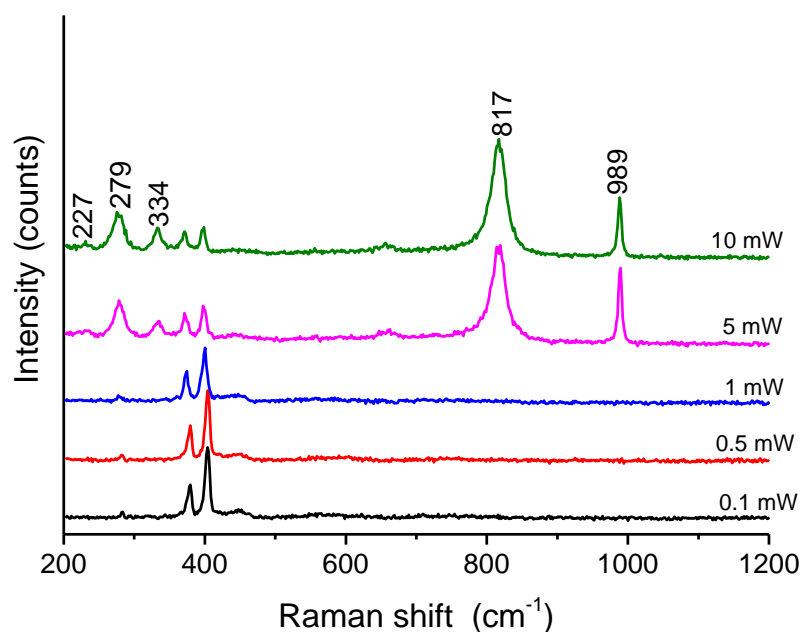
Figure 6-6. Raman spectra of MoS$_2$ microcrystalline powder obtained with 488 nm laser at various laser powers as indicated in the Figure. The spectra were obtained at 1s exposure time and 1 accumulation. The spectra are plotted on the same scale and have been shifted vertically for clarity.

Significant differences were observed when MoS$_2$ powders and MoDTC tribofilms were damaged by the laser. In MoS$_2$ powder, prominent MoO$_3$ peaks were observed whereas in MoDTC tribofilms iron oxide peaks were observed.

95

Figure 6-7 shows the influence of laser power on MoS_2 peak frequencies in microcrystalline MoS_2 powder. It was observed that when the laser power was increased from 0.01 mW to 10 mW, the E^1_{2g} peak shifted from 382 cm⁻¹ to 371 cm⁻¹ while the A_{1g} peak shifted from 408 cm⁻¹ to 398 cm⁻¹ (-10 cm⁻¹). The red shift to lower wavenumbers with increase in laser power is in agreement with previous literature [111].

Compared to MoDTC tribofilms, laser power had a greater influence on MoS_2 peak positions in MoS_2 powder. MoS_2 in MoDTC tribofilms is present in a carbon matrix. The high laser energies at high laser powers are therefore easily dissipated away from MoS_2 by the carbon matrix. This would explain why the peak frequency shift at high laser powers was not as large in MoDTC tribofilms as it was in MoS_2 powder.
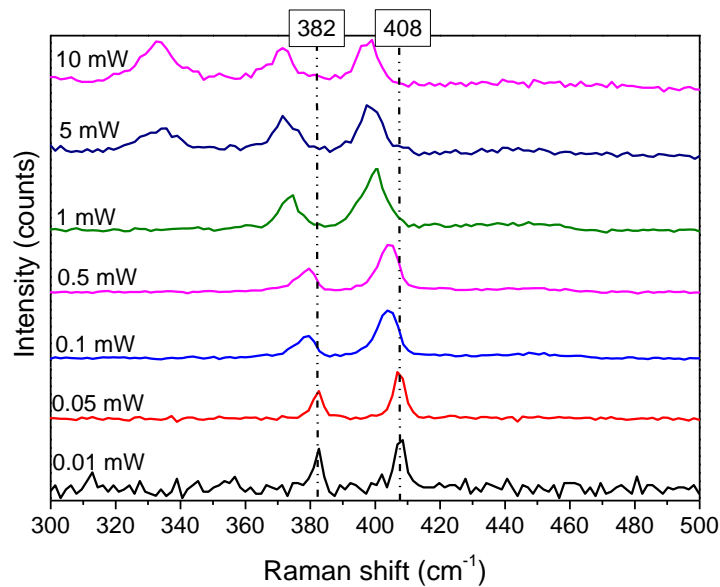
Figure 6-7. Influence of laser power on MoS₂ peak frequency in microcrystalline powder. The spectra were obtained with 488 nm laser at 1s exposure time, 1 accumulation.

Due to the sensitivity of the MoDTC tribofilms to laser damage at higher laser powers, spectra of tribofilms presented in the following sections were obtained at 1 mW laser power. To improve the SNR, at least 20 accumulations were

obtained in each spectra acquisition. It was observed that increasing the number of accumulation did not damage the sample since burn spots were not observed on the tribofilm and no additional peaks were observed on the acquired spectra.

6.4   Influence of exposure time

To further understand the influence of lasers on MoDTC tribofilms, the influence of laser exposure time at high laser powers was also investigated. Figure 6-8 shows spectra obtained at 10 mW laser power at 1s and 20s exposure times.
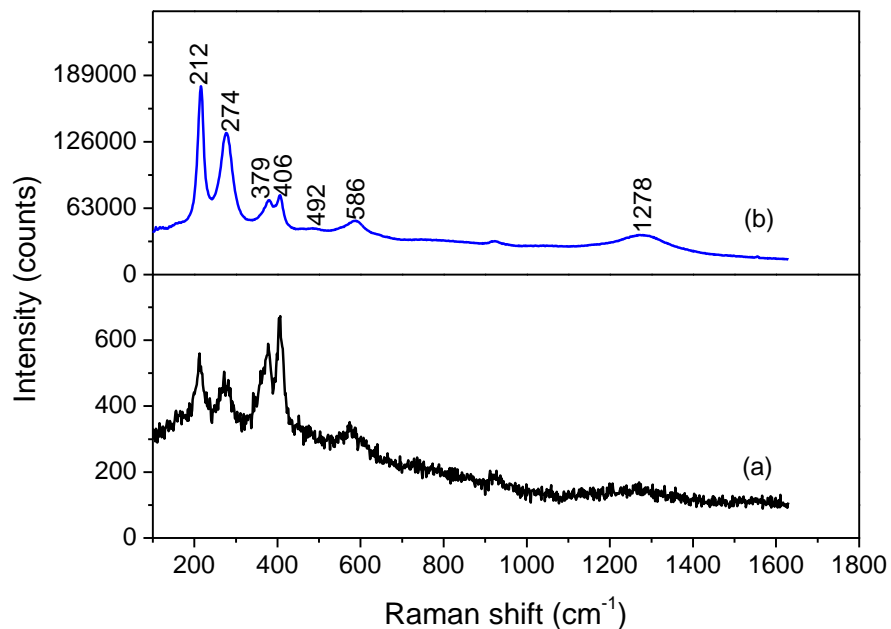
Figure 6-8. Raman spectra of MoDTC tribofilm obtained at 10 mW laser power at (a) 1s and (b) 20s exposure time.

In both Raman spectra, peaks were observed at 212 cm^{-1}, 274 cm^{-1}, 379 cm^{-1}, 406 cm^{-1}, 492 cm^{-1}, 586 cm^{-1} and 1278 cm^{-1}. The peaks at 379 cm^{-1} and 406 cm^{-1} were assigned to MoS$_2$ vibration modes. The intensity of the 212 cm^{-1} and 274 cm^{-1} peaks in relation to MoS$_2$ peaks increased with exposure time. As mentioned earlier in Section 6.3, it was observed that at 10

mW laser power a peak around 390 cm⁻¹ emerged in the region where MoS_2 peaks are observed peaks. At 20s exposure time, the intensity of this peak (around 390 cm⁻¹) was also seen to increase such that it almost completely overlapped the MoS_2 peaks. At longer exposure times the intensity of this peak increased and completely overlapped the MoS_2 peaks resulting in a broad single peak such that the MoS_2 double peak could not be distinguished from the spectrum. The peaks observed at 212 cm⁻¹, 274 cm⁻¹, 390 cm⁻¹, 492 cm⁻¹, 586 cm⁻¹ and 1278 cm⁻¹ are believed to be due to formation of haematite (Fe_2O_3) within the tribofilm at high laser powers. It is noteworthy to mention that MoS_2 in MoDTC tribofilm was not partially oxidised to MoO_3 even with increased laser power and exposure time.

6.5   Influence of laser polarisation

Raman spectra obtained from MoS_2 crystals are greatly influenced by the polarisation of the laser used due to the crystal lattice layer structure [97]. Figure 6-9 shows spectra obtained from the same spot within MoDTC tribofilms. The spectra were obtained using three laser polarisations: circular, normal and orthogonal. In all the spectra, MoS_2 E^1_{2g} and A_{1g} peaks were observed at 380 cm⁻¹ and 410 cm⁻¹, respectively. Although there were no differences in the peak intensities, slight differences in the A_{1g}/E^1_{2g} peak intensity ratio were observed. The A_{1g}/E^1_{2g} ratio was 1.54, 2.14 and 1.90 for circular, normal (*s-*) and orthogonal (*p-*) polarisation, respectively.

Since the laser polarisation did not seem to affect Raman spectrum from MoDTC tribofilms, the normal polarisation was selected to be used in obtaining Raman spectra presented elsewhere in this Chapter and subsequent Chapters.
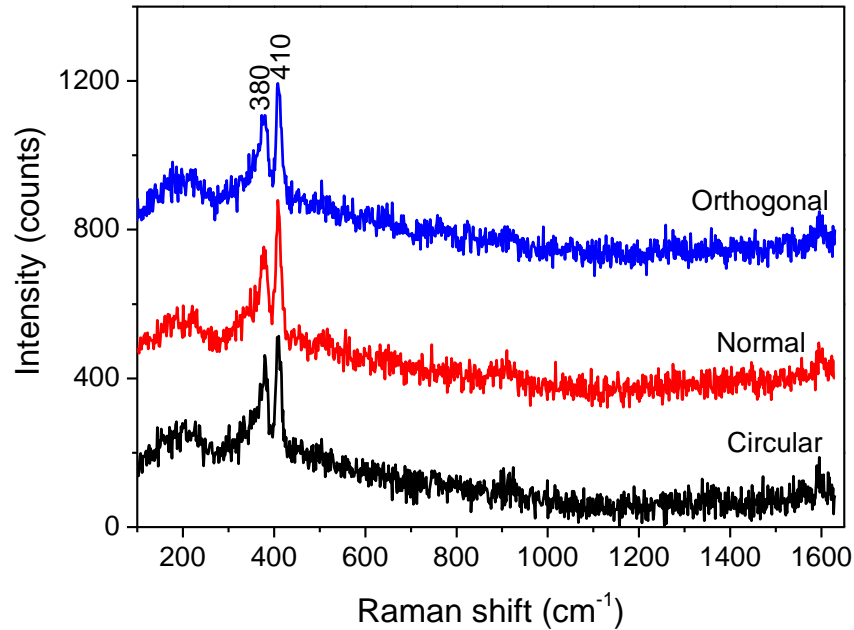
Figure 6-9. Raman spectra obtained from MoDTC tribofilm at different laser polarisations. Spectra were obtained at 1 mW, 1s exposure time, 20 accumulations.

6.6   Summary

- Raman spectra of MoDTC tribofilms obtained with the 488 nm laser show distinct MoS_2 peaks while spectra obtained with the 785 nm wavelength laser have a high background which obscures MoS_2 peaks from being observed.

- Raman analysis of MoDTC tribofilm obtained with 488 nm laser revealed that MoS_2 second-order peaks were observed in microcrystalline MoS_2 powder and not in MoDTC tribofilms.

- Spectra acquisition at higher laser powers and longer exposure times causes laser damage to samples and dark spots are observed after analysis. Laser damage results in additional iron oxide peaks being observed in MoDTC tribofilms. In MoS_2 microcrystalline powder, laser damage causes MoO_3 peaks to be observed due to partial oxidation of MoS_2. Proper care should be taken with regard

to laser power and exposure times when obtaining spectra from MoDTC tribofilms to avoid wrong interpretation of the spectra.

- Laser power does not affect MoS_2 peak frequencies in MoDTC tribofilms as much as it does in microcrystalline MoS_2 powder.

- Laser polarisation used in this study did not significantly affect the spectra pattern obtained with the 488 nm wavelength laser.

Based on the results in this Chapter, Raman analysis of MoDTC tribofilms in subsequent Chapters was carried out with the 488 nm wavelength laser at 1 mW laser power, 1s exposure time. Several accumulations (20-100) were obtained in each spectrum to improve the signal to noise ratio. Spectra were obtained under normal laser polarisation.

Chapter 7

Surface chemistry changes during evolution of MoDTC tribofilms and the influence of oil layer during Raman analysis of MoDTC tribofilms

7.1 Introduction

Previous studies have shown that tribotests with MoDTC-containing lubricants have unique friction behaviour. During the beginning of the test there is high friction and after rubbing for a few minutes there is an abrupt and rapid friction drop to lower friction values. Post-test analysis with X-ray Photoelectron Spectroscopy (XPS) and Raman spectroscopy reveal that the rubbed surfaces contain MoS_2. The formed MoS_2 is believed to be responsible for the low friction observed at longer rubbing times. It is therefore of interest to understand how the surface chemistry changes at the contact interface during the initial stages of tests with MoDTC lubricants.

In this Chapter, Raman spectroscopy was employed to understand the evolution of MoDTC tribofilms and how this impacts friction behaviour. Raman analysis does not require samples to be cleaned prior to analysis as is the case with vacuum-based techniques such as XPS. Raman spectroscopy thus shows great potential as an *in-situ* analysis technique for lubricated contacts. To investigate the capability of Raman spectroscopy in analysing uncleaned rubbed contacts, the influence of the oil layer during Raman analysis of MoDTC tribofilms was also studied. Tribotests were carried out using the high speed pin-on-disc tribometer at 0.5 wt% MoDTC, 100ºC, 200 rpm (0.3 m/s), 2.12 GPa.

7.2 Friction results

Figure 7-1 shows friction curves obtained during tests with MoDTC lubricant. For comparison, friction curves of tests conducted under dry lubrication and mineral base oil are also included. The test under dry lubrication was stopped after rubbing for 5 minutes due to cold welding of the disc and the ball. The friction coefficient was μ=0.13 at the end of the test. In tests carried out in base oil, friction was high (μ=0.10) at the beginning of the test and increased gradually during the duration of the test. The friction coefficient at the end of the test was μ=0.12. The friction coefficient in tests with base oil was slightly lower than that observed under dry lubrication. In tests with MoDTC lubricant, friction was high at the beginning of the test (μ=0.10) for a few minutes before rapidly dropping to lower values. Steady low values of about μ=0.06 were obtained at the end of the test. The induction time, which is the time taken from the beginning of the test to the time when low friction is obtained, was 2 minutes.
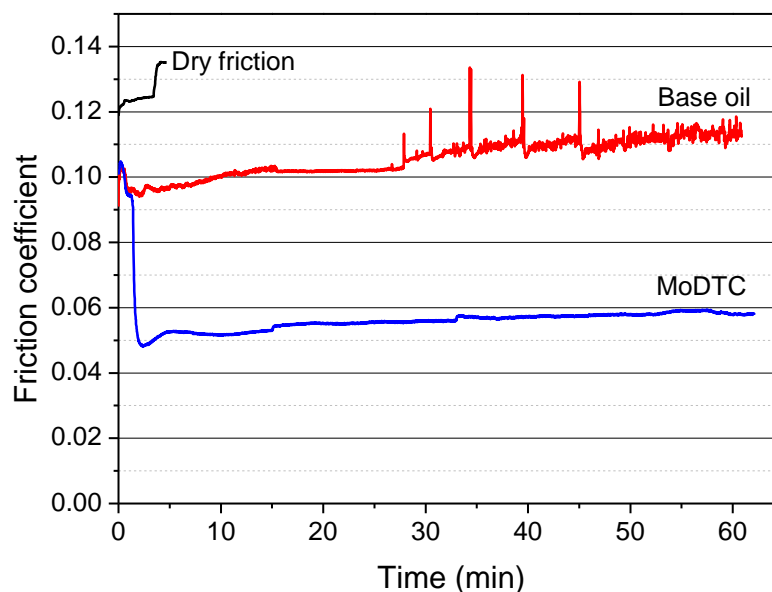
Figure 7-1. Friction curves during tests carried out under dry friction (without any lubricant), mineral base oil and 0.5 wt% MoDTC lubricant. Tests were conducted at 200 rpm (0.3 m/s), 2.12 GPa, 100ºC

In order to study changes in surface chemistry that occur at the tribocontact in the initial stages of the tests with MoDTC lubricant, separate tests were conducted at shorter test durations; 1, 2, 5 and 20 minutes. Figure 7-2 shows the friction curves obtained during these short duration tests. In the test carried out for 1 minute, friction was still high (μ=0.13) at the end of the test. The 2 minute tests were stopped once the friction had dropped down to μ=0.06. The 5 and 20 minute tests showed low friction at the end of the test (μ=0.05-0.06) and had a 2 minute induction time.
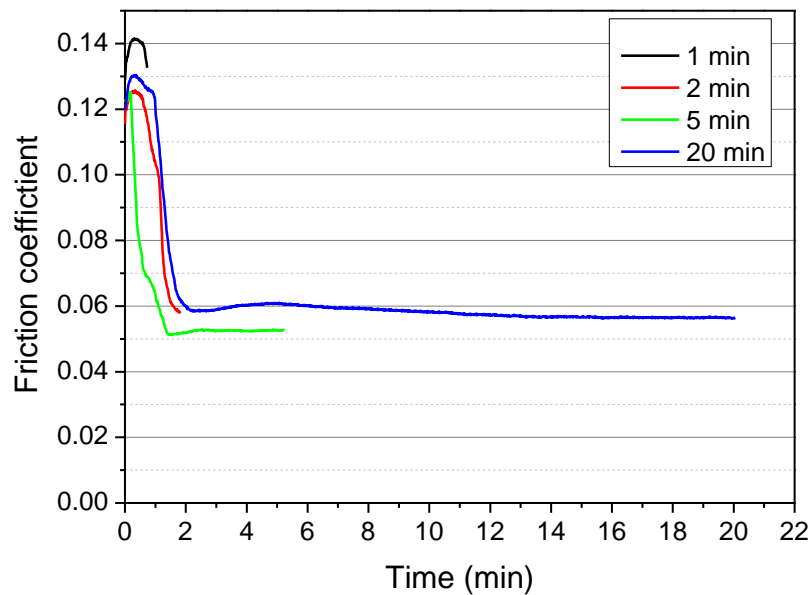
Figure 7-2. Friction curves obtained during tests with 0.5 wt% MoDTC lubricant at shorter test durations. Tests were conducted at 200 rpm (0.3 m/s), 2.12 GPa, 100ºC

7.3   Morphology of wear scars

Figure 7-3 show optical images of tribopair wear scars after tests under no lubrication, with mineral base oil and MoDTC lubricant. In the dry friction test, the ball wear scar had numerous grooves. The disc wear scar was also very severely worn out. Although tests under dry friction were carried out for only 5 minutes, the ball wear scar diameter was the largest (1227 μm) compared to tests with mineral base oil (808 μm) and MoDTC (372 μm). The presence

of MoDTC additive in mineral base oil not only reduced friction but also reduced wear of the steel ball. The improved wear performance with MoDTC lubricant over base oil is in agreement with previous reports [143].

| Balls | Discs |

(a)

(b)

(c)
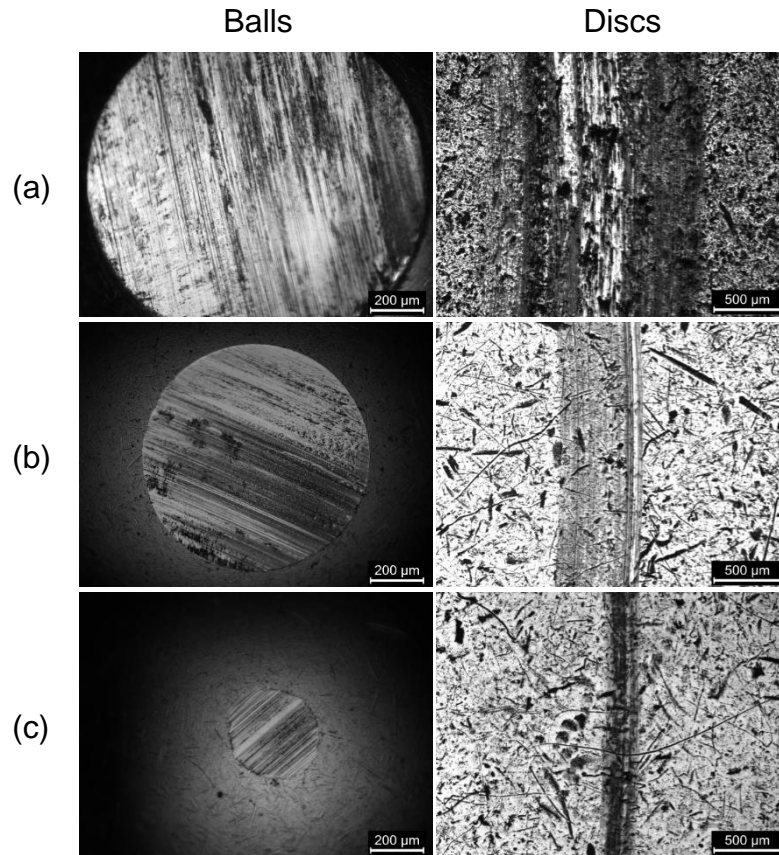
Figure 7-3. Optical images of ball and disc wear scars after 60 minutes tests (a) under dry friction (b) mineral base oil (c) MoDTC lubricant

Figure 7-4 shows optical images of the wear scar of the tribopair after tests with MoDTC at short test durations. The ball wear scar after 1 minute tests was covered with dark films in some regions. The morphology inside the disc wear scar was not significantly different from that outside the wear scar. The wear scar was only slightly polished and has a brownish colour. Tribopair wear scars after 2 minute tests were similar to those observed after 1 minute tests. In the 5 minute tests, the ball wear scar was covered with a film (dark green regions). The ball wear scar after 20 minute test was also covered with a film although numerous grooves were observed.
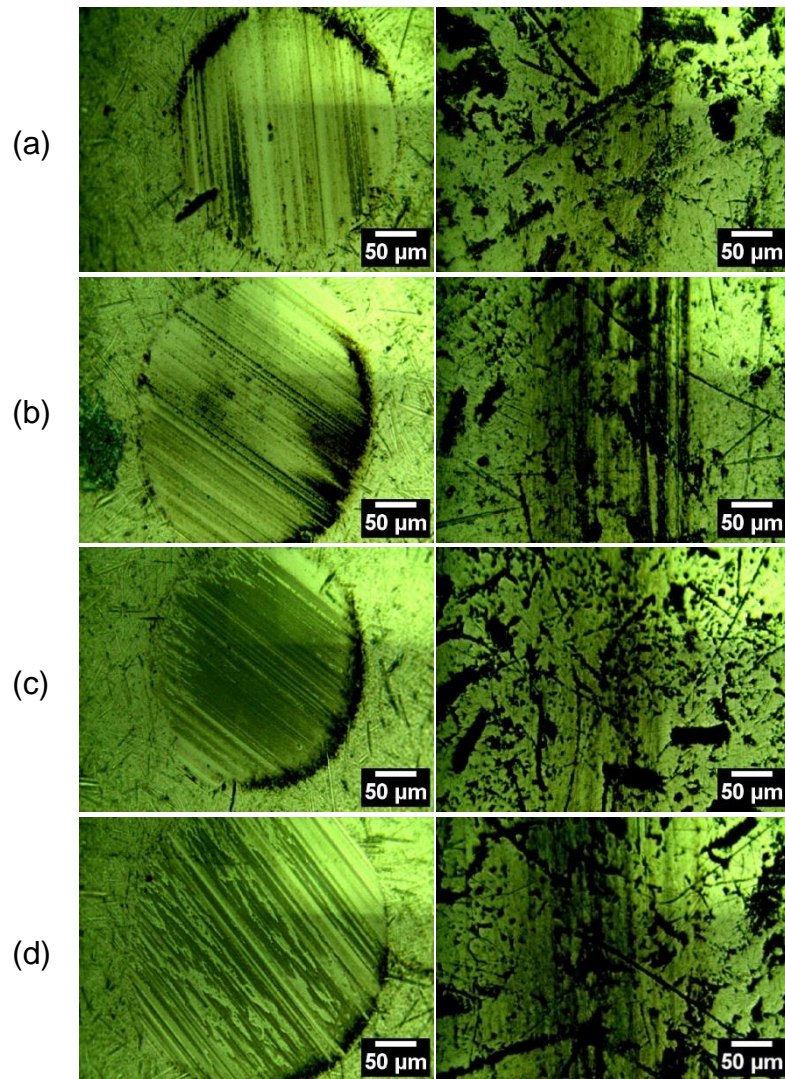
Figure 7-4. Optical images of ball (left) and disc (right) wear scars after with MoDTC at different test durations. (a) 1 minute (b) 2 minutes (c) 5 minutes (d) 20 minutes

7.4   Raman analysis: Tests without MoDTC additive

Figure 7-5 shows Raman spectra obtained from the tribopair wear scars after tests under dry lubrication and with base oil. The peaks at 222 cm⁻¹, 291 cm⁻¹, 404 cm⁻¹, 495 cm⁻¹ and 1322 cm⁻¹ were assigned to haematite (Fe_2O_3), while peaks at 310 cm⁻¹, 540 cm⁻¹ and 666 cm⁻¹ were assigned to magnetite (Fe_3O_4). The formation of magnetite in tests using PAO has been reported in a previous study [144].
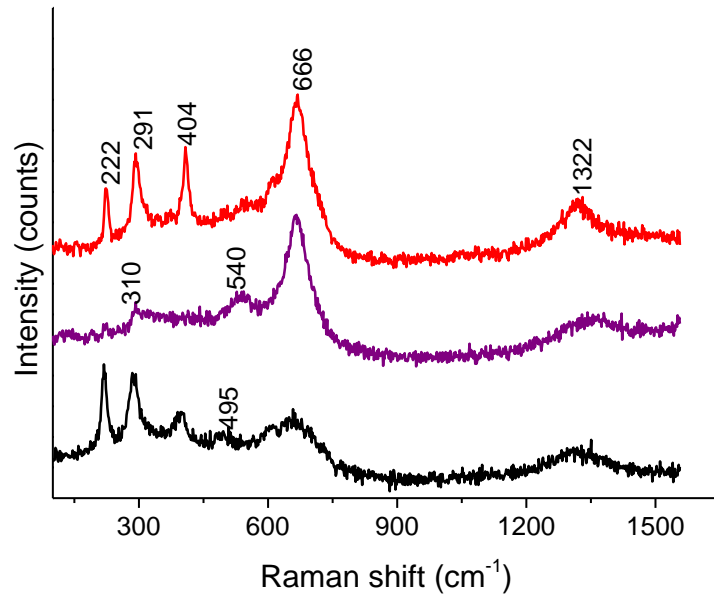
Figure 7-5. Raman spectra obtained from tribopair wear scars after tests under dry friction and with base oil. The 3 spectra were obtainded from different regions on the wear scars and are representative of the spectra obtained from samples

7.5   Raman analysis: Tests with MoDTC

Spectra obtained from different regions on tribopair wear scars after tests with MoDTC at different test durations are shown in Appendix A. The spectral information is summarised in Table 7-1. The broad peak observed in the region 100-250 cm⁻¹ could be due to vibration of sulphur or stress-induced disorder in MoS_2 crystal structure [142, 145]. This is discussed in greater detail in Section 7.7. The broad peak at 335 cm⁻¹ was assigned to the formation of amorphous sulphur-rich molybdenum compounds, MoS_x (x>2). The peak at 925 cm⁻¹ was assigned to stretching of terminal oxygen v(Mo=O) in $FeMoO_4$ [76, 80]. The assignment of the peaks at 335 cm⁻¹ and 925 cm⁻¹ is further discussed in Chapter 8. Less intense peaks at 510 cm⁻¹ and 550 cm⁻¹ were assigned to v(S-S) vibration in molybdenum compounds with bridging sulphur atoms (S_2^{2-}) [80, 146]. The origin of the S-S bond is discussed in Section 7.7.2. The peak observed at 750 cm⁻¹ was assigned to v(Mo-O-Mo) vibration in oxygen bridged molybdenum (V) species [132].

106

Table 7-1. Summary of Raman spectra obtained from tribopair wear scars after tests with MoDTC lubricant at different test durations

Duration	Raman peaks (cm⁻¹)	Notes
1 minute	100-250 (MoS_2) 335 (MoS_x) 380, 410 (MoS_2) 666 (Fe_3O_4) 925 ($FeMoO_4$)	- Spectra varied from spot-to-spot - Trace amounts of MoS_2
2 minutes	100-250 (MoS_2) 335 (MoS_x) 380, 410 (MoS_2) 666 (Fe_3O_4) 925 ($FeMoO_4$)	- Spectra varied from spot-to-spot - Higher coverage of MoS_2
5 minutes	100-250 (MoS_2) 380, 410 (MoS_2) 510 (S-S) 666 (Fe_3O_4)	- Spectra were similar in different regions within wear scars - Less Fe_3O_4 and $FeMoO_4$
20 minutes	100-250 (MoS_2) 380, 410 (MoS_2) 510 (S-S) 666 (Fe_3O_4) 925 ($FeMoO_4$)	- Spectra were similar in different regions within wear scars - Less Fe_3O_4 and $FeMoO_4$
60 minutes	100-250 (MoS_2) 380, 410 (MoS_2) 453 (Mo-S) 510, 550 (S-S) 666 (Fe_3O_4) 750 (Mo-O-Mo) 925 ($FeMoO_4$)	- Spectra were similar in different regions within wear scars - Less Fe_3O_4 and $FeMoO_4$

From Table 7-1, it can be seen that the surface chemistry changed with rubbing time. At the beginning of the test (1 minute), Fe_3O_4 and $FeMoO_4$ were

dominant on the surface. Increasing the rubbing time to 2 minutes resulted in formation of more MoS$_2$ at the contact. With further rubbing, more MoS$_2$ was formed and less FeMoO$_4$ and Fe$_3$O$_4$ were formed.

7.6   Effect of oil layer in Raman analysis of MoDTC tribofilms

Figure 7-6 shows optical images of the uncleaned disc after 60 minutes test with MoDTC lubricant. The wear scar was not easily distinguished due to the presence of an oil layer. At shorter test durations, it was very difficult to distinguish the wear track on unrinsed samples. Thus, although Raman analysis can be carried out on unrinsed samples, one major problem of such analysis is the inability to clearly see the wear track. Brown wear debris were observed on the outside regions of the wear scar. At longer test durations, more wear debris was formed as can be seen in Figure 7-7 where the test was carried out for 6h.
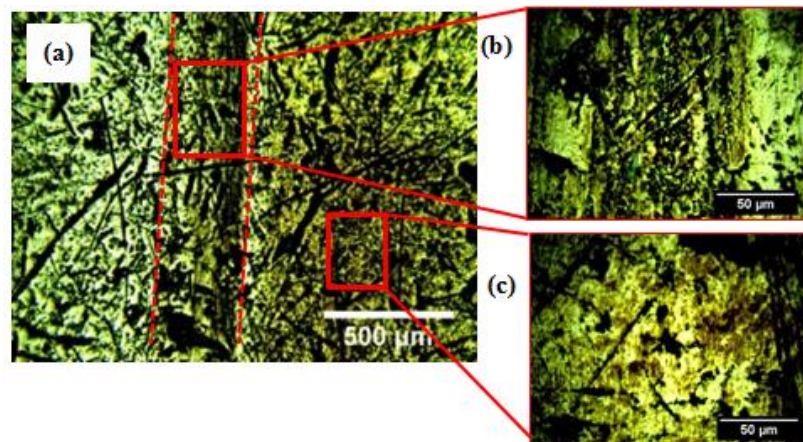
Figure 7-6. (a) Optical image of the uncleaned disc after 60 minutes test with MoDTC lubricant (b) image from inside the wear scar (c) image of wear debris on the disc outside the wear scar
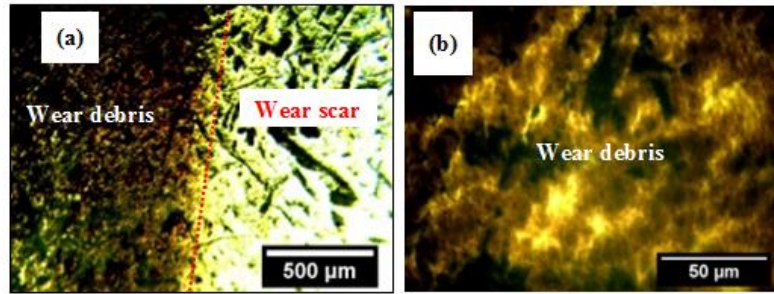
Figure 7-7. (a) Optical images of an uncleaned disc after 6h test with MoDTC (b) Image of wear debris formed outside the wear scar.

Figure 7-8 shows Raman spectra obtained from the uncleaned disc. Spectra from the wear scar show the presence of MoS_2 peaks at 380 cm⁻¹ and 410 cm⁻¹. Peaks at 1069 cm⁻¹, 1149 cm⁻¹, 1302 cm⁻¹ and 1448 cm⁻¹ are from the mineral base oil used to blend the additive. The less intense peaks at 453 cm⁻¹, 510 cm⁻¹, 550 cm⁻¹ and 750 cm⁻¹ which were observed in the wear scar of the rinsed disc could not be observed in the uncleaned disc. Another difference observed between spectra obtained from rinsed and unrinsed discs is that spectra from unrinsed disc had high backgrounds at higher wavenumbers due to fluorescence caused by the presence of the oil layer.
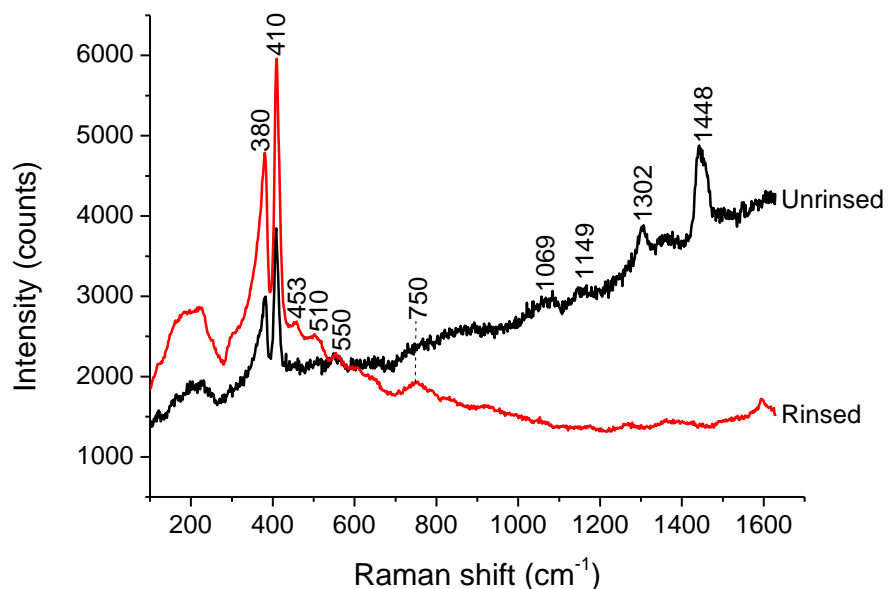
Figure 7-8. Comparison of Raman spectra obtained from rinsed and unrised discs after 60 minutes test with MoDTC lubricant.

Figure 7-9 shows Raman spectra obtained from the wear debris on the unrinsed disc. MoS_2 peaks were observed at 380 cm⁻¹ and 410 cm⁻¹. The presence of MoS_2 in the wear debris is in agreement with high resolution TEM images obtained from wear debris after tests with MoDTC lubricant [56]. Less intense peaks were also observed at 510 cm⁻¹ v(S-S) and 550 cm⁻¹ v(S-S). Peaks at higher wavenumbers are from the mineral base oil. Spectra from the wear debris were very similar to those obtained from within the wear scar indicating that they were formed from wear of MoDTC tribofilm.
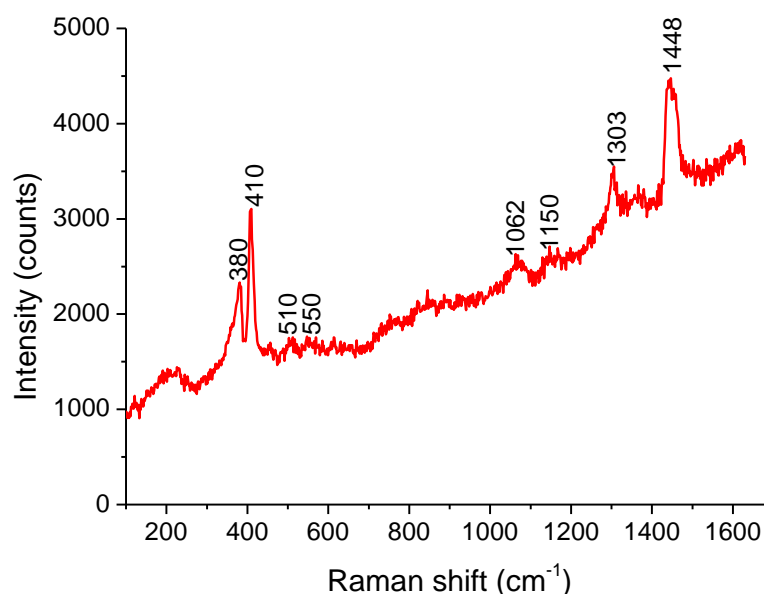
Figure 7-9. Raman spectra obtained from wear debris on the unrinsed disc after 60 minutes test with MoDTC lubricant.

7.7 MoS_2 Raman peaks in MoDTC tribofilms: Comparison with microcrystalline MoS_2 powder

7.7.1 MoS_2 peaks in MoDTC tribofilms

Raman spectra obtained from rinsed samples generated after 60 minutes tests with MoDTC lubricant showed slight differences in MoS_2 peaks when compared to microcrystalline MoS_2 powder. Figure 7-10 shows spectra of MoS_2 powder and MoDTC tribofilms. Spectra from MoDTC tribofilm were

obtained from the ball wear scar and are an average of the spectra shown in Figure A5. The differences observed are as follows:

- The E_{1g} peak at 283 cm⁻¹ observed in MoS_2 powder was not observed in MoDTC tribofilms.

- MoS_2 second-order peaks were observed in MoS_2 powder and not in MoDTC tribofilms.
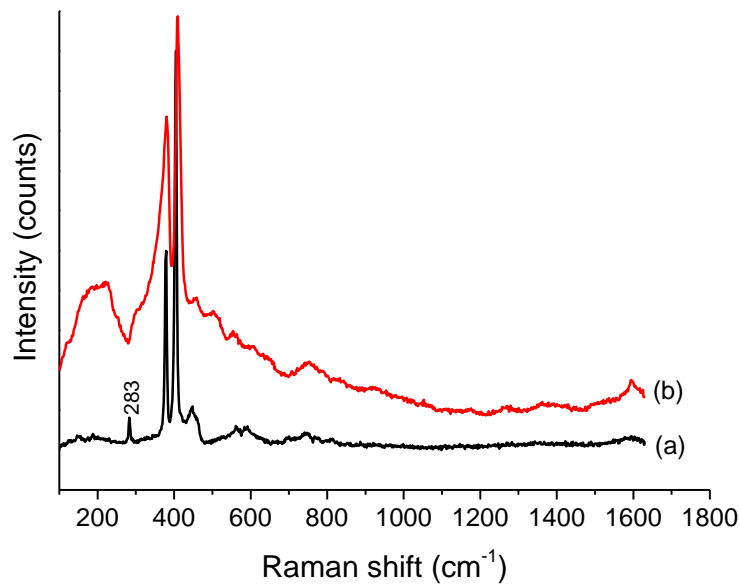
Figure 7-10. Raman spectra obtained from (a) microcrystalline MoS₂ powder (b) MoDTC tribofilm

Figure 7-11 shows the spectra in the region 300 cm⁻¹ to 450 cm⁻¹ where MoS_2 first-order E^1_{2g} and A_{1g} peaks are observed. Table 7-2 shows peak information after curve fitting. The following differences were observed.

- In MoDTC tribofilm, the E^1_{2g} peak was observed to be very broad and asymmetrical compared to that of MoS_2 powder which was narrow and symmetrical. The E^1_{2g} peak in MoDTC tribofilm was fitted better with three Gaussian curves at 354 cm⁻¹, 374 cm⁻¹ and 382 cm⁻¹.

- The A_{1g} peak was broader in MoDTC tribofilm than in MoS_2 powder.

111

- MoS$_2$ peaks in MoS$_2$ powder were observed at lower wavenumber than in MoDTC tribofilm.
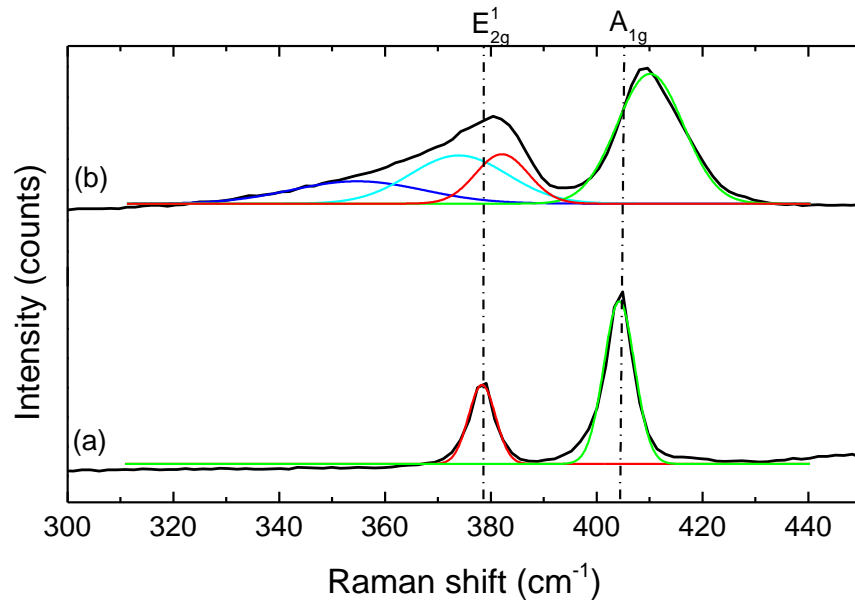
Figure 7-11. Raman spectra showing MoS$_2$ first-order peaks in (a) MoS$_2$ powder (b) MoDTC tribofilm

Table 7-2. MoS$_2$ Raman peak information of MoS$_2$ powder and MoDTC tribofilm

Sample	Peak frequency (cm^{-1})	Peak width (FWHM)
MoS$_2$ powder	378.3	6.0
	404.3	6.9
MoDTC tribofilm	354.7	29.5
	373.9	21.7
	382.1	11.8
	410.1	14.8

Broadening of the E$^1_{2g}$ peaks is indicative of slight disorder in arrangement of Mo and S atoms in the *x-y* plane [75, 147]. Broadening of the A$_{1g}$ peaks can also be due to disorder in the *z*-axis induced by stress during tribological tests. The influence of tribological processes on the crystal structure of MoS$_2$ is discussed in Section 7.7.2.

The presence of MoS_2 peaks at lower wavenumbers in the powder than in the tribofilm can be attributed to the high laser power (1 mW) used to acquire the spectra. As mentioned earlier in Chapter 6, MoS_2 peaks of MoS_2 powder shift to lower wavenumbers with increase in laser power while MoS_2 peaks in MoDTC tribofilms are only slightly affected. At a lower laser power of 0.05 mW, the A_{1g} and E^1_{2g} peaks of MoS_2 powder were observed at 407 cm^{-1} and 382 cm^{-1}, respectively. It can thus be seen that at lower laser powers, the position of MoS_2 peaks in MoS_2 powder are similar to those in MoDTC tribofilms at 1 mW laser power.

It should be noted that for Raman spectra obtained under similar acquisition parameters, the intensity of both MoS_2 peaks was about 10 times higher in MoS_2 microcrystalline powder than in MoDTC tribofilm. The large difference in intensity can be attributed to the highly crystalline nature of the MoS_2 powder compared to MoS_2 in the tribofilm.

7.7.2 Influence of tribological processes on MoS_2 Raman peaks: MoS_2 coatings

Analysis of MoS_2 peaks in MoDTC tribofilms revealed that they were broader and asymmetrical compared to microcrystalline MoS_2 powder (Figure 7-11). Broadening of these peaks was attributed to stress-induced disorder in MoS_2 crystal structure during tribological tests. To verify this hypothesis, it was necessary to subject pure crystalline MoS_2 to tribological process and then conduct Raman analysis on the MoS_2 after tribotest. To simulate tribological process on crystalline MoS_2, steel discs coated with MoS_2 were rubbed against an uncoated steel ball. Tribotests were conducted in the high speed pin-on-disc tribometer under a load of 206 N and 200 rpm (0.3 m/s) speed. The test was conducted at room temperature for 30 minutes and no lubricant was used.

Figure 7-12 shows optical images of the as-prepared MoS$_2$ coatings and the tribopair wear scars after tribotests. From optical images in Figure 7-12 it was observed that MoS$_2$ coating was transferred to the wear scar on the ball. MoS$_2$ from the disc that is transferred to the ball during the rubbing process can experience disorder in its crystal structure due to stress. By analysing Raman spectra obtained from MoS$_2$ transferred on the ball, the influence of tribological processes on MoS$_2$ Raman peaks can be investigated.

| (a) | (b) | (c) |
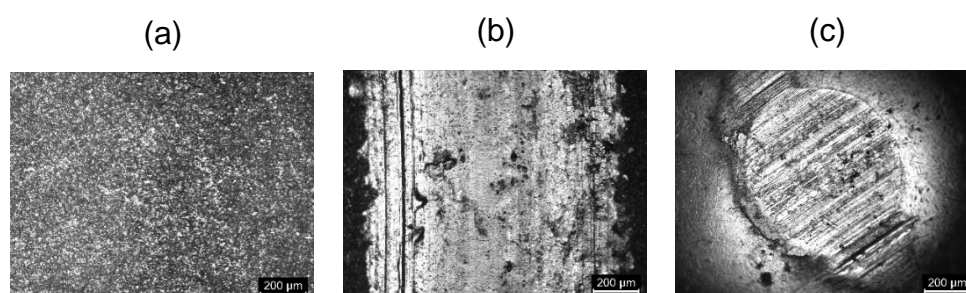
Figure 7-12. Optical images of (a) as-prepared MoS$_2$ coating on steel disc (b) MoS$_2$ coated disc after tribotests (c) ball wear scar after test on MoS$_2$ coated disc

Figure 7-13 (a) shows the spectrum obtained from the as-prepared MoS$_2$ coating. MoS$_2$ first-order peaks were observed at 286 cm⁻¹ (E$_{1g}$), 383 cm⁻¹ (E$^1_{2g}$) and 408 cm⁻¹ (A$_{1g}$). MoS$_2$ second-order peaks were also observed in regions 560-630 cm⁻¹ and 750-820 cm⁻¹. The broad peaks at 1378 cm⁻¹ and 1601 cm⁻¹ were due to the presence of amorphous carbon in the coating [148]. Figure 7-13 (b) shows spectra obtained from different regions on the ball wear scar after tribotests. MoS$_2$ peaks were observed in the spectra indicating that MoS$_2$ from the coated disc was transferred to the ball during rubbing. The following differences were observed between spectra from the ball wear scar and as-prepared MoS$_2$ coating.

- In spectra from the ball wear scar, new peaks were observed at 100-250 cm⁻¹, 510 cm⁻¹, 750 cm⁻¹ and 925 cm⁻¹. These peaks were absent in spectra obtained from the as-prepared MoS$_2$ coatings.

- MoS$_2$ E$_{1g}$ peak (286 cm⁻¹) and second-order peaks observed in the as-prepared MoS$_2$ coating were not observed in the ball wear scar.

- At similar spectra acquisition parameters, the intensities of MoS$_2$ peaks in spectra obtained from the ball wear scars were lower than in as-prepared MoS$_2$ coating. This suggests that the crystallinity of MoS$_2$ coating decreased when it was rubbed.
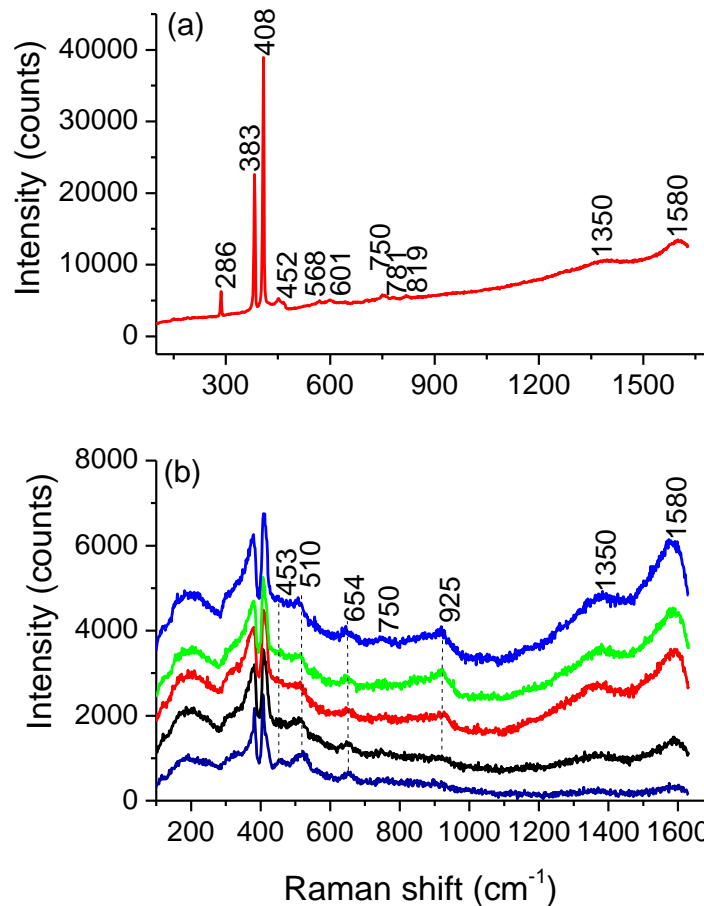
Figure 7-13. (a) Raman spectrum obtained from the as-prepared MoS$_2$ coatings on steel discs (b) Raman spectra from different regions on the ball wear scar after tribotests on MoS$_2$ coated disc

The broad peak in region 100-250 cm⁻¹ observed after tribotests on MoS$_2$ coatings was also observed in spectra obtained from MoDTC tribofilms. This confirms that the peak in the region 100-250 cm⁻¹ in MoDTC tribofilms is due to stress induced to MoS$_2$ crystal structure during tribological tests. It has been

reported that the broad peak at 100-250 is due to local disorder in the MoS_2 structure [149].

Raman peaks observed at 510 cm⁻¹ and 750 cm⁻¹ in the ball wear scar after tests with the MoS_2 coating were also observed in wear scars generated with MoDTC lubricant. The peak at 510 cm⁻¹ is due to v(S-S) vibrations in molybdenum compounds with bridging sulphur atoms (S_2^{2-}) while the peak at 750 cm⁻¹ is due to bridging oxygen atoms v(Mo-O-Mo). These results indicate that rubbing MoS_2 results in formation of bonds between adjacent sulphur atoms in MoS_2 crystal structure. Adjacent molybdenum atoms also become partially linked via oxygen atoms. The peak at 925 cm⁻¹ further indicates that the ferrous counterpart reacts with MoS_2 coating forming $FeMoO_4$.

The E_{1g} (286 cm⁻¹) peak was observed in the as-prepared MoS_2 coating but was not observed in the transferred coating on the ball wear scar. The E_{1g} peak has been shown to be highly dependent on the orientation of the MoS_2 crystal. This mode is only observed when the observation plane is in the z-axis [98]. In the as-prepared MoS_2 coating the crystals have different orientations including along the z-axis therefore the E_{1g} mode was observed. Since this peak was not observed in the transferred MoS_2 coating on the ball, it was concluded that the MoS_2 layers were oriented basally due to rubbing. Figure 7-14 illustrates the orientation of MoS_2 layers in as-prepared coating and in transferred coating after tribotests.
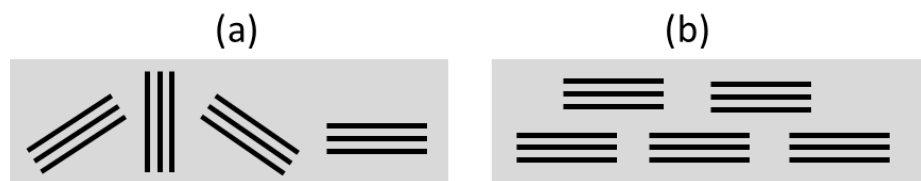
Figure 7-14. (a) Orientation of MoS₂ layers in the as-prepared MoS₂ (b) orientation of MoS₂ layers in transferred MoS₂ coating after tribotests.

Figure 7-15 shows spectra from the ball wear scar and the as-prepared MoS_2 coating in the spectral region 300-450 cm⁻¹ where E^1_{2g} and A_{1g} peaks are

observed. The MoS_2 peaks were fitted with Gaussian curves. Table 7-3 shows information of the peak fitting.
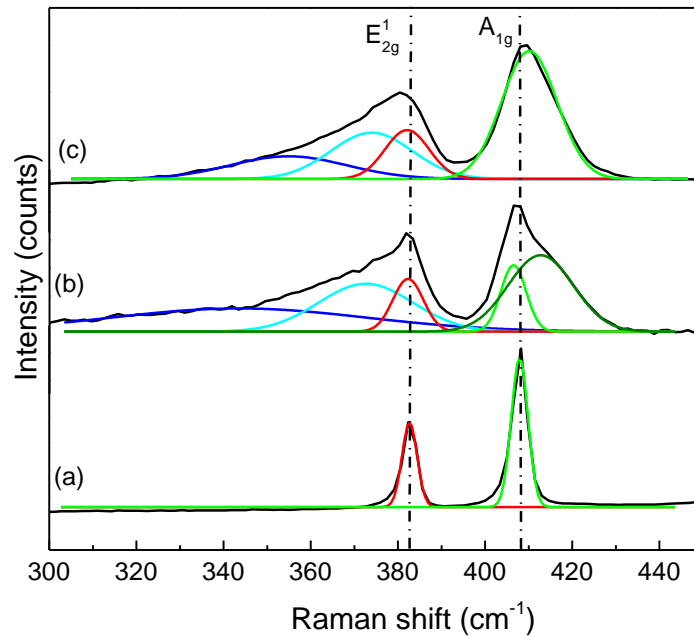
Figure 7-15. Raman spectra showing MoS₂ peaks in (a) as-prepared MoS₂ coating (b) transferred MoS₂ coating on the ball wear scar (c) MoDTC tribofilm

Table 7-3. MoS₂ peak fitting information for as-prepared MoS₂ coatings and MoS₂ transferred onto steel balls after tribotests

Sample	Peak frequency (cm⁻¹)	Peak width (cm⁻¹)
As-prepared MoS₂ coating	382.6	4.1
	407.9	4.5
Transferred MoS₂ on steel ball after tribotests	343.4	68.8
	372.5	25.5
	382.3	8.2
	406.4	6.8
	412.7	17.6

MoS_2 peaks from the ball wear scar were broader compared to the as-prepared coating. Both A_{1g} and E^1_{2g} peaks in the transferred MoS_2 were asymmetrical and were properly fitted with two or three Gaussian curves. The

E^1_{2g} peak was fitted with curves at 343 cm⁻¹, 373 cm⁻¹ and 382 cm⁻¹ while the A_{1g} peaks was fitted with peaks at 406 and 413 cm⁻¹.

The asymmetry observed in the E^1_{2g} peak in the MoS_2 coating after tribological tests was similar to that observed in MoDTC tribofilms confirming that the crystal structure in *x-y* axis of MoS_2 changes when subjected to tribological processes. The A_{1g} mode in transferred MoS_2 coating was as broad as that in MoDTC tribofilm indicating only slight disorder at atomic scale in the *z*-axis without significant defects in the structure [150]. Peak asymmetry and broadness observed in MoS_2 peaks from MoDTC tribofilms as well as the presence of the broad peak in the region 100-250 cm⁻¹ can thus be attributed to stress-induced disorder in the crystal structure of MoS_2.

7.7.3   Influence of tribological processes on MoS_2 Raman peaks: MoS_2 from MoDTC thermal decomposition

In Chapter 5, it was shown that MoS_2 was formed from thermal decomposition of $MoDTC/Fe_3O_4$ lubricant. MoS_2 formed from thermal decomposition is not subjected shear stress. Therefore, to investigate the influence of tribological process on the crystal structure of MoS_2 formed from decomposition of MoDTC, MoS_2 peaks from MoDTC tribofilm and $MoDTC/Fe_3O_4$ deposits on were compared. Figure 7-16 and Table 7-4 show MoS_2 peaks from MoDTC tribofilms, $MoDTC/Fe_3O_4$ deposits and microcrystalline MoS_2 powder.

MoS_2 formed from thermal decomposition of MoDTC ($MoDTC/Fe_3O_4$ deposits) has peaks which are symmetrical, similar to those of the microcrystalline MoS_2 powder. The only difference is that peaks from $MoDTC/Fe_3O_4$ deposits were broader. This indicates that MoS_2 from the thermal decomposition of MoDTC has low crystallinity compared to the microcrystalline MoS_2 powder [147].
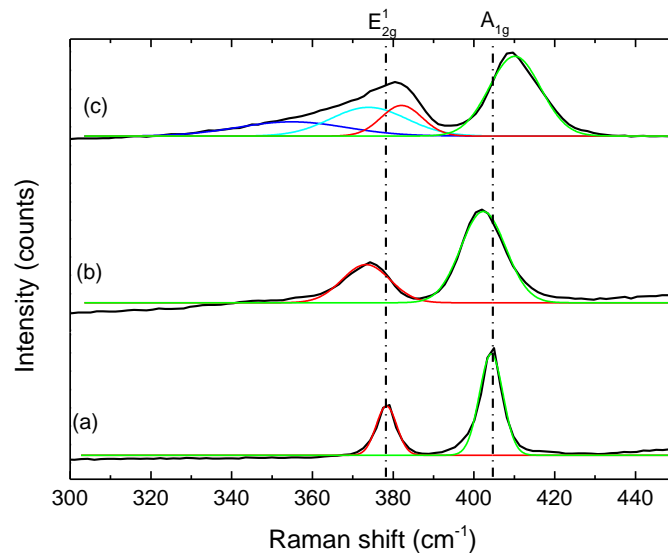
Figure 7-16. Raman spectra showing MoS$_2$ peaks in (a) MoS$_2$ powder, (b) MoDTC/Fe$_3$O$_4$ deposits (c) MoDTC tribofilm.

Table 7-4. MoS$_2$ peaks fitting information for MoS$_2$ formed under tribological and non-tribological conditions

Sample	Peak frequency (cm^{-1})	Peak width (FWHM)
MoS$_2$ powder	378.3	6.0
	404.3	6.9
MoDTC/Fe$_3$O$_4$ deposits	373.3	14.0
	402.3	13.1
MoDTC tribofilm	354.7	39.5
	373.9	21.7
	382.1	11.8
	410.1	14.8

Broadening of MoS$_2$ peaks in MoDTC tribofilms is therefore also attributed to low crystallinity. This assumption is supported by a previous study which showed that MoS$_2$ in MoDTC tribofilms and wear debris was composed of about 2 layers and thus lacked long-range order [56]. Further broadening of MoS$_2$ peaks in MoDTC tribofilms can occur during tribological tests as was shown in Figure 7-15. It may be argued that the broad MoS$_2$ peaks in MoDTC/Fe$_3$O$_4$ deposits and MoDTC tribofilms were due to a smaller grain

size compared to MoS_2 microcrystalline powder [147]. However, this cannot be true since MoS_2 nanoparticles analysed with the same laser wavelength and laser power have been shown to have peak widths ranging from 4-9 cm⁻¹ [102].

The E^1_{2g} peak in MoDTC/Fe_3O_4 deposits was symmetrical while in MoDTC tribofilms the peak was asymmetrical. These results further confirm that asymmetry of the E^1_{2g} peak in MoDTC tribofilms is due to tribological processes.

7.8   Summary

- Tribotest carried out without MoDTC additive had high friction and wear. The generated wear scars were mainly composed of iron oxides; haematite (Fe_2O_3) and magnetite (Fe_3O_4). Addition of MoDTC to base oil resulted in friction reduction as well as a decrease in the ball wear scar diameter.

- During tests with MoDTC, surface chemistry of the tribocontact changes rapidly during the first few minutes of rubbing.

- Raman spectroscopy can be used to characterise MoDTC lubricated surfaces after tribotests. However, the mineral oil has strong Raman signals which can obscure weak signals from MoDTC decomposition compounds such as MoS_x and $FeMoO_4$.

- Raman spectroscopy can be used to probe the crystal structure of MoS_2 present in MoDTC tribofilms. It has been observed that MoS_2 present in MoDTC tribofilms undergoes slight disorder within its crystal structure due to stress induced during tribological tests. The stress-induced disorder in MoS_2 crystal structure results in broad and asymmetrical MoS_2 peaks. Shear stress on MoS_2 also causes a broad

peak to be observed in the region 100-250 cm^{-1}. Shear stress also causes S-S and Mo-O-Mo bonds to form within MoS$_2$.

- FeMoO$_4$ easily forms in ferrous contacts when rubbed in the presence of molybdenum compounds such as MoS$_2$.

Chapter 8

Effect of contact parameters on chemical composition of MoDTC tribofilms

8.1   Introduction

Friction performance of MoDTC containing lubricant in steel/steel sliding contacts is dependent on contact parameters such as temperature, additive concentration, stroke length, sliding speed and surface roughness [12, 57, 58, 60, 62]. Low friction has been observed when MoS_2 is present at the tribocontact while high friction has been observed when only iron oxides are formed [12]. The chemical composition of MoDTC tribofilms at intermediate friction values has not been reported. In this Chapter, chemical composition of MoDTC tribofilms formed at different test conditions was investigated. Tribotests were conducted using the high speed pin-on-disc tribometer at varying temperatures, MoDTC concentrations and contact pressures. MoDTC decomposition products formed on the rubbing surfaces after tests were analysed using Raman spectroscopy.

8.2   Influence of temperature

8.2.1   Friction and wear results

Figure 8-1 (a) shows friction curves obtained during tests at different temperatures. For tests conducted at 20ºC, friction was high (μ=0.1) at the beginning of the test and decreased gradually with rubbing time. The friction coefficient at the end of the test was 0.09. In tests carried out at 40ºC, there was rapid friction drop to low steady friction values after an induction time of about 10 minutes. The friction coefficient after the friction drop was 0.07. Tests conducted at 60ºC and 100ºC also showed rapid friction drop to low values (0.05-0.06) after only a short induction time.
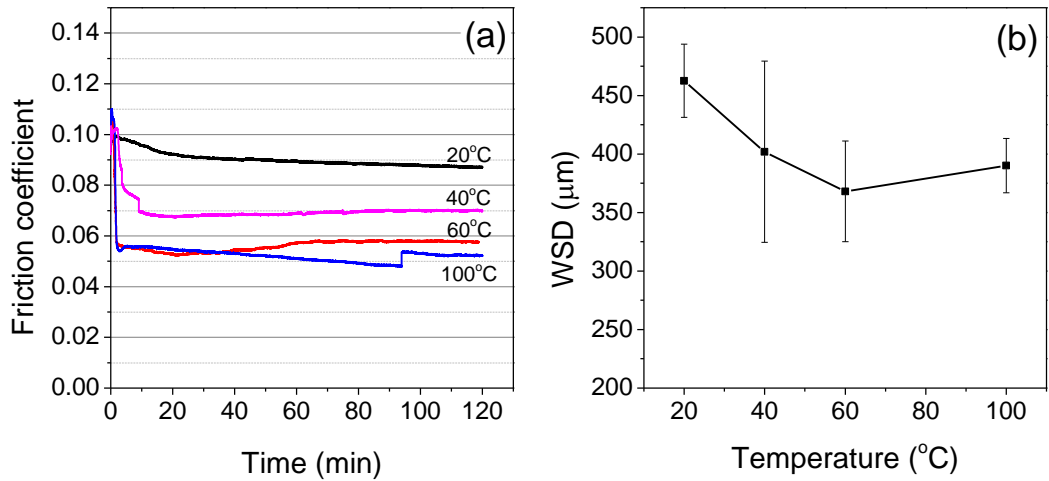
Figure 8-1. (a) Friction coefficient obtained during tests with MoDTC at various temperatures. (b) Ball wear scar diameters (WSD) at different temperatues. Tests were conducted with 0.5 wt% MoDTC at 200 rpm, 2.12 GPa

Figure 8-1 (b) shows the wear scar diameter (WSD) of wear scars formed on the balls at different temperatures. The WSD was highest at 20°C and decreased to lower values when the temperature was increased.

8.2.2 Morphology of tribopair wear scars

Figure 8-2 shows optical images of tribopair wear scars after tests at different temperatures. In tests conducted at 20ºC, Figure 8-2 (a), the tribopair wear scars were covered with dark brown films. At 40ºC, Figure 8-2 (b), the tribopair wear scars were also covered by brown films. At 60ºC (Figure 8-2c) the ball wear scar appeared to be covered with patchy films with a different colour than those observed at lower temperatures. The disc wear scar was however still covered with brown films similar to those observed at lower temperatures. At 100ºC, Figure 8-2 (d), both tribopair wear scars were covered with non-brown patchy films.
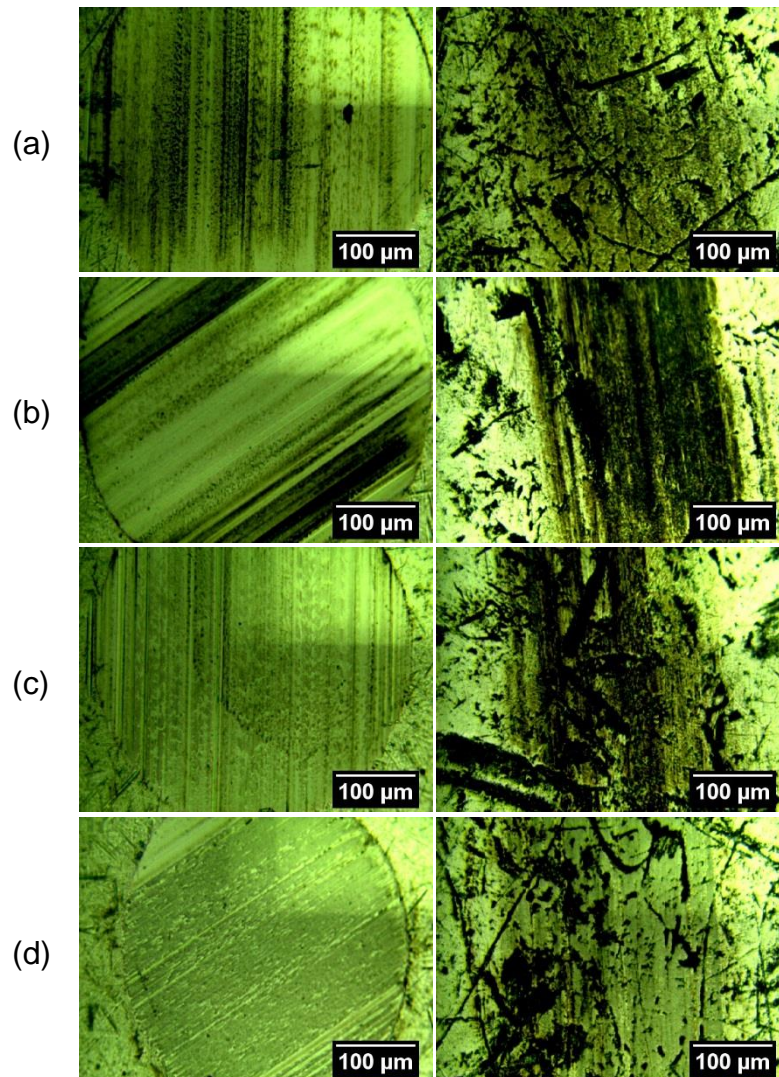
Figure 8-2. Optical images showing tribopair wear scars after tests at various temperatures (a) 20ºC (b) 40ºC (c) 60ºC and (d) 100ºC. Left: ball wear scars, Right: disc wear scars

8.2.3 Chemical composition of MoDTC tribofilms

Figure 8-3 shows representative Raman spectra obtained from tribopair wear scars after tests at different temperatures. It should be highlighted that the chemical composition in the wear scars was non-uniform especially for tests conducted at 40ºC and 60ºC. Consequently, spectra obtained from different regions of the wear scars varied greatly. Spectra obtained from different positions within the tribopair wear scars are provided in Appendix B.1. The Raman spectral information is summarised in Table 8-1.

124
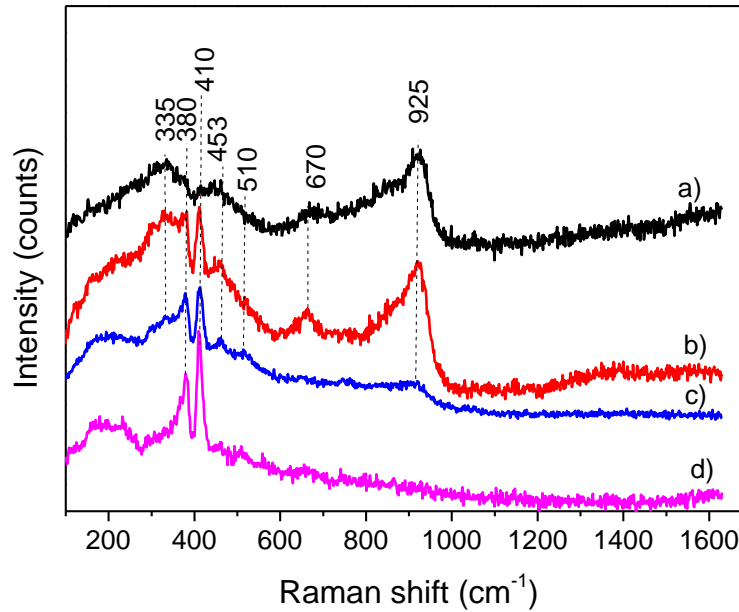
Figure 8-3. Raman spectra obtained from tribopair wear scars after tests at different temperatures (a) 20ºC (b) 40ºC (c) 60ºC (d) 100ºC

Table 8-1. Chemical composition of MoDTC tribofilms formed at different temperatures

Temperature	Raman peaks (cm^{-1})	Notes
20ºC	335, 453 (MoS_x) 670 (Fe_3O_4) 925 ($FeMoO_4$)	- Chemical composition uniform within wear scars
40ºC	335, 453 (MoS_x) 380, 410 (MoS_2) 670 (Fe_3O_4) 925 ($FeMoO_4$)	- Chemical composition non-uniform within wear scars
60ºC	380, 410 (MoS_2) 670 (Fe_3O_4) 925 ($FeMoO_4$)	- Chemical composition non-uniform within wear scars - $FeMoO_4$ intensity decreases
100ºC	380, 410 (MoS_2)	- Chemical composition uniform within wear scars

In previous Raman studies on the MoDTC tribofilms, there have been no reports of spectra similar to those shown in Figure 8-3 (a). This can be due to the fact that no Raman analysis has been carried out on samples generated at 20ºC. Most of the previous studies analysed samples generated at higher

temperatures and Raman spectra showed MoS_2 peaks [57]. Tribofilms generated at higher temperatures did indeed have MoS_2 peaks but this was not the case for samples generated at lower temperatures. This is the first time Raman peaks at 335 cm^{-1}, 453 cm^{-1} and 925 cm^{-1} have been observed in tests with MoDTC. Observation of these peaks has given a new insight on the mechanism of MoDTC decomposition which is discussed in detail in Section 12.2.4.

From previous reports, probable MoDTC decomposition products are molybdenum oxides such as MoO_2 [64, 65], MoO_3 [56, 65] molybdenum oxysulphide (MoS_xO_{2-x}) [56] and MoS_2 [151]. These chemical species were identified using X-ray photoelectron spectroscopy (XPS). However, by carefully examining Raman spectra obtained from pure MoO_2 and MoO_3 powders (Appendix C) and those reported in literature (Table 8-2), it was concluded that MoO_2, MoO_3 and $MoS_xO_{(2-x)}$ were not present in MoDTC tribofilms generated in this study.

Table 8-2. Raman peaks of molybdenum compounds reported in literature

Pure powders	Raman peaks (cm^{-1})	Reference
MoO_2	200, 228, 360, 459, 495, 566, 738	[72, 84]
MoO_3	284, 335, 664, 817, 993	[72, 85, 152]
$MoS_xO_{(2-x)}$	220-230, 440-480, 300-400, 500-550, 800-1000	[134, 136]
$FeMoO_4$	823, 879 (weak shoulder peaks) 926	[76, 83, 137]

Based on reported literature, the broad peak at 925 cm^{-1} observed in this study was assigned to Mo=O stretching in $FeMoO_4$. The broad peaks at 335 cm^{-1} and 453 cm^{-1} were   assigned to the formation of amorphous sulphur-rich molybdenum compounds, MoS_x (x>2), with bridging sulphur atoms (S_2^{2-}) [80, 126, 135, 146, 153, 154]. Formation of amorphous MoS_x from MoDTC decomposition has not been reported in literature but examples of

MoS$_x$ compounds from decomposition of other compounds have been reported [80, 81, 155-159].

Raman results showed that MoS$_2$ peaks emerged from broad MoS$_x$ peaks as the temperature was increased from 20ºC to 40ºC. Above 60ºC, MoS$_x$ peaks completely disappeared from the spectra and only MoS$_2$ peaks were observed. The intensity of the FeMoO$_4$ peaks also decreased with increase in temperature and completely disappeared at 60ºC.

8.3 Influence of MoDTC concentration

8.3.1 Friction and wear results

Figure 8-4 (a) shows the friction results after tests at different MoDTC concentrations. The friction coefficient was high (0.10) at the beginning in all tests. In the tests with 0.1 wt% MoDTC, the friction decreased gradually and reached µ=0.06 at the end of the test. In tests conducted with 0.5 wt% and 0.9 wt% MoDTC, high friction coefficient was only observed at the beginning of the test and rapidly dropped to low values (0.06) after a very short induction time.
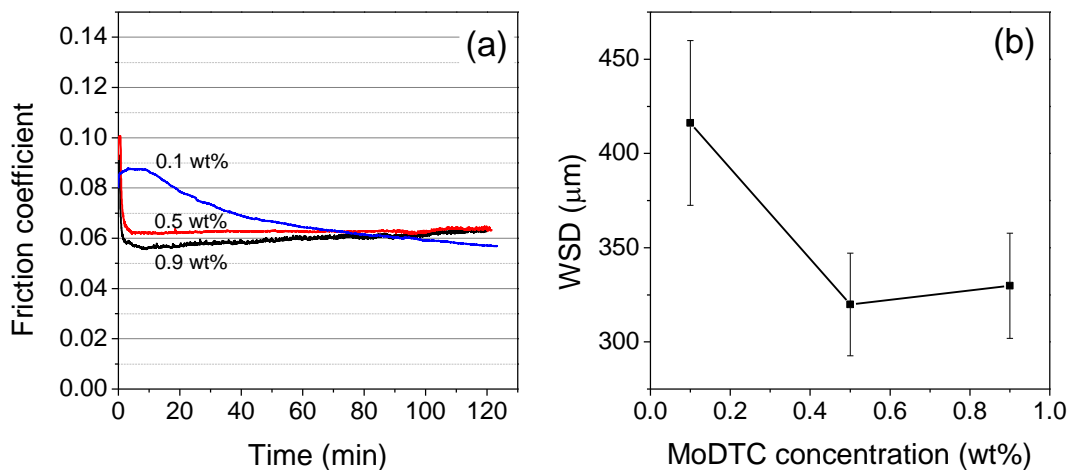
Figure 8-4. (a) Friction curves during tests with varying MoDTC concentrations. (b) Ball wear scar diameters (WSD) at different MoDTC concentrations. Tests were conducted at 60ºC, 400 rpm, 1.67 GPa.

From wear results presented in Figure 8-4 (b), it was observed that the WSD decreased when MoDTC concentration was increased from 0.1 to 0.5 wt%.

8.3.2 Morphology of tribopair wear scars

Figure 8-5 shows optical images of tribopair wear scar after tests at various MoDTC concentrations. Significant differences were observed in balls wear scars. In tests conducted using 0.1 wt% MoDTC, Figure 8-5 (a), the ball wear scar appeared polished with dark brown patches in various regions of the wear scar. When MoDTC concentration was increased to 0.5 wt%, Figure 8-5 (b), the wear scar appeared to be covered with patchy films (dark green regions). Grooves were also observed in the wear scar. At a higher concentration of 0.9 wt%, Figure 8-5 (c), the ball wear scar had numerous grooves and was covered with a dark brown film.
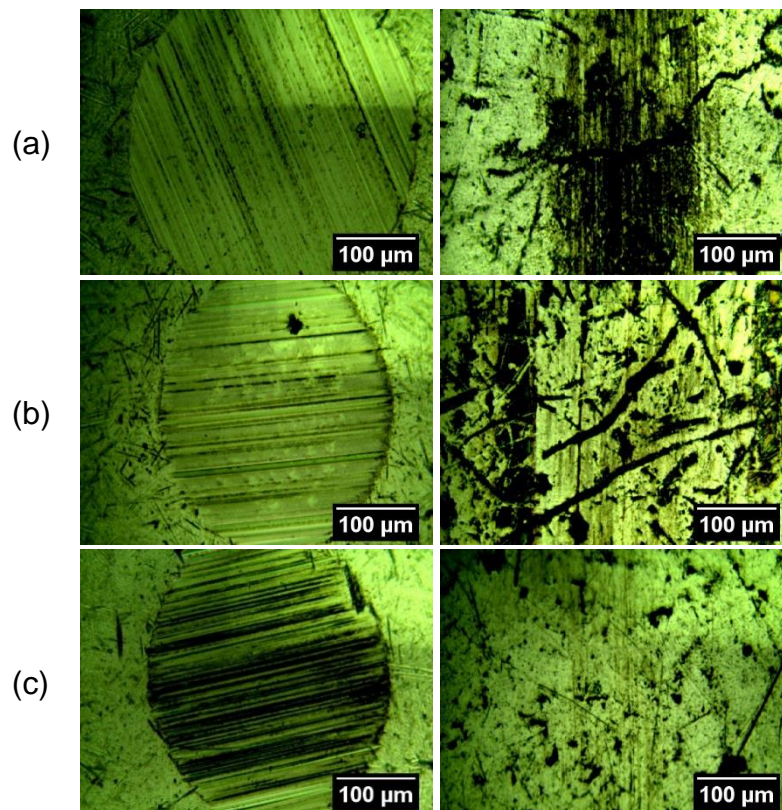
Figure 8-5. Optical images of ball wear scars after tests with varying MoDTC concentrations (a) 0.1 wt% (b) 0.5 wt% (c) 0.9 wt%. Left: ball wear scars, Right: disc wear scars

8.3.3 Chemical composition of MoDTC tribofilms

Raman spectra obtained from different regions within generated wear scars are shown in Appendix B.2. Representative spectra at various MoDTC concentrations are shown in Figure 8-6. Information obtained from the Raman spectra is summarised in Table 8-3.
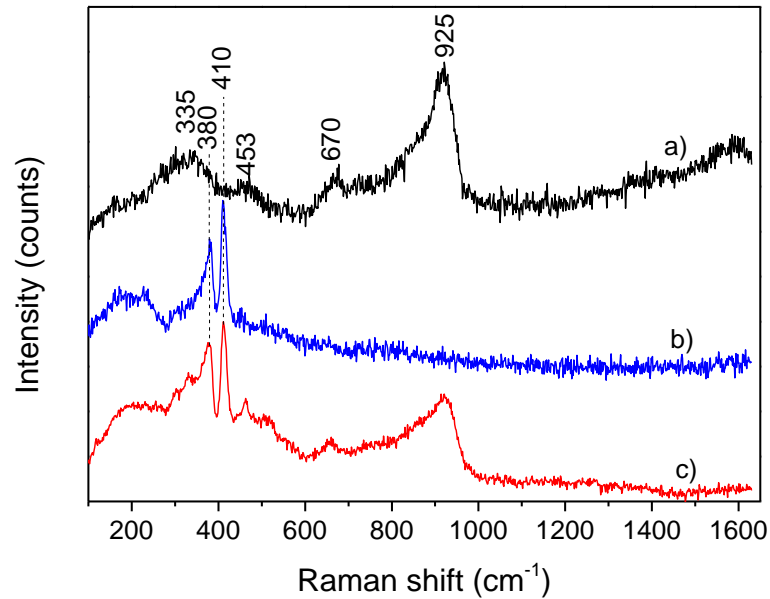
Figure 8-6. Raman spectra obtained from the tribopair wear scars after tests at varying MoDTC concentrations (a) 0.1 wt% (b) 0.5 wt% (c) 0.9 wt%

Table 8-3. Chemical composition of MoDTC tribofilms formed at different MoDTC concentrations

MoDTC concentration	Raman peaks (cm⁻¹) and assignment	Notes
0.1 wt%	335, 453 (MoS_x) 670 (Fe_3O_4), 925 ($FeMoO_4$)	- Chemical composition uniform within wear scars
0.5 wt%	380, 410 (MoS_2) 670 (Fe_3O_4), 925 ($FeMoO_4$)	- Chemical composition uniform within wear scars
0.9 wt%	335, 453 (MoS_x) 380, 410 (MoS_2) 670 (Fe_3O_4), 925 ($FeMoO_4$)	- Chemical composition non-uniform within wear scars

Results obtained showed that increasing MoDTC concentration from 0.1 wt% to 0.5 wt% resulted in chemical composition of the wear scars changing from MoS_x, $FeMoO_4$ to MoS_2. Further increase in MoDTC concentration to 0.9 wt% led to chemical composition changing from MoS_2 to MoS_2, MoS_x and $FeMoO_4$.

8.4 Influence of contact pressure

8.4.1 Friction and wear results

Figure 8-7 (a) shows friction curves observed during tests at various contact pressures. Friction behaviour was similar at all contact pressures. There was high friction (μ=0.10) at the beginning of the test followed by a rapid drop to low steady friction values (μ=0.07 - 0.06) after a very short induction time. The ball wear scar diameter (Figure 8-7b) increased with contact pressure as expected.
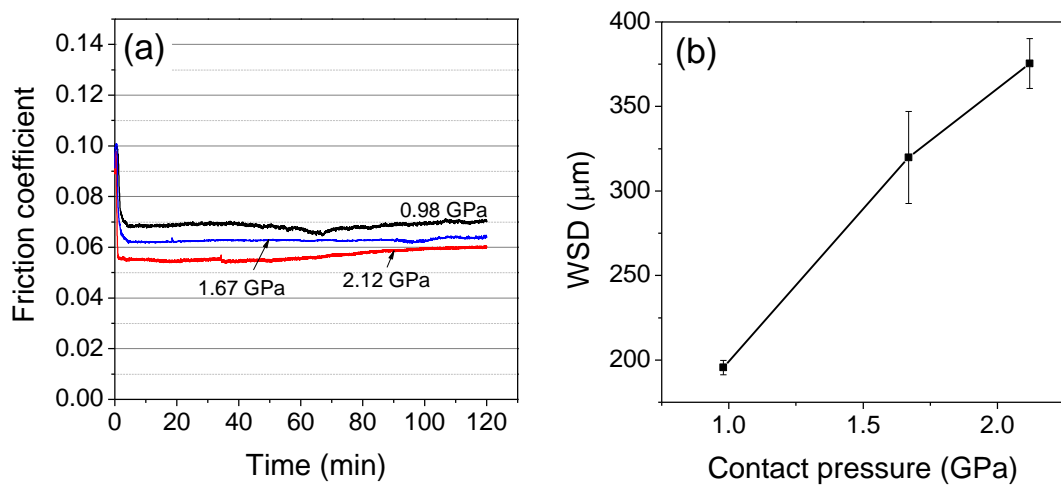
Figure 8-7. (a) Friction curves during tests at varying contact pressures. (b) ball wear scar diameters (WSD) at different contact pressures.Tests were conducted at 0.5 wt% MoDTC, 60ºC, 400 rpm.

8.4.2 Morphology of tribopair wear scars

Figure 8-8 shows optical images of the tribopair wear scars after tests at the various contact pressures. In tests conducted at 0.98 GPa, the ball wear scar

had grooves in the sliding direction and was covered with dark brown films. The disc wear scar was barely visible. In tests conducted at 1.67 GPa and 2.12 GPa, grooves were observed on the ball wear scars similar to those observed at 0.98 GPa. Patchy films (dark green regions) were also observed on the wear scars. Wear scars on the discs were more distinct at higher contact pressures than at 0.98 GPa.
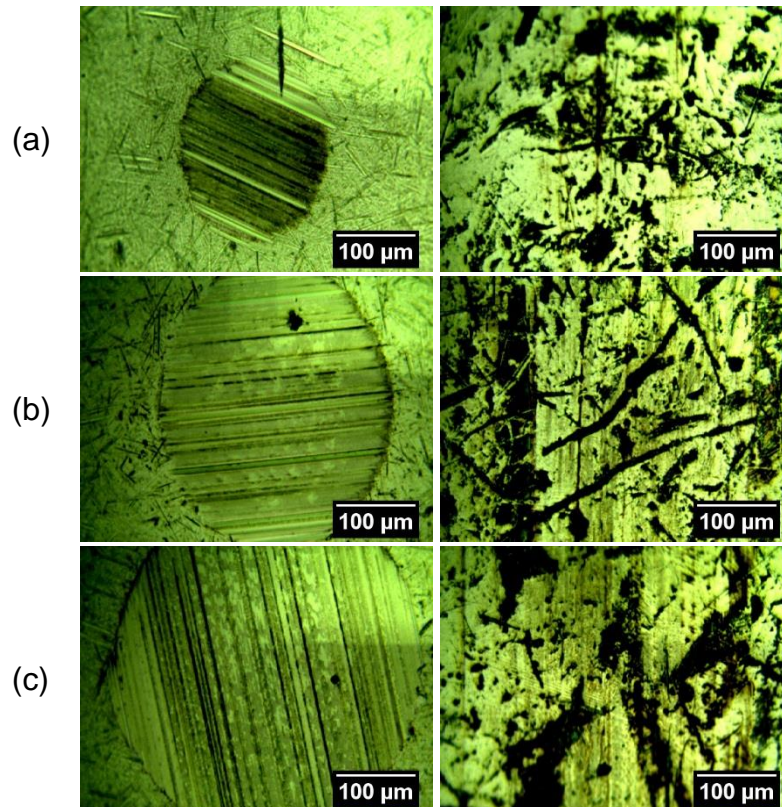
Figure 8-8. Optical images of ball wear scars after tests at varying contact pressures (a) 0.98 GPa (b) 1.67 GPa (c) 2.12 GPa. Left: ball wear scars, Right: disc wear scars

8.4.3 Chemical composition of MoDTC tribofilms

Raman spectra obtained from different regions within wear scars generated at varying contact pressures are shown in Appendix B.3. Figure 8-9 shows representative spectra obtained at different contact pressures. The spectral information is summarised in Table 8-4.
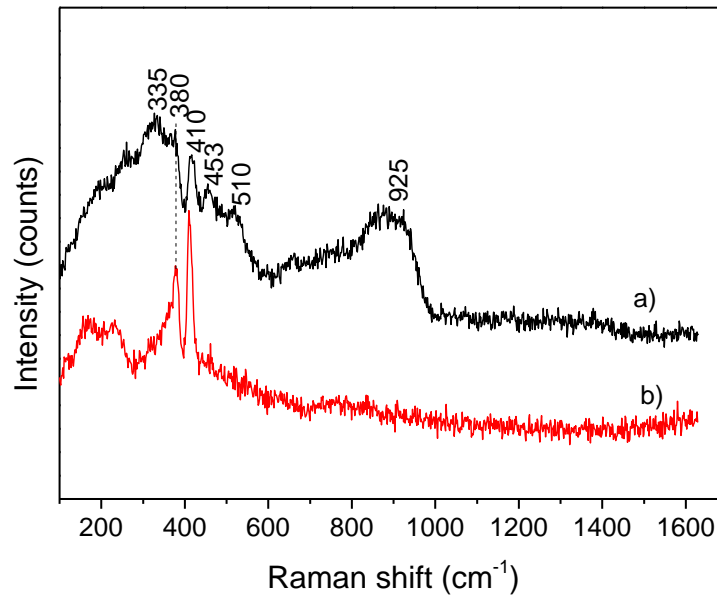
Figure 8-9. Raman spectra obtained from the tribopair wear scars after tests at (a) 0.98 GPa (b) 2.12 GPa.

Table 8-4. Chemical composition of MoDTC tribofilms formed at different initial contact pressures

Contact pressure	Raman peaks (cm^{-1})	Notes
0.98 GPa	380, 410 (MoS_2) 335, 453 (MoS_x) 925 ($FeMoO_4$)	- Chemical composition non-uniform within wear scars
1.67 GPa	380, 410 (MoS_2) 670 (Fe_3O_4) 925 ($FeMoO_4$)	- Chemical composition uniform within wear scars
2.12 GPa	380, 410 (MoS_2)	- Chemical composition non-uniform within wear scars

MoS_x was transformed to MoS_2 when the Hertzian contact pressure was increased from 0.98 GPa to 2.12 GPa. Also, less $FeMoO_4$ and Fe_3O_4 were formed at high contact pressures.

8.5   Summary

- MoDTC decomposition in a steel/steel contact is highly dependent on test conditions. MoDTC decomposes to form MoS_2, $FeMoO_4$ and MoS_x.

- MoS_x formed at lower temperatures, concentrations and contact pressures is converted to MoS_2 at higher temperatures, concentrations and contact pressures.

- The various MoDTC decomposition products formed within the tribocontact affected the friction performance. High friction was observed when MoS_x and $FeMoO_4$ are present at the tribocontact while low friction was observed when MoS_2 was present at the tribocontact.

Chapter 9

Effect of contact parameters on friction and wear performance of MoDTC lubricants in sliding/rolling contacts

9.1 Introduction

Although the influence of test conditions on friction has been investigated in previous studies [12, 57], there has been no mention of the influence of test parameters on the growth of MoDTC tribofilms or wear performance. This study therefore focuses on understanding the influence of test conditions on MoDTC tribofilm growth and wear.

In this Chapter, the central composite design was used in the design of experiments. The test parameters that were investigated were temperature, MoDTC concentration, speed and contact pressure. Table 4-6 lists all the tests that were conducted. Tests were conducted using the MiniTraction Machine at a slide-roll ratio of 100%. Steel discs (R_a=150 nm) and balls (R_a=10 nm) were used in the tribotests.

9.2 Friction results

Figure 9-1 shows the average friction coefficient during the last 1h of the tests conducted using 0.3 wt% and 0.7 wt% MoDTC. For tests conducted at 0.3 wt% MoDTC, friction decreased with increase in temperature only for tests conducted at lower contact pressure (0.7 GPa). For tests conducted at 0.7 wt% MoDTC, the friction at 50ºC was generally lower than that observed with 0.3 wt% MoDTC. At 50ºC, high friction (µ=0.06) was observed in tests conducted at 0.8 m/s while low friction (µ=0.04) was observed in tests conducted at 0.4 m/s.
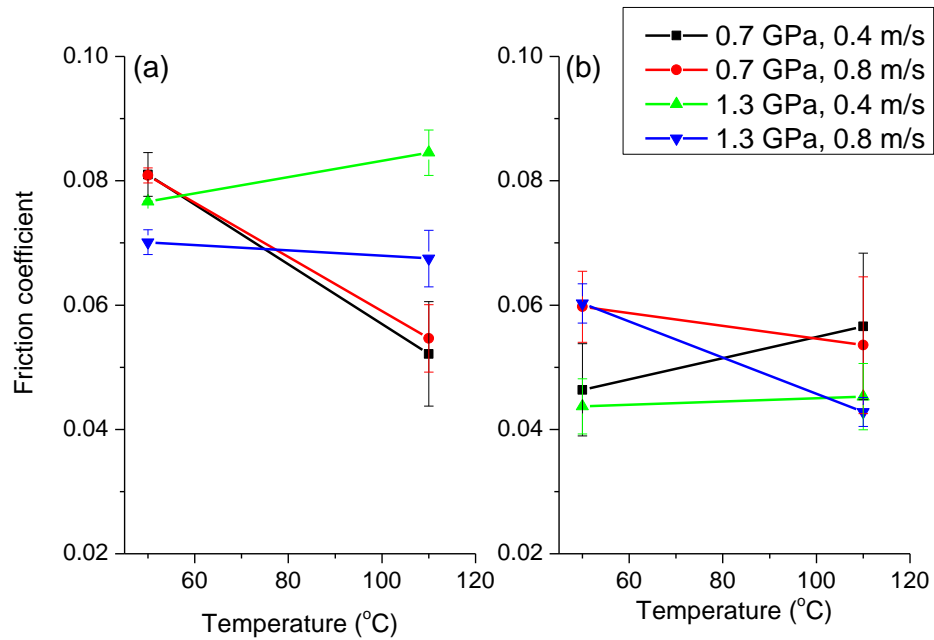
Figure 9-1. Friction as a function of contact parameters for tests conducted using (a) 0.3 wt% MoDTC (b) 0.7 wt% MoDTC. Friction values are an average of friction during the last 1h of test

To further understand the influence of contact parameters on friction, friction values from all tests shown in Table 4-6 were plotted as a function of lambda ratio (Figure 9-2). Lambda ratio (λ) is ratio of minimum film thickness (h_{min}) and composite roughness (R_a), h_{min}/R_a. In all tests, the initial composite roughness was 150.3 nm therefore λ was determined by the minimum film thickness. The four plots in Figure 9-2 show the same friction values (average value of last 1h) but highlight the influence of MoDTC concentration, temperature, contact pressure and speed on friction and lambda ratio. High friction values were observed at high lambda ratios ($\lambda>0.2$) while at low lambda ratios ($\lambda<0.2$), both high and low friction values were observed. From this, it can be seen that lambda values alone cannot explain the friction behaviour of MoDTC. The effect of the individual parameters has to be taken into account. This is discussed in detail in Sections 12.2.5 and 12.2.6.
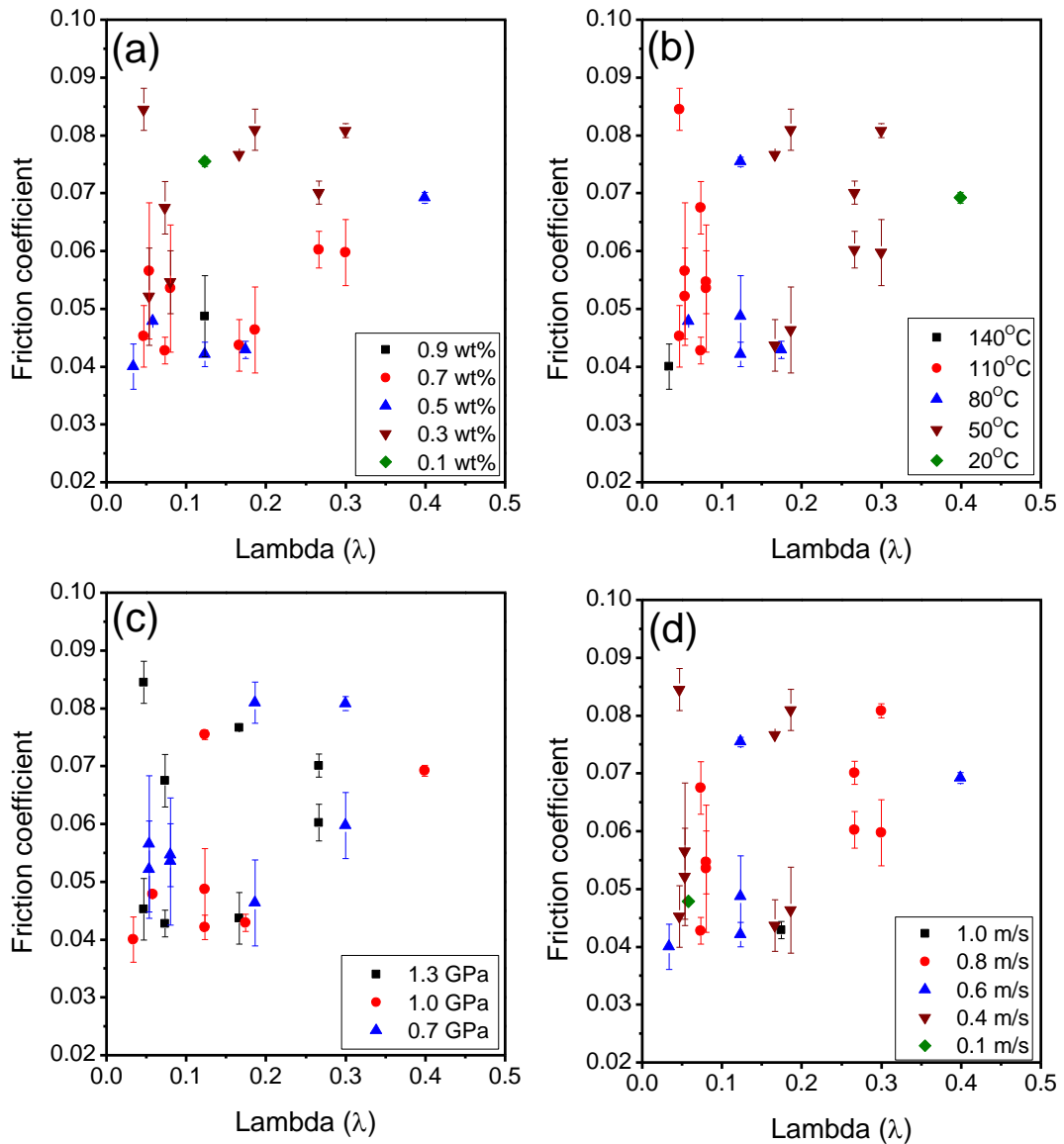
Figure 9-2. Friction coefficient as a function of initial lambda ratio. (a) MoDTC concentration (b) temperature (c) contact pressure (d) speed

9.3 Morphology and surface analysis of rubbed surfaces: Tests conducted with 0.3 wt% MoDTC

Figure 9-3 shows optical images of ball wear scars after tests with 0.3 wt% MoDTC. At 110ºC, very large wear scars were generated when the tests were conducted at 1.3 GPa. Figure 9-4 shows interference images obtained during tests at 110ºC. Severe wear of the ball at 1.3 GPa resulted in the images

appearing cylindrical in shape as opposed to the circular shape observed at 0.7 GPa. At 1.3 GPa, the generated wear scars were 783 μm wide and 6 μm deep.
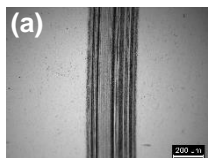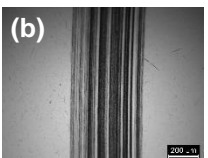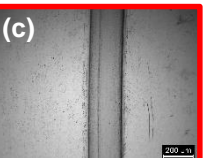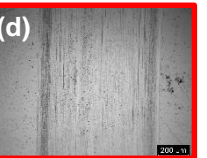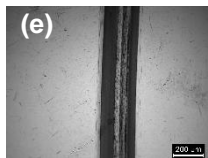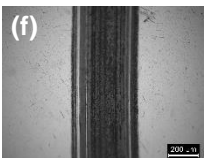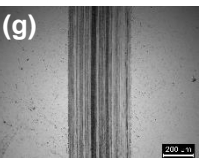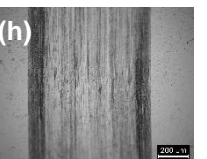
	50⁰C		110⁰C	
	0.7 GPa	1.3 GPa	0.7 GPa	1.3 GPa
0.4 m/s	(a) μ=0.08	(b) μ=0.08	(c) μ=0.05	(d) μ=0.08
0.8 m/s	(e) μ=0.08	(f) μ=0.07	(g) μ=0.05	(h) μ=0.07

Figure 9-3. Optical images of ball wear scars after tests conducted with 0.3 wt% MoDTC. Interference images of samples highlighted in red are shown in Figure 9-4

	0 min	30 min	60 min	120 min	Depth profile
(a)					
(b)					
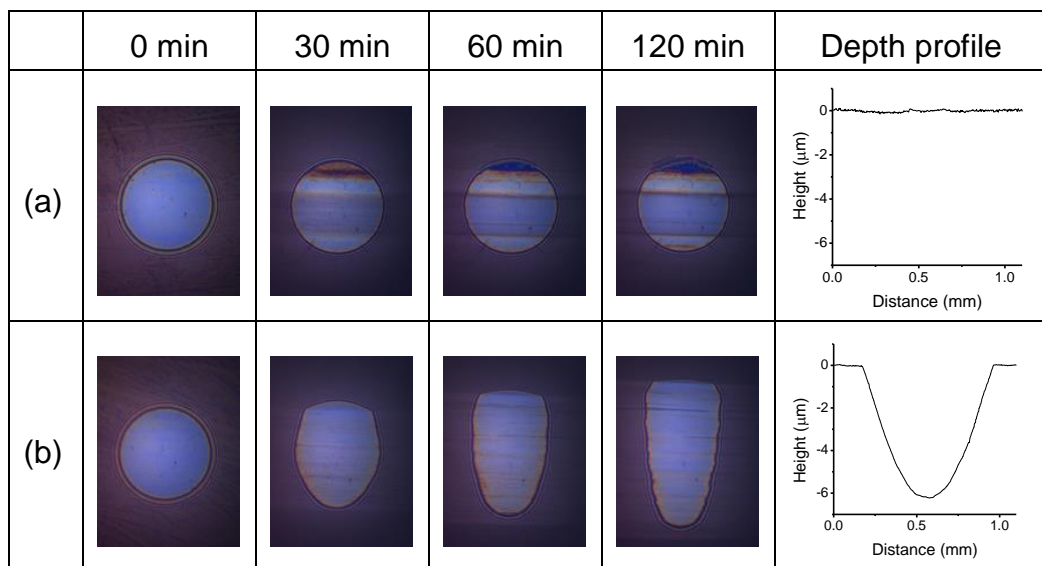
Figure 9-4. Interference images during tests with 0.3 wt% MoDTC at 110⁰C, 0.4 m/s (a) 0.7 GPa (b) 1.3 GPa.The depth profiles are after 120 minutes tests.

Table 9-1 shows the chemical composition of wear scars obtained at different test conditions. Samples generated at 50⁰C showed the presence of MoS_x

and $FeMoO_4$. The chemical composition of samples generated at 110°C was dependent on contact pressure. Samples generated at 0.7 GPa were composed of MoS_2, Fe_3O_4 and $FeMoO_4$ while samples generated at 1.3 GPa were composed of MoS_x, Fe_2O_3, Fe_3O_4 and $FeMoO_4$.

Table 9-1. Chemical composition of wear scars generated after tests with 0.3 wt% MoDTC

Temperature	Parameters	Friction coefficient (μ)	Chemical composition
50°C	0.7 GPa, 0.4 m/s	0.08	MoS_x, $FeMoO_4$
	1.3 GPa, 0.4 m/s	0.08	
	0.7 GPa, 0.8 m/s	0.08	
	1.3 GPa, 0.8 m/s	0.07	
110°C	0.7 GPa, 0.4 m/s	0.05	MoS_2
	1.3 GPa, 0.4 m/s	0.08	Fe_2O_3, Fe_3O_4, $FeMoO_4$
	0.7 GPa, 0.8 m/s	0.05	MoS_2, Fe_3O_4, $FeMoO_4$
	1.3 GPa, 0.8 m/s	0.07	MoS_x, Fe_3O_4, $FeMoO_4$

9.4   Morphology and surface analysis of rubbed surfaces: Tests conducted with 0.7 wt% MoDTC

Figure 9-5 shows optical images of ball wear scars after tests using 0.7 wt% MoDTC. It was generally observed that tribofilms were formed at both 50°C and 110°C. MoDTC tribofilms formed at 50°C had grooves present while those formed at 110°C did not exhibit grooves within the tribofilms as can be seen in the 3D images in Figure 9-6. Increasing the contact pressure at 110°C did not cause the severe wear that was observed in tests conducted with 0.3 wt% MoDTC. As expected, the wear scars formed at 1.3 GPa were wider than those formed at 0.7 GPa.
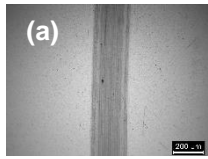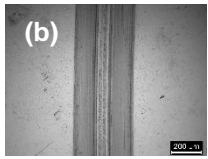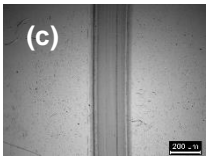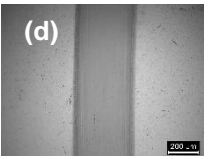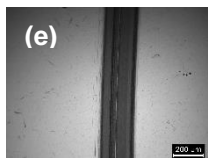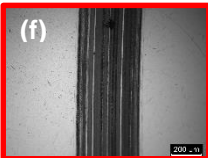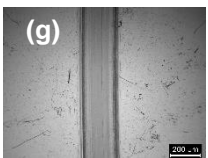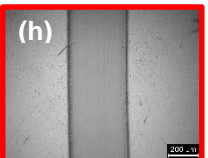
	50ºC		110ºC	
	0.7 GPa	1.3 GPa	0.7 GPa	1.3 GPa
0.4 m/s	(a) μ=0.05	(b) μ=0.04	(c) μ=0.05	(d) μ=0.04
0.8 m/s	(e) μ=0.06	(f) μ=0.06	(g) μ=0.05	(h) μ=0.04

Figure 9-5. Optical images of ball wear scars after tests with 0.7 wt% MoDTC. 3D images of samples highlighted in red are shown in Figure 9-6
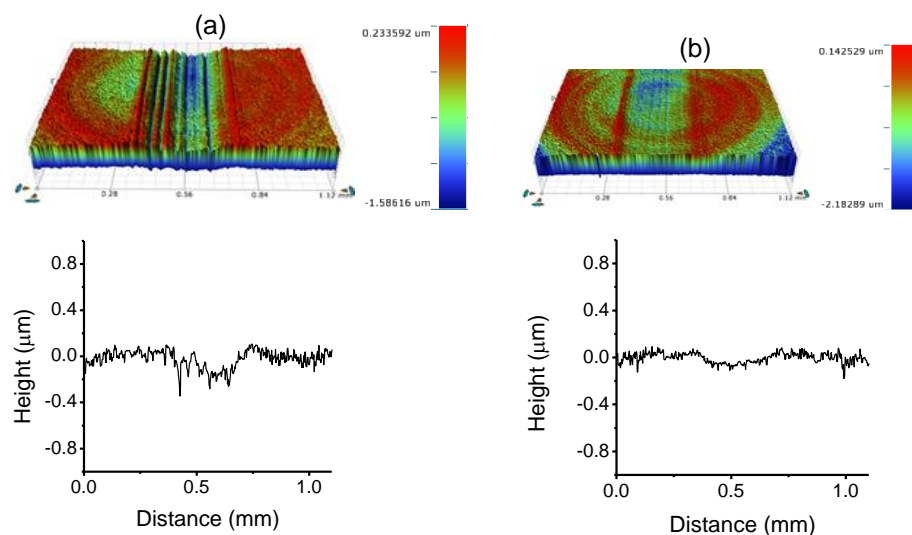
Figure 9-6. 3D images and depth profiles of ball wear scars formed at (a) 50ºC and (b) 110ºC in tests conducted at 0.8 m/s, 1.3 GPa, 0.7 wt% MoDTC

Table 9-2 shows the chemical composition of wear scars that were generated at different test conditions using 0.7 wt% MoDTC. For samples generated at 50ºC, the chemical composition was dependent on speed. MoS_2 was formed at low speeds (0.4 m/s), while MoS_x and $FeMoO_4$ were formed at high speeds

(0.8 m/s). All samples generated at 110ºC showed the presence of MoS_2 irrespective of the speed.

Table 9-2. Chemical composition of wear scars generated after tests with 0.7 wt% MoDTC

Temperature	Parameters	Friction coefficient (μ)	Chemical composition
50ºC	0.7 GPa, 0.4 m/s	0.04	MoS_2
	1.3 GPa, 0.4 m/s	0.04	
	0.7 GPa, 0.8 m/s	0.06	MoS_x, $FeMoO_4$
	1.3 GPa, 0.8 m/s	0.06	
110ºC	0.7 GPa, 0.4 m/s	0.05	MoS_2
	1.3 GPa, 0.4 m/s	0.04	
	0.7 GPa, 0.8 m/s	0.05	
	1.3 GPa, 0.8 m/s	0.04	

9.5 Morphology and surface analysis of rubbed surfaces: Tests at levels 0 and ±2

Figure 9-7 shows optical images of ball wear scars after tests at different speeds. Under the test conditions used, the speed did not affect the formation of MoDTC tribofilms. Tribofilms formed at the different speeds were composed of MoS_2 (Table 9-3).

| (a) μ=0.05 | (b) μ=0.04 | (c) μ=0.04 |
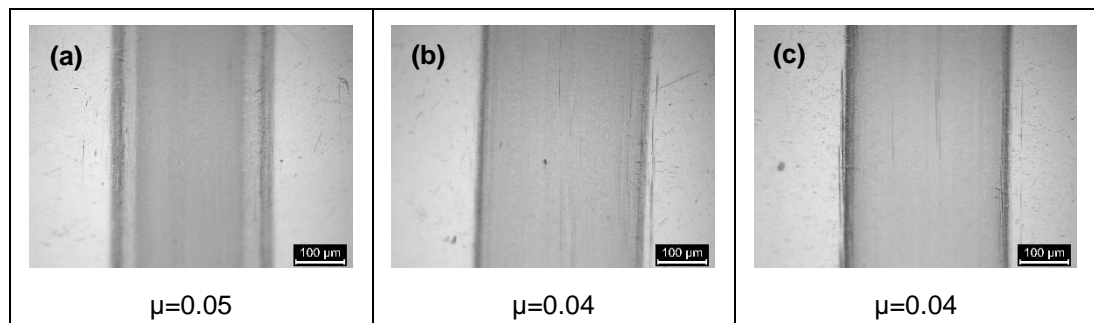
Figure 9-7. Optical images of ball wear scars after tests at different speeds (a) 0.2 m/s (b) 0.6 m/s (c) 1 m/s. Tests were conducted at 0.5 wt%, 80ºC, 1 GPa

Table 9-3. Chemical composition at various contact parameters

Parameter	Level	Friction coefficient (μ)	Chemical composition
Speed	0.2 m/s	0.05	MoS_2
	0.6 m/s	0.04	MoS_2
	2 m/s	0.04	MoS_2
MoDTC concentration	0.1 wt%	0.08	Fe_2O_3, Fe_3O_4, $FeMoO_4$
	0.5 wt%	0.04	MoS_2
	0.9 wt%	0.05	MoS_2
Temperature	20ºC	0.07	Fe_2O_3, Fe_3O_4, $FeMoO_4$
	80ºC	0.04	MoS_2
	140ºC	0.04	MoS_2

Figure 9-8 shows optical and 3D images of ball wear scars after tests at varying MoDTC concentrations. Uniform tribofilms were formed at 0.9 wt% MoDTC while patchy films were formed at 0.1 wt% MoDTC. Wear scars generated at 0.1 wt% were composed of Fe_2O_3, Fe_3O_4 and $FeMoO_4$ while those generated at 0.9 wt% were composed of MoS_2 (Table 9-3).
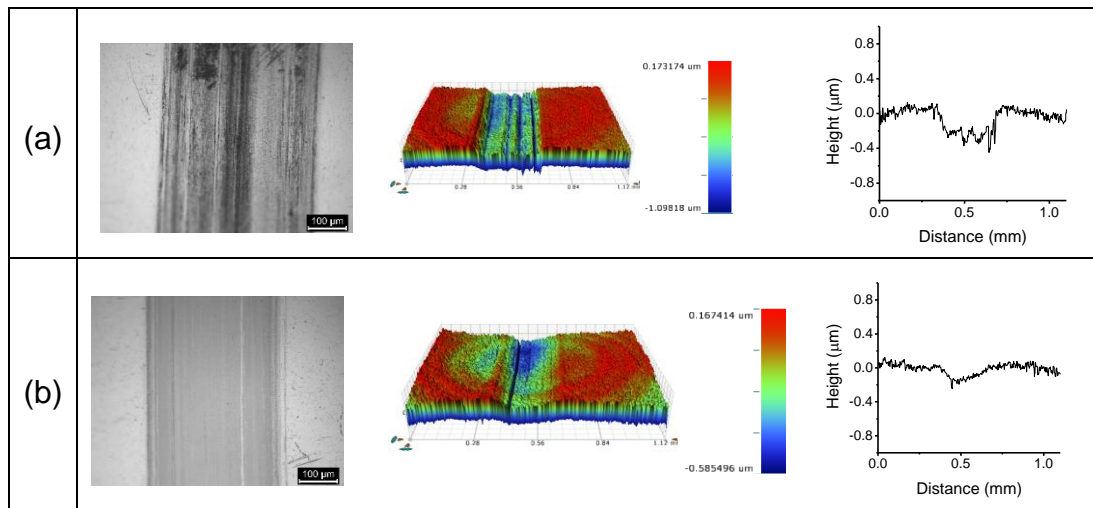
Figure 9-8. Optical images of ball wear scars after test at different MoDTC concentrations (a) 0.1 wt%, (b) 0.9 wt%. Tests were conducted at 1 GPa, 0.6 m/s, 80ºC

Figure 9-9 shows optical and 3D images of ball wear scars after tests at different temperatures. At 20⁰C, the wear scar had numerous grooves and was covered with patchy tribofilms composed of Fe_2O_3, Fe_3O_4 and $FeMoO_4$. At higher temperature (140⁰C), the wear scars were covered with uniform tribofilms composed of MoS_2 (Table 9-3)
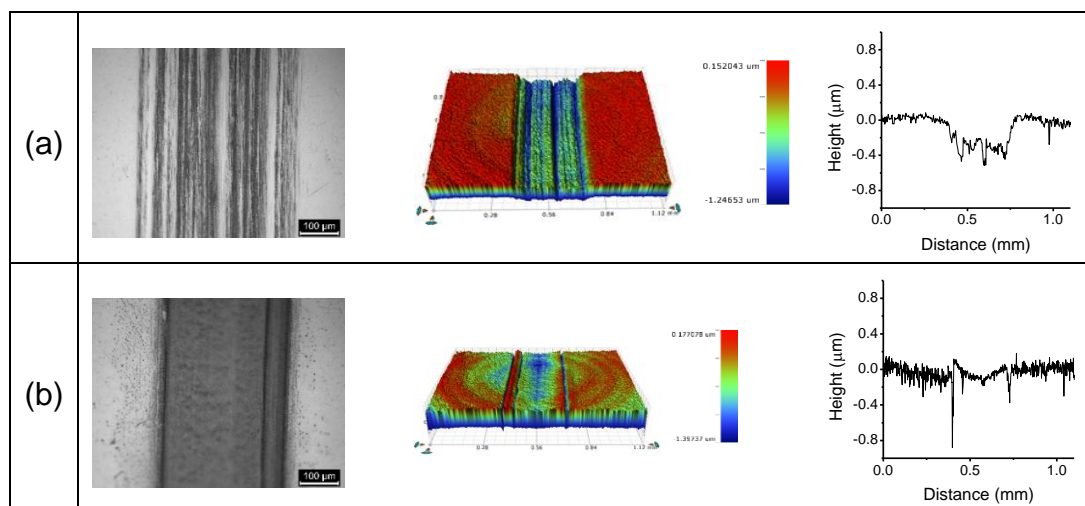
Figure 9-9. Optical and 3D images of ball wear scars after tests at different temperatures (a) 20⁰C (b) 140⁰C. Tests were conducted at 0.5 wt%, 0.6 m/s, 1 GPa

9.6   Summary

- MoDTC concentration, temperature, contact pressure and speed affect the friction behaviour of MoDTC-containing lubricants.

- MoDTC decomposes to various decomposition products depending on the contact parameters.

- MoDTC tribofilms provide wear protection to the tribopair. However at certain test conditions (low MoDTC concentrations, high temperatures, and high contact pressures) MoDTC is incapable of providing wear protection and severe wear occurs.

Chapter 10

Effect of surface roughness and slide-roll ratio on surface chemistry and friction performance of MoDTC lubricants

10.1   Introduction

Surface roughness has been shown to have a significant effect on the friction performance of MoDTC lubricants in steel/steel contacts [12, 62]. In this Chapter, the effect of surface roughness and slide-roll ratio (SRR) on friction performance, morphology and chemical composition of MoDTC tribofilms was investigated. Tribotests were conducted using the MiniTraction Machine at the following tests conditions: 0.5 wt% MoDTC lubricant, 1 GPa, 100ºC. Tests were conducted using rough (R_a=150 nm) and smooth (R_a=10 nm) steel discs sliding against smooth steel balls (R_a=10 nm) at SRR=100% and SRR=200%.

10.2   Friction results

Figure 10-1 shows friction curves obtained during tribotests. At SRR=100%, tests with rough discs showed an initial high friction coefficient of µ=0.11 that decreased rapidly within the first few minutes to low values of µ=0.035 before increasing slightly to reach a steady state value of µ=0.04. In tests with smooth discs, friction coefficient was low at the beginning of the test and reached a steady-state value of µ=0.04.

At SRR=200%, tests conducted with rough discs showed low friction coefficient from the beginning of the test. Steady low values of µ=0.04-0.05 were observed throughout the duration of the test. The friction observed was similar to that observed at SRR=100%. In tests with smooth discs at SRR=200%, friction was generally high (µ=0.1) especially during the first 30 minutes of the test. At longer rubbing times the friction decreased to µ=0.05-0.07. The friction observed with smooth discs at SRR=200% was

generally higher than that observed at SRR=100% and had large friction fluctuations.
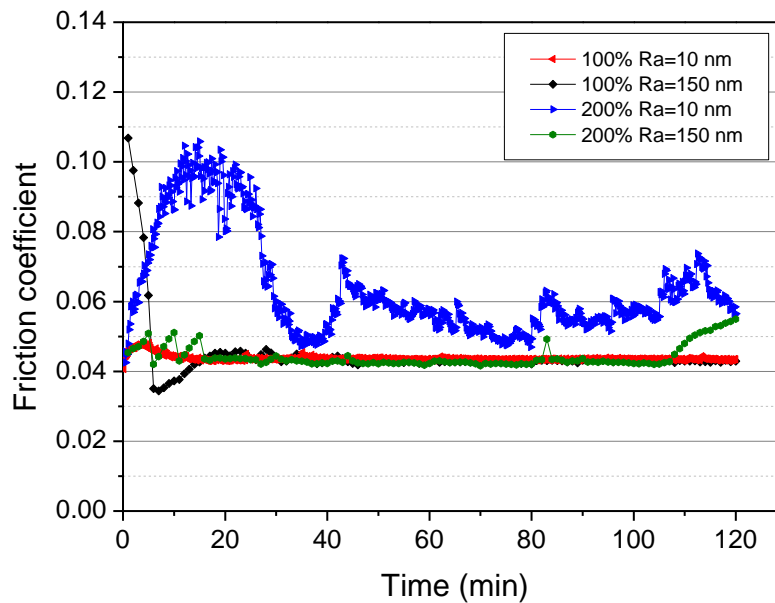
Figure 10-1. Friction curves of tests conducted at SRR=100% and 200% using smooth and rough discs

10.3   Morphology of tribopair wear scars

Interference images of ball wear scars during tests at SRR=200% were similar to those observed at SRR=100%. Figure 10-2 shows interference images obtained during tests at SRR=100% with rough discs and smooth discs. Figure 10-3 shows optical images of ball wear scars after 2h tests. Interference images in Figure 10-2 (a) show that during tests with rough discs, a wear track was formed on the ball after 5 minutes of rubbing and was gradually covered by a tribofilm as rubbing continued. After 2h of sliding, a very thick tribofilm was observed on the ball wear track. Optical images in Figure 10-3 (a) and (c) confirmed that the wear scars were fully covered with tribofilms.
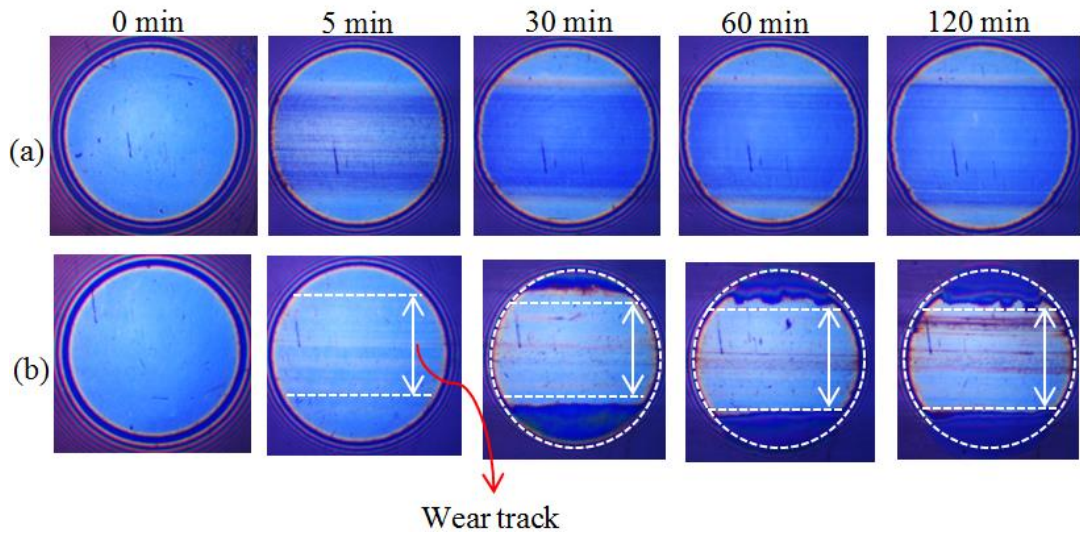
Figure 10-2. Interference images of ball wear scars during tests at SRR=100% (a) rough discs (b) smooth discs
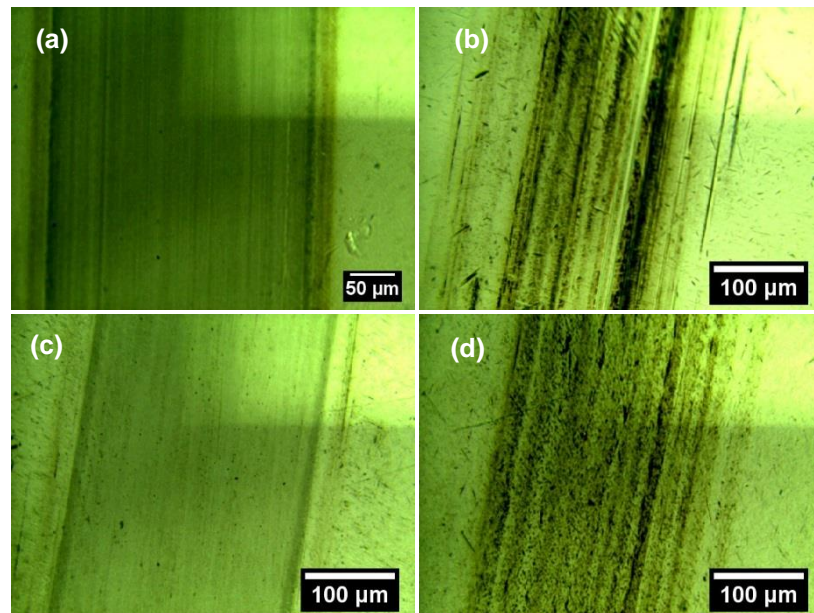
Figure 10-3. Optical images of ball wear scars after tests with (a) rough disc at SRR=100% (b) smooth disc at SRR=100% (c) rough discs at SRR=200% (d) smooth discs at SRR=200%

Interference images in Figure 10-2 (b) showed that during tests with smooth discs, the wear scar on the ball was barely noticeable after 5 minutes rubbing. At longer rubbing times, patchy brown films were observed on the wear track.

145

Optical images in Figure 10-3 (b) and (d) showed wear scars covered with patchy dark brown films.

Figure 10-4 shows 3D interference images of discs after tests. Wear scars generated after tests with smooth discs at both SRR=100% and 200% were very rough and had deep grooves. The high regions in the wear scars were due to formation of tribofilms; this was confirmed by optical images of the wear scars. Although wear scars after tests with rough discs were clearly observed optically, it was not possible to detect any height difference between rubbed and unrubbed regions with white light interferometry as shown in Figure 10-4 (c).
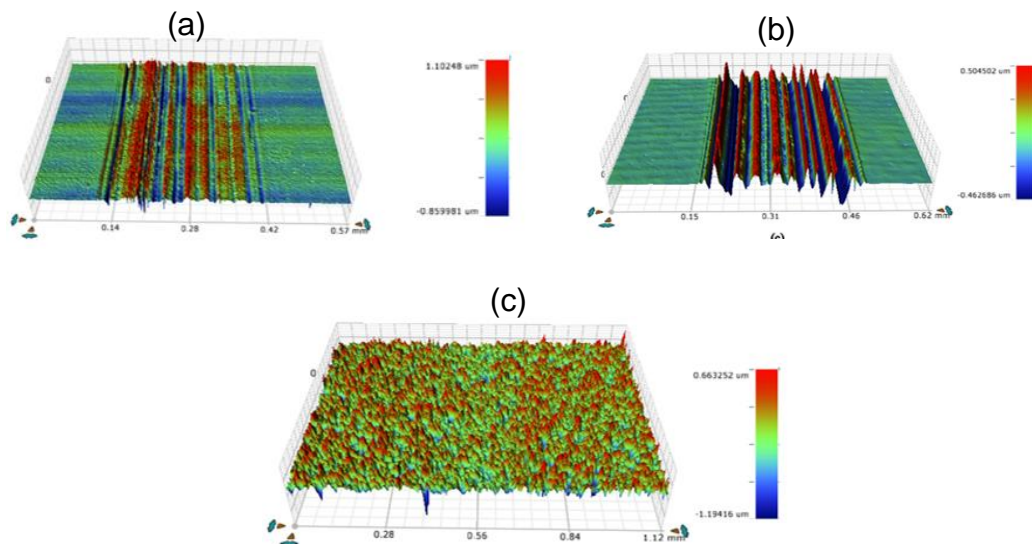
Figure 10-4. 3D images of discs after tests (a) smooth disc at SRR=100% (b) smooth disc at SRR=200% (c) rough disc at SRR=200%

10.4   Raman analysis of MoDTC tribofilms

Raman analysis was carried out on the tribopair wear scars at the end of the 2h test. As discussed above, the morphology of the wear scars was observed to be non-uniform in some samples. For this reason, Raman analysis was conducted by obtaining several Raman spectra from different regions within

each wear scar. This was done so as to determine the uniformity of the surface chemistry within the wear scars. Representative spectra from each wear scar are shown in the Appendix D. The spectral information is summarised in Table 10-1.

Table 10-1. Raman analysis from wear scars after tests at varying surface roughness and slide-roll ratios

Disc roughness	Slide-Roll Ratio (SRR)	Raman peak (cm^{-1})	Notes
R_a=10 nm	100%, 200%	335,453 (MoS_x) 380, 410 (MoS_2) 670 (Fe_3O_4) 925 ($FeMoO_4$) 1370,1580 (carbon)	- Chemical composition non-uniform within wear scars
R_a=150 nm	100%, 200%	380, 410 (MoS_2) 670 (Fe_3O_4) 960 (MoDTC) 1370,1580 (carbon)	- Chemical composition uniform within wear scars

The chemical composition of MoDTC tribofilms was only affected by the roughness of the disc. MoDTC tribofilms formed with smooth discs had a non-uniform chemical composition and spectra obtained varied greatly from spot-to-spot. Wear scars generated after tests with smooth discs were composed of a mixture of MoS_x, MoS_2, Fe_3O_4 and $FeMoO_4$. On the other hand, MoDTC tribofilms generated with rough discs were composed of MoS_2 with traces of Fe_3O_4. The results obtained in rough discs are in agreement with those obtained by Cousseau et al. [68].

10.5   Simulation of local contact pressures

The calculated Hertzian contact pressure assumes that the applied load is supported by the entire contact area. This is not accurate for real surfaces

where the load is supported by the asperities and local pressures at the asperities can be significantly higher that the Hertzian contact pressure. The local contact pressure is thus dependent on the surface roughness. Simulation of local pressures in contacts with smooth and rough discs was conducted. The numerical model used was based on the model developed by Ghanbarzadeh et al. [160] which incorporates a Boundary Element simulation for contact of rough surfaces. The model considers an elastic-perfectly plastic contact and the hardness of the material is used as a criterion for the plastic flow. Although this method can underestimate the deformations of the surfaces it is widely accepted in literature for finding the true contact area. The plastic model is explained in detail in the study by Sahlin et al. [161]. Digitised surfaces are used as inputs of the numerical model. Surfaces are created using the method introduced by Hu and Tonder [162] which is flexible to simulate surfaces with desired surface roughness and asperity lateral size.

In this simulation, two surfaces with different surface roughness were generated, surface 1 (R_a=10 nm) and surface 2 (R_a=150 nm). The roughness of the two surfaces is similar to that of the two discs used to conduct tribological tests. A third surface (surface 3) with the surface roughness R_a=10 nm was also generated to simulate the roughness of the ball used in the tribological tests. Simulation of the local contact pressure was carried out for cut off size of 64 μm × 64 μm with each node being 1 μm. Surface 3 was placed on top of surfaces 1 and 2 and a contact pressure of 1 GPa was applied on surface 3. The load used ensured that the surfaces in contact were in boundary lubrication regime and the load applied was carried by the asperities.

Figure 10-5 shows results of the simulation. Figure 10-5 (a) shows a 2D map of local pressures between surface 1 and 3. Figure 10-5 (b) shows a 2D map of local pressures between surface 2 and 3. Figure 10-5 (c) shows the average of local asperity pressures obtained in Figure 10-5 (a) and (b). From the simulation results it can be seen that despite the Hertzian contact pressure

being the same, the average local pressure was 2.5 times higher in the rough surface than in the smooth surface.
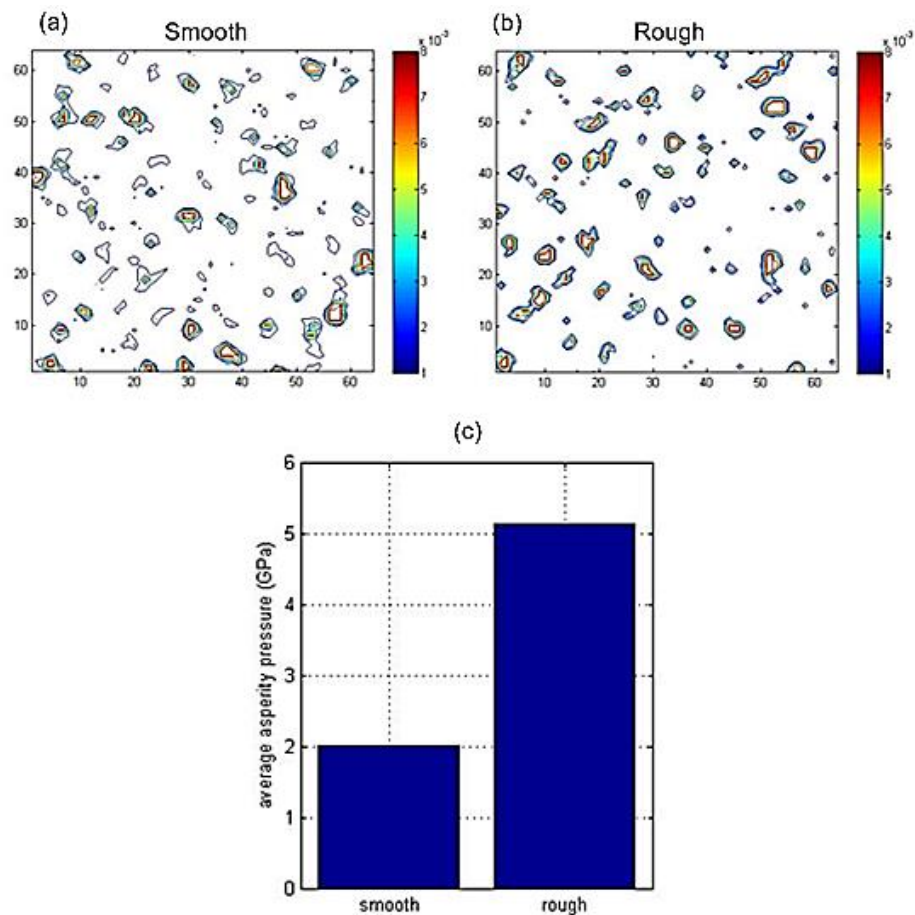
Figure 10-5. Simulation results of local contact pressures for smooth and rough discs. The unit for the local pressure in (a) and (b) is Pa

10.6 Relationship between MoS$_2$ Raman signal and MoDTC tribofilm thickness

To investigate whether MoS$_2$ Raman signal can be used to determine the thickness of MoDTC tribofilms, tribotests were conducted using MoDTC lubricant and stopped at 5, 20, 40, 60, 90 and 120 minutes. Figure 10-6 shows optical images of ball wear scars after tests at different durations. After 5 minutes test, the wear scar was not completely covered with a tribofilm. The

tribofilm grew rapidly with rubbing time and full coverage was obtained after rubbing for 20 minutes.
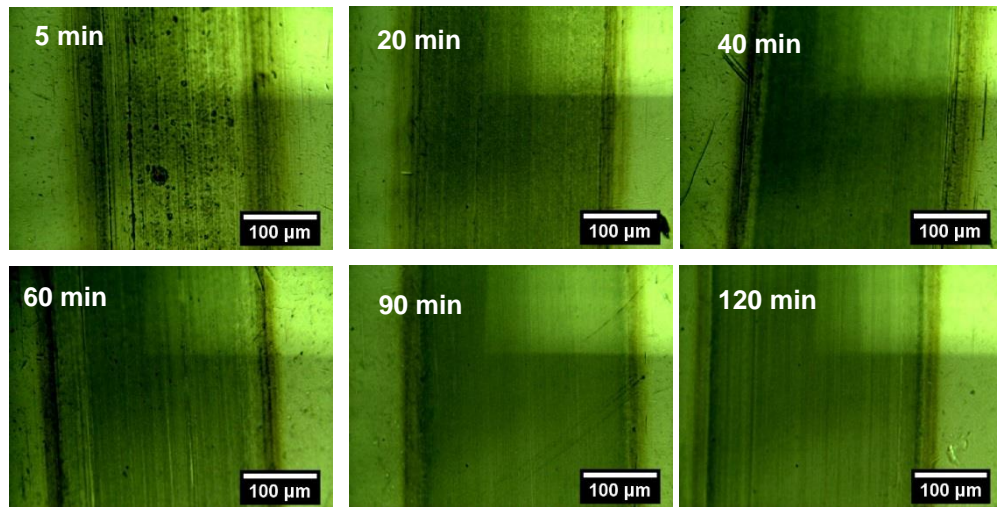
Figure 10-6. Optical images of ball wear scars after tests at different test durations as indicated. Tests were conducted using 0.5 wt% MoDTC lubricant, 1 GPa, 100ºC, SRR=100%, Disc R_a=150 nm

Figure 10-7 shows Raman spectra obtained from ball wear scars at different test durations. Each spectrum is an average of several spectra obtained from different regions of the wear scar. All the spectra showed the presence of MoS_2 peaks as expected. It should however be noted that for the wear scar generated after 5 minutes test, MoS_2 peaks were mostly observed in spectra obtained along the edges of the wear scar. There was no significant change in MoS_2 peak intensity with rubbing time. Despite the formation of thicker films after 2h test, MoS_2 peak intensity was similar to that obtained after 5 minutes test. In a previous Raman study by Scharf and Singer [163] on DLC coatings, it was shown that Raman intensity could be used to determine film thickness. However, from the Raman results in Figure 10-7, it can be seen that MoS_2 peak intensity could not be used to determine the thickness of MoDTC tribofilms.
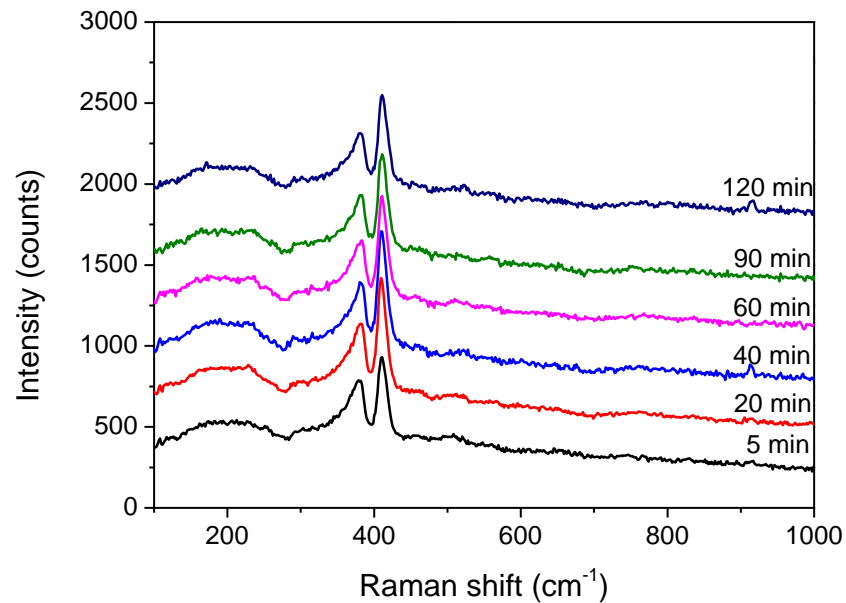
Figure 10-7. Raman spectra obtained from ball wear scars at different test durations. Each spectra is an average of several spectra obtained from different regions of the same wear scar

10.7   Summary

- Friction performance of MoDTC was only affected by slide-roll ratio in tests conducted with smooth discs.

- Only the surface roughness affected surface chemistry. Tests with rough discs resulted in wear scars composed of MoS_2 while tests with smooth discs had wear scars composed of a mixture of MoS_2, MoS_x (x>2) and $FeMoO_4$.

- Tests with rough discs resulted in formation of thicker films with a higher coverage than smoother discs. Formation of MoDTC tribofilms in tests with rough discs occurred very rapidly. Full tribofilm coverage on ball wear scars was observed after rubbing for 20 minutes. The intensities of MoS_2 Raman peaks could not be used to monitor the thickness of MoDTC tribofilms.

Chapter 11

Durability of MoDTC tribofilms and the effect on friction performance

11.1   Introduction

MoDTC additive in lubricants is consumed during tests due to thermal degradation and can be completely depleted after long duration tests [62, 164]. Depletion of MoDTC in tribological contact has been shown to result in high friction [66]. It has been suggested that the increase in friction is due to MoDTC tribofilms being removed from the tribocontact. It is however not clear whether friction increase is due to removal of MoDTC tribofilms or changes in the chemical composition. In this study, physicochemical changes that occur to pre-formed MoDTC tribofilms during MoDTC depletion have been investigated. The depletion of MoDTC at the tribocontact was simulated by replacing MoDTC-containing lubricant with MoDTC-free lubricant during tribotests.

Tribotests were conducted using high speed pin-on-disc (HSPOD) tribometer and the MiniTraction Machine (MTM) under unidirectional linear sliding and sliding/rolling conditions, respectively. Tribotests in the HSPOD tribometer were conducted at the following test conditions: 200 rpm (0.3 m/s), 80ºC, 1.67 GPa. Tribotests in MTM tribometer were conducted using rough discs (R_a=150 nm) sliding against smooth balls (R_a=10 nm) at the following tests conditions: 0.3 m/s entrainment speed (SRR=100%), 100ºC, 1 GPa (40 N). The MoDTC-containing lubricant used was 0.5 wt% MoDTC while the MoDTC-free lubricant used was BO

11.2 Tribotests under sliding/rolling conditions

11.2.1 Friction results

Figure 11-1 shows the friction curve obtained during the formation and removal of MoDTC tribofilms in BO. In the presence of MoDTC lubricant, there was initial high friction coefficient value of 0.11 followed by a rapid friction drop to low steady values (0.03-0.05). When MoDTC lubricant was replaced with BO, the friction rapidly increased and reached high values of $\mu=0.12$.
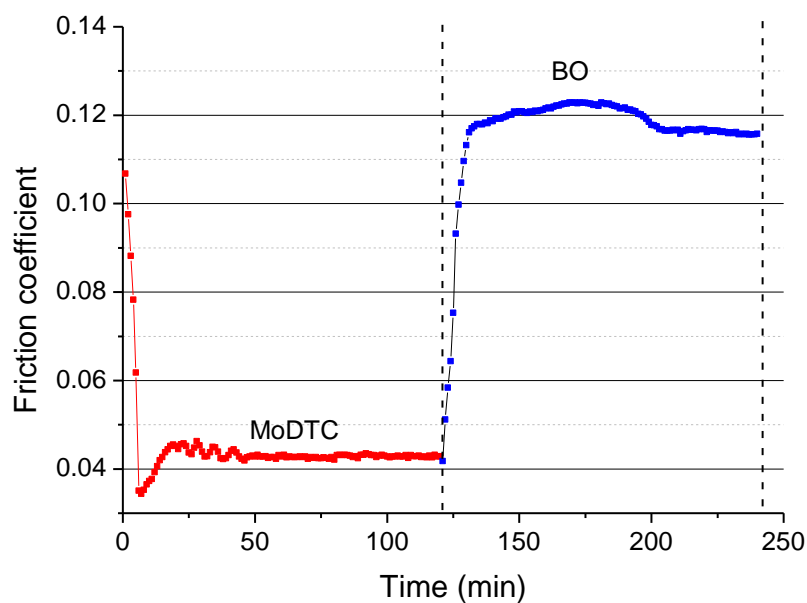
Figure 11-1. Friction coefficient during tests with MoDTC lubricant followed by tests with BO in sliding/rolling conditions. Tests were conducted using 0.3 m/s (SRR=100%), 40 N, 100ºC, Discs: R_a=150 nm, Balls: R_a=10 nm

11.2.2 Morphology of tribopair wear scar

Figure 11-2 shows interference images of balls during tests with MoDTC and when the lubricant was changed to BO. Figure 11-3 shows optical and 3D images of ball wear scars after tests. Figure 11-2 (a) shows typical images obtained during the initial 2h of MoDTC tribofilm formation. MoDTC tribofilms were rapidly formed on the ball wear scar and a complete tribofilm was

153

observed after rubbing or 60 minutes. Optical image of the ball after rubbing for 2h shows that the wear track was covered with a tribofilm.
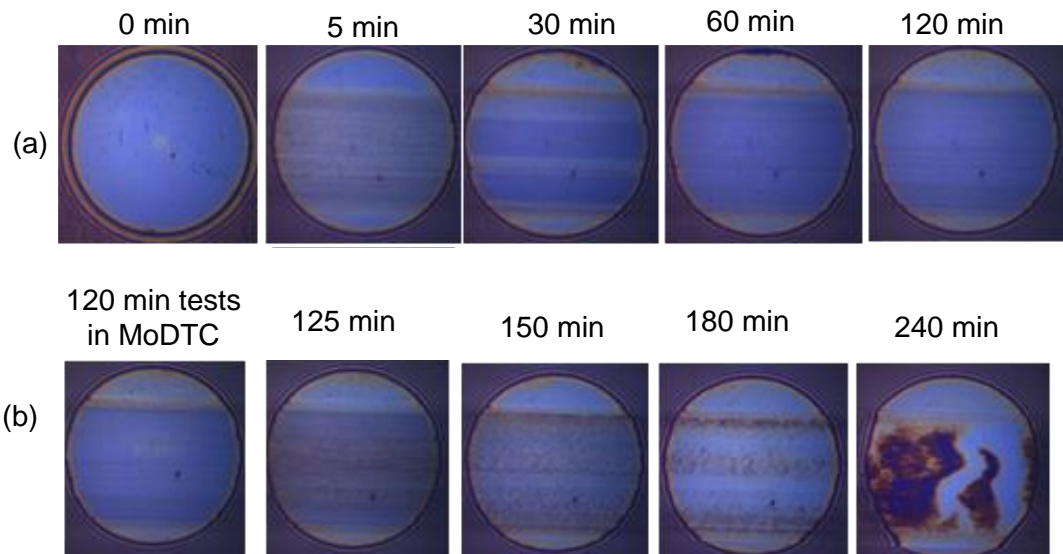
Figure 11-2. Interference images of ball wear scars during tests with (a) MoDTC (b) MoDTC followed with BO
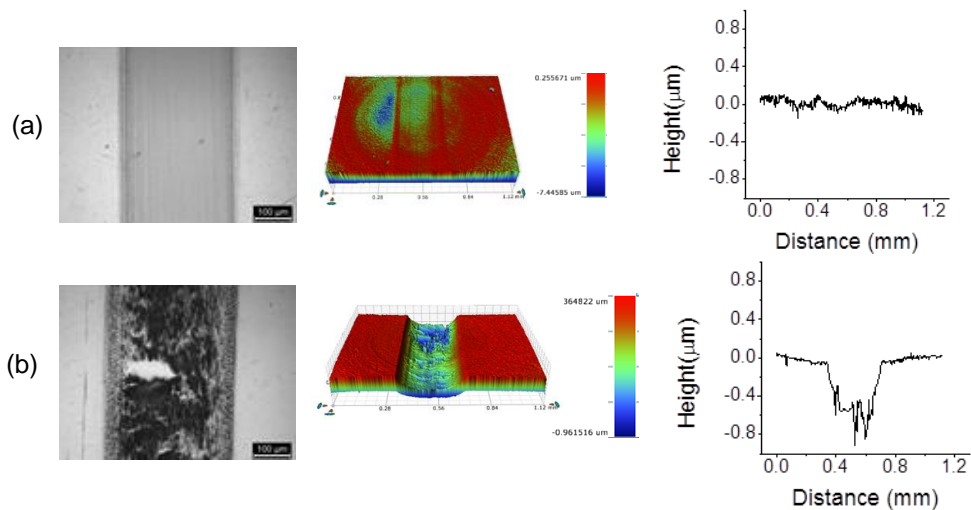
Figure 11-3. Optical and 3D images of ball wear scars after 2h tests in different lubricants (a) MoDTC (b) MoDTC followed by BO

Figure 11-2 (b) shows interference images during rubbing of pre-formed MoDTC tribofilm with BO. The tribofilm was almost completely removed after

154

rubbing for 2h in BO. Optical images of the wear scar after 2h rubbing in BO, Figure 11-3 (b), show that the MoDTC tribofilm that was initially present in the scar was mostly removed. Some regions of the wear scar appeared covered with a thin film. 3D image of the ball clearly show that most of the MoDTC tribofilm was removed from the wear scar. The depth profile across the wear scar after tests with BO shows that the wear scar had a depth of 400 nm.

11.2.3 Raman analysis of tribopair wear scars

Figure 11-4 shows Raman spectra obtained from tribopair wear scars after tests with MoDTC and when MoDTC was replaced with BO. The spectral information is summarised in Table 11-1. MoS_2 was formed after tests with MoDTC. When MoDTC lubricant was replaced with BO, the wear scars were only composed of MoS_x, $Fe_2(MoO_4)_3$ [73, 165] and $FeMoO_4$.
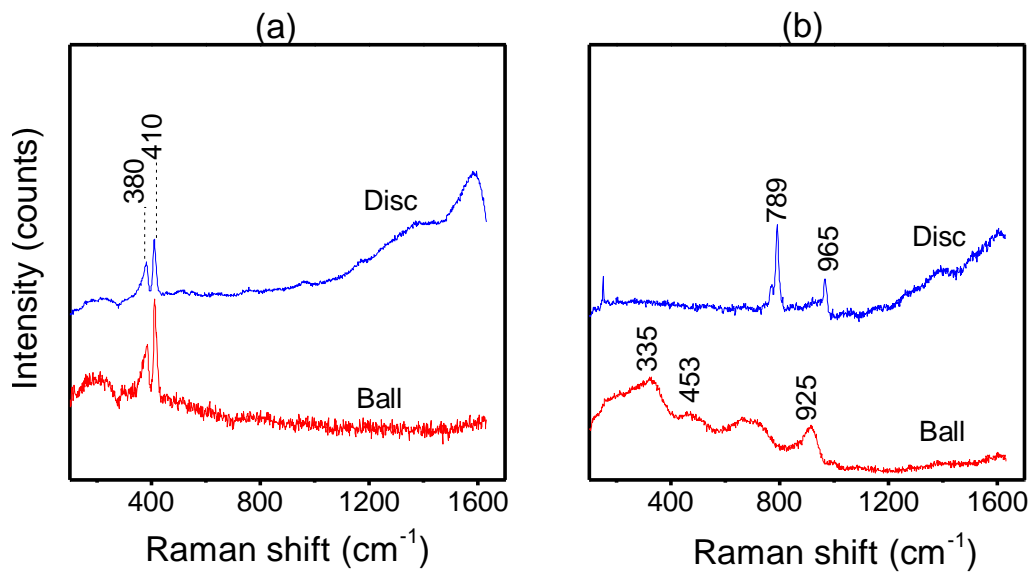
Figure 11-4. Raman spectra obtained from the tribopair wear scars (a) 2h test with MoDTC (b) 2h test with MoDTC followed by 2h test with BO

Table 11-1. Chemical composition of wear scars after durability tests conducted in sliding/rolling conditions

Lubricant	Raman peak (cm⁻¹)	Notes
MoDTC	380, 410 (MoS_2) 1350, 1580 (carbon)	- Chemical composition uniform within wear scars
MoDTC followed by BO	335, 453 (MoS_x) 789, 965 ($Fe_2(MoO_4)_3$) 925 ($FeMoO_4$) 1350, 1580 (carbon)	- Chemical composition non-uniform within wear scars

11.3 Tribotests under unidirectional linear sliding conditions

Tests were conducted using two types of substrates; (1) fresh steel samples and (2) oxidised steel samples. Steel samples in this study were oxidised by rubbing in BO for 60 minutes in order to generate iron oxides on the surfaces of the samples. The reason why oxidised steel samples were used is because oxidation is likely to occur on steel surface in tests with MoDTC. It has been reported that MoDTC lubricants can have induction times as long as 120 minutes [66]. Since iron oxides are mostly formed during the induction period (Table 7-1), having long induction times would result in the formation of more iron oxides on the steel surface. MoDTC tribofilms formed after such long induction times are thus formed on oxidised surfaces and not directly on fresh steel surfaces.

11.3.1 Friction results

Figure 11-5 shows friction curves during tests. In the first stage where MoDTC lubricant was used, there was high friction coefficient (0.10) at the beginning of the test which rapidly dropped to lower values (0.05) after a short induction time of 30s. When MoDTC lubricant was replaced with BO, the friction coefficient remained low (0.05-0.06) in tests conducted with fresh samples

while in tests conducted with oxidised samples there was a rapid rise in friction to values of about μ=0.08-0.09. The friction behaviour observed with the oxidised sample is in agreement with that reported in literature [66].
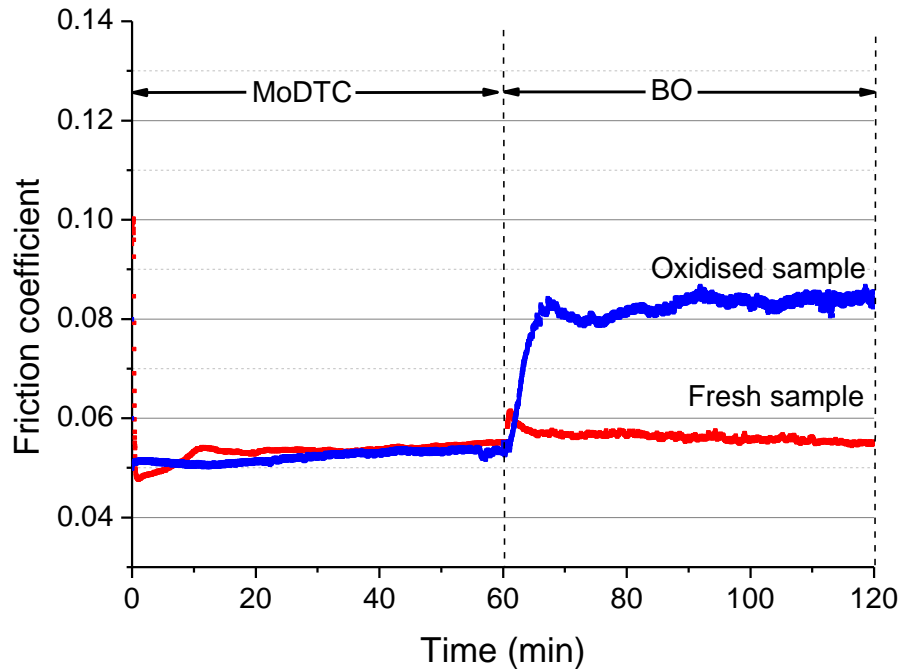
Figure 11-5. Friction curves obtained during tests with MoDTC followed by BO in unidirectional linear sliding conditions. Tests were conducted at 80⁰C, 200 rpm (0.3 m/s), 1.67 GPa

11.3.2 Morphology of wear scars

Figure 11-6 shows optical images of the tribopair wear scars after tests with fresh steel samples. At the end of tests with MoDTC, a wear scar measuring 300 μm in diameter was formed on the ball. The wear scar appeared covered with a patchy tribofilm. The disc wear scar also appeared intermittently covered with tribofilms. When the lubricant was changed to BO, the resulting ball wear scar was covered with a thicker tribofilm. The coverage of the tribofilm was higher compared to that at the end of tests with MoDTC. The morphology of the disc wear scar did not change significantly when the lubricant was changed to BO.
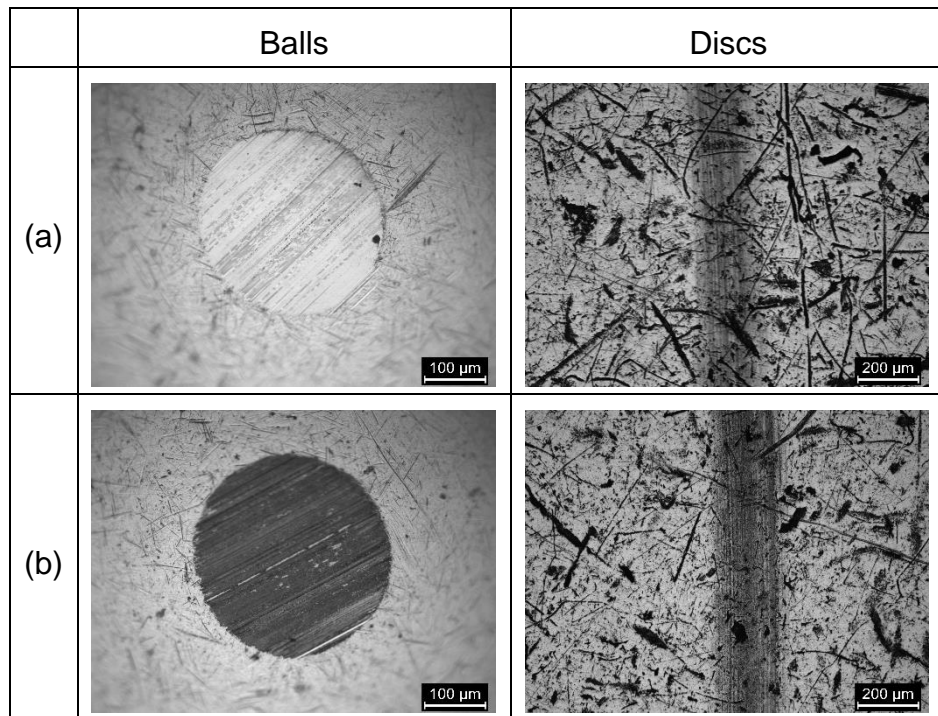
Figure 11-6. Optical images of tribopair wear scars after tests on fresh steel samples (a) MoDTC (b) MoDTC followed by BO

Figure 11-7 shows optical images of the tribopair wear scars after tests on oxidised steel samples. The diameter of wear scars generated on the ball after tests with MoDTC (700 µm) was 2 times larger than that observed in tests with fresh steel samples (Figure 11-6). The high wear was generated during the initial test with BO since MoDTC was not present to provide wear protection [143]. After tests with MoDTC, patchy films were formed in the wear scar. A very thick film was formed on the disc wear scar. When the lubricant was changed to BO, the patchy films previously formed on the ball wear scar in MoDTC were mostly removed. This is in contrast to what happened in tests with fresh steel samples when the lubricant was changed from MoDTC to BO.
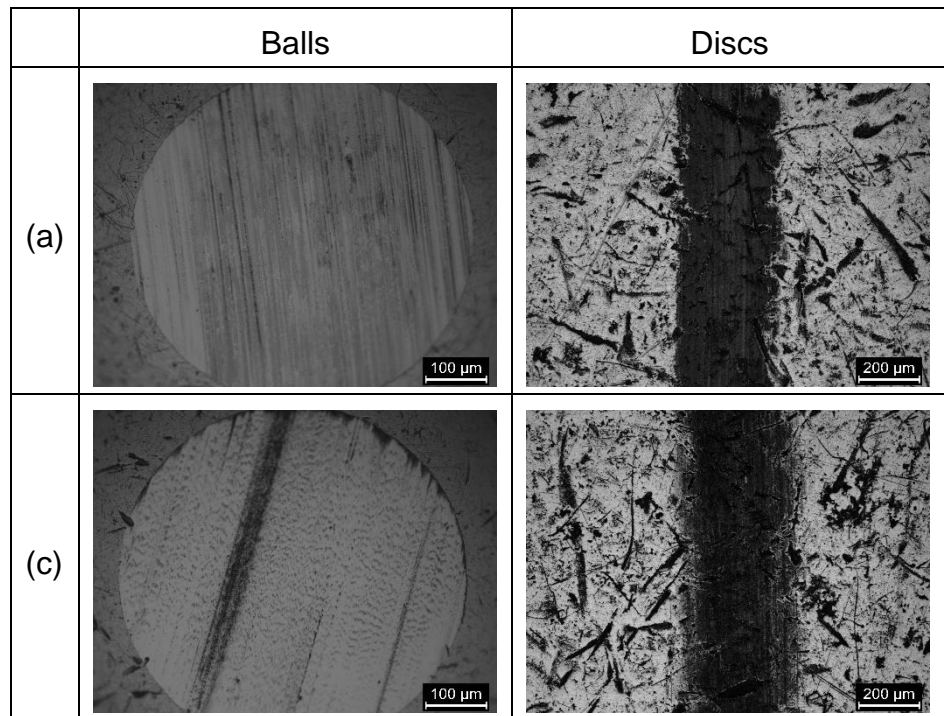
Figure 11-7. Optical images of tribopair wear scars after tests on oxidised steel samples. (a) MoDTC (b) MoDTC followed by BO

11.3.3 Raman analysis of wear scars

Spectra obtained from tribopair wear scars are shown in Appendix E. Table 11-2 shows the chemical composition of wear scars at different stages during tests. In tests conducted using fresh steel samples, MoDTC tribofilms composed of MoS_2 were formed after tests with MoDTC as expected. Rubbing the pre-formed MoDTC tribofilms in BO resulted in partial amorphisation of MoS_2 within the tribofilm and formation of $FeMoO_4$.

In tests conducted with oxidised steel samples, MoDTC tribofilms formed after tests with MoDTC were composed of MoS_2 and iron oxides. Rubbing the pre-formed MoDTC tribofilm in BO resulted in complete amorphisation of MoS_2 to MoS_x and the formation of iron molybdates ($Fe_2(MoO_4)_3$, $FeMoO_4$) [166].

Table 11-2. Chemical composition of wear scars after durability tests conducted under unidirectional linear sliding conditions

Sample	Raman peaks (cm⁻¹) and assignment	
	MoDTC	MoDTC followed by BO
Fresh steel sample	380, 410 (MoS_2)	100-400 (MoS_x) 380, 410 (MoS_2) 650 (Fe_3O_4) 925 ($FeMoO_4$)
Oxidised steel sample	380, 410 (MoS_2) 225, 295 (Fe_2O_3) 667 (Fe_3O_4)	335, 453 (MoS_x) 225, 295 (Fe_2O_3) 667 (Fe_3O_4) 751 $Fe_2(MoO_4)_3$ 925 ($FeMoO_4$)

11.4 Summary

- When rubbed with BO, the durability of MoDTC tribofilms formed on fresh steel samples is dependent on the sliding configuration. MoDTC tribofilms are more durable under unidirectional linear sliding conditions than under sliding/rolling conditions.

- In unidirectional linear sliding conditions, MoDTC tribofilm formed on oxidised steel sample were less durable than those formed on fresh steel samples when rubbed in BO.

- Surface chemistry of wear scars changes when pre-formed MoDTC tribofilms are rubbed in BO.

Chapter 12 Discussion

Results from tribological tests with MoDTC clearly show that test parameters affected the tribological performance (friction and wear) of the lubricant. Through detailed chemical analysis using Raman spectroscopy and wear analysis, the knowledge gaps on MoDTC, highlighted in Section 3.7.2, have been addressed. Overall, the study shows that tribochemistry is key to understanding tribological performance of lubricated systems in boundary lubrication regime. Furthermore, Raman spectroscopy has proven to be a very effective technique in studying tribochemical reactions of MoDTC. In this Chapter, results obtained from this study are discussed. This discussion is split into the following seven key points.

- Thermal decomposition of MoDTC

- Tribological tests with MoDTC

- Friction performance of MoDTC

- Wear performance of MoDTC

- The growth of MoDTC tribofilms

- Durability of MoDTC tribofilms

- Chemical characterisation using Raman spectroscopy

12.1 Thermal decomposition of MoDTC

12.1.1 MoDTC lubricant

Table 12-1 summarises the results obtained from chemical characterisation after thermal tests with MoDTC in Chapter 5. It was observed that the degradation of MoDTC in the lubricant was very slow. It took more than 3h before decomposition products were observed. Furthermore, it was observed

that MoDTC decomposed to form MoS_x instead of MoS_2. The formation of MoS_x could be due to the low temperature used 150ºC. It has been reported that MoDTC forms MoS_2 at temperatures above 300ºC [54, 55]. From thermal analysis conducted by Watanabe et al. [167] the formation of MoS_2 from MoDTC, with a similar structure as MoDTC used in this study, occurred at 336ºC. The formation of MoS_x should however be considered as a precursor to the formation of MoS_2 [168] (see Section 12.2.1).

Table 12-1. Thermal decomposition of MoDTC

Sample	Duration	Temperature	Chemical composition
MoDTC concentrate	1h	100ºC	MoS_x
MoDTC lubricant	1h	150ºC	MoDTC
MoDTC lubricant + Fe_3O_4	1h	100ºC	MoS_2, $FeMoO_4$
MoDTC lubricant	3h	150ºC	MoDTC
MoDTC lubricant (deposits)	5h	150ºC	MoS_x

The rate of formation of MoS_x (r_{MoS_x}) during thermal decomposition of MoDTC can be defined by Equation 12-1.

$$\frac{d[MoS_x]}{dt} = r_{MoS_x} = k_{thermo}[MoDTC]$$

12-1

Where k_{thermo} is the reaction constant and [MoDTC] the concentration of MoDTC. As the reaction is thermally-activated, k_{thermo} is described by the Arrhenius Equation 12-2.

$$k_{thermo} = A_0 e^{\frac{-E_a}{RT}}$$

12-2

Where A_0 is the pre-exponential factor, R the gas constant and T the absolute temperature and E_a the activation energy.

Therefore, the reaction rate increases with increase in MoDTC concentration and temperature. This reaction kinetics explain the differences observed in tests with MoDTC concentrate (55-65 wt%) and MoDTC lubricant (1 wt%). The formation of MoS_x was faster (1h) in MoDTC concentrate than in the lubricant (>3h) due to the high concentration.

Formation of brown deposits after 5h thermal tests with MoDTC lubricant indicated that the decomposition product was not soluble in the base oil. This suggests that the product formed did not have alkyl groups. The formation of brown deposits in MoDTC lubricants was also reported by De Feo et al. [169]. In the mentioned study, the mechanism shown in Figure 12-1 was proposed for the degradation process. Although Raman analysis conducted in this study showed that the brown deposits were composed of MoS_x, it is also possible that at longer heating times, oxidation would occur leading to the formation of molybdenum oxysulphides (MoS_xO_y) as suggested by De Feo et al. [169].
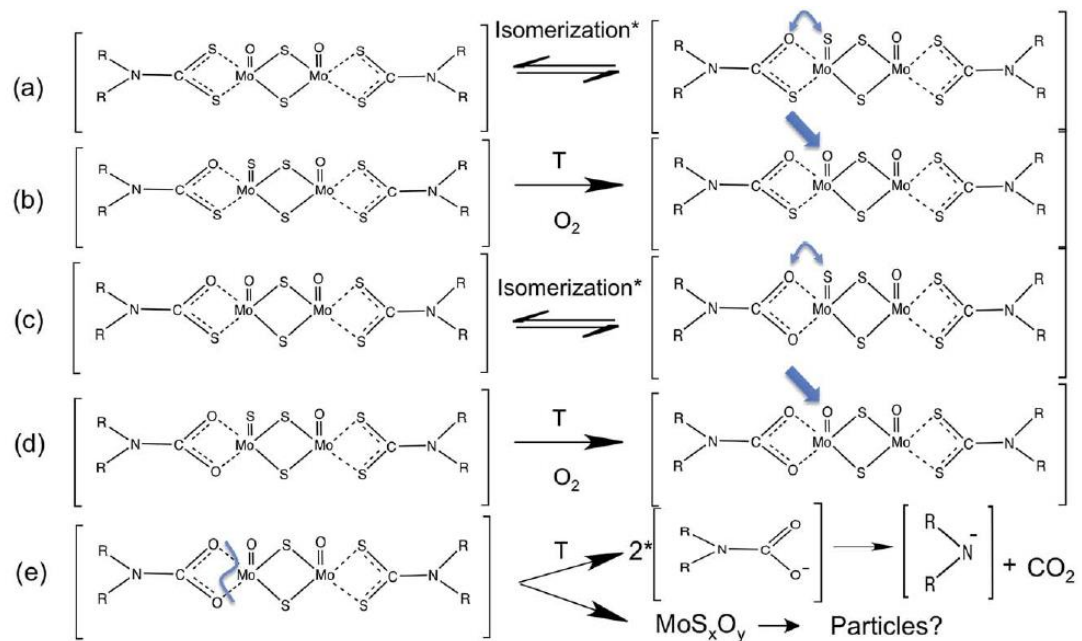
Figure 12-1. Mechanism for the thermal degradation of MoDTC proposed by De Feo et al. [152]

One interesting finding in this study was that when Fe_3O_4 was added to MoDTC lubricant, MoS_2 was formed despite the temperature being lower the formation temperature of MoS_2 in MoDTC (>300ºC). In addition, MoS_2 was formed after only 1h. This is a very short time compared to the time it took for decomposition products to be formed when Fe_3O_4 was not present.

In thermally-activated reactions, reactions will only occur when energy in the system is greater than the activation energy (E_a). The energy of the system can be increased by increasing the temperature of the system. Thermally-activated reactions can occur at lower temperatures when catalysts are used since catalysts provide an alternative reaction route that allows the reaction to occur at lower activation energies.

Since MoS_x is a precursor for the formation of MoS_2, the activation energy (E_a) for the formation of MoS_2 is considered to be higher than that for the formation of MoS_x. This means that more energy is required in the system to form MoS_2. At similar test temperatures (same energy in the system), MoS_x was formed in the absence of Fe_3O_4 while MoS_2 was formed in the presence of Fe_3O_4. These results indicate that the presence of Fe_3O_4 resulted in a reaction route that allowed MoS_2 to be formed at a lower activation energy.

Fe-based compounds have been reported to catalyse decomposition reactions of lubricating oils and additives. Huq et al. [170] reported that FeF_3 catalysed the decomposition of ZDDP resulting in lower decomposition temperatures and faster decomposition rates. Nehme [171] reported that thicker tribofilms were formed when FeF_3 was added to ZDDP oils probably due to the faster decomposition rate of ZDDP. Colclough [35] reported that $Fe(C_5H_7O_2)_3$ catalysed the decomposition of mineral oil. From these reports, it can be inferred that Fe_3O_4 probably acted as a catalyst in the decomposition of MoDTC in this study.

12.1.2 MoDTC thermal films and tribochemical films

Table 12-2 compares the chemical composition of MoDTC films formed from thermal and tribological decomposition at 100ºC. MoDTC thermal films were found to be composed of MoDTC while MoDTC tribofilms were composed of MoS_2. The formation of MoS_2 in MoDTC tribofilms was very rapid (after rubbing for only 2 minutes). The slow rate of MoDTC decomposition under thermal conditions explains why MoDTC thermal films did not have any decomposition product after 1h (Section 12.1.1). Overall, these results show that the decomposition of MoDTC is accelerated in tribological conditions.

Table 12-2. Chemical composition of MoDTC films formed from thermal and tribological reactions at 100ºC

Condition	Sample	Duration	Chemical composition
Thermal	MoDTC thermal film	1h	MoDTC
Tribochemical	MoDTC tribofilm	2 minutes	MoS_2, $FeMoO_4$, Fe_3O_4
	MoDTC tribofilm	1h	MoS_2

The rapid decomposition of MoDTC in tribological contacts is believed to be due to MoDTC being decomposed on the rubbing surfaces of the tribopair and not in the bulk oil. The decomposition of MoDTC on the rubbing surfaces is also supported by the fact that decomposition products were only observed within the rubbed surfaces. For MoDTC decomposition to occur at the rubbing surface, MoDTC has to adsorb on the surfaces. Onodera et al. [87] showed that MoDTC adsorbs on nascent steel surfaces via S atoms. The initial rubbing of steel surfaces at the beginning of tribological tests causes the removal of the top oxide layer resulting in the generation of nascent surfaces on which MoDTC can adsorb. As adsorption of MoDTC is an important step in the decomposition process, test conditions that promote adsorption would increase the rate of decomposition. The influence of test conditions on MoDTC adsorption is discussed in detail in Section 12.2.5.

12.2 Tribological tests with MoDTC lubricant

Tribological tests with MoDTC resulted in the formation of MoDTC tribofilms composed of MoS_2, MoS_x and $FeMoO_4$ in different concentrations depending on test conditions. Although the formation of MoS_2 has been widely reported, the formation of $FeMoO_4$ and MoS_x has not been reported before. Key information about these two compounds is presented below.

12.2.1 MoS_x

MoS_x ($x>2$) compounds are normally formed at lower temperatures than MoS_2 and have been reported to undergo recrystallization at high temperatures to form MoS_2 [80, 82, 159, 172, 173]. Recrystallization of MoS_x has also been observed under tribological conditions. Lince et al. [174] reported the formation of MoS_2 after tribological tests on MoS_3 coatings. Based on this information, it can be concluded that MoS_x is an intermediate compound in the formation of MoS_2 and that the transformation of MoS_x to MoS_2 is dependent on temperature and shear stress. It should be noted that sulphur-rich MoS_x compounds appear dark brown in colour while MoS_2 is grey in colour [159, 172]

12.2.2 $FeMoO_4$

Considering the quaternary diagram shown in Figure 3-5, it is not surprising that $FeMoO_4$ was formed in tests with MoDTC since Fe, O and Mo were present at the steel/steel contact. In literature, it has been reported that $FeMoO_4$ is formed from a reaction of molybdenum compounds with iron oxides at temperatures of about 120⁰C [175, 176]. It has also been reported that metal molybdates can be formed at room temperature via mechanical activation (mechanical milling) [177].

In this study, the formation of $FeMoO_4$ was also observed in the following instances.

- During thermal degradation of MoDTC lubricant in the presence of Fe_3O_4 at 100°C (Figure 5-8)

- During tribotests on MoS_2 coated discs (Figure 7-13b).

From knowledge gained in literature and results from this study, it can be deduced that in tribotests with MoDTC lubricant, $FeMoO_4$ was probably formed from a reaction of molybdenum compounds with iron oxides on the steel surface. Also, that this reaction was mechanically-activated.

12.2.3 Tribochemical reactions

In tests conducted at 20°C, it was observed that MoDTC decomposed to form MoS_x and $FeMoO_4$ (Figure 8-3). This is an interesting observation as such a reaction would not happen in non-tribological conditions since the temperature is too low to cause thermal decomposition of MoDTC. These results indicate that the tribochemical reaction was not necessarily driven by temperature as is the case for thermally-activated reactions. Tribochemical reactions cannot therefore be described by the Arrhenius Equation in 12-2. The presence of shear stress in tribological tests promoted the decomposition MoDTC. These results are supported by simulation studies conducted by Onodera et al. [87] where it was reported that decomposition of adsorbed MoDTC occurred only when pressure and sliding were applied. Numerical studies have shown that tribochemical reactions also occur in other molecules when shear stress is applied [178]. The addition of shear stress has been reported to initiate and accelerate reactions [179-181]. It is therefore suggested that tribochemical reactions of MoDTC are best described by the modified Arrhenius Equation in 12-3.

$$k_{tribo} = A_o \, exp^{\frac{\sigma V - E_a}{k_B T}}$$ 12-3

Where A_o is the pre-exponential factor, σ the shear stress, V the material constant, E_a the activation energy, T the temperature and k_B the Boltzmann constant.

The rate of MoDTC decomposition in tribological contacts is therefore dependent on shear stress, temperature as well as MoDTC concentration. The shear stress component in Equation 12-3 reduces the activation energy which in turn enables MoDTC decomposition to occur at low temperatures.

12.2.4 Proposed mechanism for MoDTC decomposition

The mechanism for MoDTC decomposition proposed by Grossiord et al. [56] cannot be used to explain MoDTC decomposition products obtained at 20ºC as MoS_2, MoO_2 or MoO_3 were not detected in the wear scars. The previously proposed mechanism suggests the formation of MoO_2 and MoO_3 however these oxides were not detected by Raman spectroscopy in this study. Therefore, a new decomposition pathway for MoDTC has to be proposed to accommodate the observations made in this study.

In determining the new reaction pathway, the chemical composition of MoDTC tribofilms formed at various contact parameters was considered (Table 8-1, Table 8-3, Table 8-4). As discussed in Section 12.2.3, shear stress participates in the decomposition of MoDTC probably through rupturing of bonds. To determine which bonds would be most susceptible to rupturing under shear stress, bond dissociation energies of bonds in MoDTC were obtained from literature. Table 12-3 shows bond dissociation energies for various bonds in MoDTC. The C-S bond has the lowest bond dissociation energy therefore it is the weakest bond and can be easily ruptured under shear stress [43, 50]. Figure 12-2 shows the proposed reaction pathway for MoDTC decomposition.

Table 12-3. Bond dissociation energy for bonds in MoDTC

Bond type	Bond dissociation energy (kJ/mol) [182]
Mo-S	450
Mo=O	420
C-H	410
C-C	350
C-N	300
C-S	260
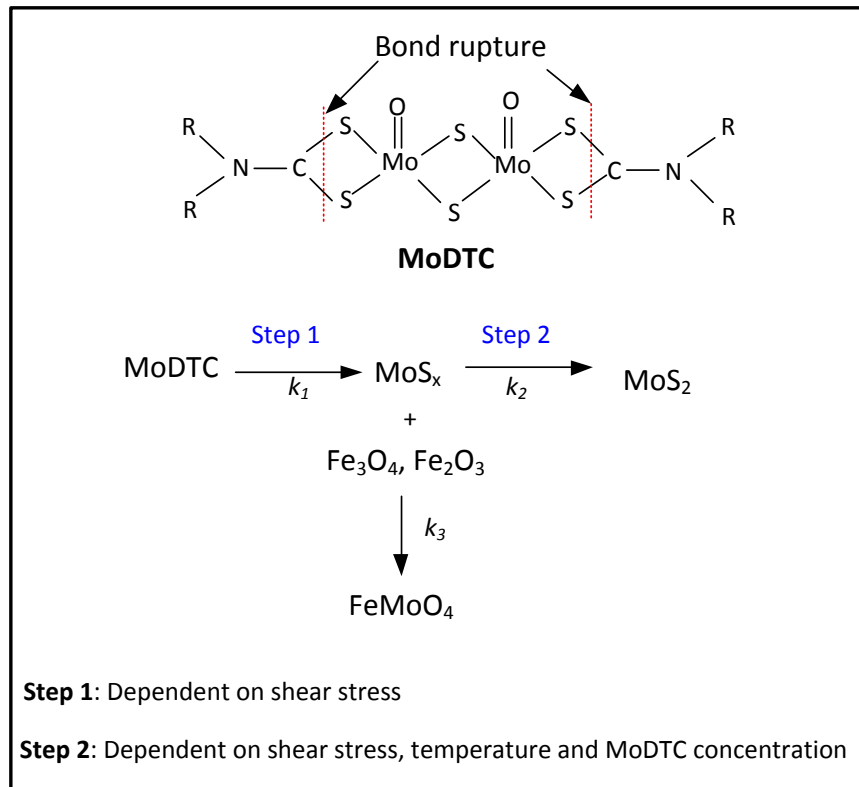
Figure 12-2. Proposed reaction pathway for decomposition of MoDTC in a tribological contact

The decomposition process occurs as follows.

1   MoDTC first adsorbs on the tribopair surfaces.

2   In Step 1, shear stress applied on the adsorbed MoDTC molecules causes decomposition to occur. The decomposition process begins by rupturing of C-S bonds forming molybdenum intermediate compound

which undergoes intramolecular sulphonation forming amorphous MoS_x.

3 In Step 2, MoS_x is converted to MoS_2. Since $E_{a(MoS_2)} > E_{a(MoS_x)}$, MoS_2 can be formed from MoS_x either through increasing the energy at the contact by increasing temperature or lowering the activation energy by increasing shear stress.

4 $FeMoO_4$ is formed from a reaction of iron oxides on the steel surfaces with MoS_x.

The rates of reactions for the formation of the various MoDTC decomposition products are shown in Equations 12-4 to 12-6. It should be noted that these are simplified expressions as the order of the reactions is currently unknown.

$$r_{MoS_x} = k_1[MoDTC] \qquad\qquad 12\text{-}4$$

$$r_{MoS_2} = k_2[MoS_x] \qquad\qquad 12\text{-}5$$

$$r_{FeMoO_4} = k_3[MoS_x]\,[iron\ oxides] \qquad\qquad 12\text{-}6$$

Although exact values for reaction rate constants k_1, k_2 and k_3 have not been determined in this study, it is believed that the reaction constants can be described by Equation 12-3 [50].

Reaction constant k_1 is not dependent on temperature as MoS_x is formed even at 20°C given that shear stress is applied. Reaction constant k_2 is dependent on both temperature and shear stress since recrystallization of MoS_x is dependent on these two parameters (Section 12.2.1). Varying the temperature and shear stress will therefore affect k_2 values which will in turn affect the decomposition products as follows.

$$k_1 \gg k_2 \qquad \text{MoS}_x$$

$$k_1 > k_2 \qquad \text{MoS}_x, \text{MoS}_2$$

$$k_1 \ll k_2 \qquad \text{MoS}_2$$

From results obtained in Section 8.2.3, it was observed that the formation of $FeMoO_4$ was inversely proportional to the formation of MoS_2. The reason for this can be attributed to two competing reactions occurring at the tribocontact; oxidation of the surface and formation of MoS_2. Formation of $FeMoO_4$ is dependent on the presence of iron oxides at the tribocontact. Iron oxides are formed as a result of surface oxidation. Oxidation of the steel substrate is favoured when the formation of MoS_2 at the contact is inhibited. On the other hand, rapid formation of MoS_2 at the contact will hinder surface oxidation and the subsequent formation of $FeMoO_4$.

12.2.5 Effect of temperature and MoDTC concentration

Results presented in Table 8-1 showed that the chemical composition of MoDTC tribofilms changed from MoS_x, $FeMoO_4$ to MoS_2 when the temperature was increased from 20ºC to 100ºC. In the study by Morina et al. [60] it was observed that tribofilms formed at 30ºC had lower amounts of Mo and S than those formed at higher temperatures (100ºC, 150ºC). It was also reported in the same study that more Mo oxides (MoO_3) were formed at 30ºC than at higher temperatures.

MoDTC concentration was also found to affect the composition of MoDTC tribofilms (Table 8-3). At low concentration (0.1 wt%) MoS_x and $FeMoO_4$ were formed while at 0.5 wt% MoS_2 was formed. At 0.9 wt% a mixture of MoS_2, MoS_x and $FeMoO_4$ was formed. In a previous study, it was reported that sulphates were formed at low MoDTC concentration (Mo 100 ppm) while at high concentration MoS_2 was formed [70]. In another study, it was reported that the amount of MoS_2 increased with MoDTC concentration [77].

Reports in literature on the influence of temperature and MoDTC concentration on the composition of MoDTC tribofilms are not in complete agreement with findings in this study. This can be attributed to differences in analysis techniques used in this study and in the previous studies (XPS, XAS). This is because different techniques have varying capabilities when distinguishing molybdenum compounds. This is further discussed in Section 12.7.1.

In order to explain the results obtained in this study, the effect of temperature and MoDTC concentration on MoDTC decomposition has to be considered. Temperature and MoDTC concentration affect MoDTC decomposition in the following three ways.

1. Affecting the adsorption of MoDTC on the rubbing surfaces

2. Determining the nature of products formed

3. Affecting the rate of the decomposition reaction

Adsorption of additives has been shown to increase with increase in temperature and concentration [183, 184]. At low MoDTC concentrations and low temperatures, there is less MoDTC adsorbed on the surface. Lower MoDTC coverage will promote oxidation of the steel surface while higher MoDTC coverage will hinder oxidation of the steel surface.

From the mechanism proposed in Section 12.2.4, it can be seen that high temperatures will promote the formation of MoS_2 formed while low temperatures will lead to formation of MoS_x. High temperatures will also lead to rapid formation of MoS_2. From Equation 12-4, it can be seen that high MoDTC concentrations will increase the rate of MoS_x formation.

The insights presented above on MoDTC adsorption and decomposition can be used to explain the trends observed in this study at varying temperatures and MoDTC concentrations.

Observations made at varying temperatures can be explained as follows. The formation of $FeMoO_4$ at low temperatures is due high surface oxidation due to low MoDTC coverage. The decrease in $FeMoO_4$ amount with increase in temperature is due to a decrease in surface oxidation as the formation of MoS_2 on the surface occurs instead.

Observations made at varying MoDTC concentrations can be explained as follows. At low concentrations, $FeMoO_4$ is formed due to presence of an oxidised surface as a result of low MoDTC coverage. At the temperature used (60ºC), the formation of MoS_2 was expected. However, MoS_x was formed instead of MoS_2. The formation of MoS_x can be attributed to the slow rate of MoS_x formation due to a lower MoDTC concentration (Equation 2-4). Consequently, the rate of MoS_x conversion to MoS_2 was very slow because of low MoS_x concentration (Equation 12-5). The formation of MoS_2 would therefore require a longer time than the duration used in the test (2h). Increasing MoDTC concentration from 0.1 wt% to 0.5 wt% resulted in the formation of MoS_2 as expected. This is because the formation of MoS_x was faster. Increasing the concentration further to 0.9 wt% MoDTC resulted in a mixture of MoS_x and MoS_2 which was unexpected. This observation can be due to the rate of MoS_x formation being too high to balance the rate of MoS_2 formation. To increase the rate of MoS_2 formation, k_2 values have to be increased. This can be done either by increasing the temperature or the contact pressure. This was confirmed by formation of MoS_2 in tests conducted with 0.9 wt% at 80ºC (Table 9-3).

12.2.6 Effect of surface texture and contact pressure

In results presented in Section 10.4, it was observed that rough surfaces resulted in the formation of MoS_2 while MoS_2, MoS_x and $FeMoO_4$ were formed in smooth surfaces. Cousseau et al. [68] reported that MoS_2 was only formed in rough discs and not smooth surface. It should however be noted that in the mentioned study tests were conducted with a fully formulated oil unlike tests conducted in this study where only MoDTC in base oil was used. Cousseau et al. [68] suggested that rough surfaces promoted the formation of MoS_2 through removal of surface oxides. The authors of the mentioned study arrived at this conclusion by considering that the removal of iron oxides was a prerequisite for the formation of MoS_2. However in this study, it was observed that MoS_2 was formed on oxidised samples (Table 11-2). Based on the results contained from this study it is believed that the removal of iron oxides is not a prerequisite for the formation of MoS_2. The formation of MoS_2 in rough surfaces is therefore explained by a different mechanism other than the removal of iron oxide films.

Based on the decomposition mechanism proposed in Section 12.2.4, it is expected that MoS_2 would be formed at the temperature used in the tests (100ºC). MoS_2 was formed in rough surfaces as expected. But in smooth surfaces MoS_x was observed in some regions.

Surface roughness has been shown to affect the distribution of pressure at the tribocontact. Rough surfaces have been reported to have extremely high local pressures in comparison to smooth surfaces [185]. Thus during sliding, rough surfaces will experience higher shear stresses than smooth surface due to high local pressures [68]. Simulation results in this study showed higher local contact pressures in rough surfaces than in smooth surfaces (Figure 10-5). It is thus believed that the varying chemical composition observed in this study at different surface roughness can be attributed to differences in shear stresses.

Numerical studies have shown that when sufficient shear stress is applied to molecules, chemical bond dissociation and reorganisation occurs [178]. In the case of MoDTC, high shear stress leads to recrystallization of MoS_x to MoS_2. It is proposed that the high stresses in rough surfaces promoted the formation of MoS_2 while low shear stresses in some regions of the smooth surface resulted in the formation of MoS_x.

In unidirectional sliding conditions, increasing the contact pressure from 0.98 to 2.12 GPa resulted in formation of tribofilms composed of MoS_2 instead of a mixture MoS_2 and MoS_x (Figure 8-9). Formation of MoS_2 at higher contact pressures can also be explained by the presence of higher shear stresses at the contact.

12.2.7 Effect of sliding configuration

Studies on the impact of test conditions on MoDTC decomposition were investigated in both unidirectional linear sliding and sliding/rolling contacts. Generally, the influence of the contact parameters was similar in the two sliding configurations. However, there were a few exceptional cases where the sliding configuration affected MoDTC decomposition. These instances have been highlighted in Table 12-4. It is noted that the contact pressure and speeds were different in the two sliding configurations.

From Table 12-4, it can be seen that differences in the chemical composition of MoDTC decomposition products were only noticeable at 20ºC and 0.1 wt% MoDTC concentration. At higher temperatures and MoDTC concentrations, the chemical composition of the wear scars was the same for both sliding configurations. For tests conducted at 20ºC, MoS_x and $FeMoO_4$ were formed in unidirectional linear sliding while iron oxides and $FeMoO_4$ were formed in sliding/rolling conditions. At a higher temperature of 100ºC, MoS_2 was formed in both sliding configurations despite the contact pressure and speed being different. This suggests that the difference in chemical composition observed

in tests conducted at 20ºC cannot be attributed to the difference in test conditions but instead can be attributed to the sliding configuration.

Table 12-4. MoDTC decomposition products formed in unidirectional linear sliding and sliding/rolling contacts

Parameter	Levels	Unidirectional linear sliding	Sliding/rolling
Temperature	20ºC	[1] MoS_x, $FeMoO_4$	[2] Fe_2O_3, Fe_3O_4, $FeMoO_4$
	100ºC	[3] MoS_2	[4] MoS_2
MoDTC concentration	0.1 wt%	[5] MoS_2	[6] Fe_2O_3, Fe_3O_4, $FeMoO_4$
	0.5 wt%	[7] MoS_2	[8] MoS_2

(1) 2.12 GPa, 0.15 m/s, 0.5 wt% (2) 1 GPa, 0.6 m/s, 0.5 wt%
(3) 2.12 GPa, 0.15 m/s, 0.5 wt% (4) 1 GPa, 0.3 m/s, 0.5 wt%
(5) 1.67 GPa, 0.3 m/s, 100ºC   (6) 1 GPa, 0.6 m/s, 80ºC
(7) 2.12 GPa, 0.15 m/s, 100ºC   (8) 1 GPa, 0.6 m/s, 80ºC

In unidirectional sliding conditions, MoS_x was present at the tribocontact while in sliding/rolling conditions MoS_x was not observed and instead iron oxides were observed. These results indicate that more iron oxides are formed in sliding/rolling conditions while the formation of iron oxides is inhibited in unidirectional sliding conditions. This suggests that there is less coverage of adsorbed MoDTC in sliding/rolling conditions than in unidirectional sliding conditions. The observations made at 20ºC were also observed in tests conducted at 0.1 wt% MoDTC.

At both 20ºC and 0.1 wt% MoDTC, the coverage of adsorbed MoDTC is expected to be low. The rolling motion in sliding/rolling conditions causes further reduction in adsorbed MoDTC at the tribocontact for tests conducted at 20ºC and 0.1 wt% MoDTC. The removal of adsorbed MoDTC is illustrated in Figure 12-3. The removal of adsorbed MoDTC at the contact exposes the

nascent surface to oxidation. This explains the presence of high amounts of iron oxides in sliding/rolling conditions.
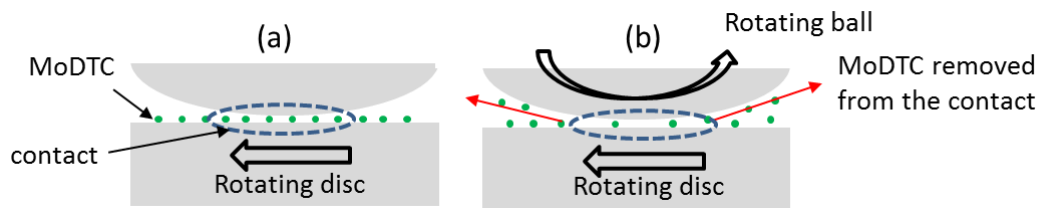
Figure 12-3. Schematic diagram showing adsorbed MoDTC at the tribocontact in (a) unidirectional linear sliding conditions (b) sliding/rolling conditions

12.2.8 Formation of MoS$_2$

Compiling chemical composition information obtained from Chapter 8, Chapter 9 and Chapter 10, it can be said that the following test conditions are ideal for complete decomposition of MoDTC to MoS$_2$ in steel/steel contacts.

- At least one of the tribopair should have a rough finish (R$_a$ >100 nm) to increase local contact pressures and shear stresses. In tests conducted under unidirectional sliding and sliding/rolling conditions the ball had a smoother finish, R$_a$=10 nm, while the discs had a rougher finish, R$_a$>100 nm.

- For tests conducted at low MoDTC concentration (0.1-0.3 wt%), it is important to use high temperatures (>80ºC), low contact pressures (< 0.7 GPa) and low entrainment speeds (0.4 m/s).

- For tests conducted at high MoDTC concentration (0.5-0.9 wt%), the only requirement is that tests are conducted at high temperatures (>50ºC)

12.3 Friction performance of MoDTC lubricants

12.3.1 The link between surface chemistry and friction

Table 12-5 summarises the chemical composition of wear scars at different friction values. These results were obtained from tests in sliding/rolling conditions. It can be seen that MoDTC decomposition products present in wear scars dictated the friction obtained in the tribosystem.

Table 12-5. Chemical composition of wear scars at different friction values

Friction coefficient	Chemical composition of wear scars
0.04-0.05	MoS_2
0.05-0.06	MoS_2, Fe_3O_4, $FeMoO_4$
0.06-0.07	MoS_x, Fe_3O_4, $FeMoO_4$
0.07-0.08	Fe_2O_3, Fe_3O_4, $FeMoO_4$

MoS_2 is well known to reduce friction and the mechanism by which it does this has been presented in Section 3.5.2. Reports in literature however reveal that the friction performance of MoS_2 is affected by contact parameters such as temperature and contact pressures. Friction decreases with increase in Hertzian contact pressure and temperature [186-188]. In this study, MoS_2 was formed at high temperatures therefore low friction was always observed. MoS_x compounds such as MoS_3 have also been reported to provide friction reduction [174]. However, the friction reduction is less than that observed with MoS_2 [189]. Fe_2O_3, Fe_3O_4 and $FeMoO_4$ have not been reported to have any friction reduction capabilities. This knowledge on the friction properties of different chemical species explains the friction observed in this study.

12.3.2 The link between test conditions and friction

Friction results obtained in sliding/rolling conditions (Chapter 9) showed that friction was influenced by MoDTC concentration, temperature, contact pressure and speed. This is in agreement with previous studies [12, 57]. In

the previous studies, the reason for the varying friction values at different test conditions was not presented.

It is clear that test conditions affect the chemical composition of MoDTC tribofilms and that the chemical composition of MoDTC tribofilms (or rubbed surface) determines the friction achieved in the tribosystem (Table 12-5). It is thus possible to link test conditions to friction performance via the MoDTC decomposition products. This is the first time that such a link has been established and highlights the importance of tribochemistry in understanding friction performance of MoDTC lubricants. Figure 12-4 summarises the friction results obtained in sliding/rolling contacts. The low friction values were due to MoS_2 being formed since ideal test conditions were used (Section 12.2.7). High friction values were due to the formation of a mixture of MoS_x, MoS_2, $FeMoO_4$ and Fe_3O_4 under non-ideal test conditions. High friction was also observed when severe wear occurred since there were no/few MoDTC tribofilms at the contact to reduce friction. The reason for the severe wear is discussed in Section 12.5.
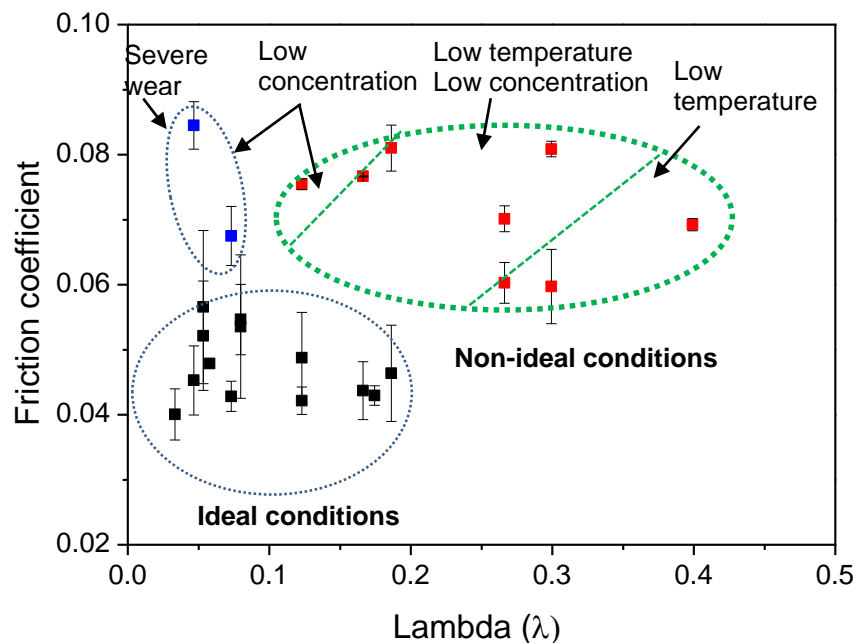
Figure 12-4. Plot summarising friction obtained in sliding/rolling contacts

179

12.3.3 Effect of slide-roll ratio (SRR) on friction in smooth surfaces

Results obtained from tests with smooth surfaces showed that the induction time increased with increase in slide-roll ratio from 100% to 200%. These results show that for smooth surfaces, the friction reducing capability of MoDTC reduces as the slide-roll ratio increases. In a previous study, it was reported that friction reduction (μ=0.1) did not occur in smooth surfaces under pure sliding conditions [12]. It has been suggested that the friction behaviour observed with smooth surfaces is due to formation of micro-elastohydrodynamic (EHD) films [12]. This means that there is no direct contact between the tribopair. However, results obtained from this study show that metal-metal contact occurred in smooth surfaces since MoDTC decomposition products were observed. The contact was however not as severe as that in rough surfaces as evidenced by the presence of MoS_x. Poor asperity-asperity contact in smooth surfaces can explain the long induction time observed at high slide-roll ratios.

12.3.4 Friction behaviour of MoDTC

With the exception of tests conducted at certain test conditions, friction curves during most tests with MoDTC revealed high friction at the beginning of the test which was followed by a rapid drop to low friction values in agreement with previous studies [62, 66]. In this study, an induction time of 2 minutes was observed and significant changes in the surface chemistry were observed within the tribocontact during the first 5 minutes of sliding (Table 7-1). During the first 1 minute of sliding, MoDTC decomposition occurred with MoS_x and $FeMoO_4$ being formed in the wear scars. After rubbing for 2 minutes, the coverage of MoS_2 at the rubbing interface had increased tremendously. With further rubbing, the amount of $FeMoO_4$ and Fe_3O_4 decreased in the wear scars. The chemical composition of wear scars before friction drop was also studied by Morina et al. [65]. In the mentioned study, it was reported that the wear scars had elements Fe, O, S, C and N before the friction drop. The

results from the previous study are in agreement with those obtained from this study.

The friction behaviour of MoDTC lubricant can be explained in three main stages. During the first stage, where high friction is observed, oxidation of the surface occurs which may be accompanied by formation of MoS_x and $FeMoO_4$. Although MoS_2 is also formed during this stage, high friction is still observed probably due to lower coverage of MoS_2 within the wear scars. It is possible that MoS_2 should attain a certain critical coverage for low friction to be attained. The duration of the first stage can be very short (a few seconds) or very long (30 mins - 2h) depending on the test conditions. It has been reported that the duration of stage 1 decreases with increase in MoDTC concentration [58]. This can be explained by the increase in the rate of MoDTC decomposition with concentration (Section 12.2.5). During the second stage, the critical MoS_2 coverage is attained which precipitates the drop in friction. Results from this study showed that a higher amount of MoS_2 was formed during this stage. This is agreement with a previously proposed mechanism which suggested an autocatalytic reaction in this stage [12]. In the third stage, further rubbing results in formation of more MoS_2 and low friction is maintained. Low friction will be maintained as long as MoDTC is continually replenished at the contact.

12.4   Growth of MoDTC tribofilms

12.4.1   Effect of rubbing time

Decomposition of MoDTC in tribocontacts resulted in the formation of tribofilms. From optical images in Figure 10-6 it was observed that the coverage and thickness of MoDTC tribofilms increased with rubbing time. Interference images in Figure 11-2, showed that MoDTC tribofilms were rapidly removed in sliding/rolling conditions when MoDTC was not replenished

at the contact. These results indicate that tribofilm formation and removal was simultaneously occurring at the tribocontact.

The schematic diagram in Figure 12-5 illustrates the growth of MoDTC tribofilms with rubbing time under ideal test conditions. In the initial stages of rubbing (running-in) the substrate is worn out generating a wear scar. In most tests conducted under sliding/rolling conditions with MoDTC, the generated wear scar had a wear depth of less than 0.4 µm. The formation MoDTC tribofilms after the induction period prevents further wear of the substrate. MoDTC tribofilms have been reported to reduce wear of the tribopair [143]. MoDTC tribofilms act as sacrificial layers and are sheared off instead of the steel substrate. Despite the tribofilm being sheared off it was observed that the tribofilm grew with further rubbing time (Figure 10-6).

Figure 12-5. Growth of MoDTC tribofilm with rubbing time

In order to explain the growth of MoDTC tribofilms in tribocontacts, two important aspects need to be taken into consideration; (1) tribofilm formation (2) tribofilm removal. The rate of formation of MoDTC tribofilms is affected by the rate of MoDTC decomposition. Tribofilm removal occurs due to the presence of shear stress at the tribocontact [190]. For the tribofilm to grow in the wear scar, the rate of tribofilm formation has to be greater than the rate of tribofilm removal. From Equation 12-3 it can be seen that the rate of tribofilm formation increases by conducting tests at high temperatures, high MoDTC concentrations and high contact pressures as these conditions increase the rate of decomposition. High temperature (100ºC) and high MoDTC concentration (0.5 wt%) were used in results presented in Figure 10-6. The fact that tribofilm grew with rubbing time indicates that the rate of tribofilm formation was higher than the rate of tribofilm removal.

MoDTC tribofilms did not continue to grow indefinitely, the growth stopped once a certain limiting thickness was achieved. Tribofilms from other additives such as ZDDP have also been shown to reach a limiting thickness [191]. In literature, it has been suggested that tribofilms form as a result of intermixing of reaction products formed at the rubbing interface with atoms of the bulk metal substrate [51, 192]. It has been suggested that the Mott-Cabrera growth mechanism is responsible for the growth of tribofilms [193]. According to the Mott-Cabrera growth mechanism, the growth of films on substrates is dependent on an electric field (Mott potential) that is formed between the metal substrate and deposited film [194, 195]. The film will continue to grow as long as the electric field is still present. As the film becomes thicker, the electric field is reduced and the growth of the film is halted. The limiting thickness achieved in MoDTC tribofilms can be explained by this growth mechanism.

12.4.2 Thickness of MoDTC tribofilms

The limiting thickness of MoDTC tribofilms was dependent on test conditions. Thicker MoDTC tribofilms were formed in rough surfaces while thinner patchy films were formed in smooth surface (Figure 10-3). A similar observation has also been reported for ZDDP tribofilms [196]. In the study by Gosvami et al. [18], it was reported that the rate of ZDDP tribofilm growth increased with increase in contact pressure. This means that for a given test duration, thicker tribofilms will form at high contact pressures than at low contact pressures. As discussed in Section 12.2.6, rough surface have higher local pressures than smooth surfaces. The formation of thicker ZDDP tribofilms in rough surfaces than in smooth surfaces can thus be attributed to local pressures. If the reaction kinetics for the growth of ZDDP tribofilms is considered to be similar to that of MoDTC tribofilms, then formation of thicker MoDTC tribofilms in rough surfaces can also be attributed to higher local pressures (Figure 10-5).

In this study, it was observed that MoDTC tribofilms formed faster in rough surfaces than in smooth surfaces (Figure 10-2).The influence of surface

roughness on the rate of formation of other tribofilms has been reported in previous studies. Kubiak et al. [197] reported that ZDDP tribofilms were formed faster in rough surfaces than in smooth surfaces. In the mentioned study, it was proposed that the rapid formation of ZDDP tribofilms was attributed to a lower activation energy in rough surfaces. The growth rate model in Equation 3-4 for the formation of ZDDP shows that the growth rate is dependent on contact pressure. Higher contact pressures reduce the activation energy resulting in faster tribofilm growth. The faster growth of ZDDP tribofilms in rough surfaces is therefore due to high local pressures which reduce the activation energy. If rate of MoDTC decomposition is considered to be proportional to the rate of MoDTC tribofilm formation, then the rate of MoDTC tribofilm formation will also be dependent on the contact pressure. As is the case for ZDDP tribofilms, the rapid formation of MoDTC tribofilms in rough surface can also be attributed to the higher local pressures.

12.5   Wear performance of MoDTC

Figure 12-6 summarises wear results obtained in Chapter 8 where tests were conducted under unidirectional linear sliding conditions. The wear scar diameter (WSD) values shown were obtained at varying MoDTC concentrations and temperatures. It was observed that the ball WSD decreased by about 50% when MoDTC was added to BO. This is in agreement with previous studies [77, 143]. Wear reduction can be attributed to the formation of MoDTC tribofilms. It has been reported that MoDTC tribofilms have a lower hardness (0.4-0.5 GPa) than steel [69]. This means that, the tribofilms can be easily sheared instead of the steel substrate. This way MoDTC tribofilms protect the substrate from wear.
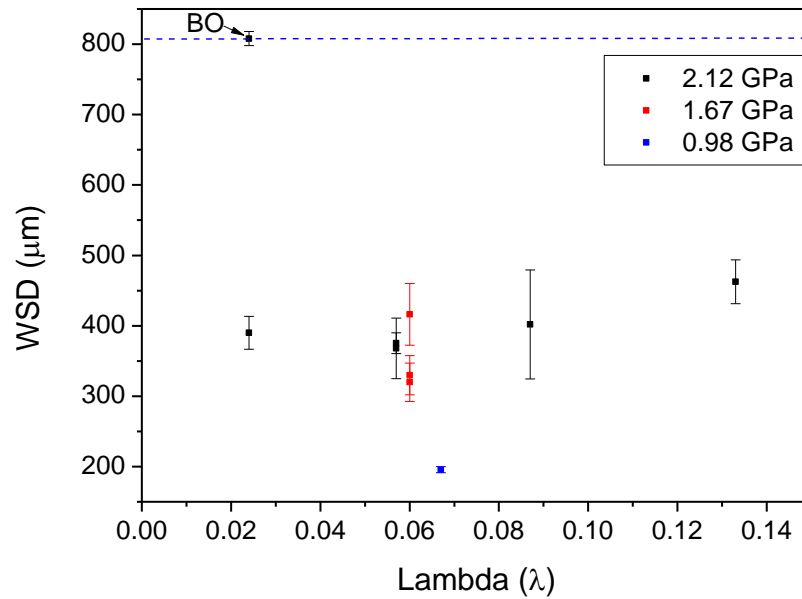
Figure 12-6. Wear results of tests conducted under unidirectional linear sliding conditions with MoDTC lubricants

Larger WSD were observed at low temperatures and low concentrations (Figure 8-1b, Figure 8-4b). At these conditions, it was also observed that the induction time was longer than that observed at higher temperatures and higher concentrations. The longer induction times indicate that the formation of MoDTC tribofilms was delayed (Section 12.3.4). The absence of MoDTC tribofilms during the running-in process could explain the higher wear observed at low temperatures and low MoDTC concentrations.

Wear results obtained in sliding/rolling conditions (Sections 9.3, 9.4 and 9.5) also showed that wear of the substrate was minimal when MoDTC was used. In most tests, the wear depth was less than 0.4 µm. However, severe wear (wear depth 6 µm) was observed at low concentrations, high contact pressures and high temperatures (Figure 9-3). Interference images in Figure 9-4 (b) showed that wear of the substrate increased with rubbing time.

The severe wear can be explained by the rate of tribofilm formation being much lower than the rate of tribofilm removal such that any MoDTC tribofilms formed were rapidly removed [198]. The removal of MoDTC tribofilms made

the substrate susceptible to wear. Given that rate of MoDTC decomposition is proportional to the rate of tribofilm formation, it can be seen that rate of tribofilm formation was low at low MoDTC concentrations used in the test (Section 12.2.5). The rate of tribofilm removal was high at high contact pressures and high temperatures (low lambda ratios) used in the tests.

From results obtained in this study, it can be seen that MoDTC provides wear protection only at test conditions which promote the presence of tribofilms at the tribocontact.

12.6 Durability of MoDTC tribofilms

12.6.1 Effect of sliding configuration

Results presented in Chapter 11 show that the durability of MoDTC tribofilms when rubbed in BO was dependent on the sliding configuration. In sliding/rolling contacts, pre-formed MoDTC tribofilms were rapidly removed when rubbed in BO resulting in instantaneous friction increase (μ=0.12). In tests conducted in unidirectional linear sliding conditions, pre-formed MoDTC tribofilm were not removed when rubbed in BO and friction remained low (μ=0.05-0.06).

These results suggest that the rolling motion accelerated the removal of MoDTC tribofilm in the sliding/rolling contact. In the study by Suzuki [199] on MoS_2 coatings, it was observed that the durability of MoS_2 coatings decreased as the sliding/rolling ratio decreased (more rolling). It was proposed that high tensile stress, achieved at high sliding/rolling ratios (more sliding), was necessary for good adherence of MoS_2. In relation to results obtained in this study, it can be concluded that higher tensile stress in pure sliding conditions provided better adherence of MoDTC tribofilms than in sliding/rolling conditions.

12.6.2 Effect of iron oxide films

Although MoDTC tribofilms were found to be durable under unidirectional sliding conditions, the durability was dependent on the nature of the surface on which the tribofilms were generated. When rubbed in BO, MoDTC tribofilms generated on fresh steel samples were not removed while tribofilms generated on oxidised steel samples were rapidly removed. These results show that MoDTC tribofilms formed on iron oxide films are not strongly adhered to the substrate and were therefore less durable compared to those formed directly on the substrate. The differences in durability could be due to the varying adhesion strengths of MoS_2 on the steel surface and iron oxide [200]. In a previous study Stephen et al. [201], it was reported that the adhesion of MoS_2 was enhanced when the iron oxide layer was removed from the steel surface.

The results obtained in this study with fresh steel samples are in disagreement with those reported by Morina and Neville [66]. In the mentioned study, it was observed that friction rapidly increased when MoDTC tribofilms generated on fresh samples were rubbed in BO. This discrepancy can be addressed by considering the induction time taken during tests with MoDTC. In the previous study, the induction time varied between 60 and 120 minutes whereas in this study the induction time was 30s. Oxidation of the steel surface during the long induction period in the previous study can explain the formation of less durable MoDTC tribofilms than those formed in this study.

12.6.3 Surface chemistry

Although, MoDTC tribofilms were removed in sliding/rolling contacts and in unidirectional sliding contacts (oxidised samples), MoDTC decomposition products were still observed in the wear scars after rubbing in BO. This could be due to the tribofilm not being completely removed or wear debris being entrained back to the contact. Either way, rubbing in BO resulted in a change in the surface chemistry of the wear scars.

In sliding/rolling contacts, rubbing pre-formed MoDTC tribofilms resulted in the formation of MoS_x, $Fe_2(MoO_4)_3$ and $FeMoO_4$ (Figure 11-4b). The high friction observed when rubbing in BO can be explained by the presence of these compounds at the contact (Table 12-5). In unidirectional linear sliding contacts, MoS_2 in pre-formed MoDTC tribofilms also underwent amorphisation to MoS_x when rubbed in BO. For tribofilms generated on fresh samples, MoS_2 was only partially transformed to MoS_x. The low friction observed during rubbing in BO can be attributed to the presence of MoS_2 at the contact. In contrast, complete amorphisation of MoS_2 occurred in tribofilms formed on oxidised samples. This explains the high friction observed in oxidised samples.

12.7   Chemical characterisation using Raman spectroscopy

12.7.1   Comparison with other techniques

In this study, it was observed that MoDTC tribofilms formed at certain test conditions were composed of MoS_x and $FeMoO_4$. These species were not detected in previous studies where XPS and XAS analysis were used to characterise the tribofilms. To explain this, the qualitative capabilities of XPS and XAS in characterising MoS_x and $FeMoO_4$ species were explored. These capabilities are compared to those of Raman spectroscopy.

12.7.1.1 MoS_x species: Comparison with XAS and XPS analysis

Raman and XPS analysis on molybdenum sulphide with varying Mo/S ratios was conducted in a previous study [168]. Figure 12-7 shows results of the analysis. With XPS analysis, no differences were observed in the $3d_{5/2}$ and the $3d_{3/2}$ peaks at different S/Mo ratios. Differences were only observed in the S region where the contributions of bridging and apical sulphur bonds decreased with decrease in S/Mo ratio. On the other hand, Raman analysis was able to show varying spectral patterns at different S/Mo ratios. At high S/Mo ratios (>2.40), broad Mo-S peaks were observed as well as peaks due to S-S bonds.

The peaks observed had low intensity in comparison to peaks observed at low S/Mo ratios. At low S/Mo ratios (>2.40), the intensity of the double peaks increased with decrease in S/Mo ratio indicating an increase in crystallinity.

Bakunin et al. [189] conducted XAS analysis on MoS_3 and MoS_2. It was observed that Mo L-edge and S K-edge of MoS_3 were similar to those of MoS_2. It is therefore difficult to distinguish these two compounds using XAS. These results show that with XAS it is not possible to distinguish molybdenum sulphide compounds with varying Mo/S ratios.
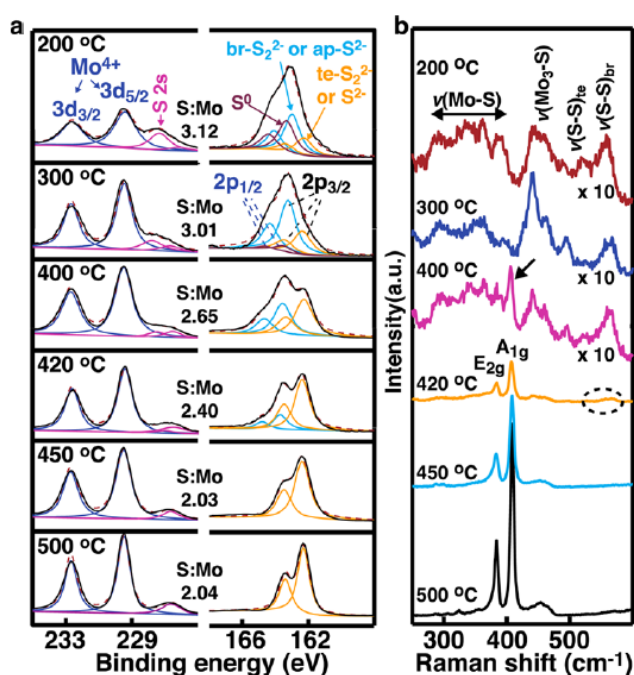
Figure 12-7. (a) XPS analysis and (b) Raman analysis of molybdenum sulphide compounds grown at different temperatures [168]

With this knowledge, it can be seen that only Raman spectroscopy and XPS are capable of differentiating molybdenum sulphur compounds with varying Mo/S ratios. With XPS, detailed analysis of the S region is necessary. Looking at the XPS spectra obtained in S region in the study by Yamamoto and Gondo [58], it can be seen that the Mo compounds formed contained bringing S-S bonds and therefore had a high S/Mo ratio. The authors in the previously mentioned study did not analyse the S peak in detail and therefore did not

arrive at the same conclusion. In previous studies where XPS analysis was conducted on MoDTC tribofilms, the Mo region which cannot distinguish molybdenum sulphur compounds was mostly analysed [56, 67]. This can be one reason why MoS_x has not been reported in XPS studies. Another possible reason could be that MoDTC tribofilms analysed with XPS were not composed of MoS_x. As illustrated in this study, MoS_x only forms at certain test conditions.

12.7.1.2 $FeMoO_4$ species: Comparison with XPS analysis

XPS analysis of $FeMoO_4$ shows Mo 3d peaks at 232.3 and 235.5 eV suggesting that molybdenum is at an oxidation state of +6 [78, 83]. Although XPS can characterise $FeMoO_4$, it is incapable of distinguishing $FeMoO_4$ from other Mo compounds which have the same oxidation state (+6).This is because Mo peaks are observed at the same binding energy. For example, it is impossible to distinguish $FeMoO_4$ from MoO_3 using the Mo 3d peaks. Raman spectroscopy shows unique spectral patterns for MoO_3 [100] and $FeMoO_4$ [76] therefore these two compounds can clearly be distinguished from each other. From this, it can be seen that Raman spectroscopy is superior to XPS in distinguishing molybdenum oxide compounds.

Previous XPS analysis of MoDTC tribofilms showed Mo 3d peaks at 229, 232.3 and 235 eV [56, 151]. From these XPS studies it was concluded that MoDTC tribofilms were composed of MoO_3 due to the presence of Mo $3d_{5/2}$ peak at 232.3 eV. MoO_3 was suggested to be present since MoO_3 was used as a reference. There are no XPS studies that have used $FeMoO_4$ as a reference. If $FeMoO_4$ was to be used as reference, then the conclusion would be that the MoDTC tribofilms were composed of $FeMoO_4$. The use of MoO_3 as a reference instead of $FeMoO_4$ explains why $FeMoO_4$ has not been reported in previous XPS studies.

In this study, Raman peaks belonging to $FeMoO_4$ were observed while those belonging to MoO_3 were not observed at all in MoDTC tribofilms. It is therefore

possible that the Mo (6+) peak observed in MoDTC tribofilms in previous XPS studies is due to the presence of $FeMoO_4$ and not MoO_3.

12.7.2 Advantages of using Raman spectroscopy

In this study, the use of Raman spectroscopy in chemical characterisation of MoDTC tribofilms has proven to be advantageous in many ways. These benefits are highlighted below.

- It was shown for the first time that MoDTC tribofilm can be composed of molybdenum sulphide with varying Mo/S ratios. This finding was very significant as it was used to account for friction behaviour at certain test conditions.

- It was possible to capture the intermediate stages during the recrystallization of MoS_x to MoS_2. This provided valuable information on the influence of contact parameters on decomposition of MoDTC in tribological contacts.

- It was shown for the first time that MoDTC tribofilms were composed of $FeMoO_4$.

- It was demonstrated for the first time that MoS_2 in MoDTC tribofilms undergoes slight structural disorder.

- It was shown for the first time that MoS_2 in MoDTC tribofilms undergoes amorphisation to MoS_x when MoDTC is not replenished at the contact. This finding was useful in explaining friction observed when pre-formed MoDTC tribofilms were rubbed in MoDTC-free lubricants.

12.7.3 Challenges with Raman spectroscopy

12.7.3.1 Effect of oil layer

Raman analysis of lubricated surfaces after tests with MoDTC lubricant showed that characterisation of MoDTC tribofilms was possible when an oil layer was present. There were however a few challenges with such analysis.

Firstly, the presence of an oil layer decreases the visibility of the wear scar. Visibility of the wear scar is further reduced in short duration tests where the contact area is very small. In order to ensure that analyses are being done within the wear scar, larger contact areas should be generated.

The second problem that arises with analysing lubricated surfaces is the strong Raman signal from the mineral base oil (Figure 7-8). MoS_x and $FeMoO_4$ observed during the initial stages of the test have very weak Raman signals in comparison to the mineral base oil. Analysing MoDTC lubricated samples after 1-2 minutes test would therefore only show the strong signals from the base oil. Detection of Fe_3O_4 in uncleaned samples generated after 1 minute in base oil has also been found to be difficult [202]. In long duration tests, the strong signals from the base oil will also obscure weak signals from MoS_x and $FeMoO_4$ observed at certain test conditions. One may be tempted to increase the laser power in an attempt to increase the Raman signal from MoS_x and $FeMoO_4$. This is however strongly discouraged because analysing MoDTC lubricant films at high laser powers promotes laser-induced reactions which results in formation of MoS_2, MoO_2 and MoO_3 (Table 5-4).This would in turn provide wrong interpretation of the chemical composition of the analysed surface.

12.7.3.2 Laser-induced reactions

When a laser is focused on a very small area on a sample, the temperature rises within the analysed region. The increase in temperature causes various

reactions such as oxidation, crystallisation and structural transformation to occur within the sample. In literature, there are several reports on laser-induced reactions in molybdenum compounds. Thin metallic molybdenum films have been shown to oxidise to MoO_2 and Mo_4O_{11} when radiated at longer exposure times [141, 203]. Amorphous MoO_3 has also been shown to undergo laser-induced structural transformation to its crystalline form [152]. It has also been shown that laser treatment of MoS_x film can result in formation of highly crystalline MoS_2 [142] or oxidation to MoO_3 [155].

Results obtained in Chapter 6, revealed that laser-induced reactions can occur to MoDTC tribofilms especially at high laser powers and exposure times. In MoDTC tribofilms composed of MoS_2, Raman analysis at high laser powers resulted in the formation of Fe_2O_3. Laser damage in MoDTC tribofilms was different from that observed in MoS_2 powder. In the case of MoS_2 power, laser damage caused partial oxidation of MoS_2 to MoO_3. Laser damage to MoDTC tribofilms during Raman analysis has been reported although no specific details on its effect on Raman spectra was given [57].

In tests with MoDTC lubricant, iron oxides were formed in the wear scars in the initial stages of the rubbing process (Table 7-1). Further rubbing causes iron/iron oxide from the steel surface to be ejected from the surface and subsequently embedded within the growing MoDTC tribofilm. The growth of the tribofilm inhibits further oxidation of the ferrous surface resulting in a lower concentration of iron oxides in the tribofilm. This explains the absence of iron oxide peaks in MoDTC tribofilms when analysed at low laser powers. Generated MoDTC tribofilms are composed of Fe embedded within a MoS_2-carbon matrix. Irradiation of the tribofilms at high laser powers causes the iron particles to react with atmospheric air forming iron oxide as evidenced by the formation of dark spots within the tribofilm.

The discussion above explains why Fe_2O_3 is observed at high laser powers but does not explain why MoS_2 in the tribofilm was not partially oxidised to

MoO_3 as was the case in MoS_2 powder. Windom et al. [100] observed that natural MoS_2 crystal did not partially oxidise to form MoO_3 even at high laser powers while MoS_2 microcrystalline powder oxidised easily. They attributed the lack of MoS_2 oxidation of the natural crystal to the orientation of the analysed surface. In the case of the natural crystal, the analysed surface was cleaved along the z-axis and did not have its polar edge sites available for oxidation. One explanation for the lack of oxidation of MoS_2 in the MoDTC tribofilms could be that MoS_2 nanocrystals were basally orientated in the tribofilm and as such the polar edges were unavailable for oxidation. Another possible explanation for this lack of oxidation could be due to the fact that MoS_2 was present in an organic matrix in the tribofilm which shielded MoS_2 polar edges from oxidation.

Although there is a risk of damaging MoDTC tribofilms during Raman analysis, the systematic study in Chapter 5 has provided suitable parameters for conducting Raman analysis on the tribofilms. The study also provided indicators to look out for in case laser damage occurred on MoDTC tribofilms formed in steel/steel contacts.

Laser-induced reactions were also observed when analysing MoDTC thermal films and $MoDTC/Fe_3O_4$ deposits at high laser power and longer exposure times (Figure 5-8, Figure 5-12). In the case of MoDTC lubricated films, MoO_2, MoO_3 and MoS_2 were observed as products of laser-induced reactions. These results show that MoDTC lubricant films are very susceptible to laser-induced reaction and utmost care should be taken during Raman analysis.

Chapter 13
Conclusions and Future work

13.1 Conclusions

13.1.1 Thermal degradation of MoDTC

- In air, MoDTC additive concentrate decomposes at 100°C to form MoS_x (x>2). However, MoDTC in MoDTC lubricant is not easily decomposed at 150°C, it takes about 5h for MoS_x to be formed. The decomposition of MoDTC in MoDTC lubricant can be significantly enhanced by adding Fe_3O_4 powders to the lubricant. In this case, MoDTC decomposes to form MoS_2 instead of MoS_x.

- MoDTC thermal films formed on steel discs at 100°C for 1h were not composed of MoDTC decomposition products.

13.1.2 Tribochemical decomposition of MoDTC and its effect on friction and wear

- During tribological tests with MoDTC lubricant, MoDTC decomposes into three main products namely: MoS_x, MoS_2 and $FeMoO_4$, depending on the test conditions. Formation of MoS_2 has been reported in previous literature but the formation of MoS_x and $FeMoO_4$ has not been reported.

- Decomposition of MoDTC within a tribocontact is due to the presence of shear stress and occurs even at room temperature (20°C). A new mechanism for MoDTC decomposition has been proposed.

- MoDTC decomposition leads to growth of tribofilms in the tribocontact. The presence of MoDTC tribofilms provides wear protection to the steel substrate. There are however certain test conditions that inhibit the growth of MoDTC tribofilm and severe wear of the substrate occurs.

195

- Friction observed in tests with MoDTC lubricants at long test durations was dependent on the surface chemistry at the rubbing surfaces.

13.1.3 Durability of MoDTC tribofilms

- Under sliding/rolling conditions, pre-formed MoDTC tribofilms formed directly on steel substrates were rapidly removed from the tribocontact when rubbed in base oil and friction increased rapidly to high values (μ=0.12).

- Under unidirectional linear sliding conditions, pre-formed MoDTC tribofilms formed on fresh steel samples were not easily removed when rubbed in base oil and low friction was observed.

- Pre-formed MoDTC tribofilms on oxidised steel samples were easily removed when rubbed in base oil. The removal of MoDTC tribofilms caused a rapid increase in friction. The reduced durability of MoDTC tribofilms formed on oxidised steel surfaces is attributed to poor adhesion of MoS_2 to iron oxide.

13.1.4 Raman spectroscopy as an analysis technique

- Raman analysis of MoDTC lubricant revealed that Raman peaks of mineral oil (base oil) are significantly stronger than peaks belonging to MoDTC. For this reason, it is difficult to detect MoDTC in MoDTC lubricants at low concentrations.

- Lubricant films formed from adsorption of MoDTC such as MoDTC thermal films are susceptible to laser-induced reactions when analysed at high laser powers (10 mW) and longer exposure times. Laser-induced reactions can lead to MoS_2, MoO_2 and MoO_3 being observed from MoDTC thermal films. These compounds are only a product of laser-induced reaction and are not an accurate representation of the chemical composition of MoDTC thermal films.

- The 488 nm wavelength laser was more suitable in analysing MoDTC tribofilms than the 785 nm wavelength laser because it gave more distinct Raman peaks and did not have a high background (fluorescence).

- Laser-induced reactions can occur in MoDTC tribofilms when the tribofilms are analysed with 488 nm laser at high laser powers (>5 mW) and exposure times. Laser-induced reactions of the MoDTC tribofilm results in strong iron oxide peaks (Fe_2O_3) being observed in the Raman spectra.

- Laser-induced reactions that occurred in MoDTC tribofilms were different from those that occurred in microcrystalline MoS_2 powder. Laser-induced reactions in MoS_2 powder caused oxidation of MoS_2 to MoO_3. In MoDTC tribofilms, oxidation of MoS_2 to MoO_3 did not occur even at high laser power and longer exposure times. Inhibition of MoS_2 oxidation in MoDTC tribofilms was considered to be either due to the presence of carbon surrounding MoS_2 nanocrystals or the basal orientation of MoS_2 layers on the wear scars which keeps away the polar edges of MoS_2 from oxidation.

- Laser polarisation did not have any significant effects on Raman spectra obtained from MoDTC tribofilms. MoS_2 peaks were observed when MoDTC tribofilms were analysed under circular, normal and orthogonal polarisation. The intensity of MoS_2 peaks was the same under the different polarisations. The ratio of A_{1g}/E^1_{2g} slightly varied under the different laser polarisations.

- Detailed analysis of MoS_2 Raman peaks from MoDTC tribofilms revealed that MoS_2 in the tribofilm was subjected to stress-induced disorder which caused the MoS_2 Raman peaks to be slightly broad and asymmetrical. Shear stress in MoS_2 also led to formation of a broad peak in the region 150-250 cm⁻¹. The broad peak was attributed to

v(Mo-Mo) vibration in the sheared MoS_2 crystal. In addition, shear stress caused S-S bonds to be formed within the MoS_2 structure and was evidenced by the appearance of the peaks at 450 cm^{-1}, 510 cm^{-1} and 550 cm^{-1}.

- Uncleaned samples from tribotests with MoDTC can be analysed using Raman analysis when the main MoDTC decomposition product is MoS_2 since it has an equally strong Raman peaks as those of the base oil. Raman signal from the mineral base oil is very strong in comparison to signals from MoS_x and $FeMoO_4$. Therefore it may be difficult to analyse uncleaned samples which have MoS_x and $FeMoO_4$ as the main MoDTC decomposition products since they have weak Raman signals.

13.2   Future work

13.2.1   Mo/S ratio in MoS_x species

MoS_x was formed as a decomposition product in certain test conditions. The exact ratio of Mo/S was not determined in this study. Future work should use other techniques such as XPS and X-Ray Diffraction (XRD) to determine the ratio of Mo/S.

13.2.2   Numerical simulation studies

MoDTC decomposition in tribological contacts has been shown to be initiated by shear stress. Future studies should therefore focus on conducting numerical simulations to study the effect of shear stress on MoDTC decomposition.

One interesting result from this study was that the roughness of the tribopair affects MoDTC tribochemical reactions. Further tests should be carried at different surface roughness to determine optimum substrate roughness that will ensure MoDTC decomposition. Numerical simulation studies can also

provide a better insight on how roughness affects interfacial processes (shear stress, lubricant retention etc.).

13.2.3 Measurement of MoDTC tribofilm thickness

In this study it has been shown that under ideal test conditions, thick MoDTC tribofilms were formed at the tribocontact. Under non-ideal test conditions, thin patchy tribofilms were formed. It was however difficult to measure the exact thickness of the tribofilms formed especially those formed on the balls. MoDTC tribofilms form rapidly on the smoother counterpart given that the other counterpart is rough. Although MoDTC tribofilms also form on the rough counterpart (discs in this case) it would be difficult to measure the tribofilm thickness due to the uneven topography. Therefore, future work should focus on designing a suitable set-up that can allow the tribofilm thickness on the smoother counterpart to be measured. *In-situ* AFM analysis has recently been used to measure the thickness of ZDDP tribofilms. This technique can be employed to study the thickness of MoDTC tribofilms. Real-time measurement of MoDTC tribofilm thickness will be useful in reaction kinetics studies.

13.2.4 Quantitative analysis of MoDTC tribofilms

Raman analysis of wear scars generated at certain test conditions showed that the chemical composition was non-uniform and was composed of a mixture of MoS_x, MoS_2 and $FeMoO_4$. The lowest friction was observed when MoS_2 was formed at the tribocontact while intermediate to high friction was observed when MoS_x, $FeMoO_4$ and iron oxides were present at the tribocontact. It is not clear how the concentration of MoS_x, $FeMoO_4$ and iron oxides affect the friction response. Future work should therefore focus on quantification of the various compounds within the entire wear scars. Semi-quantitative analysis can be done by Raman mapping of the wear scars. When analysing entire wear scars, it is advised that smaller wear scars are generated since Raman mapping of large wear scars such as those generated in this study can be extremely time consuming.

13.2.5 Reaction kinetics studies

In this study, it has been shown that MoDTC decomposition and growth of MoDTC tribofilms are dependent on test conditions. There was however no attempt to study the reaction kinetics involved in the MoDTC decomposition or tribofilm growth. In order to conduct reaction kinetic studies, real-time measurements of at least one property of the tribochemical reaction should be made. Real-time quantitative analysis of the decomposition products (MoS_2, MoS_x and $FeMoO_4$) and/or the thickness of the tribofilm are suitable properties to be used in studying the rates of reactions. MoDTC tribofilm thickness can be measured using *in-situ* AFM analysis or other suitable optical techniques while *in-situ* Raman spectroscopy can be used in quantitative analysis of the various decomposition products. However, in order to conduct *in-situ* Raman analysis, the problem of strong Raman signals from the base oil has to be resolved. Further investigations should focus on finding alternative base oils with lower Raman signal or enhancing signals from MoDTC decomposition products by employing Surface Enhanced Raman spectroscopy (SERs) techniques.

13.2.6 The influence of other additives

Considerable knowledge on the decomposition of MoDTC has been obtained from this study. These tests were however conducted using base oil containing only MoDTC. In actual engine lubricants, the base oil contains many other additives which may interact with MoDTC affecting its performance. Using results obtained from this study as a basis, future work should investigate the interactions between MoDTC and other chemically active additives (antiwear additives, detergents, dispersants) and their effect on MoDTC decomposition.

References

1. K. Holmberg, P. Andersson, and A. Erdemir, *Global energy consumption due to friction in passenger cars.* Tribology International, 2012. **47**(0): p. 221-234.

2. R. I. Taylor and R. C. Coy, *Improved fuel efficiency by lubricant design: A review.* Proceedings of the Institution of Mechanical Engineers, Part J: Journal of Engineering Tribology, 2000. **214**(1): p. 1-15.

3. M. Ratoi, V. B. Niste, H. Alghawel, Y. F. Suen, and K. Nelson, *The impact of organic friction modifiers on engine oil tribofilms.* RSC Advances, 2014. **4**(9): p. 4278-4285.

4. H. A. Spikes, *Film-forming additives - Direct and indirect ways to reduce friction.* Lubrication Science, 2002. **14**(2): p. 147-167.

5. P. Rabaso, F. Dassenoy, F. Ville, M. Diaby, B. Vacher, T. Le Mogne, M. Belin, and J. Cavoret, *An Investigation on the Reduced Ability of IF-MoS2 Nanoparticles to Reduce Friction and Wear in the Presence of Dispersants.* Tribology Letters, 2014. **55**(3): p. 503-516.

6. L. Cizaire, B. Vacher, T. Le Mogne, J. M. Martin, L. Rapoport, A. Margolin, and R. Tenne, *Mechanisms of ultra-low friction by hollow inorganic fullerene-like MoS2 nanoparticles.* Surface and Coatings Technology, 2002. **160**(2–3): p. 282-287.

7. L. Rapoport, O. Nepomnyashchy, I. Lapsker, A. Verdyan, A. Moshkovich, Y. Feldman, and R. Tenne, *Behavior of fullerene-like WS2 nanoparticles under severe contact conditions.* Wear, 2005. **259**(1–6): p. 703-707.

8. A. Erdemir, *Large-scale manufacturing of nanoparticulate-based lubrication additives for improved energy efficiency and reduced emissions*, 2013, Argonne National Laboratory, Technical report.

9. E. Ali and D. Christophe, *Tribology of diamond-like carbon films: recent progress and future prospects.* Journal of Physics D: Applied Physics, 2006. **39**(18): p. R311-R327.

10. H. A. Tasdemir, T. Tokoroyama, H. Kousaka, N. Umehara, and Y. Mabuchi, *Friction and Wear Performance of Boundary-lubricated*

DLC/DLC Contacts in Synthetic base Oil. Procedia Engineering, 2013. **68**: p. 518-524.

11. STLE. [cited 2015 18-8-2015]; Available from: www.stle.org/resources/lubelearn/lubrication/.

12. J. Graham, H. Spikes, and S. Korcek, *The friction reducing properties of molybdenum dialkyldithiocarbamate additives: Part I - Factors influencing friction reduction.* Tribology Transactions, 2001. **44**(4): p. 626-636.

13. F. M. Piras, A. Rossi, and N. D. Spencer, *Growth of Tribological Films: In Situ Characterization Based on Attenuated Total Reflection Infrared Spectroscopy.* Langmuir, 2002. **18**(17): p. 6606-6613.

14. F. M. Piras, A. Rossi, and N. D. Spencer, *In situ attenuated total reflection (ATR) spectroscopic analysis of tribological phenomena*, in *Tribology Series*, M.P.G.D. D. Dowson and A.A. Lubrecht, Editors. 2002, Elsevier. p. 199-206.

15. J. M. Martin, T. Le Mogne, C. Grossiord, and T. Palermo, *Tribochemistry of ZDDP and MoDDP chemisorbed films.* Tribology Letters, 1996. **2**(3): p. 313-326.

16. J. M. Martin, T. Le Mogne, C. Grossiord, and T. Palermo, *Adsorption and friction in the UHV tribometer.* Tribology Letters, 1997. **3**(1): p. 87-94.

17. H. Fujita and H. A. Spikes, *Study of Zinc Dialkyldithiophosphate Antiwear Film Formation and Removal Processes, Part II: Kinetic Model.* Tribology Transactions, 2005. **48**(4): p. 567-575.

18. N. N. Gosvami, J. A. Bares, F. Mangolini, A. R. Konicek, D. G. Yablon, and R. W. Carpick, *Mechanisms of antiwear tribofilm growth revealed in situ by single-asperity sliding contacts.* Science, 2015. **348**(6230): p. 102-106.

19. STLE. [cited 2016 15/2/2016]; Available from: http://www.stle.org/files/What_is_tribology/Tribology_Applications.aspx.

20. G. W. Stachowiak and A. W. Batchelor, *Engineering Tribology (3rd Edition)*, Elsevier.

21. R. W. Bruce, *Handbook of Lubrication and Tribology*. Theory and Design. Vol. II. 2012: CRC press.

22. J. A. Greenwood and J. B. P. Williamson, *Contact of Nominally Flat Surfaces.* Proceedings of the Royal Society of London A: Mathematical, Physical and Engineering Sciences, 1966. **295**(1442): p. 300-319.

23. J. E. Booth, *THe Feasibility of using electrostatic charge condition monitoring for lubricant additive screening*, 2008, University of Southampton.

24. H. A. Francis, *Interfacial temperature distribution within a sliding Hertzian contact.* ASLE Trans, 1971. **14**(1): p. 41-54.

25. J. F. Archard, *The temperature of rubbing surfaces.* Wear, 1959. **2**(6): p. 438-455.

26. J. A. Greenwood, *An interpolation formula for flash temperatures.* Wear, 1991. **150**(1-2): p. 153-158.

27. X. Tian and F. E. Kennedy, *Maximum and average flash temperatures in sliding contacts.* Journal of Tribology, 1994. **116**(1): p. 167-174.

28. B. J. Hamrock and D. Dowson, *Isothermal Elastohydrodynamic Lubrication of Point Contacts: Part III—Fully Flooded Results.* Journal of Lubrication Technology, 1977. **99**(2): p. 264-275.

29. C. Roelands, *Correlational aspects of the viscosity-temperature-pressure relationship of lubricating oils*, 1966, PhD thesis, Technische Hogeschool Delft, The Netherlands.

30. R. Roshan, M. Priest, A. Neville, A. Morina, X. Xia, C. P. Warrens, and M. J. Payne, *Friction Modelling in Boundary Lubrication Considering the Effect of MoDTC and ZDDP in Engine Oils.* Tribology Online, 2011. **6**(7): p. 301-310.

31. M. Priest, *Lecture notes.*

32. S. M. Hsu and R. S. Gates, *Boundary lubricating films: formation and lubrication mechanism.* Tribology International, 2005. **38**(3): p. 305-312.

33. R. M. Mortier and S. T. Orszulik, *Chemistry and technology of lubricants.* Second ed. Friction, wear and the role of additives in their control, ed. C.H. Bovington. 1997, London: Blackie Academic & Professional.

34. S. M. Hsu, *Molecular basis of lubrication.* Tribology International, 2004. **37**(7): p. 553-559.

35. T. Colclough, *Role of additives and transition metals in lubricating oil oxidation.* Industrial and Engineering Chemistry Research, 1987. **26**(9): p. 1888-1895.

36. P. A. Willermet, D. P. Dailey, R. O. Carter Iii, P. J. Schmitz, and W. Zhu, *Mechanism of formation of antiwear films from zinc dialkyldithiophosphates.* Tribology International, 1995. **28**(3): p. 177-187.

37. J. Lahijani, F. E. Lockwood, and E. E. Klaus, *Influence of metals on sludge formation.* ASLE transactions, 1982. **25**(1): p. 25-32.

38. M. Fuller, *Ph.D. thesis, University of Ontario* 1998.

39. H. A. Spikes, *Additive-additive and additive-surface interactions in lubrication.* Lubrication Science, 1989. **2**(1 , Oct., 1989): p. 3-23.

40. C. M. Allen and E. Drauglis, *Boundary layer lubrication: monolayer or multilayer.* Wear, 1969. **14**(5): p. 363-384.

41. T. Fischer, *Tribochemistry.* Annual Review of Materials Science, 1988. **18**(1): p. 303-323.

42. G. Heinicke, *Tribochemistry*. 1984: John Wiley & Sons.

43. H. L. Adams, M. T. Garvey, U. S. Ramasamy, Z. Ye, A. Martini, and W. T. Tysoe, *Shear-Induced Mechanochemistry: Pushing Molecules Around.* The Journal of Physical Chemistry C, 2015. **119**(13): p. 7115-7123.

44. S. M. Hsu, E. E. Klaus, and H. S. Cheng, *A mechano-chemical descriptive model for wear under mixed lubrication conditions.* Wear, 1988. **128**(3): p. 307-323.

45. S. M. Hsu, J. Zhang, and Z. Yin, *The nature and origin of tribochemistry.* Tribology Letters, 2002. **13**(2): p. 131-139.

46. S. B. Bulgarevich, M. V. Boiko, E. N. Tarasova, V. A. Feizova, and K. S. Lebedinskii, *Kinetics of mechanoactivation of tribochemical processes.* Journal of Friction and Wear, 2012. **33**(5): p. 345-353.

47. S. B. Bulgarevich, M. V. Boiko, V. I. Kolesnikov, and K. E. Korets, *Population of Transition States of Trioactivated Chemical Processes.* Journal of Friction and Wear, 2010. **31**(4): p. 288-293.

48. S. B. Bulgarevich, M. V. Boiko, V. I. Kolesnikov, and V. A. Feizova, *Thermodynamic and Kinetic Analyses of Probable Chemical Reactions in the Tribocontact Zone and the Effect of Heavy Pressure on Evolution of Adsorption Processes.* Journal of Friction and Wear, 2011. **32**(4): p. 301-309.

49. M. K. Beyer and H. Clausen-Schaumann, *Mechanochemistry: The mechanical activation of covalent bonds.* Chemical Reviews, 2005. **105**(8): p. 2921-2948.

50. M. Mahrova, M. Conte, E. Roman, and R. Nevshupa, *Critical Insight into Mechanochemical and Thermal Degradation of Imidazolium-Based Ionic Liquids with Alkyl and Monomethoxypoly(ethylene glycol) Side Chains.* The Journal of Physical Chemistry C, 2014. **118**(39): p. 22544-22552.

51. O. J. Furlong, B. P. Miller, P. Kotvis, and W. T. Tysoe, *Low-Temperature, Shear-Induced Tribofilm Formation from Dimethyl Disulfide on Copper.* ACS Applied Materials & Interfaces, 2011. **3**(3): p. 795-800.

52. P. C. H. Mitchell, *Oil-soluble MO-S compounds as lubricant additives.* Wear, 1984. **100**(1–3): p. 281-300.

53. H. H. Farmer and E. V. Rowan, *Molybdenum oxysulfide dithiocarbamates and processes for their preparation*, 1967, Google Patents.

54. T. Sakurai, H. Okabe, and H. Isoyama, *The Synthesis of Di-μ-thio-dithio-bis (dialkyldithiocarbamates) Dimolybdenum (V) and Their Effects on Boundary Lubrication.* Bulletin of The Japan Petroleum Institute, 1971. **13**(2): p. 243-249.

55. H. Isoyama and T. Sakurai, *The lubricating mechanism of di-u-thio-dithio-bis (diethyldithiocarbamate) dimolybdenum during extreme pressure lubrication.* Tribology, 1974. **7**(4): p. 151-160.

56. C. Grossiord, K. Varlot, J. M. Martin, T. Le Mogne, C. Esnouf, and K. Inoue, *MoS2 single sheet lubrication by molybdenum dithiocarbamate.* Tribology International, 1998. **31**(12): p. 737-743.

57. K. T. Miklozic, J. Graham, and H. Spikes, *Chemical and physical analysis of reaction films formed by molybdenum dialkyl-dithiocarbamate friction modifier additive using Raman and atomic force microscopy.* Tribology Letters, 2001. **11**(2): p. 71-81.

205

58. Y. Yamamoto and S. Gondo, *Friction and Wear Characteristics of Molybdenum Dithiocarbamate and Molybdenum Dithiophosphate.* Tribology Transactions, 1989. **32**(2): p. 251-257.

59. R. Roshan, M. Priest, A. Neville, A. Morina, X. Xia, C. P. Warrens, and M. J. Payne, *A Boundary Lubrication Friction Model Sensitive to Detailed Engine Oil Formulation in an Automotive Cam/Follower Interface.* Journal of Tribology, 2011. **133**(4): p. 042101-042101.

60. A. Morina, A. Neville, M. Priest, and J. H. Green, *ZDDP and MoDTC interactions in boundary lubrication—The effect of temperature and ZDDP/MoDTC ratio.* Tribology International, 2006. **39**(12): p. 1545-1557.

61. Y. Yamamoto and S. Gondo, *Environmental Effects on the Composition of Surface Films Produced by an Organo-Molybdenum Compound©.* Tribology Transactions, 1994. **37**(1): p. 182-188.

62. J. Graham, H. Spikes, and R. Jensen, *The friction reducing properties of molybdenum dialkyldithiocarbamate additives: Part II - Durability of friction reducing capability.* Tribology Transactions, 2001. **44**(4): p. 637-647.

63. M. Muraki and H. Wada, *Influence of the alkyl group of zinc dialkyldithiophosphate on the frictional characteristics of molybdenum dialkyldithiocarbamate under sliding conditions.* Tribology International, 2002. **35**(12): p. 857-863.

64. M. Muraki, Y. Yanagi, and K. Sakaguchi, *Synergistic effect on frictional characteristics under rolling-sliding conditions due to a combination of molybdenum dialkyldithiocarbamate and zinc dialkyldithiophosphate.* Tribology International, 1997. **30**(1): p. 69-75.

65. A. Morina, A. Neville, M. Priest, and J. H. Green, *ZDDP and MoDTC interactions and their effect on tribological performance - Tribofilm characteristics and its evolution.* Tribology Letters, 2006. **24**(3): p. 243-256.

66. A. Morina and A. Neville, *Understanding the composition and low friction tribofilm formation/removal in boundary lubrication.* Tribology International, 2007. **40**(10-12): p. 1696-1704.

67. A. Morina, A. Neville, J. H. Green, and M. Priest, *Additive/additive interactions in boundary lubrication — a study of film formation and tenacity*, in *Tribology and Interface Engineering Series*, M.P.G.D. D. Dowson and A.A. Lubrecht, Editors. 2005, Elsevier. p. 757-767.

68. T. Cousseau, J. S. Ruiz Acero, and A. Sinatora, *Tribological response of fresh and used engine oils: The effect of surface texturing, roughness and fuel type.* Tribology International, 2015.

69. S. Bec, A. Tonck, J. M. Georges, and G. W. Roper, *Synergistic Effects of MoDTC and ZDTP on Frictional Behaviour of Tribofilms at the Nanometer Scale.* Tribology Letters, 2004. **17**(4): p. 797-809.

70. M. Kasrai, J. N. Cutler, K. Gore, G. Canning, G. M. Bancroft, and K. H. Tan, *The Chemistry of Antiwear Films Generated by the Combination of ZDDP and MoDTC Examined by X-ray Absorption Spectroscopy.* Tribology Transactions, 1998. **41**(1): p. 69-77.

71. I. Singer, *A thermochemical model for analyzing low wear-rate materials.* Surface and Coatings Technology, 1991. **49**(1): p. 474-481.

72. P. A. Spevack and N. S. McIntyre, *Thermal reduction of molybdenum trioxide.* The Journal of Physical Chemistry, 1992. **96**(22): p. 9029-9035.

73. S. S. Saleem, *Infrared and Raman spectroscopic studies of the polymorphic forms of nickel, cobalt and ferric molybdates.* Infrared Physics, 1987. **27**(5): p. 309-315.

74. P. Colomban, S. Cherifi, and G. Despert, *Raman identification of corrosion products on automotive galvanized steel sheets.* Journal of Raman Spectroscopy, 2008. **39**(7): p. 881-886.

75. N. T. McDevitt, J. S. Zabinski, M. S. Donley, and J. E. Bultman, *Disorder-Induced Low-Frequency Raman Band Observed in Deposited MoS2 Films.* Applied Spectroscopy, 1994. **48**(6): p. 733-736.

76. Y. Wang, P. He, W. Lei, F. Dong, and T. Zhang, *Novel FeMoO4/graphene composites based electrode materials for supercapacitors.* Composites Science and Technology, 2014. **103**(0): p. 16-21.

77. Y. Yamamoto, S. Gondo, T. Kamakura, and N. Tanaka, *Frictional characteristics of molybdenum dithiophosphates.* Wear, 1986. **112**(1): p. 79-87.

78. Z. Zhang, C. Hu, M. Hashim, P. Chen, Y. Xiong, and C. Zhang, *Synthesis and magnetic property of FeMoO4 nanorods.* Materials Science and Engineering: B, 2011. **176**(9): p. 756-761.

79. P. A. Spevack and N. S. McIntyre, *A Raman and XPS investigation of supported molybdenum oxide thin films. 2. Reactions with hydrogen sulfide.* The Journal of Physical Chemistry, 1993. **97**(42): p. 11031-11036.

80. T. Weber, J. C. Muijsers, and J. W. Niemantsverdriet, *Structure of Amorphous MoS3.* The Journal of Physical Chemistry, 1995. **99**(22): p. 9194-9200.

81. G. F. Khudorozhko, L. G. Bulusheva, L. N. Mazalov, V. E. Fedorov, J. Morales, E. A. Kravtsova, I. P. Asanov, G. K. Parygina, and Y. V. Mironov, *Synthesis and study of the electronic structure of molybdenum tetrasulfide and its lithium intercalates.* Journal of Physics and Chemistry of Solids, 1998. **59**(2): p. 283-288.

82. T. Weber, J. C. Muijsers, J. H. M. C. van Wolput, C. P. J. Verhagen, and J. W. Niemantsverdriet, *Basic Reaction Steps in the Sulfidation of Crystalline MoO3 to MoS2, As Studied by X-ray Photoelectron and Infrared Emission Spectroscopy.* The Journal of Physical Chemistry, 1996. **100**(33): p. 14144-14150.

83. Z. Zhang, W. Li, T.-W. Ng, W. Kang, C.-S. Lee, and W. Zhang, *Iron(ii) molybdate (FeMoO4) nanorods as a high-performance anode for lithium ion batteries: structural and chemical evolution upon cycling.* Journal of Materials Chemistry A, 2015. **3**(41): p. 20527-20534.

84. L. Can, L. Zhengcao, and Z. Zhengjun, *MoO x thin films deposited by magnetron sputtering as an anode for aqueous micro-supercapacitors.* Science and Technology of Advanced Materials, 2013. **14**(6): p. 065005.

85. S.-H. Lee, M. J. Seong, C. E. Tracy, A. Mascarenhas, J. R. Pitts, and S. K. Deb, *Raman spectroscopic studies of electrochromic a-MoO3 thin films.* Solid State Ionics, 2002. **147**(1–2): p. 129-133.

86. H. Li, Q. Zhang, C. C. R. Yap, B. K. Tay, T. H. T. Edwin, A. Olivier, and D. Baillargeat, *From Bulk to Monolayer MoS2: Evolution of Raman Scattering.* Advanced Functional Materials, 2012. **22**(7): p. 1385-1390.

87. T. Onodera, R. Miura, A. Suzuki, H. Tsuboi, N. Hatakeyama, A. Endou, H. Takaba, M. Kubo, and A. Miyamoto, *Development of a quantum chemical molecular dynamics tribochemical simulator and its application to tribochemical reaction dynamics of lubricant additives.* Modelling and Simulation in Materials Science and Engineering, 2010. **18**(3): p. 034009.

88. T. Onodera, Y. Morita, A. Suzuki, M. Koyama, H. Tsuboi, N. Hatakeyama, A. Endou, H. Takaba, M. Kubo, F. Dassenoy, C. Minfray, L. Joly-Pottuz, J.-M. Martin, and A. Miyamoto, *A Computational Chemistry Study on Friction of h-MoS2. Part I. Mechanism of Single Sheet Lubrication.* The Journal of Physical Chemistry B, 2009. **113**(52): p. 16526-16536.

89. H. Fujita, R. P. Glovnea, and H. A. Spikes, *Study of Zinc Dialkydithiophosphate Antiwear Film Formation and Removal Processes, Part I: Experimental.* Tribology Transactions, 2005. **48**(4): p. 558-566.

90. M. Fuller, Z. Yin, M. Kasrai, G. M. Bancroft, E. S. Yamaguchi, P. R. Ryason, P. A. Willermet, and K. H. Tan, *Chemical characterization of tribochemical and thermal films generated from neutral and basic ZDDPs using X-ray absorption spectroscopy.* Tribology International, 1997. **30**(4): p. 305-315.

91. Z. Yin, M. Kasrai, M. Fuller, G. M. Bancroft, K. Fyfe, and K. H. Tan, *Application of soft X-ray absorption spectroscopy in chemical characterization of antiwear films generated by ZDDP Part I: the effects of physical parameters.* Wear, 1997. **202**(2): p. 172-191.

92. R. G. Dickinson and L. Pauling, *The crystal structure of molybdenite.* Journal of the American Chemical Society, 1923. **45**(6): p. 1466-1471.

93. B. Radisavljevic, A. Radenovic, J. Brivio, V. Giacometti, and A. Kis, *Single-layer MoS2 transistors.* Nat Nano, 2011. **6**(3): p. 147-150.

94. X. Luo, Y. Zhao, J. Zhang, Q. Xiong, and S. Y. Quek, *Anomalous frequency trends in MoS2 thin films attributed to surface effects.* Physical Review B, 2013. **88**(7): p. 075320.

95. J. L. Verble and T. J. Wieting, *Lattice Mode Degeneracy in MoS2 and Other Layer Compounds.* Physical Review Letters, 1970. **25**(6): p. 362-365.

96. T. J. Wieting, *Long-wavelength lattice vibrations of MoS2 and GaSe.* Solid State Communications, 1973. **12**(9): p. 931-935.

97. J. M. Chen and C. S. Wang, *Second order Raman spectrum of MoS2.* Solid State Communications, 1974. **14**(9): p. 857-860.

98. T. J. Wieting and J. L. Verble, *Infrared and Raman Studies of Long-Wavelength Optical Phonons in Hexagonal MoS2.* Physical Review B, 1971. **3**(12): p. 4286-4292.

99. Y. Wang, C. Cong, C. Qiu, and T. Yu, *Raman Spectroscopy Study of Lattice Vibration and Crystallographic Orientation of Monolayer MoS2 under Uniaxial Strain.* Small, 2013. **9**(17): p. 2857-2861.

100. B. Windom, W. G. Sawyer, and D. Hahn, *A Raman Spectroscopic Study of MoS2 and MoO3: Applications to Tribological Systems.* Tribology Letters, 2011. **42**(3): p. 301-310.

101. B. L. Evans and P. A. Young, *Optical Absorption and Dispersion in Molybdenum Disulphide.* Proceedings of the Royal Society of London. Series A, Mathematical and Physical Sciences, 1965. **284**(1398): p. 402-422.

102. G. L. Frey, R. Tenne, M. J. Matthews, M. S. Dresselhaus, and G. Dresselhaus, *Raman and resonance Raman investigation of MoS2 nanoparticles.* Physical Review B, 1999. **60**(4): p. 2883-2892.

103. H. Zeng, B. Zhu, K. Liu, J. Fan, X. Cui, and Q. M. Zhang, *Low-frequency Raman modes and electronic excitations in atomically thin MoS2 films.* Physical Review B, 2012. **86**(24): p. 241301.

104. A. M. Stacy and D. T. Hodul, *Raman spectra of IVB and VIB transition metal disulfides using laser energies near the absorption edges.* Journal of Physics and Chemistry of Solids, 1985. **46**(4): p. 405-409.

105. C. Lee, H. Yan, L. E. Brus, T. F. Heinz, J. Hone, and S. Ryu, *Anomalous Lattice Vibrations of Single- and Few-Layer MoS2.* ACS Nano, 2010. **4**(5): p. 2695-2700.

106. B. Chakraborty, H. S. S. R. Matte, A. K. Sood, and C. N. R. Rao, *Layer-dependent resonant Raman scattering of a few layer MoS2.* Journal of Raman Spectroscopy, 2013. **44**(1): p. 92-96.

107. A. G. Bagnall, W. Y. Liang, E. A. Marseglia, and B. Welber, *Raman studies of MoS2 at high pressure.* Physica B+C, 1980. **99**(1–4): p. 343-346.

108. T. Livneh and E. Sterer, *Resonant Raman scattering at exciton states tuned by pressure and temperature in 2H-MoS2.* Physical Review B, 2010. **81**(19): p. 195209.

109. S. Sugai and T. Ueda, *High-pressure Raman spectroscopy in the layered materials 2H-MoS2, 2H-MoSe2, and 2H-MoTe2.* Physical Review B, 1982. **26**(12): p. 6554-6558.

110. A. P. Nayak, T. Pandey, D. Voiry, J. Liu, S. T. Moran, A. Sharma, C. Tan, C.-H. Chen, L.-J. Li, M. Chhowalla, J.-F. Lin, A. K. Singh, and D. Akinwande, *Pressure-Dependent Optical and Vibrational Properties of Monolayer Molybdenum Disulfide.* Nano Letters, 2015. **15**(1): p. 346-353.

111. S. Sahoo, A. P. S. Gaur, M. Ahmadi, M. J. F. Guinel, and R. S. Katiyar, *Temperature-Dependent Raman Studies and Thermal Conductivity of Few-Layer MoS2.* The Journal of Physical Chemistry C, 2013. **117**(17): p. 9042-9047.

112. M. Thripuranthaka, R. V. Kashid, C. Sekhar Rout, and D. J. Late, *Temperature dependent Raman spectroscopy of chemically derived few layer MoS2 and WS2 nanosheets.* Applied Physics Letters, 2014. **104**(8): p. doi:http://dx.doi.org/10.1063/1.4866782.

113. S. Najmaei, P. M. Ajayan, and J. Lou, *Quantitative analysis of the temperature dependency in Raman active vibrational modes of molybdenum disulfide atomic layers.* Nanoscale, 2013. **5**(20): p. 9758-9763.

114. N. A. Lanzillo, A. Glen Birdwell, M. Amani, F. J. Crowne, P. B. Shah, S. Najmaei, Z. Liu, P. M. Ajayan, J. Lou, M. Dubey, S. K. Nayak, apos, and T. P. Regan, *Temperature-dependent phonon shifts in monolayer MoS2.* Applied Physics Letters, 2013. **103**(9): p. -.

115. L. Su, Y. Zhang, Y. Yu, and L. Cao, *Dependence of coupling of quasi 2-D MoS2 with substrates on substrate types, probed by temperature dependent Raman scattering.* Nanoscale, 2014. **6**(9): p. 4920-4927.

116. S. Najmaei, Z. Liu, P. M. Ajayan, and J. Lou, *Thermal effects on the characteristic Raman spectrum of molybdenum disulfide (MoS2) of varying thicknesses.* Applied Physics Letters, 2012. **100**(1): p. -.

117. K. Elangovan, V. Balasubramanian, and S. Babu, *Developing an Empirical Relationship to Predict Tensile Strength of Friction Stir Welded AA2219 Aluminum Alloy.* Journal of Materials Engineering and Performance, 2008. **17**(6): p. 820-830.

118. P. Larkin, *Chapter 2 - Basic Principles*, in *Infrared and Raman Spectroscopy.* 2011, Elsevier: Oxford. p. 7-25.

119. Renishaw. [cited 2015 17-8-2015]; Available from: http://www.renishaw.com/en/raman-spectroscopy-in-more-detail--25806

120. Cornell. [cited 2015 17-8-2015]; Available from: http://www.ccmr.cornell.edu/igert/modular/docs/Appl_of_Raman_Spectroscopy.pdf.

121. G. Gouadec and P. Colomban, *Raman Spectroscopy of nanomaterials: How spectra relate to disorder, particle size and mechanical properties.* Progress in Crystal Growth and Characterization of Materials, 2007. **53**(1): p. 1-56.

122. H. Harima, *Raman scattering characterization on SiC.* Microelectronic Engineering, 2006. **83**(1): p. 126-129.

123. M. T. Islam, R.-H. Nair, S. Ciotti, and C. Ackermann, *The Potential of Raman Spectroscopy as a Process Analytical Technique During Formulations of Topical Gels and Emulsions.* Pharmaceutical Research, 2004. **21**(10): p. 1844-1851.

124. L. Mandrile, A. M. Giovannozzi, F. Pennecchi, A. Saverino, C. Lobascio, and A. M. Rossi, *Direct detection and quantification of molecular surface contaminants by infrared and Raman spectroscopy.* Analytical Methods, 2015. **7**(6): p. 2813-2821.

125. P. T. T. Wong, T. E. Chagwedera, and H. H. Mantsch, *Structural aspects of the effect of pressure on the Raman and infrared spectra of n‐hexadecane.* The Journal of Chemical Physics, 1987. **87**(8): p. 4487-4497.

126. A. Müller, R. Jostes, W. Jaegermann, and R. Bhattacharyya, *Spectroscopic investigation on the molecular and electronic structure of [Mo3S13]2−, a discrete binary transition metal sulfur cluster.* Inorganica Chimica Acta, 1980. **41**(0): p. 259-263.

127. A. Muller, R. Jostes, W. Eltzner, C.-s. Nie, E. Diemann, H. Bogge, M. Zimmermann, M. Dartmann, U. ReinschVogell, and S. Che, *Synthetic, spectroscopic, X-ray structural, and quantum-chemical studies of cyanothiomolybdates with Mo2S, Mo2S2, Mo3S4, and Mo4S4 cores- A remarkable class of species existing with different electron populations and having the same central units as the ferrodoxins.* Inorganic Chemistry 1985. **24**(19): p. 2872-2884.

128. V. P. Fedin, B. A. Kolesov, Y. V. Mironov, and V. Y. Fedorov, *Synthesis and vibrational (IR and Raman) spectroscopic study of triangular thio-complexes [Mo3S13]2− containing 92Mo, 100Mo and 34S isotopes.* Polyhedron, 1989. **8**(20): p. 2419-2423.

129. H. Oku, N. Ueyama, and k. Nakamura, *Thiolato-Activated Oxo-Metal Bond Features in Molybdenum and Tungsten Oxidoreductase Models As Revealed by Raman Spectroscopy.* INORGANIC CHEMISTRY, 1995. **34**(14): p. 3667-3676.

130. A. Müller, R. G. Bhattacharyya, N. Mohan, and B. Pfefferkorn, *On the preparation of binuclear S, S bridged molybdenum(V) complexes crystal and molecular structure of [Mo2S4(Et2dtc)2].* Zeitschrift für anorganische und allgemeine Chemie, 1979. **454**(1): p. 118-124.

131. N. Ueyama, M. Nakata, T. Araki, A. Nakamura, S. Yamashita, and T. Yamashita, *Raman and resonance Raman spectra of sulphur-bridged binuclear molybdenum (V) complexes of cysteine-containing chelate anions.* Chemistry Letters, 1979. **8**(4): p. 421-424.

132. V. R. Ott, D. S. Swieter, and F. A. Schultz, *Di-.mu.-oxo, .mu.-oxo-.mu.-sulfido, and di-.mu.-sulfido complexes of molybdenum(V) with EDTA, cysteine, and cysteine ester ligands. Preparation and electrochemical and spectral properties.* INORGANIC CHEMISTRY, 1977. **16**(10): p. 2538-2545.

133. N. Ueyama, M. Nakata, T. Araki, A. Nakamura, S. Yamashita, and T. Yamashita, *Raman and resonance Raman spectra of oxomolybdenum(VI) and -(V) complexes of cysteine and related thiolate ligands.* Inorganic Chemistry, 1981. **20**(6): p. 1934-1937.

134. G. L. Schrader and C. P. Cheng, *In situ laser raman spectroscopy of the sulfiding of Moγ-Al2O3 catalysts.* Journal of Catalysis, 1983. **80**(2): p. 369-385.

135. A. Maezawa, M. Kitamura, Y. Okamoto, and T. Imanaka, *Characterization of Active Sites in Sulfided Molybdenum/ Alumina Hydrodesulfurization Catalysts.* Bulletin of the Chemical Society of Japan, 1988. **61**(7): p. 2295-2301.

136. Z. Wei, Q. Xin, and G. Xiong, *Investigation of the sulfidation of Mo/TiO2-Al2O3 catalysts by TPS and LRS.* Catalysis Letters, 1992. **15**(3): p. 255-267.

137. W. Kuang, Y. Fan, and Y. Chen, *State and Reactivity of Lattice Oxygen Ions in Mixed Fe−Mo Oxides.* Langmuir, 2000. **16**(3): p. 1440-1443.

138. R. Srivastava and L. L. Chase, *Raman spectra of CrO2 and MoO2 single Crystals.* Solid State Communications, 1972. **11**(2): p. 349-353.

139. Horiba. *Raman scattering and Flourescence.* 22/10/2015]; Available from: http://www.horiba.com/fileadmin/uploads/Scientific/Documents/Raman/Fluorescence01.pdf.

140. P. A. Willermet, R. O. Carter, P. J. Schmitz, M. Everson, D. J. Scholl, and W. H. Weber, *Formation, structure, and properties of lubricant-derived antiwear films.* Lubrication Science, 1997. **9**(4): p. 325-348.

141. S. Camacho-López, M. A. Camacho-López, R. E. Oscar Olea Mejía, G. C. Vega, M. A. Camacho-López, M. H. Zaldivar, A. E. García, and J. G. B. Muñetón, *Processing of metallic thin films using Nd:YaG laser pulses, Nd YAG Laser*, D.D.C. Dumitras, Editor 2012, InTech.

142. T. R. Jervis, J.-P. Hirvonen, and M. Nastasi, *Post deposition excimer laser processing of MoS x thin films.* Journal of Materials Research, 1991. **6**(06): p. 1350-1357.

143. B. Vengudusamy, J. H. Green, G. D. Lamb, and H. A. Spikes, *Behaviour of MoDTC in DLC/DLC and DLC/steel contacts.* Tribology International, 2012. **54**: p. 68-76.

144. S. Berkani, F. Dassenoy, C. Minfray, J.-M. Martin, H. Cardon, G. Montagnac, and B. Reynard, *Structural Changes in Tribo-Stressed Zinc Polyphosphates.* Tribology Letters, 2013. **51**(3): p. 489-498.

145. S. L. González-Cortés, T.-C. Xiao, T.-W. Lin, and M. L. H. Green, *Influence of double promotion on HDS catalysts prepared by urea-matrix combustion synthesis.* Applied Catalysis A: General, 2006. **302**(2): p. 264-273.

146. A. Müller, W.-O. Nolte, and B. Krebs, *[(S2)2Mo(S2)2Mo(S2)2]2−, a Novel Complex Containing Only S 22− Ligands and a Mo☐Mo Bond.* Angewandte Chemie International Edition in English, 1978. **17**(4): p. 279-279.

147. N. T. McDevitt, J. S. Zabinski, and M. S. Donley, *The use of Raman scattering to study disorder in pulsed laser deposited MoS2 films.* Thin Solid Films, 1994. **240**(1–2): p. 76-81.

148. J. S. Zabinski and N. T. MacDevitt, *Raman spectra of inorganic compounds related to solid state tribochemical studies*, 1996, USAF Wright Laboratory Report No. WL-TR-96-4034.

149. N. T. McDevitt, J. E. Bultman, and J. S. Zabinski, *Study of Amorphous MoS2 Films Grown by Pulsed Laser Deposition.* Applied Spectroscopy, 1998. **52**(9): p. 1160-1164.

150. G. Gouadec, L. Bellot-Gurlet, D. Baron, and P. Colomban, *Raman Mapping for the Investigation of Nano-phased Materials*, in *Raman Imaging*, A. Zoubir, Editor. 2012, Springer Berlin Heidelberg. p. 85-118.

151. R. Unnikrishnan, M. C. Jain, A. K. Harinarayan, and A. K. Mehta, *Additive-additive interaction: An XPS study of the effect of ZDDP on the AW/EP characteristic of molybdenum based additives.* Wear, 2002. **252**(3-4): p. 240-249.

152. E. Haro-Poniatowski, C. Julien, B. Pecquenard, J. Livage, and M. A. Camacho-López, *Laser-induced structural transformations in MoO3 investigated by Raman spectroscopy.* Journal of Materials Research, 1998. **13**(04): p. 1033-1037.

153. T. Sekine, K. Uchinokura, T. Nakashizu, E. Matsuura, and R. Yoshizaki, *Dispersive Raman Mode of Layered Compound 2H-MoS2 under the Resonant Condition.* Journal of the Physical Society of Japan, 1984. **53**(2): p. 811-818.

154. A. Müller, N. Weinstock, and H. Schulze, *Laser-Raman-Spektren der Ionen MoS42−, WS42−, MoOS32− und WOS32− in wässriger Lösung sowie der entsprechenden kristallinen Alkalisalze.* Spectrochimica Acta Part A: Molecular Spectroscopy, 1972. **28**(6): p. 1075-1082.

155. C. H. Chang and S. S. Chan, *Infrared and Raman studies of amorphous MoS3 and poorly crystalline MoS2.* Journal of Catalysis, 1981. **72**(1): p. 139-148.

156. T. Wang, J. Zhuo, K. Du, B. Chen, Z. Zhu, Y. Shao, and M. Li, *Electrochemically Fabricated Polypyrrole and MoSx Copolymer Films as a Highly Active Hydrogen Evolution Electrocatalyst.* Advanced Materials, 2014. **26**(22): p. 3761-3766.

157. R. N. Bhattacharya, C. Y. Lee, F. H. Pollak, and D. M. Schleich, *Optical study of amorphous MoS3: Determination of the fundamental energy gap.* Journal of Non-Crystalline Solids, 1987. **91**(2): p. 235-242.

158. C. Sourisseau, O. Gorochov, and D. M. Schleich, *Comparative IR and Raman studies of various amorphous MoS3 and LixMoS3 phases.* Materials Science and Engineering: B, 1989. **3**(1–2): p. 113-117.

159. D. A. Rice, S. J. Hibble, M. J. Almond, K. A. H. Mohammad, and S. P. Pearse, *Novel low-temperature route to known (MnS and FeS2) and new (CrS3, MoS4 and WS5) transition-metal sulfides.* Journal of Materials Chemistry, 1992. **2**(8): p. 895-896.

160. A. Ghanbarzadeh, M. Wilson, A. Morina, D. Dowson, and A. Neville, *Development of a new mechano-chemical model in boundary lubrication.* Tribology International.

161. F. Sahlin, R. Larsson, A. Almqvist, P. M. Lugt, and P. Marklund, *A mixed lubrication model incorporating measured surface topography. Part 1: Theory of flow factors.* Proceedings of the Institution of Mechanical Engineers, Part J: Journal of Engineering Tribology, 2010. **224**(4): p. 335-351.

162. Y. Hu and K. Tonder, *Simulation of 3-D random rough surface by 2-D digital filter and fourier analysis.* International Journal of Machine Tools & Manufacture, 1992. **32**(1-2): p. 83-90.

163. T. W. Scharf and I. L. Singer, *Thickness of diamond-like carbon coatings quantified with Raman spectroscopy.* Thin Solid Films, 2003. **440**(1-2): p. 138-144.

164. M. I. De Barros Bouchet, J. M. Martin, T. Le Mogne, P. Bilas, B. Vacher, and Y. Yamada, *Mechanisms of MoS2 formation by MoDTC in presence of ZnDTP: effect of oxidative degradation.* Wear, 2005. **258**(11–12): p. 1643-1650.

165. H. Tian, C. A. Roberts, and I. E. Wachs, *Molecular Structural Determination of Molybdena in Different Environments: Aqueous Solutions, Bulk Mixed Oxides, and Supported MoO3 Catalysts.* The Journal of Physical Chemistry C, 2010. **114**(33): p. 14110-14120.

166. H. Tian, I. E. Wachs, and L. E. Briand, *Comparison of UV and Visible Raman Spectroscopy of Bulk Metal Molybdate and Metal Vanadate Catalysts.* The Journal of Physical Chemistry B, 2005. **109**(49): p. 23491-23499.

167. I. Watanabe, M. Otake, M. Yoshimoto, K. Sakanishi, Y. Korai, and I. Mochida, *Behaviors of oil-soluble molybdenum complexes to form very fine MoS2 particles in vacuum residue.* Fuel, 2002. **81**(11–12): p. 1515-1520.

168. Y. Li, Y. Yu, Y. Huang, R. A. Nielsen, W. A. Goddard, Y. Li, and L. Cao, *Engineering the Composition and Crystallinity of Molybdenum Sulfide for High-Performance Electrocatalytic Hydrogen Evolution.* ACS Catalysis, 2015. **5**(1): p. 448-455.

169. M. De Feo, C. Minfray, M. I. De Barros Bouchet, B. Thiebaut, and J. M. Martin, *MoDTC friction modifier additive degradation: Correlation between tribological performance and chemical changes.* RSC Advances, 2015. **5**(114): p. 93786-93796.

170. M. Z. Huq, X. Chen, P. B. Aswath, and R. L. Elsenbaumer, *Thermal degradation behavior of zinc dialkyldithiophosphate in presence of catalyst and detergents in neutral oil.* Tribology Letters, 2005. **19**(2): p. 127-134.

171. G. Nehme, *Fluorinated FeF3 catalyst interactions in three different oil formulations using design of experiment optimization and chemistry characterization of tribofilms.* Lubrication Science, 2011. **23**(4): p. 153-179.

172. J. C. Wildervanck and F. Jellinek, *Preparation and Crystallinity of Molybdenum and Tungsten Sulfides.* Zeitschrift für anorganische und allgemeine Chemie, 1964. **328**(5-6): p. 309-318.

173. X. Li, W. Zhang, Y. Wu, C. Min, and J. Fang, *Solution-Processed MoSx as an Efficient Anode Buffer Layer in Organic Solar Cells.* ACS Applied Materials & Interfaces, 2013. **5**(18): p. 8823-8827.

174. J. Lince, A. Pluntze, S. Jackson, G. Radhakrishnan, and P. Adams, *Tribochemistry of MoS3 Nanoparticle Coatings.* Tribology Letters, 2014. **53**(3): p. 543-554.

175. M. Bowker, C. Brookes, A. F. Carley, M. P. House, M. Kosif, G. Sankar, I. Wawata, P. P. Wells, and P. Yaseneva, *Evolution of active catalysts for the selective oxidative dehydrogenation of methanol on Fe2O3 surface doped with Mo oxide.* Physical Chemistry Chemical Physics, 2013. **15**(29): p. 12056-12067.

176. L.-b. Wu, L.-h. Wu, W.-m. Yang, and A. I. Frenkel, *Study of the local structure and oxidation state of iron in complex oxide catalysts for*

propylene ammoxidation. Catalysis Science & Technology, 2014. **4**(8): p. 2512-2519.

177. J. Temuujin, K. J. D. MacKenzie, G. Burmaa, D. Tsend-Ayush, T. Jadambaa, and A. v. Riessen, *Mechanical activation of MoS2 + Na2O2 mixtures.* Minerals Engineering, 2009. **22**(4): p. 415-418.

178. S. M. Haw and N. J. Mosey, *Tribochemistry of Aldehydes Sheared between (0001) Surfaces of α-Alumina from First-Principles Molecular Dynamics.* The Journal of Physical Chemistry C, 2012. **116**(3): p. 2132-2145.

179. J. Liang and J. M. Fernández, *Kinetic measurements on single-molecule disulfide bond cleavage.* Journal of the American Chemical Society, 2011. **133**(10): p. 3528-3534.

180. R. Schnurmann and I. S. Stringer, *Initiation of chemical reactions by mechanical forces.* Nature, 1960. **187**(4737): p. 587-588.

181. S. R. Koti Ainavarapu, A. P. Wiita, L. Dougan, E. Uggerud, and J. M. Fernandez, *Single-Molecule Force Spectroscopy Measurements of Bond Elongation during a Bimolecular Reaction.* Journal of the American Chemical Society, 2008. **130**(20): p. 6479-6487.

182. S. J. Blanksby and G. B. Ellison, *Bond Dissociation Energies of Organic Molecules.* Accounts of Chemical Research, 2003. **36**(4): p. 255-263.

183. B. Dacre and C. H. Bovington, *The Adsorption and Desorption of Zinc Di-isopropyldithiophosphate on Steel.* A S L E Transactions, 1982. **25**(4): p. 546-554.

184. B. Vengudusamy, A. Grafl, F. Novotny-Farkas, and W. Schöfmann, *Influence of Surface Roughness on the Tribological Behavior of Gear Oils in Steel–Steel Contacts: Part I—Boundary Friction Properties.* Tribology Transactions, 2014. **57**(2): p. 256-266.

185. J. Seabra and D. Berthe, *Influence of Surface Waviness and Roughness on the Normal Pressure Distribution in the Hertzian Contact.* Journal of Tribology, 1987. **109**(3): p. 462-469.

186. I. L. Singer, R. N. Bolster, J. Wegand, S. Fayeulle, and B. C. Stupp, *Hertzian stress contribution to low friction behavior of thin MoS2 coatings.* Applied Physics Letters, 1990. **57**(10): p. 995-997.

187. T. Kubart, T. Polcar, L. Kopecký, R. Novák, and D. Nováková, *Temperature dependence of tribological properties of MoS2 and MoSe2 coatings.* Surface and Coatings Technology, 2005. **193**(1–3): p. 230-233.

188. H. S. Khare and D. L. Burris, *The Effects of Environmental Water and Oxygen on the Temperature-Dependent Friction of Sputtered Molybdenum Disulfide.* Tribology Letters, 2013. **52**(3): p. 485-493.

189. V. N. Bakunin, G. N. Kuzmina, M. Kasrai, O. P. Parenago, and G. M. Bancroft, *Tribological behavior and tribofilm composition in lubricated systems containing surface-capped molybdenum sulfide nanoparticles.* Tribology Letters, 2006. **22**(3): p. 289-296.

190. R. Heuberger, A. Rossi, and N. D. Spencer, *Pressure Dependence of ZnDTP Tribochemical Film Formation: A Combinatorial Approach.* Tribology Letters, 2007. **28**(2): p. 209-222.

191. H. A. Spikes and H. Fujita, *The formation of zinc dithiophosphate antiwear films.* Proceedings of the Institution of Mechanical Engineers, Part J: Journal of Engineering Tribology, 2004. **218**(4): p. 265-278.

192. O. Furlong, B. Miller, P. Kotvis, H. Adams, and W. T. Tysoe, *Shear and thermal effects in boundary film formation during sliding.* RSC Advances, 2014. **4**(46): p. 24059-24066.

193. N. Cabrera and N. F. Mott, *Theory of the oxidation of metals.* Reports on Progress in Physics, 1949. **12**(1): p. 163.

194. J. D. Baran, H. Grönbeck, and A. Hellman, *Mechanism for Limiting Thickness of Thin Oxide Films on Aluminum.* Physical Review Letters, 2014. **112**(14): p. 146103.

195. N. Cai, G. Zhou, K. Müller, and D. E. Starr, *Tuning the Limiting Thickness of a Thin Oxide Layer on Al(111) with Oxygen Gas Pressure.* Physical Review Letters, 2011. **107**(3): p. 035502.

196. L. Taylor, A. Dratva, and H. A. Spikes, *Friction and wear behavior of zinc dialkyldithiophosphate additive.* Tribology Transactions, 2000. **43**(3): p. 469-479.

197. K. J. Kubiak, T. G. Mathia, and M. Bigerelle, *Influence of roughness on ZDDP tribofilm formation in boundary lubricated fretting.* Tribology - Materials, Surfaces & Interfaces, 2012. **6**(4): p. 182-188.

198. Y. C. Lin and H. So, *Limitations on use of ZDDP as an antiwear additive in boundary lubrication.* Tribology International, 2004. **37**(1): p. 25-33.

199. M. Suzuki, *Comparison of tribological characteristics of sputtered MoS2 films coated with different apparatus.* Wear, 1998. **218**(1): p. 110-118.

200. G. C. Barton and S. V. Pepper, *Transfer of molybdenum disulfide to various metals.* NASA STI/Recon Technical Report N, 1977. **77**: p. 30296.

201. V. D. Stephen, R. H. Michael, and D. F. Paul, *The Influence of Steel Surface Chemistry on the Bonding of Lubricant Films*, in *Surface Science Investigations in Tribology*. 1992, American Chemical Society. p. 43-57.

202. M. Miyajima, K. Kitamura, and K. Matsumoto, *Characterization of Tribofilm with the Remaining Lubricating Oil by Raman Spectroscopy.* Tribology Online, 2015. **10**(3): p. 225-231.

203. M. Cano-Lara, S. Camacho-López, A. Esparza-García, and M. A. Camacho-López, *Laser-induced molybdenum oxide formation by low energy (nJ)–high repetition rate (MHz) femtosecond pulses.* Optical Materials, 2011. **33**(11): p. 1648-1653.

Appendix A
Raman spectra: Evolution of MoDTC tribofilms with rubbing time
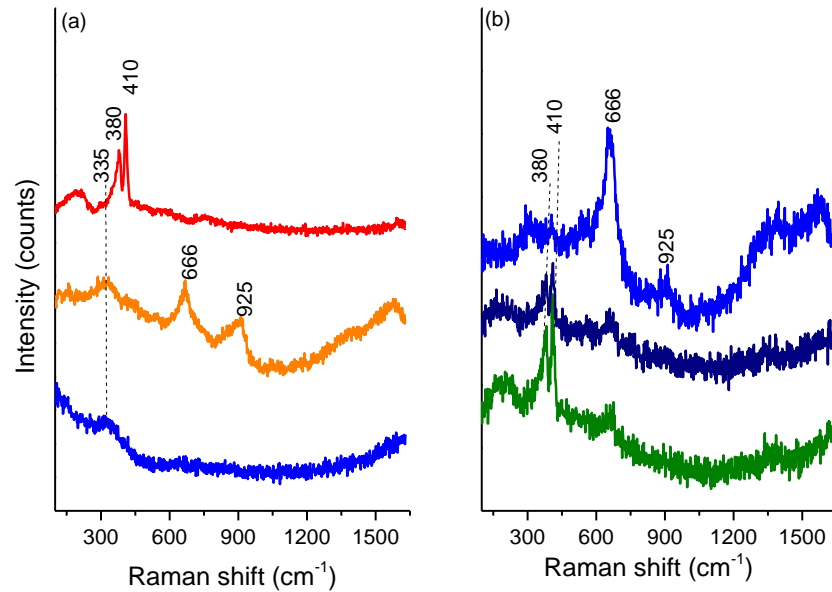
Figure A1. Raman spectra from tribopair wear scars after 1 minute test. (a) Ball wear scar (b) disc wear scar.
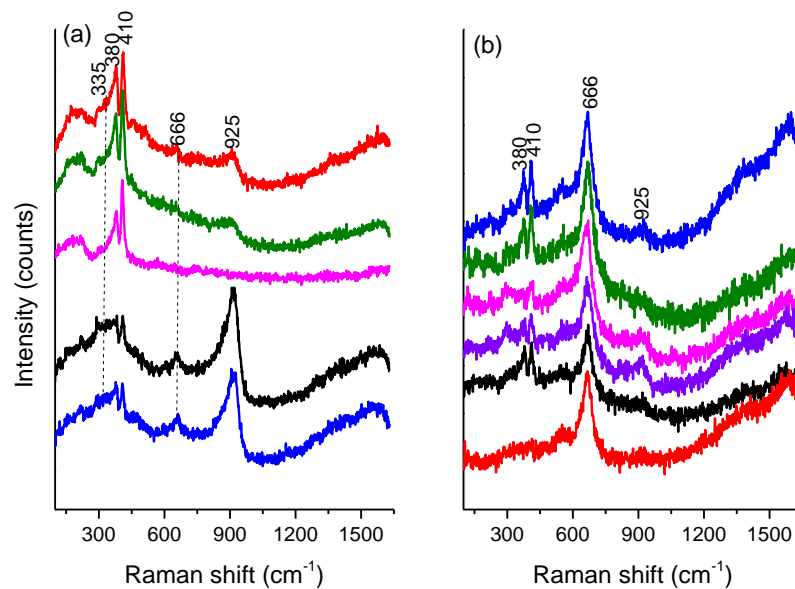
Figure A2. Raman spectra obtained from tribopair wear scars after 2 minute tests. (a) Ball wear scar (b) disc wear scar.
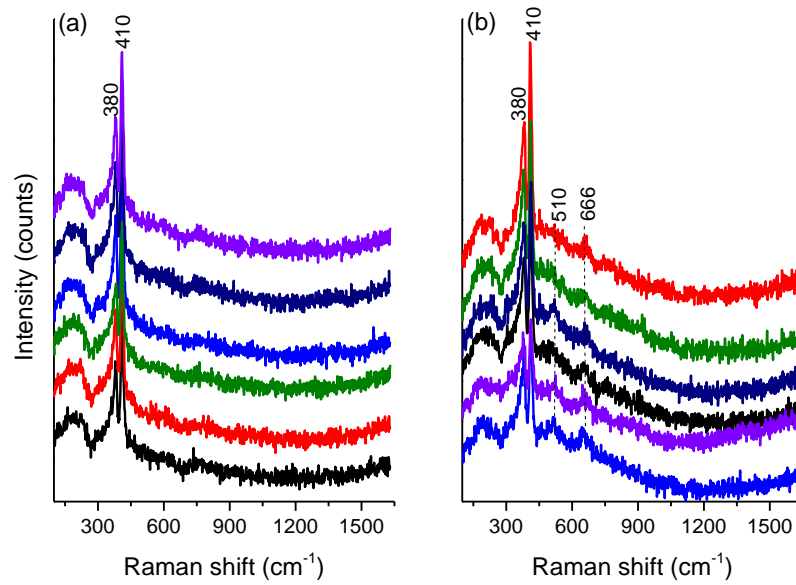
Figure A3. Raman spectra obtained from tribopair wear scar after 5 minutes test. (a) Ball wear scar (b) disc wear scar
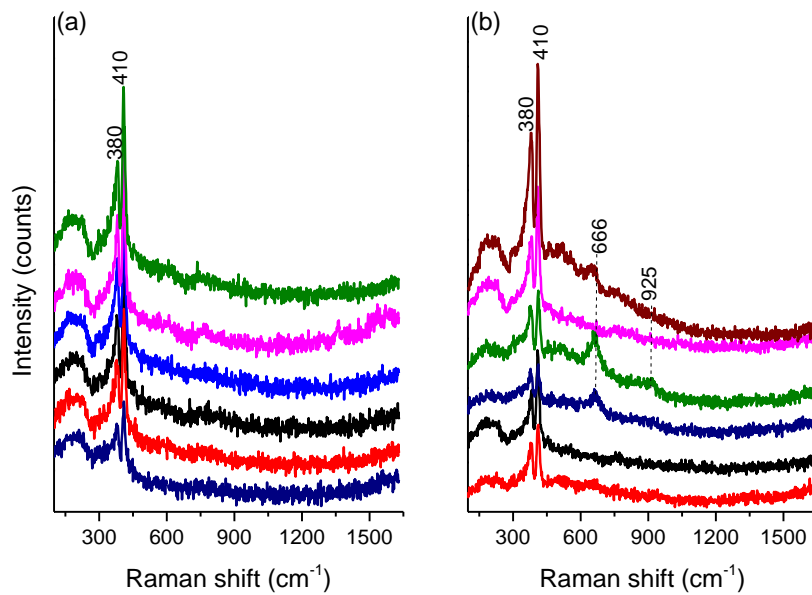
Figure A4. Raman spectra obtained from tribopair wear scar after 20 minutes test. (a) Ball wear scar (b) disc wear scar
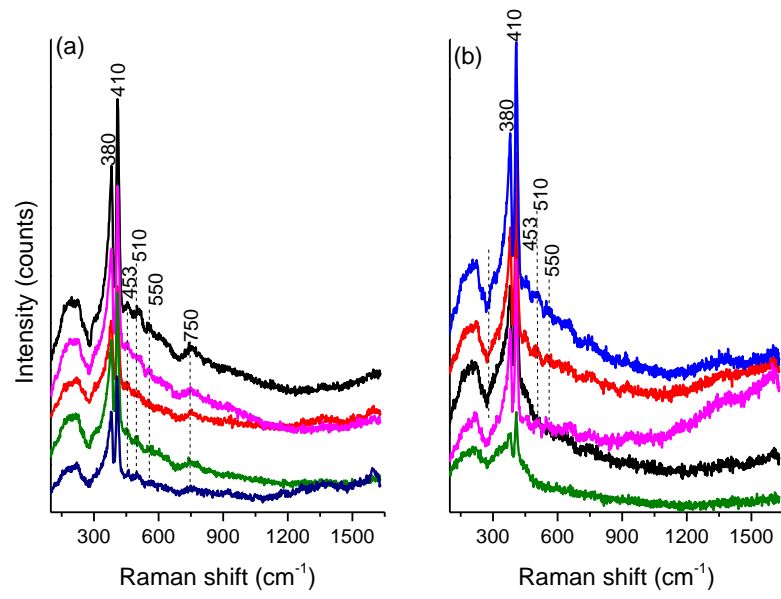
Figure A5. Raman spectra obtained from tribopair wear scars after 60 minutes test. (a) Ball wear scar (b) disc wear scar

Appendix B
Raman spectra: Influence of test conditions on chemical composition of MoDTC tribofilms

B.1. Influence of temperature
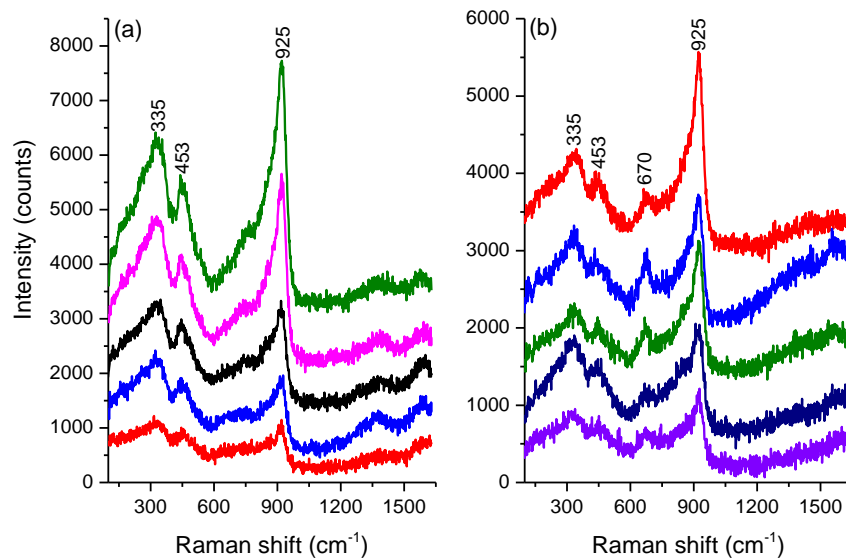
Figure B1. Tribopair wear scar after tests at 20⁰C. (a) Ball wear scar (b) disc wear scar
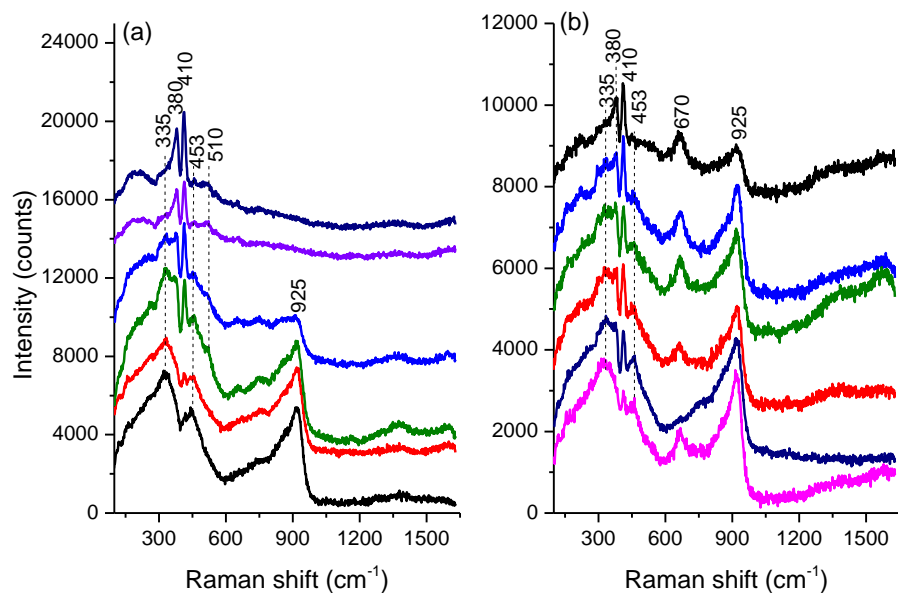
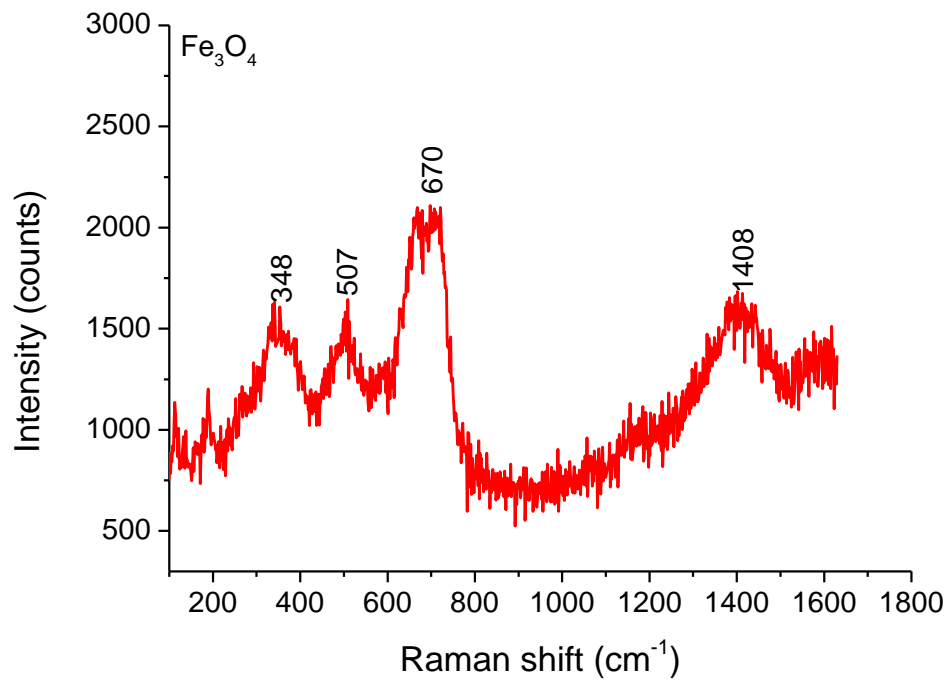**Figure B2. Tribopair wear scars after tests with 0.5 wt% MoDTC at 40⁰C. (a) Ball wear scar (b) disc wear scar.**
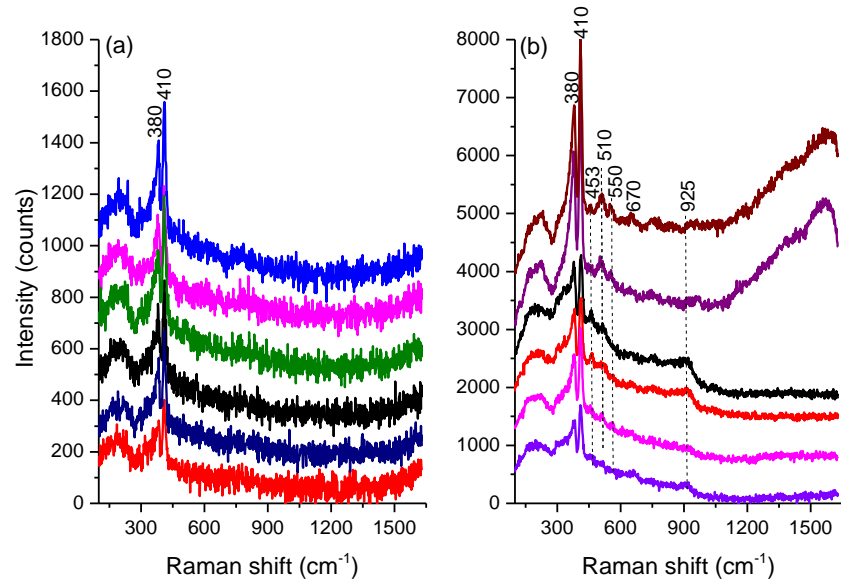
Figure B3. Tribopair wear scars after tests with 0.5 wt% MoDTC at 60⁰C. (a) Ball wear scar (b) disc wear scar
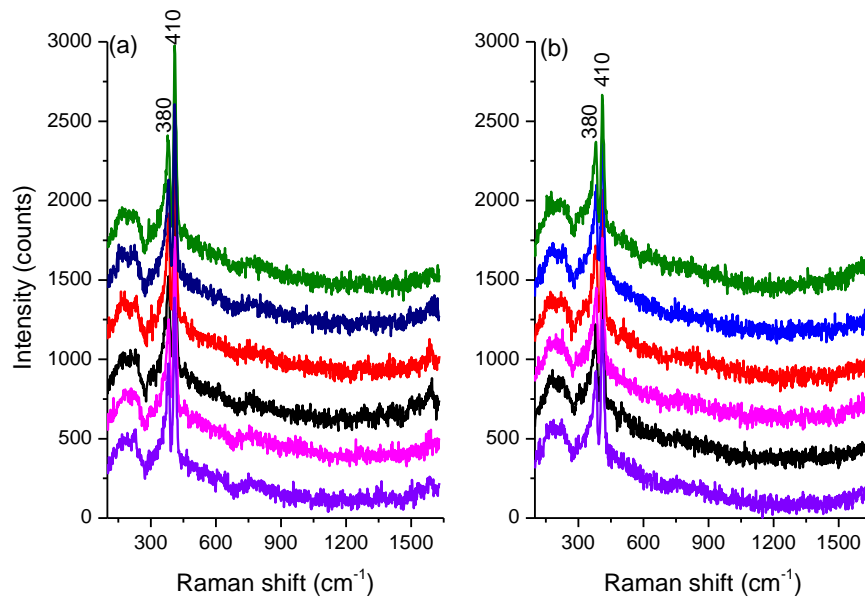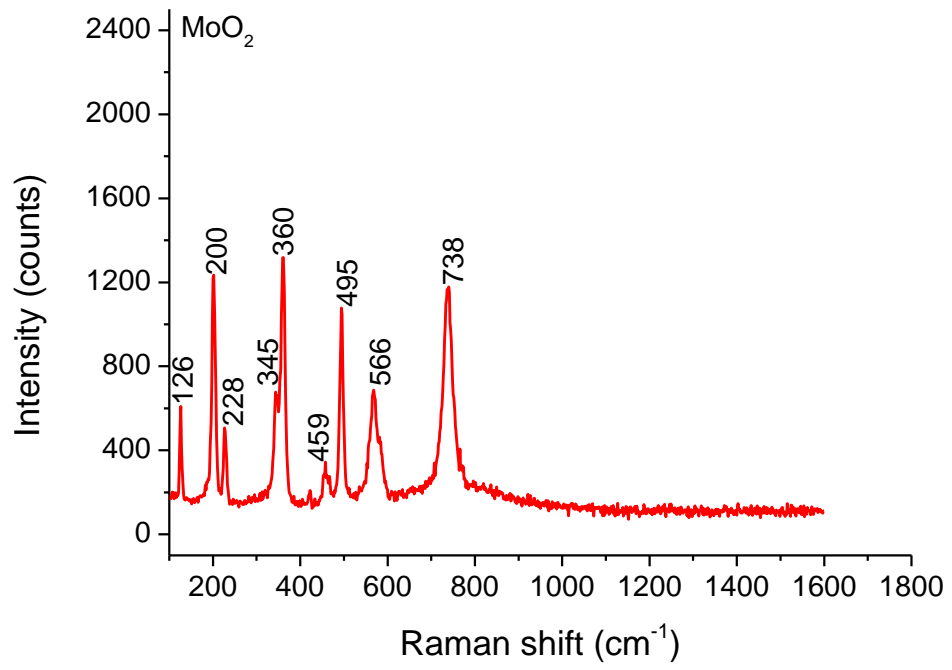

Figure B4. Tribopair wear scars after tests with 0.5 wt% at 100⁰C. (a) Ball wear scar (b) disc wear scar

B.2. Influence of MoDTC concentration
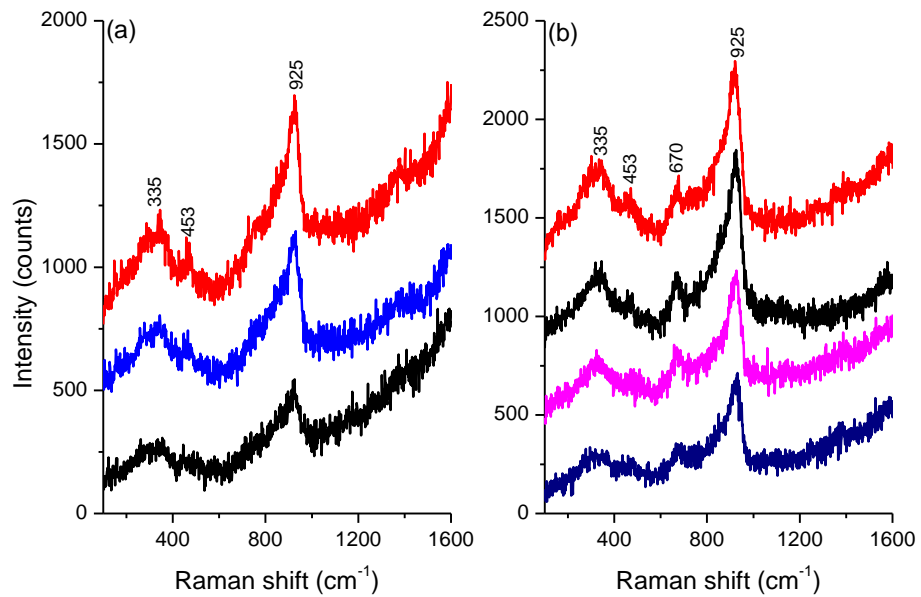
Figure B5. Tribopair wear scars after tests with 0.1 wt% MoDTC at 60ºC. (a) Ball wear scar (b) disc wear scar
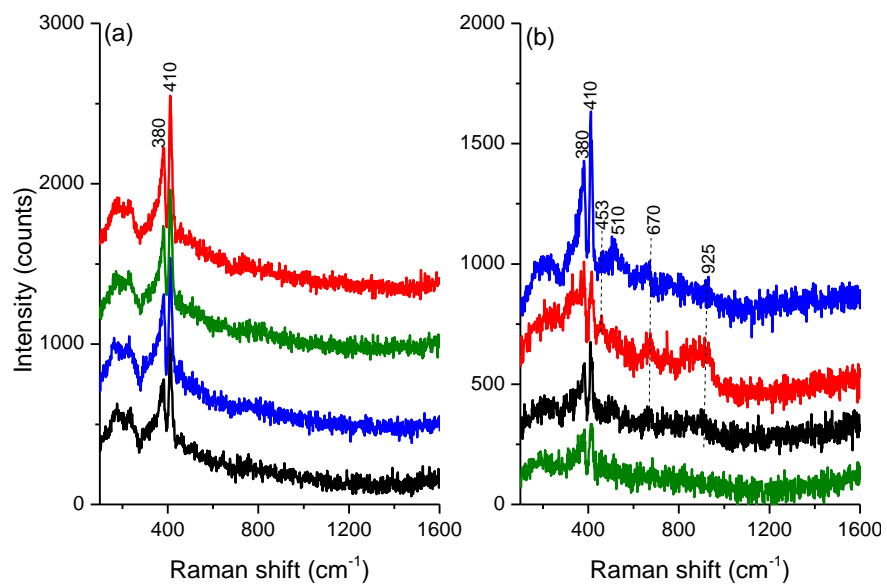
Figure B6. Tribopair wear scars after tests with 0.5 wt% MoDTC at 60℃. (a) Ball wear scar (b) disc wear scar
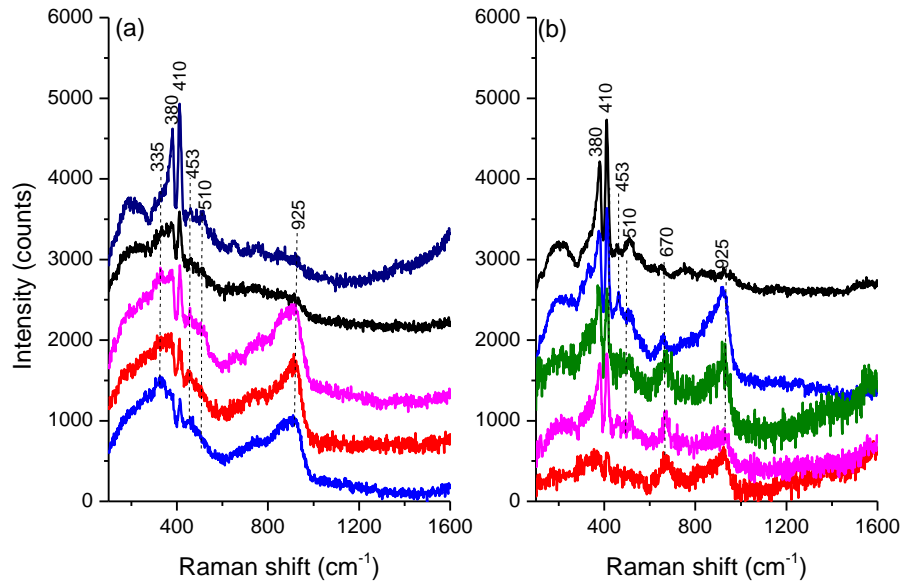
Figure B7. Tribopair wear scars generated with 0.9 wt% MoDTC at 60ºC. (a) Ball wear scar (b) disc wear scar

B.3. Influence of contact pressure
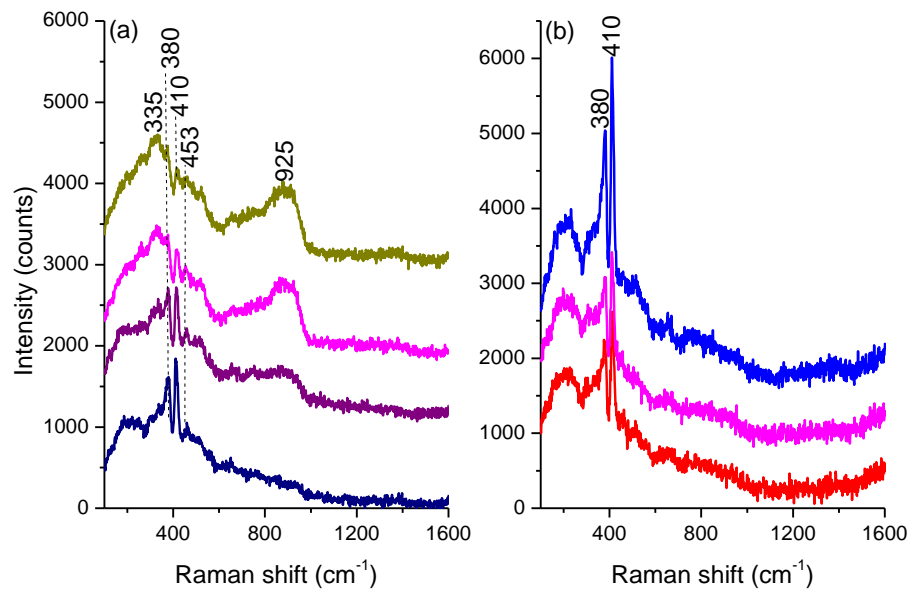
Figure B8. Tribopair wear scars after tests at 0.98 GPa. (a) Ball wear scar (b) disc wear scar
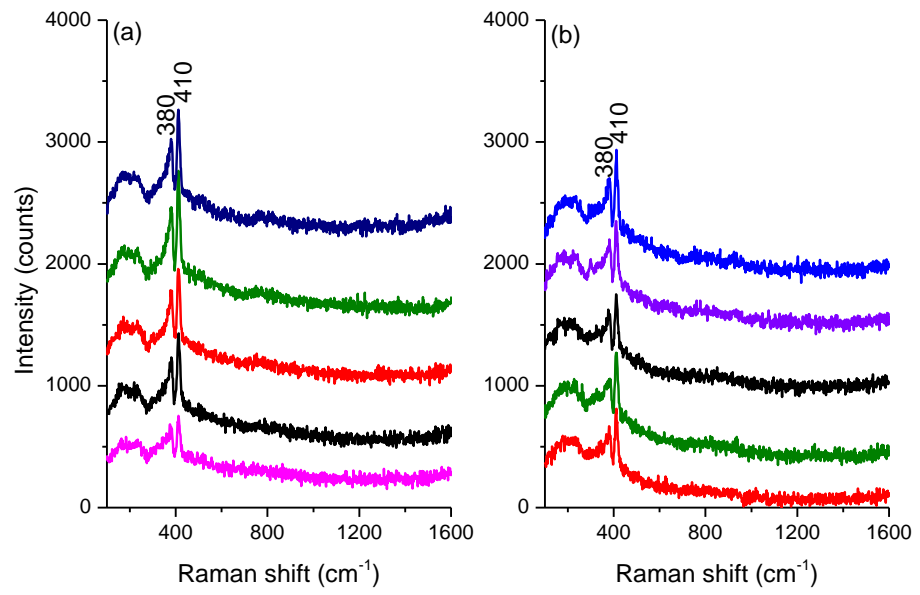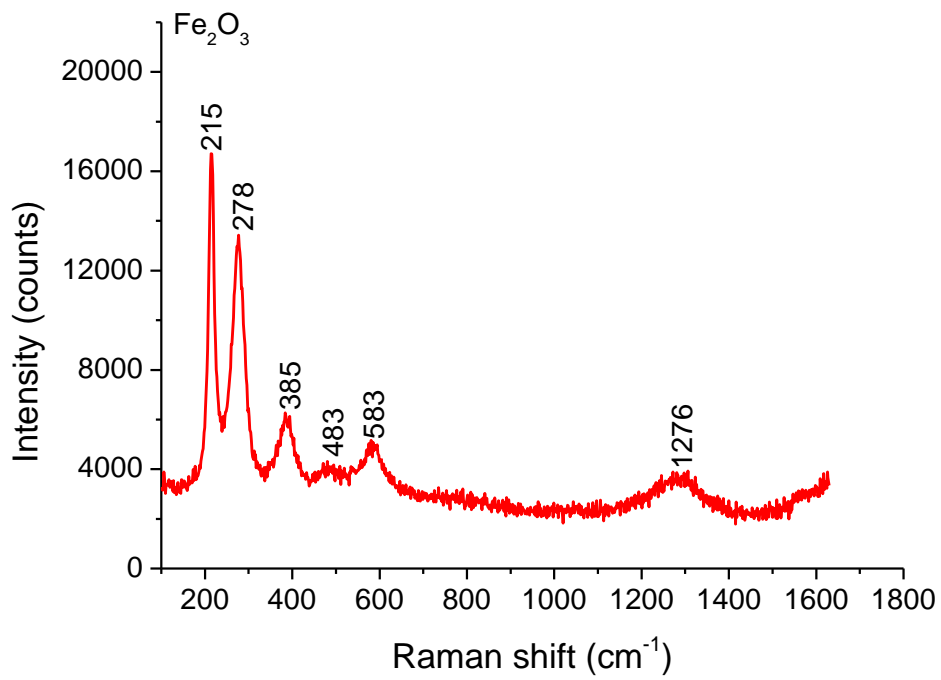
Figure B9. Tribopair wear scars after tests at 2.12 GPa at 60ºC. (a) Ball wear scar (b) disc wear scar

Appendix C
Raman spectra of pure powders

MoO$_3$

82, 116, 157, 283, 337, 666, 818, 995

Intensity (counts)

Raman shift (cm^{-1})

MoS$_2$

280, 374, 400, 442, 555, 586, 734, 770, 812

Intensity (counts)

Raman shift (cm^{-1})

FeSO₄ Raman spectrum with peaks labeled at 218, 271, 423, 494, 619, 663, 1018, 1091, and 1195 cm⁻¹.
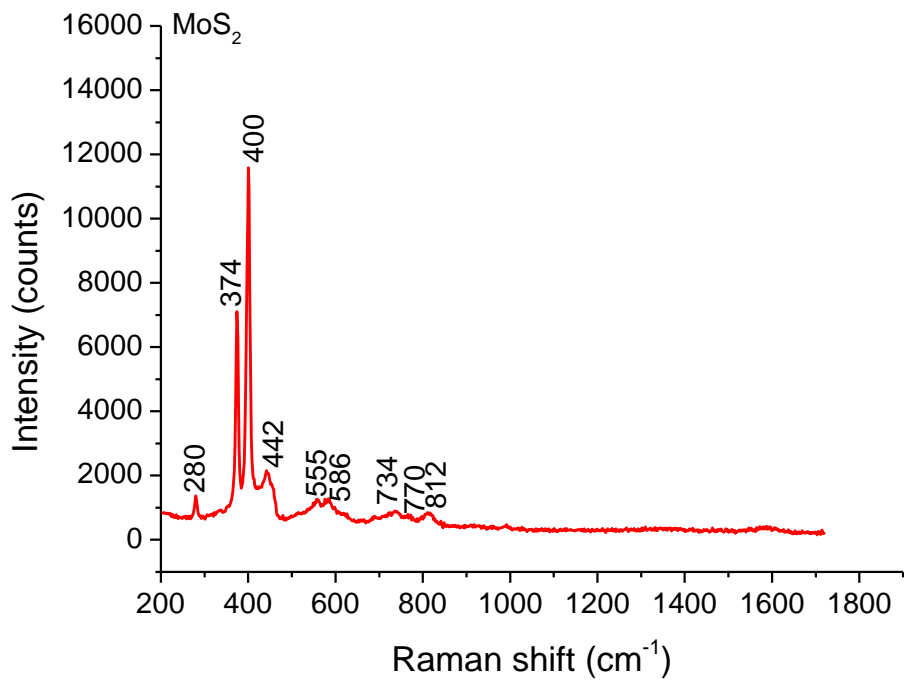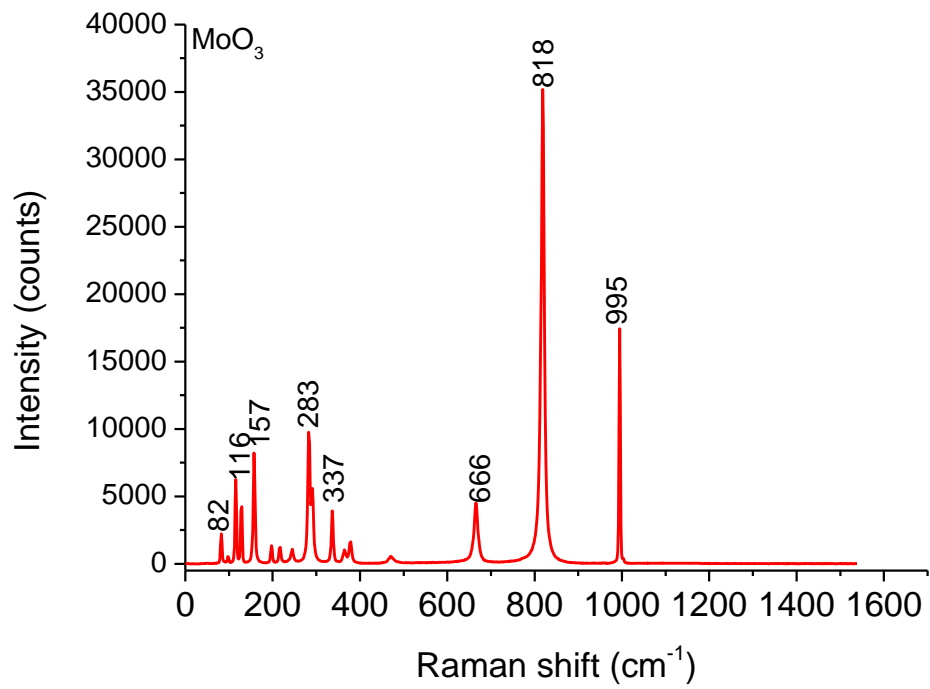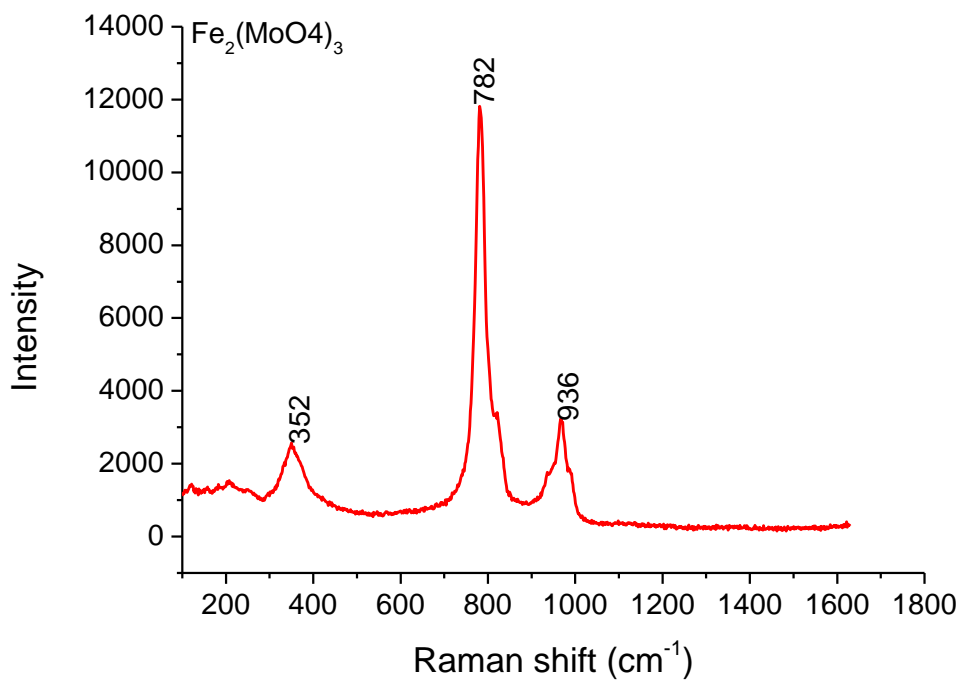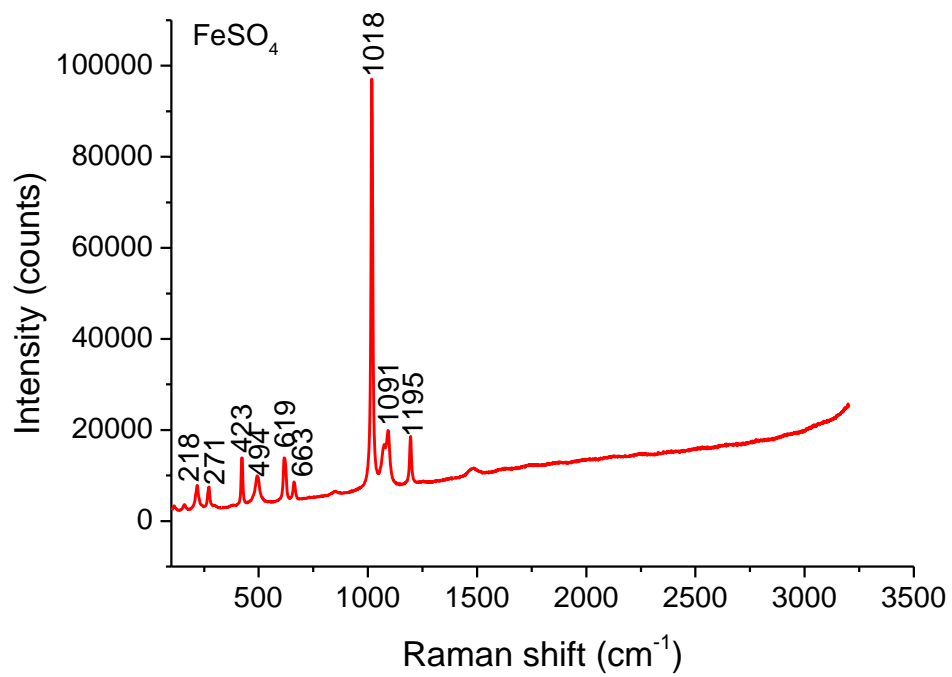
Appendix D
Raman spectra: Influence of surface roughness and slide-roll ratio (SRR)

Tribotests were conducted using the MiniTraction Machine at the following tests conditions: 0.5 wt% MoDTC lubricant, 1 GPa, 100ºC
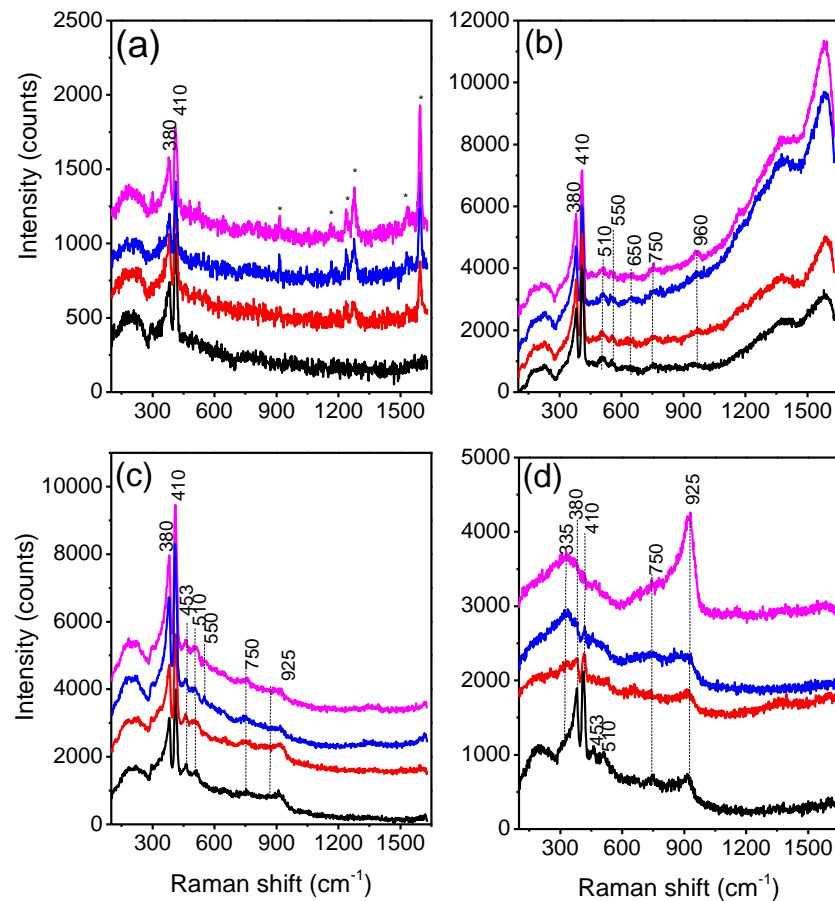

Figure D1. Raman spectra obtained from tribopair wear scars after 2h tests at SRR=100%. (a) Ball rubbed against rough discs (b) rough disc (c) ball rubbed against smooth disc (d) smooth disc. Peaks indicated by asterisk are from the adhesive used to fix samples on glass slides during analysis.
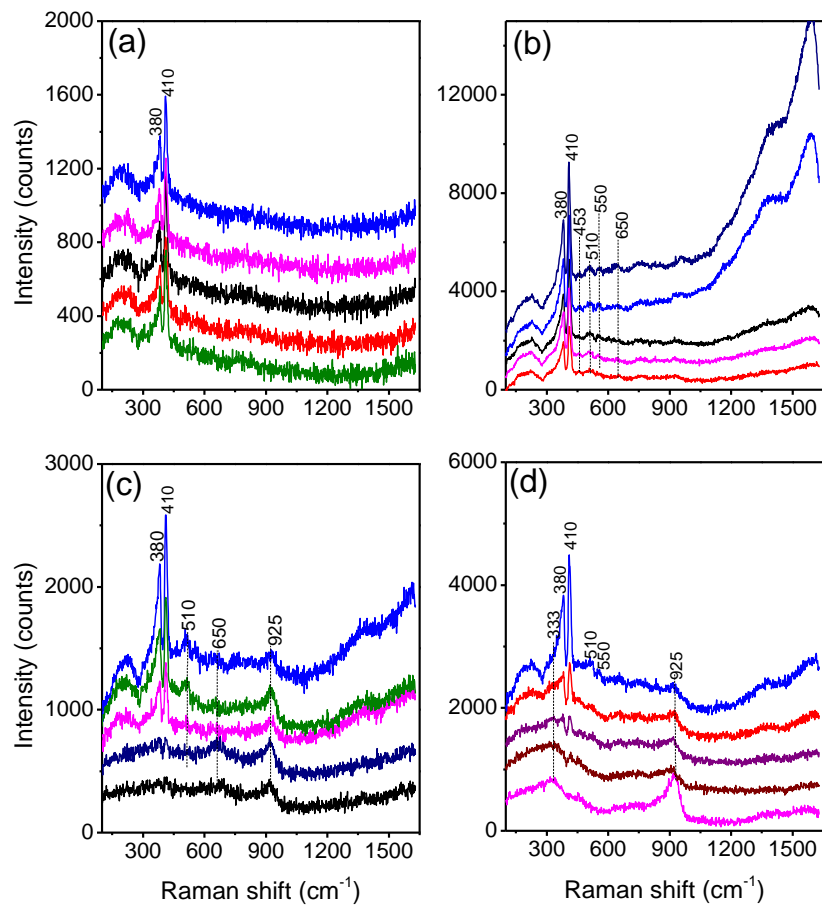
Figure D2. Raman spectra obtained from tribopair wear scars after 2h tests at SRR=200%. (a) Ball rubbed against rough discs (b) rough disc (c) ball rubbed against smooth disc (d) smooth disc.

Appendix E
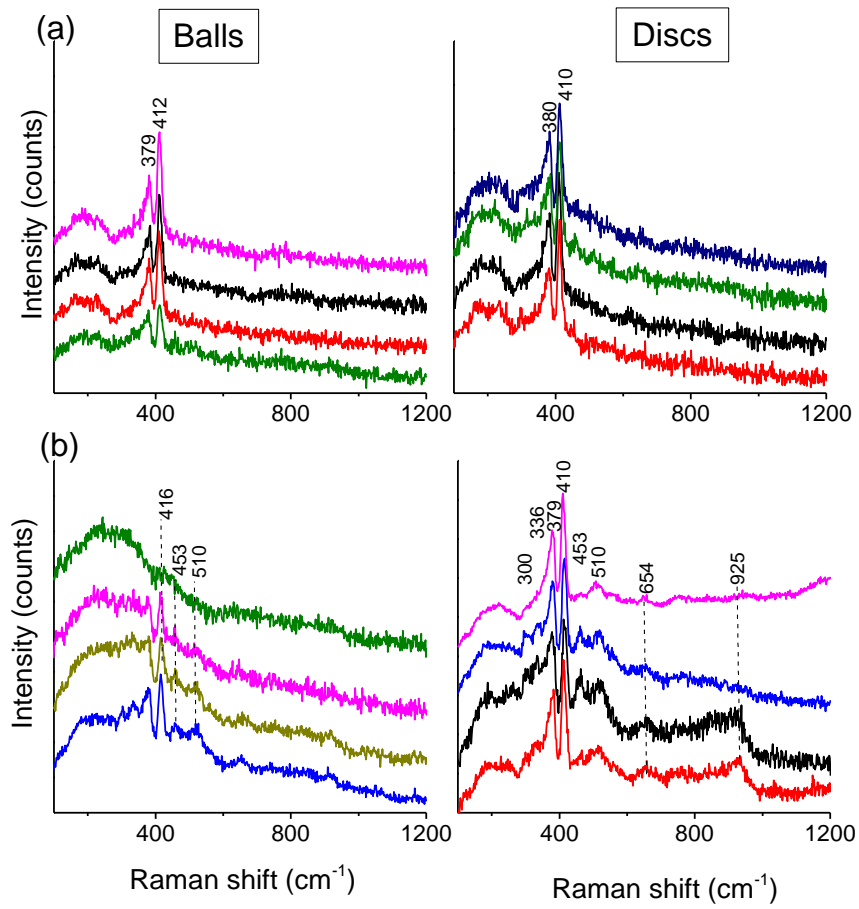## Raman spectra: Durability of MoDTC tribofilms

Figure E1. Raman spectra obtained from different regions within the tribopair wear scars after tests with fresh steel samples (a) MoDTC (b) MoDTC followed by BO
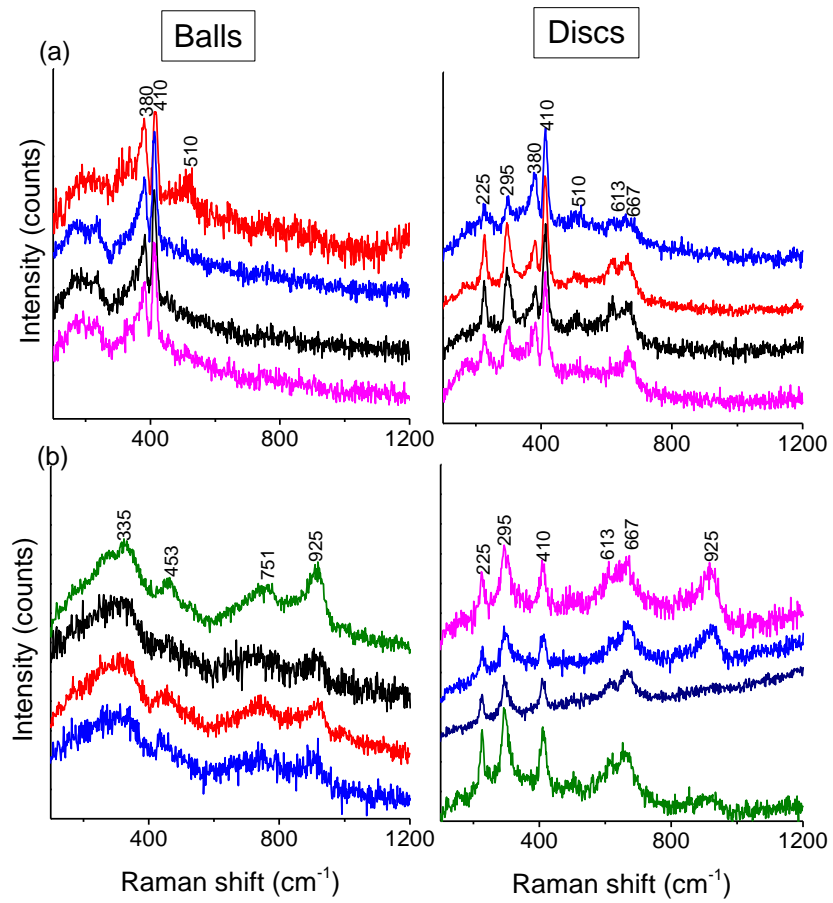
Figure E2. Raman spectra obtained from different regions within tribopair wear scars after tests with oxidised steel samples (a) MoDTC (b) MoDTC followed by BO